Nottingham Transportation Engineering Centre (NTEC)
Department of Civil Engineering
Faculty of Engineering

EARLY-OPENING-TO-TRAFFIC ASPHALT PAVEMENT FOR AIRFIELD REHABILITATION

By

Taqia Rahman

Thesis submitted to the University of Nottingham
for the degree of Doctor of Philosophy

March 2021

Abstract

A large number of scheduled flights at major civil airports has made it necessary that runway repair and overlay be carried out without interfering with flight schedules. Asphalt overlaying at night has become one practical solution to this issue. Using this method, the runway is closed at night for several hours and immediately opened to aircraft traffic in the morning. Generally, at the end of the time window, several hours are needed for the pavement to cool down before re-opening. For a busy airport, the cooling is an otherwise undesirable use of time. Shortening the asphalt cooling time would allow airport authorities to quickly open the new pavement to traffic and thus reduce airport closures. It would also allow contractors to place the maximum amount of HMA each night, increasing the target length to be paved, thus shortening the overall project contract and increasing construction efficiency.

This thesis investigates strategies for reducing the cooling time of asphalt overlays to accelerate airport pavement construction while still delivering satisfactorily constructed pavements during airfield pavement repair/rehabilitation. Three strategies were reviewed: (1) Defining and selecting the warmest hot-mix-asphalt (HMA) temperature at opening to traffic commensurate with adequate performance and safe operations, (2) Reducing the cooling time by using warm-mix-asphalt (WMA), (3) Decreasing the pavement temperature by spraying cool water onto the new asphalt.

To investigate the first and second strategies, laboratory evaluation of rutting performance and interface shear strength at high temperature and high loads was performed to investigate the allowable asphalt temperature for trafficking of HMA and WMA airfield pavements. Bituminous mixtures with unmodified bitumen (40/60 pen. grade), SBS polymer modified binder, and both binders containing WMA additives (wax and chemical) were manufactured and tested to examine the bitumen effect on the pavement performance at different opening temperatures. The rutting performance and interface shear bond strength of the bituminous mixtures at traffic opening temperatures were then predicted using a simple linear viscous approach and the Mohr-Coulomb failure model, respectively. Moreover, to simulate the effect of each strategy on airport closure time and pavement construction period, a one-dimensional (1D) heat-transfer model, using a finite element (FE) program (ABAQUS) was developed.

To investigate the third strategy, small-scale 11-cm-thick asphalt slabs were constructed inside steel moulds to measure cooling rates due to both natural cooling and water spray cooling, using embedded thermocouples and an infrared thermometer. Various temperatures and flow rates of water spraying were considered. A three-dimensional (3D) heat transfer analysis of the laboratory-scale FE model was then used to determine the heat transfer coefficients of the water cooling by trial-and-error matching of temperature in the 3D model to the temperatures from the thermocouple readings. In addition, cores were taken from the asphalt slabs for Cantabro and indirect tensile strength (IDT) testing so as to investigate the possible drawbacks of water cooling of newly laid asphalt in terms of the long-term durability and moisture susceptibility.

Regarding the first strategy, the results indicate that at the traffic-opening temperature of 60°C, as set by many agencies and specifications, the newly laid asphalt has gained sufficient strength to resist permanent deformation and interface failure caused by aircraft load and braking. The results, however, suggested that different mixtures and tack coat materials, particularly those containing polymer-modified bitumen (PMB), could be re-opened to air traffic at a considerably higher temperature (up to 80°C). This result encourages airport authorities and agencies to be more adaptive with the traffic-opening temperature specification, particularly for asphalt with PMBs. The cooling analysis showed that for the cases studied, raising the critical trafficking temperature could reduce the closure of an airport during night-time construction by 17-114 minutes (26-63% reductions) depending on the asphalt mixture type, environmental condition (wind speed) and traffic-opening temperature.

For the second strategy, the laboratory tests indicate that, in general, the WMAs have a rutting performance at high temperatures during the opening to traffic similar to, or better than HMA. It was found that, compared to HMA, a WMA having a wax additive showed excellent rutting resistance, enabling the pavement to be opened to traffic at a higher temperature. This is likely because, at in-service temperatures, the wax additives solidify (crystallize) and thus improve stiffness and rutting resistance of the mixture. Moreover, the cooling analysis showed that, in comparison to HMA, the use of this WMA could shorten the closure time of airport during the night-time construction by 8–67 min (5–73% reductions compared to HMA cooling time) depending on the asphalt overlay thickness, specified traffic opening temperature and WMA production temperature.

Concerning the third strategy, the results indicate that the heat loss of newly laid asphalt is significantly affected by water cooling depending on the water temperatures, flow rate, spray duration and travel time of water (to drain). The 3D heat transfer model was found to be sufficiently accurate for estimating the heat transfer coefficient of water spraying. The reduced cooling time due to spray water cooling, however, is much less effective for asphalt with greater overlay thickness, since the water only cools the crust/surface of asphalt temporarily, with the bottom of the newly laid asphalt not being much affected. Limited Cantabro and indirect tensile strength testing indicated that the spray water application onto newly paved asphalt, so as to permit earlier trafficking, does not necessarily adversely affect the asphalt durability and/or the moisture damage of asphalt pavement.

Keywords: airfield rehabilitation, runway resurfacing, asphalt cooling response, temperature of opening to traffic, warm-mix asphalt, newly laid asphalt, spray water cooling

Publications

The following conference papers and journal articles have been published based on the research undertaken as part of the PhD program.

- Rahman, T., Dawson, A. and Thom, N. 2019. '*Investigation of the Permissible Temperature of Asphalt Overlay for Opening to Traffic during Airfield Pavement Rehabilitation*.' 7th International Conference Bituminous Mixtures and Pavements, 12-14 June 2019, Thessaloniki, Greece (published).
- Rahman, T., Thom, N., Dawson, A. 2019. '*Strategies for Reduced Cooling Time of Asphalt for Airfield Pavement Overlay*.' 2019 International Airfield and Highway Pavements Conference, July 21–24, 2019, Chicago (published).
- Rahman, T., Dawson, A. and Thom, N. 2020. Warm mix asphalt (WMA) for rapid construction in airfield pavement. *Construction and Building Materials*, 246, 118411 (published).

  Rahman, T., Dawson, A., Thom, N., Ahmed, I. and Carvajal-Munoz, J. S. 2020. Determining the allowable opening-to-traffic asphalt temperature for airport pavements. *International Journal of Pavement Engineering*, 1-19 (published online).

In addition, the following publications are either prepared for submission, submitted for peer review or are in pre-publication processing:

- Rahman, T., Dawson, A. and Thom, N. 2021. Spray Water Cooling of Newly Laid Asphalt Pavement for Rapid Opening to Traffic. *Road Materials and Pavement Design* (prepared for submission).

Acknowledgements

First of all, I want to thank Allah Almighty who gave me the power, the patience and the love to be able to complete my study in the best way.

I would like to give special thanks to my supervisors, Dr Andrew Dawson and Dr Nick Thom for their knowledge, advice, guidance and encouragement throughout this study, without their guidance this thesis would not have been possible. I have learned many valuable lessons from you. I will never forget your help.

I am grateful to my internal assessor Prof. Gordon Airey for his kind advice during my research.

My sincere thanks go to Nottingham Transportation Engineering Centre for making laboratory facilities available for the study. The technical support from Jon Watson, Richard Blakemore, Lawrence Pont, Martyn Barrett and others of Nottingham Transportation Engineering Centre laboratory is highly appreciated. I am grateful to my colleagues in the research office and Indonesian students in Nottingham – PPI Nottingham and PeDLN for their supports and helps.

I would also like to acknowledge and thank LPDP (Indonesia Endowment Fund for Education), Ministry of Finance, the Republic of Indonesia and Universitas Gadjah Mada (UGM) for providing financial support for this research. The study was made possible with funding from the LPDP. Special thanks to Total UK Ltd - Bitumen Division, and AkzoNobel UK for their generosity in making materials available for this study.

I am extremely grateful to my parents, Mr M. Wildan Yahya and Mrs Enung Apandi and my brothers, my sisters and my in-laws for their patient, encouragement and continuous support. I am sorry that my mother cannot see me complete the study. Her memory will be with me always. Finally, and most importantly, I owe a debt of gratitude to my lovely wife, Bunga and our two beloved sons, Rayyan and Kafa for their supports throughout the research period.

Declaration

This is to declare that the contents of this thesis are my own work and were performed at the University of Nottingham from 2017 to 2021. This thesis has not been submitted to any other institution for another degree.

Taqia Rahman

Nottingham, March 2021

Email: taqia.rahman@nottingham.ac.uk, taqia.rahman@gmail.com

Table of Contents

List of Figures

List of Tables

List of Abbreviations

AASHTO	American Association of State Highway and Transportation Officials
APA	Asphalt Pavement Analyzer
ASTM	American Society for Testing and Materials
CBR	California Bearing Ratio
CEI	Compaction Energy Index
CML	Cantabro Mass Loss
DM	Dynamic modulus (test)
DSR	Dynamic Shear Rheometer
FAA	Federal Aviation Administration (of the USA)
FE	Finite Element
FHWA	Federal Highway Administration (of the USA)
HMA	Hot Mix Asphalt
HWTD	Hamburg Wheel Tracking Device
IATA	International Air Transport Association
ICAO	International Civil Aviation Organisation
IDT	Indirect Tensile Strength Test
ISS	Interface Shear Strength
MSCR	Multiple Stress Creep Recovery
PCC	Portland Cement Concrete
PMB	Polymer Modified Binder
RAP	Reclaimed asphalt pavement
RET	Rapid Exit Taxiway
RLAT	Repeated Load Axial Test
RSME	Root-mean-square Error
RTFO	Rolling Thin Film Oven
SBS	Styrene-Butadiene-Styrene
SC	Static creep (test)
TDI	Traffic Densification Index
TSR	Tensile Strength Ratio
TRB	Transportation Research Board (of the USA)
WMA	Warm Mix Asphalt.

List of Symbols

ν	Poisson's ratio
°C	Degree Celsius
in.	inch
kg	gram x 10^3
m	meter
km	meter x 10^3
mm	meter x 10^{-3}
Pa	Pascal
kPa	Pascal x 10^3
MPa	Pascal x 10^6
T	Temperature
A	Area
F	Force
t	Time
c	Cohesion
τ	Shear stress
h_c	Heat transfer coefficient
ρ	Density
C_p	Specific heat capacity
σ	Normal/axial stress
r	Radius
m	mass
μ	Coefficient of friction of tyre-pavement
δ	Phase angle
G^*	Complex shear modulus
ε	Strain
ε_e	Emissivity
J_{nr}	Non-recoverable creep compliance
η	Viscosity
$\dot{\varepsilon}$	Strain rate
N	Number of loading/load cycles
ϕ	Internal friction angle
ω	Angular velocity
E	Elastic modulus
E^*	Complex/dynamic modulus
d	Displacement
V	Flow rate
Q	Heat flux
k	Thermal Conductivity
v_w	Wind speed
$\tilde{\alpha}$	Albedo
S_t	Indirect tensile strength

1. Introduction

1.1. Overview and Problem Statement

Invented in the early twentieth century, air transportation has become one of the most attractive, valuable, and sophisticated industries in the world. In many parts of the world, civil aviation plays an important role as the main transportation mode (Horonjeff and McKelvey 2010). In 2016, according to IATA International Air Transport Association (2017), ICAO (2017) and Airport Council International (2017), the air transportation sector comprise more than 900 airlines and 23,000 aircraft, transported more than 3.8 billion passengers and 55 million tons of freight on more than 88 million flights to more than 17,000 commercial airports in more than 200 countries worldwide. The air transportation system, especially its airports, has developed into the backbone of global transportation of people and cargo.

The important role of airport infrastructure is to provide uninterrupted aviation services. One of an airport's most important asset is the airfield pavement structure (Pittenger 2011). Without proper design and maintenance of airfield pavements, the desired aircraft would not be able to operate to or from the airport. During airport operations, airfield pavements begin a gradual deterioration from several sources, for example, environmental conditions, aircraft loading, construction issues, and ageing (Arabali et al. 2017). In addition, the increase of air traffic movement and greater load of today's aircraft has speeded up the rate at which pavement structures reach the end of their lives (Irfan et al. 2015). This structural life is commonly designed to be 20 years based on FAA regulation (FAA 2014b). However, to achieve this intended design life, routine maintenance, repair, and rehabilitation should be performed, otherwise, the pavement will reach a weakened condition in which it is very susceptible to becoming severely distressed (Shahin 2005).

For these reasons, repairing and maintaining airfield pavements has become a critical element in airport management (Arabali et al. 2017). In the case of commercial and public airfield pavements, the chance of complete reconstruction is impracticable. The construction of new

runways is often unrealistic in today's environmentally aware world (Austin 1991). The concept of restoration by laying a new pavement layer over the existing structure is, therefore, an effective solution adopted by airfield pavements engineers. However, the increasing demand for 24-hour airport operation has limited the periods available for the execution of runway upgrade works. As airport traffic increases, airfield pavement overlaying can generate serious interruptions to airport operations and lead to flying delays, cancellations and missed connecting flights. These possible events are troublesome to passengers, cause loss of schedule integrity, and are costly to airlines (FAA 2006). Wendt et al. (2020) reported that the cost of delays due to airport closure in a typical large airport in Germany is enormous. Such delays convert into additional costs for airlines in terms of extra fuel and crew service time. The costs also comprise the passenger's cost due to longer travel time. The delay costs can be up to €0.8 million per hour.

As a solution to the aforementioned problems, rehabilitation of airside pavements during off-peak (night-time) periods can be a practical technique to manage airside paving schedules without loss of income, disruption to passengers or extreme delay of the air movement system (FAA 2006). Hayhoe et al. (1998) demonstrate that pavement rehabilitation can be completed at night-time when aircraft movement is less frequent; accordingly, the utilization of runways over the daytime will not be influenced. The off-peak period of pavement repair and overlay has become common practice in many airports around the world (Nepal 2014, Hachiya et al. 2008, Frank et al. 2013).

In major airports, the typical unoccupied time available for airfield pavement rehabilitation is as short as 6-8 hours per night. A period from 23:00 to 6:00 was specified for runway overlay at Fukuoka airport (Hachiya et al. 2008). Similar night-time construction periods can also be found in the following airport projects: San Diego International airport in 1980 (8 hours) (Wills 1982), Frankfurt airport, Germany, in 2005 (8 hours) (Aho et al. 2016) and Hong Kong airport in 2006 (8 hours) (Li et al. 2008). However, the available time has tended to be more limited recently due to airport operations, as noted by White (2017a) in relation to large Australian airports. The construction period appears to have shifted from 6-8 to 4-5 hours in the last 10 years.

During the pavement rehabilitation, at the end of the work session, contractors should allow several hours for cooling of newly placed asphalt before traffic opening (Hachiya et al. 2008). As shown in Figure 1.1, for typical road resurfacing work, the construction time is divided

into production-type activities and waiting (lags)-type activities (Wang et al. 2014b). The curing time for tack coat to set only consumes a short period; therefore, its influence on the whole project is insignificant. However, the cooling time after paving a section for trafficking may last for several hours. The same situation occurs also in airfield rehabilitation.

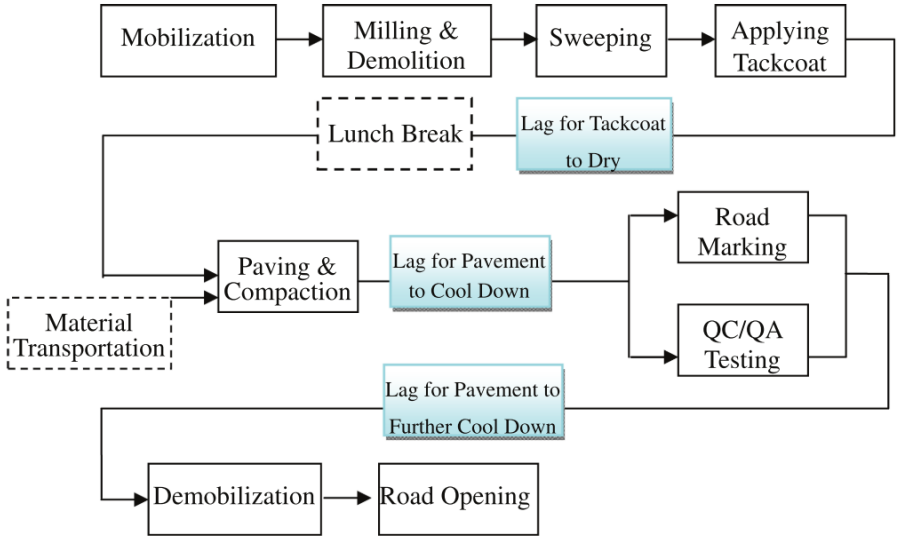

Figure 1.1 Typical activities of an asphalt road rehabilitation work (after Wang et al. (2014b))

Shortening this cooling time would allow airport authorities to quickly open the new pavement to traffic, hence reducing airport closure, and/or allow contractors to place the maximum amount of hot mix asphalt (HMA) each night. Thus, rapid asphalt pavement construction could increase the pavement target length to be paved each night, hence shortening the overall contract. This thesis aims to investigate strategies for early-opening-to-traffic asphalt pavement by reducing the cooling time of newly paved asphalt sections without adversely affecting the performance of constructed pavement. Three different strategies for a reduced cooling period were investigated in this thesis: (1) Defining and selecting the warmest asphalt temperature at opening to traffic commensurate with adequate performance and safe operations, (2) Reducing the cooling time by using warm-mix-asphalt (WMA), and (3) Decreasing the pavement temperature by spraying water onto the new asphalt.

Selecting an appropriate traffic-opening temperature of newly laid asphalt repairs would minimize the lag time and, thus, potentially shorten the runway closure and/or improve the construction productivity due to the extension of the work period. At the same time, it would prevent the development of costly premature damage of new asphalt. In this case, rutting failure

and interface shear failure are the two most likely distress types due to vehicle trafficking at high temperature. Some premature failure cases of newly laid asphalt overlay have been reported (Hachiya et al. 1997, Tashman et al. 2008, Tsubokawa et al. 2007, Horak et al. 2009, Cook et al. 2016). Excessive asphalt rutting was observed in Tribhuvan (KTM) International Airport, Nepal (Nepal 2014) immediately after the new asphalt was opened to traffic at 60°C during runway resurfacing works in the summer period. Likewise, a slippage failure in the runway of Halim Perdana Kusuma (HLP) airport, Jakarta, Indonesia was observed at the layer interface of a new asphalt overlay on July 28, 2017 (Figure 1.2). There are many factors and issues that can lead to the asphalt rutting and delamination. It is still questionable whether the early rutting and delamination failures presented in this study correlate with the decision of opening-to-traffic asphalt temperature. Currently, the allowable opening-to-traffic asphalt temperature, as set by many agencies, varied from 35 to 70°C. There is a lack of agreement between the acceptable opening-to-traffic asphalt temperature that doesn't appear to have a strong theoretical basis.

Figure 1.2 Slippage failure of newly laid asphalt overlay at HLP runway (Courtesy of Indonesia Airport Authority)

Warm-mix asphalt (WMA) is commonly mixed and compacted 15°C to 30°C below that of conventional hot mix asphalt (HMA) (West et al. 2014a). The lower production temperature of WMA is expected to give an advantage of a lower cooling time of newly laid asphalt overlay before it can be opened to traffic. In airport pavements, the use of WMA technology has been few until now. The technology has more popularly been adopted for road pavement projects than airfield pavements. However, extensive research has been carried out in the last few years on the use of WMA for airside applications. Although considerable researches have been done, there

has been no detailed investigation into the advantages of the use of WMA on shortening the construction time of pavement. It is still questionable whether the temperature at opening to traffic for WMA should be the same as HMA or not. At the same temperature of opening to traffic, the WMA could be more susceptible to rutting due to reduced bituminous binder viscosity.

Cooling of new asphalt by air-assisted water sprays has been practiced by some contractors in tropical countries to reduce prolonged cooling time. However, there is no specific research regarding the effect of water spraying onto a new asphalt surface. It is hypothesized that water spraying would adversely affect the durability and moisture susceptibility of newly paved asphalt. Asphalt Institute (2009) do not advise the spraying water on freshly laid hot mix asphalt (HMA) for speeding up the asphalt mat cooling time in order to open the pavement to traffic earlier. There is a concern that water spray would lead to reduced asphalt resistance to moisture damage and stripping. Furthermore, it is stated that spraying water on the freshly laid asphalt would not be effective, it would only cool the asphalt surface temporarily, while the temperature inside the asphalt would not be affected much.

1.2. Aim and objectives

The primary aim of this research is to investigate the permissible asphalt overlay temperature at opening to traffic, the possibility of the use of warm mix asphalt (WMA) for pavement rehabilitation (as it has advantages of reduced cooling time), and the use of water spraying for early opening to traffic. The research objectives are intended to answer the following questions:

1. What is the acceptable temperature for the opening of asphalt overlay to traffic?
2. To what extent do the binder type, tack coat type and asphalt mixtures influence the decision of opening asphalt overlay to traffic?
3. How does the rutting and interface shear bond performance of WMA compare to HMA as the overlay to an airport pavement? Is there any notable difference in WMA performance, as compared to HMA, that could have significant practical effect on the permissible temperature at opening to traffic?
4. To what extent does the use of water spraying on newly laid asphalt effect reduce the asphalt cooling time so as to permit earlier trafficking? How does the spray water cooling

on freshly laid asphalt affect the pavement performance, in term of durability and moisture susceptibility?

5. How do the traffic-opening temperature, warm mix asphalt (lower initial laying temperature) and forced water spray cooling affect the required cooling time before trafficking and/or airport closure time and construction efficiency?

1.3. Research Outcomes

The outcomes are expected to:

- Determine strategies for reducing cooling time of new asphalt to allow rapid opening of remediated pavements to traffic
- Determine the permissible temperature at opening newly laid asphalt overlay for trafficking
- Determine the feasibility of WMA application in airfield pavement rehabilitation for rapid trafficability in off-peak pavement rehabilitation/construction
- Determine the feasibility of the use of water spraying for HMA early opening to traffic
- Suggest material and mixture design considerations, including suitable bituminous binder type, optimum overlay thickness and tack coat formulations, for airfield pavement rehabilitation and maintenance

1.4. Scope of Research

This study focuses on airfield pavement resurfacing/rehabilitation in typical tropical countries or in sub-tropical countries during hot summer periods. The direct outcomes and conclusions of this research might not be suitable or beneficial for less-crowded airports and/or project locales where the ambient temperature is relatively low. The results of the research, however, are indirectly applicable to all asphalt overlay projects, subject to the following constraints:

- Where the asphalt overlay is an asphalt of similar mix design and is designed to a similar specification. In this research, dense graded asphalt concrete of 12 mm (0.5 in.) maximum aggregate size following Federal Aviation Administration (FAA) Item P-401 (FAA 2014) was used. The FAA's pavement specifications have been broadly adopted by many airports around the world.
- Where similar asphalt overlay materials and construction, including asphalt lift thickness of 60-70mm, are adopted. Unmodified and polymer modified binder were used in this research

for asphalt mixture overlay as well as tack coat material. Two different WMA technologies (organic and chemical) were also investigated as compared to HMA. Furthermore, two different existing surfaces: new HMA and PCC concrete surface were adopted for the investigation of interface shear bond strength of the newly laid asphalt overlay.

- Where the project location is in a typical busy hub-airport (or 24-hour operation) with limited closure time available for pavement repair/rehabilitation. This study focused only on airport resurfacing projects during night-time periods, with a time window of six to seven hours allocated per night. Other construction techniques such as partial runway closure and weekend airport closure for typical less-crowded airports were not studied.

1.5. Significance of Research

The primary significance of this study is to propose rapid opening of newly laid asphalt to traffic which results in satisfactorily constructed pavements during airfield pavement repair/rehabilitation. This includes the selection of the warmest permissible asphalt temperature at opening to traffic, the prevention of premature damage to newly paved asphalt repairs, the use warm mix asphalt (WMA) for airfield pavement rehabilitation and the application of water spray onto freshly paved asphalt to speed the opening to traffic.

Indirect significance includes the application of this research for the improvement of airfield pavement resurfacing/overlay work. These outcomes include:

- Understanding of the cooling response of newly laid asphalt pavement for the purpose of traffic opening decision
- Understanding of the performance of newly laid asphalt pavement, in term of rutting and interface shear bond performance, during its early life at the opening to traffic
- Determination of sufficiency of deformation resistance and interface bond strength achieved in the field under typical asphalt resurfacing techniques
- Understanding of constituent materials and characteristics that have led to rutting failure and delamination occurring during traffic-opening in airport case studies
- Estimating the heat transfer coefficient of spray water cooling onto the newly laid asphalt

1.6. Overview of Research

This thesis consists of eight chapters with each chapter detailing one phase of the research work.

Chapter 2 places the research within the context of the existing literature, including common practice of airfield pavement rehabilitation, asphalt pavement performance at high temperature and existing knowledge on warm mix asphalt (WMA). Chapter 3 briefly explains the research methodology, materials used in this research and laboratory test program and its purposes for the study. Chapter 4 reports the development of a simplified one-dimensional (1D) heat transfer model to predict the cooling response of a newly paved asphalt pavement and see the effect of proposed strategies in reducing asphalt cooling time.

Chapter 5 investigates the permissible temperature of newly paved asphalt at opening to traffic through a series of laboratory tests and analyses with regard to the rutting and interface shear failure potential of newly paved asphalt at high temperature and high load. Chapter 6 studies the rutting and interface shear bond performance of WMA compared to HMA as the overlay of an airport pavement and assesses the benefit of WMA as an airfield resurfacing material.

Chapter 7 presents the results and analysis of the investigation of the use of sprayed water cooling onto the newly laid asphalt layer as compared to a natural cooling technique. The preliminary investigation of the possible detrimental effect of water spraying onto the hot mat in terms of asphalt durability and stripping is also presented. Finally, Chapter 8 contains the conclusions, applications and recommendations for airport authorities and practitioners as well as for future studies.

2. Literature Review

2.1. Overview

A literature review on common practice in airfield pavement rehabilitation is reported in this chapter. Asphalt performance, in terms of rutting and shear failure of asphalt at elevated temperature are also considered. Furthermore, this chapter presents a literature review on Warm Mix Asphalt (WMA) technologies, spray water cooling, and previous studies on asphalt cooling prediction. It then presents existing literature and gaps in the knowledge that must be addressed to achieve the research aim.

2.2. Common Practice of off-peak Airfield Pavement Construction

Airfield pavements should be constantly maintained and, if necessary, upgraded without interfering in their regular use. However, growth in traffic volumes in commercial airports has led authorities to adopt certain strategies for pavement repair /overlay work without generating serious interruption to airport operations. Deferring construction of asphalt overlays to off-peak hours, when traffic demand is typically at its lowest levels, is commonly selected by many airport authorities (Bryden and Mace 2002). The off-peak work periods are usually at night for busy airports (Wills 1982). For a less-crowded airport, weekend airport closure is often adopted (Sander Ty and Roesler Jeffery 2006). Another method such as partial runway closure has been applied at Manchester Airport (2003) and Changi Airport, Singapore (2007), where the runway length available for take-off and landing is temporarily shortened for pavement repair work. However, partial runway closure for pavement rehabilitation leads to high-risk construction activity and is often avoided by airport authorities. Several accidents between aircraft and construction vehicle and serious runway excursion incidents, such as Chiang Kai-Shek (CKS) Airport, Taiwan in 2000 (Council 2002), and Montreal Airport, Canada in 2000 (Transportation Safety Board of Canada 2000) were reported during aircraft take-off caused by flight crew's lack

of alertness to the temporary runway closure during runway pavement maintenance (SKYbrary 2019).

Among the aforementioned strategies, night-time construction is often selected as the most feasible construction period for pavement repair work. This trend has been observed at many airports around the world. Tribhuvan International Airport, Nepal (Nepal 2014), Fukuoka Airport, Japan (Hachiya et al. 2008), Ronald Reagan Washington National Airport (DCA), The USA (Frank et al. 2013) and Brisbane airport, Australia (Figure 2.1) are several examples of airports with night-time closure for airside rehabilitation and normal airport operations during the day. Table 2.1 shows information on airfield pavement rehabilitation during off-peak times at airports around the world.

Figure 2.1 Runway overlay project at Brisbane Airport during night construction. Source: Brisbane Airport Corporation (BAC)

Night-time rehabilitation works offer considerable benefits: reduced impact to public travel, lowered pollution impact on the local environment, extended working time window, improved efficiency of material delivery, and reduced working temperatures in the period of hot summer (Holguín-Veras et al. 2003). On the other hand, night-time construction presents negative shortcomings: reduced construction quality due to insufficient lighting (reduced visibility), increased risk for the workers' safety, higher construction cost, and construction noise (Hinze and Carlisle 1990, Hancher and Taylor 2001).

2.3. Current Specification on Temperature of Asphalt Overlay for Opening to Traffic

Several Authorities regulate the permissible asphalt temperature of opening to traffic on the regulations and guidance. In airfield pavement area, according to the FAA standard (FAA 2006), aircraft traffic is not allowed on the newly laid asphalt until it cools to 150°F (65.5°C) or lower.

The purpose of this limit mentioned in the document is to prevent rutting. In Japan, Civil Aviation Bureau (2001) in Hachiya et al. (2008) limits the asphalt pavement temperature to 50^0C before it receives any traffic.

Table 2.1 Several airports in the world with rehabilitation during the off-peak period

No	Site	Year	Scope of works	Total Asphalt production (tonnes)	Available construction time per night
1	London Heathrow Airports (LHR), UK	2013	Milling and replacing 50mm runway surface with asphalt, runway lighting, and paint marking in the Southern Runway (50m x 3,658m) [b]	21,000 [b]	7.5 hours [a] (10.30 pm – 6 am)
2	Brisbane Airports (BNE), Australia	2013	275,000 m^2 asphalt overlay at BNE runway 01-19, and new installation of ground lighting [c]	18,000 [c]	6 hours [c] (11 pm – 5 am)
3	Hobart Airports (HBA), Australia	2011	Removing 800 ton of old asphalt, replaced with 1000 ton of new asphalt to resurface 45m x 2,250m runway [d]	20,000 [d]	8 hours [d] (10pm – 6am)
4	Melbourne Airports (MEL), Australia	2010-2011	Removing the existing surface layer, replacing with a new surface layer, installing new airfield lighting system, and new line markings [e]	47,000 [e]	6 hours [e] (12pm – 6am)
5	Adelaide Airports (ADL), Australia	2010	Runway resurfacing and airfield lighting installation [f]	45,000 [f]	7 hours [f] (11pm – 6am)
6	Fukuoka Airport (FUK), Japan [g]	2000 – 2002	Removing the 150mm-layer and resurfacing the layer of runway with 60m wide and 2,800m long [g]	-	7 hours [g] (11pm – 6am)
7	Dublin Airport (DUB), Ireland	2017	Planning off the existing surface, new airfield lighting and resurfacing the Runway 10/28 [i]	100,000[i]	6 hours [h] (11 pm – 5 am)
8	Ronald Reagan Washington National Airport (DCA), USA	2011	75mm mill and replacement of pavement at Runway 1-19 and reinstalling new lighting system	-	7 hours [j] (11pm – 6am)
9	Jakarta Airports (CGK), Indonesia	2017-now	19 cm asphalt overlay for the main runway (60m x 3,600m), replacing runway lighting, paint marking, and runway shoulder overlay	94,500	7 hours (11pm – 6am)

[a] Hacan (2013), [b] Express (22 Agt 2013), [c] Brisbane-Airport Australia (25 November 2013), [d] Hobart-Airport (Feb 20, 2012), [e] Fulton Hogan (2011), [f] McArdle (July 2010), [g] Hachiya et al. (2008), [h] Dublin-Airport (14 November 2016), [i] Dublin Airport (Nov 22, 2017), [j] Frank et al. (2013)

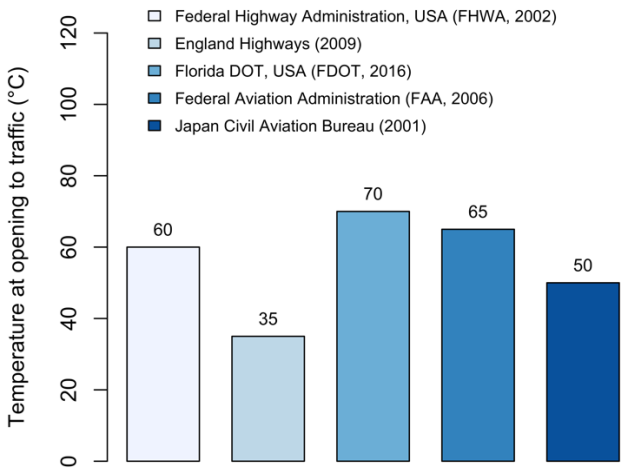

Figure 2.2. Summary of regulations of traffic-opening temperature.

Few studies (Table 2.2) described the asphalt temperature limit for opening to traffic during airfield rehabilitation projects. Hachiya et al. (2008) reported the temperature limit of 50°C before opening the runway to aircraft operation during overlay work at Fukuoka airport. In Germany, 85°C (185°F) was set as the maximum temperature at the beginning of aircraft operations during runway rehabilitation work at Frankfurt Airport (Aho et al. 2016). In general, the decision for opening to traffic resulted in good performance of asphalt pavement. However, in Tribhuvan Airport (KTM), Nepal, runway resurfacing works during summer time showed excessive asphalt rutting. The main cause of this excessive rutting was not reported. Nepal (2014) suggested that this could correlate with the decision of traffic-opening temperature.

Table 2.2 Allowable temperature for opening to traffic in several airport projects

No.	Site	Construction Year	Type of asphalt	Temperature allowed for opening to traffic	Asphalt performance
1	Tribhuvan Airport (KTM), Nepal [a]	2011	HMA	Max. 60°C	Excessive asphalt rutting occurred
2	Fukuoka Airport (FUK), Japan [b]	2002	WMA	Max. 50°C	Initial rutting was less than 2 mm
3	Frankfurt Airport (FRA), Germany [c]	2005	WMA	Max. 85°C	pavement showed acceptable performance

Sources: [a] Nepal (2014), [b] Hachiya et al. (2008), [c] Aho et al. (2016)

It is necessary to investigate the permissible temperature of newly laid asphalt for trafficking. The purpose of the asphalt temperature of opening to traffic requirement is to prevent freshly placed asphalt from being damaged, in term of rutting, shoving and delamination, by vehicular/aircraft loads when it is still hot and tender. For the airfield rehabilitation purpose, the

asphalt temperature of opening to traffic could help the airport authority to make a better decision regarding the airport closure to improve construction effectiveness, avoid air traffic delay and ensure safety. Although the allowable opening-to-traffic asphalt temperature has been set and recommended by many agencies, there is a lack of agreement between the acceptable opening-to-traffic asphalt temperature that doesn't appear to have a strong theoretical basis.

2.4. Asphalt Pavement Performance at High Temperature

To determine the allowable opening-to-traffic asphalt temperature for airport pavements, it is necessary to understand the performance of bituminous mixture at high temperature during its early life. In this case, high-temperature deformation (rutting) and interface shear failure are the two most likely distress types due to high-pressure load and braking operations of aircraft at elevated temperature. In the following section, the performances of bituminous binder and mixture against rutting and interface shear failure at high temperature are reviewed.

2.4.1. Bituminous Binder Performance

Bitumen is a residual output of the refining of crude oil in the petroleum industry. Bitumen is a binder, like cement and other water-soluble binding agents, but it has very different characteristics (Thom 2013). While cement binder produces a rigid material, bitumen acts as a plastic-like elastic solid at low temperatures and/or under fast-moving loads and remains a viscous liquid at high in-service temperatures and/or under slow-moving loads (Taylor and Airey 2015). Bitumen has been widely used in pavement engineering because it is a strong binder, remarkably waterproof, readily adhesive and a long-lasting material (Asphalt Institute 2001).

It is well known that the mechanical response of asphalt pavement is highly influenced by the properties of the bituminous binder (Moreno-Navarro et al. 2017). The bitumen contribution to bituminous mixture performance is crucial (Motamed et al. 2012). Moreover, similar bituminous mixtures with different kinds of bitumen, or identical bituminous binders can perform distinctively due to complexity in the chemical composition of the bitumen (Harnsberger et al. 2011). This finding indicates that an agreement with specifications cannot be used as an indicator to determine acceptable pavement field performance (White 2015a). Regardless of the evidence that the bitumen is not the primary constituent of asphalt pavement materials (about 5% of the total mass), the bituminous binder is the most expensive component,

representing approximately 60% of the cost of raw material (Dalhat and Al-Abdul Wahhab 2017) and approximately 20% of the total construction cost (Anderson et al. 2000).

2.4.1.1. Modified Bituminous Binder

Traditionally, unmodified or neat bituminous binders have tended to provide adequate and satisfactory performances for many years for road and airfield pavement applications (Airey 2004). However, during the last three decades, as the required mechanical properties of bituminous mixtures have increased over time, modification has been made to increase the pavement service life, and reduce the amount and severity of bituminous mixture distress, such as high-temperature rutting, fatigue cracking at low temperature and stripping/asphalt moisture damage (Read et al. 2003). Chemical agents, polymer, rubber and fibre are often used as modifiers to the original bitumen. The most common modifying agents are polymers. Polymer modified bitumen (PMB) is often chosen because it has superior mechanical properties and it is readily available at a reasonable cost. Currently, the polymers most popularly used are elastomers – styrene butadiene styrene (SBS) (Airey 2004), plastomers – ethyl vinyl acetate (EVA) and Polyethylene (Cuciniello et al. 2018), reclaimed tyre rubbers and reactive polymers (Read et al. 2003).

Polymer modifiers work by the following two approaches: (1) stiffening the bituminous binder (McNally 2011) so it will increase the load spreading ability of the pavement, improve the strength of the pavement structure and extend the predicted pavement service life (Rodrigues and Hanumanthgari 2015), and (2) improving the elastic component of the bituminous binder, thereby increasing the flexibility of the asphalt to prevent cracking at low temperature and improve pavement fatigue life (Wen et al. 2011).

Polymer modified bitumen (PMB) has been used successfully at locations of high load pressure, such as airports, intersections of busy roads, heavy vehicle stations, and racing circuits (King et al. 1999). In airfield pavements, PMBs have been adopted since the 2000s to overcome horizontal deformation, early ageing groove closure and stripping issues (White 2017b). With the increase of tyre pressures and wheel loads of large commercial aircraft, traffic volume and new axle designs, the adoption of PMB in airfield pavements is expected to overcome the reduced reliability of pavements with unmodified bituminous binder (Wang et al. 2018b).

2.4.1.2. Rheology of Bituminous Binders

Bituminous materials are characterized as time, temperature and stress-dependent materials and thus categorized as viscoelastic (Anderson et al. 1994). The idealized elastic, viscous, and viscoelastic responses to applied creep stress are displayed in Figure 2.3. A constant (or creep) load is applied to a bituminous material at t_0 and the load is released at t_1. As seen in Figure 2.3b, the elastic component of the material will instantly deform to a constant strain and instantaneously recover to its original shape when the load is released. On the other hand, a viscous Newtonian component of the material, as seen in Figure 2.3c, will flow at a constant rate under a creep load, and will maintain this deformation rate until the load is released; at which point there is no additional deformation or recovery.

As a combination of elastic and viscous responses, a viscoelastic response of bitumen undergoes an instant deformation under a creep load, followed by a gradual time-dependent deformation, as displayed in Figure 2.3d. When the load is released, the delayed elastic deformation part is gradually recovered, but not as rapidly as pure elastic deformation. Furthermore, the viscous deformation part instantly discontinues, but the deformation is not fully recovered. Hence, in creep loading, a viscoelastic material experiences only a partial recovery of the deformation.

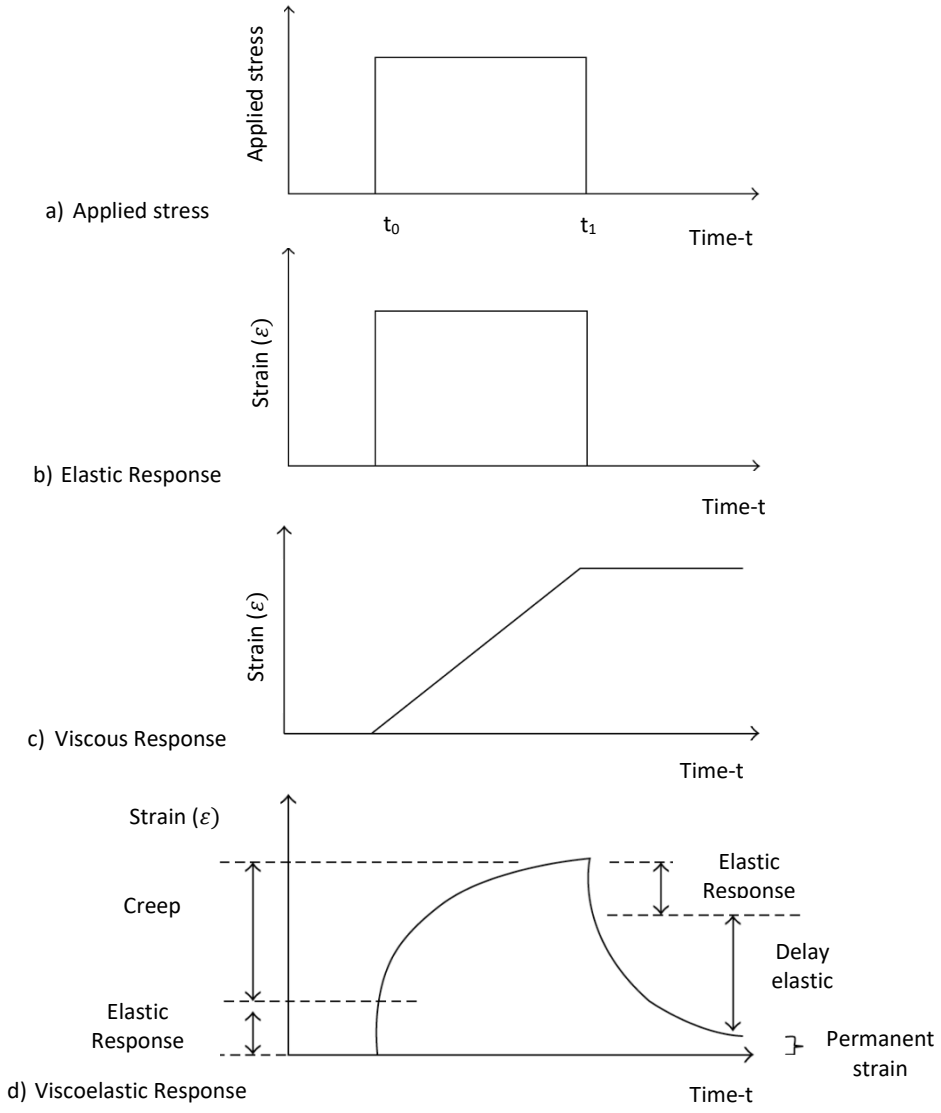

Figure 2.3 Typical response of elastic, viscous, and viscoelastic components of bituminous materials under creep stress loading, reproduced from Anderson et al. (1994)

Viscoelastic materials can be linear or nonlinear. The above-mentioned assumption applied to a linear response. Under high strains or stresses and temperature, it is well known that bituminous binders display non-linear behaviour (Delgadillo et al. 2012). In a non-linear state, the strain and strain rate are not proportional to the applied stress. However, a non-linear response is very difficult to determine in the laboratory and to model in real-life engineering problems (Anderson et al. 1994). Hence, the linear viscoelastic approach has been more commonly used to model bituminous materials.

2.4.1.3. Bituminous Binder Properties and Grading System

The performance of a bituminous mixture is highly depended on its bituminous binder properties (Elnasri et al. 2019). Bituminous binder governs the mechanical characteristics of bituminous pavements throughout their service life (Moreno-Navarro et al. 2017). Therefore, it is crucial to understand the behaviour of bituminous binders. For this reason, extensive efforts have been directed towards providing a bituminous laboratory testing and grading system according to their physical characteristics that could predict bitumen and mixture performance under the traffic and climatic conditions where they are used (Soleymani et al. 2004, Tsai et al. 2005). In this section, various testing and gradings of bituminous binder are reviewed.

a. Penetration Grade

The adoption of the penetration test for grading the consistency of bituminous binder comes from the late 19th century (Bowen 1889). The penetration test measures the penetration of a needle under a standard load of 100 grams into a bituminous binder sample at 25°C and for a duration of 5 seconds (BSI 2015a). It is expressed in one-tenths of a millimetre.

Its basic assumption is that the deeper the needle penetrates, the less viscous the bituminous binder. The test is only based on an empirical approach and does not reflect on any fundamental engineering properties such as viscosity (Roberts et al. 1991). In addition, temperature susceptibility of the bitumen (the change in bitumen rheology with temperature) cannot be measured by a single test at 25°C as normally required by the standard (Zaniewski and Pumphrey 2004). The penetration grade is also not applicable for soft binders, which would require longer needles and deeper cups (Read et al. 2003).

b. Viscosity Grade

As an improvement to the penetration grading approach, in the early 1960s, the viscosity grading system was introduced. Penetration at 25°C, the dynamic viscosity at 60°C, and the kinematic viscosity at 135°C were included in the specification. Following viscosity grading, aged residue grading was developed, where ageing was also considered and the rolling thin film oven test (RTFOT) was performed to determine relative ageing of bitumen (Kar and Nagabhushana 2019). The test can be performed on unaged (AC) or aged (AR) bituminous binder. The grading system is classified in Poises (cm-g-s = dyne-second/cm^2) or Poises divided by 100 (centiPoises); for example, AC-20 binder has a target viscosity of 2000 poises at a temperature of 60 °C.

Whereas the viscosity specification was an improved system compared to the penetration grading system, there were still some limitations when adopted into a specification. The main issue with the viscosity grading system is that the viscosity is determined in a steady-state condition, and the test can only be performed at a temperature when the bitumen is in its Newtonian fluid state (D'Angelo 2009a). The system also worked properly for typical unmodified binders, but when binder modification came into use, the viscosity grading system started to unravel. The system also failed to evaluate the low-temperature performance and long-term ageing of bituminous binder (Zaniewski and Pumphrey 2004).

c. *Superpave Performance Grading (PG)*

More recently, bituminous binder grading has shifted from using empirical approaches to a more fundamental rheological approach to address the drawbacks of the previous bitumen grading systems (Elnasri et al. 2019). The Strategic Highway Research Program (SHRP) carried out a five-year, $150 million research program from October 1987 through March 1993, to improve performance of bituminous materials for pavements. During the research program, the Superpave (Superior Performing Asphalt Pavements) mix design and the Performance Graded (PG) bituminous binder tests and grading were developed (Zaniewski and Pumphrey 2004).

The PG system measures the bitumen's resistance to permanent deformation at high temperature. It also measures fatigue cracking and brittle fracture resistance of bituminous binder at an intermediate temperature and low temperature, respectively. However, for airport pavements, the rutting performance at high temperature is the most important parameter to assess bituminous binders under the PG binder system. Low-temperature performance is of low importance for airport asphalt. Airport pavements are generally stiff and thick and traffic repetitions are low compared to road pavements. Fatigue cracking and brittle fracture of asphalt is not a common failure mode for airfield asphalt (White 2015a). Thus, this section will only discuss the high-temperature grading of PG specifications.

The original parameter used for high-temperature PG grading of bituminous binders was the Dynamic Shear Rheometer (DSR) derived $|G^*|/\sin \delta$. In the DSR test application, the bitumen sample is confined between two parallel cylindrical plates, one of the plates is fixed and the other plate is being oscillated, as displayed in Figure 2.4.

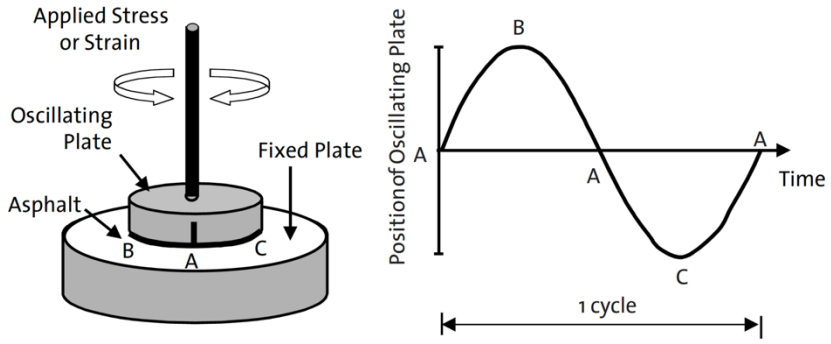

Figure 2.4 DSR principle (Uddin 2003)

The test computes a complex shear modulus (G*) and phase angle (δ) of a bituminous binder specimen (D'Andrea et al. 2014). The G* is defined as the total resistance of binder to deform when oscillated, while the phase angle (δ), is the delay between the applied shear stress and the resulting shear strain (Saowapark et al. 2019). G*/sinδ is used as a rutting indicator for binder at high temperature (Oner et al. 2017). Higher values of G*/sinδ suggest better binder resistance to rutting.

The |G*|/sin δ parameter is generally a better measure of a bitumen's rutting resistance. However, many studies suggest that it is unable to assess the response due to the addition of modifiers or distinguish between successful and unsuccessful modifiers (Elnasri et al. 2019). The |G*|/sin δ parameter is measured at low levels of stress and strain during oscillatory loading in the DSR (Santagata et al. 2013). In the case of polymer modified binder, the polymer network is never truly triggered under this very low level of stress and strain in the DSR test. It is suggested that the test captures only the hardening effects of the polymer, but not the delayed elastic effects of the polymer (FHWA 2011). A number of studies have consistently demonstrated the inadequacy of the |G*|/sin δ criterion for bitumen performance characterisation (Santagata et al. 2015). Delgadillo et al. (2006) provide a detailed review and analysis of |G*|/sin δ, its problems and inappropriateness for polymer modified binders, including the type of load used in the testing (cyclic reversible loading) and the low number of load cycles. Delgadillo et al. (2006) clearly showed that the rutting performance of bituminous mixture can be remarkably different for bituminous binders of similar |G*|/sin δ and the same PG grade, which obviously indicates the inaccuracy of the |G*|/sin δ parameters when modified bituminous binders are used.

d. Multiple Stress Creep Recovery (MSCR) Test

A new parameter was proposed by Bahia et al. (2001) in 2001 under the NCHRP 9-10 project to replace $|G^*|/\sin\delta$ as the Superpave high-temperature PG criterion, called the viscous component of the creep stiffness, G_v, derived from a repeated creep constant load test (Santagata et al. 2015). This was then improved and became known as a multiple creep recovery test (MSCR) (D'angelo et al. 2007), which originally incorporated 11 stress levels but was later decreased to two stress levels (0.1 and 3.2 kPa). The test is carried out using a DSR, which is the same equipment as that already used for Superpave PG specifications (Behnood et al. 2016).

The MSCR is quick and seemingly simple to perform in the laboratory (Soenen et al. 2013) and takes only approximately 15 minutes to finish (DuBois et al. 2014). Many studies (D'Angelo 2009b, Wasage et al. 2011, Zhang et al. 2015, Salim et al. 2019, Syed et al. 2019) have tried to validate the MSCR results against accelerated pavement testing, in situ trial performance or simulative tests in the laboratory, and have suggested that the MSCR test correlates better to permanent deformation compared with $|G^*|/\sin\delta$. It is also suggested that the test can predict the response of neat bituminous binders and those with modifiers equally well.

The output parameters of the test are the non-recoverable creep compliance (J_{nr}) and MSCR %recovery. The J_{nr} measures the proportion of permanent strain of a binder specimen after periodic stressing and relaxation, relative to the amount of applied stress. The MSCR %recovery is a proportion describing how much the binder sample returns to its initial shape after being repeatedly loaded and unloaded. The standard MSCR test is commonly performed at two stress levels (0.1 and 3.2 kPa). For each stress level, ten cycles of loading and unloading are applied, as shown in Figure 2.5. The two stress levels are proposed to assess the linear and non-linear behaviours (Wasage et al. 2011). The difference between the two provides an indication of stress sensitivity (Soenen et al. 2013). The load is applied for 1s, the specimen is then allowed a 9s rest period between each load application, see Figure 2.5.

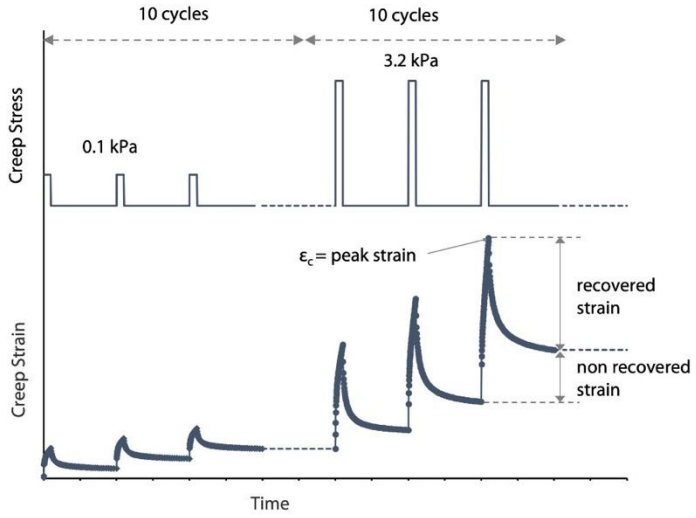

Figure 2.5 Typical MSCR test results at a stress level of 0.1 kPa and 3.2 kPa with 10 cycles creep and recovery

2.4.2. Rutting/ Permanent Deformation of Bituminous Mixtures

Rutting is often described as the accumulation of small amounts of non-recoverable (plastic) strain as a consequence of repeated trafficking of the pavement (Kandhal and Cooley 2003). The rutting is caused by the effect of cyclic traffic load on the pavement in which the materials are not purely elastic (Uzan 2004). Rutting is generally observed as a small trench or depression on the asphalt pavement surface (Qiao et al. 2014). It primarily occurs in hot environmental conditions and can often be observed in slow traffic loading areas, particularly at intersections of busy roads or in bus stop lanes (Chaturabong and Bahia 2017). In asphalt pavements, rutting is a dominant type of surface deterioration (Rushing et al. 2014, Rushing and Little 2014). Airfield pavements are susceptible to rutting, because of heavy aircraft wheel loads, high-pressure aircraft tyres, and high lateral load during aircraft ground manoeuvring. Aircraft tyres support much greater wheel loads with higher tyre pressure in contrast to truck tyres (Wang and Al-Qadi 2011).

Rutting in pavements can generally be divided into two types: structural and non-structural rutting, as displayed in Figure 2.6. The first type of rutting, structural rutting also known as subgrade rutting, occurs when the subgrade exhibits strain due to traffic loading. It is usually caused by overstressed subgrade material (perhaps because the pavement is too thin). The second type of rutting, which is the interest of this study, is asphalt mix rutting – a form of non-structural rutting. This type of rutting is related to the mixture properties, design and

compaction. It commonly occurs as a result of insufficient compaction of the asphalt mix layer and improper asphalt mix design.

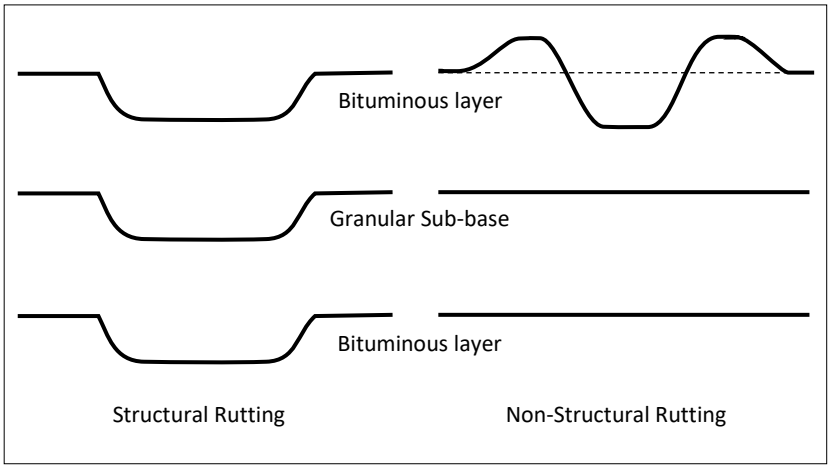

Figure 2.6 Structural and Non-Structural Rutting (Gibb 1996)

2.4.2.1. Mechanism of Rutting

Two main mechanisms contributing to rutting are densification (volume reduction) and shear plastic flow (lateral movement) (Collop et al. 1995). Researchers have observed that if a bituminous layer has been properly compacted, further permanent deformation due to the densification mechanism is unlikely to occur, and rutting is only caused by shear flow (Eisenmann and Hilmer 1987).

Hofstra and Klopm (1972) evaluated the densities of bituminous mixture specimens under wheel-path depressions and outside areas of the wheel path, and they found that both series of specimens had identical densities. It was concluded that the rutting/accumulated deformation was due to mixture shear flow, not densification (see Figure 2.7). Typically, rutting appears as longitudinal depressions under the wheel paths and sometimes occurs together with upward heaving outside the wheel paths.

2.4.2.2. Factors Affecting Permanent Deformation of Bituminous Mixtures

In general, the permanent deformation of bituminous mixtures is considered to be related to a number of factors such as the properties of aggregate (texture, grading, size and shape of aggregate), binder properties (stiffness and proportion of binder), mixture type and properties (air voids and voids in mineral aggregate, and compaction level), environmental conditions (temperatures and moisture levels), the construction process (i.e., roller compaction), traffic

loading (configurations and volumes) or a combination of these factors (Sousa et al. 1991, AASHTO 2008).

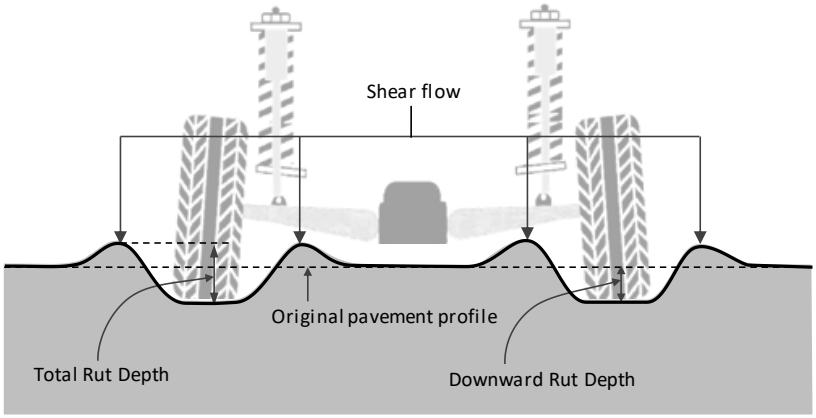

Figure 2.7 Asphalt rutting illustration, reproduced from Miljković and Radenberg (2011)

Aggregates. The aggregate properties which are crucial in promoting asphalt mix rutting resistance are: aggregate gradation, surface texture, shape and size (Taherkhani 2006). Brown and Snaith (1974) found that aggregate gradation has an important role in rutting resistance. At the test temperature of 30°C, it was found that asphalt with dense-grading exhibited better rutting resistance than that with gap-graded aggregates. However, it was also suggested that gap-graded aggregates with a high-volume portion of coarse aggregates, such as stone mastic asphalt (SMA) with coarse aggregate content greater than 70%, can exhibit a superior rutting resistance due to better contact between the aggregate particles. In terms of aggregate texture and shape, angular crushed stones and rough surface textured rocks are more favourable compared to smooth surface rocks and rounded natural stones. Button et al. (1990) investigated the effect of aggregate shape on bituminous mixture permanent deformation by replacing the crushed aggregate particles with natural (uncrushed) particles. The unconfined static and cyclic compression tests were performed on the bituminous mixture. The results suggested that asphalt mix rutting susceptibility increases when naturally rounded shape aggregate particles are used.

Bituminous Binder. It is well recognised that the rutting resistance of bituminous mixtures is significantly related to the properties of bituminous binders (Subhy 2017). The bituminous binder stiffness and its thermal susceptibility have a high correlation with the rutting potential of bituminous mixtures (Vargas-Nordcbeck 2012, Brovelli et al. 2015). Improvements have been continuously developed to enhance the rheological features of bituminous binder and rutting resistance of bituminous mixture. One of the techniques that successfully improves bituminous

mixture resistance to rutting is the addition of polymers (Airey 2004, Qi et al. 1995).

Bituminous Mixture Properties. The volumetric arrangement of bituminous mixtures determined using parameters such as bitumen content, air void content and voids in mineral aggregates (VMA) are substantial factors affecting asphalt mix rutting resistance (Gibb 1996). In general, asphalt mixes with excessive binder content have been found to have lower rutting resistance (Li et al. 2009, Walubita et al. 2012). In the case of the effect of air void content, no consistent trend has been generally accepted. For instance, Lee et al. (2007) reported that an increase in rut depths was observed with air void content increase (ranges between 2% and 11%), whereas Brown and Cross (1991) found that the rut depth increased significantly when a very low content of air void was achieved (i.e., 3% or lower). This is likely that the bitumen almost entirely fills the void between the aggregate particles, thus, this can cause the shear flow development when subjected to heavy traffic. Furthermore, another important factor is VMA. It is referred to as the inter-granular void space between aggregate particles (Asphalt Institute 2015) and used to specify the available space for the bituminous binder to sufficiently cover each aggregate particle (Dhir et al. 2017). In general, reducing the VMA leads to improved contact between aggregate particles, which is favourable to promote mix rutting resistance. However, if the VMA is too low, the bituminous mixtures could be susceptible to rutting due to inadequacy of bitumen film thickness (Gibb 1996).

Test & Field Conditions. In terms of test and field conditions, the temperature is the most crucial factor affecting the rutting resistance of bituminous mixtures. Hofstra and Klopm (1972) compared the rut depth of bituminous mixtures in laboratory wheel tracking tests at temperatures ranging from 20 to 60°C. It was observed that, over this range of temperatures, the rutting increased by two to three times. Tarefder et al. (2003) investigated several factors that affect the rutting potential of asphalt pavement by using the statistical approach. The results showed that the most significant contribution to rutting is binder grade and the second most significant factor is temperature. Another research by Chen and Xu (2009) showed that, from laboratory testing using a Rubber Wheeled Loaded Tester, the temperature had a critical effect on the rut-performance of HMA. These findings suggest that temperature is a crucial factor affecting the rutting resistance of bituminous mixtures.

Furthermore, Sousa et al. (1991) outlined the factors affecting the rutting performance of bituminous mixtures, as displayed in Table 2.3.

Table 2.3 Factors affecting bituminous mixtures resistance to rutting (Sousa et al. 1991)

	Factor	Transition in factor	Effect of factor transition on mixes resistance to rutting
Aggregate	Surface texture	Smooth to rough	Increase
	Gradation	Gap to continuous	Increase
	Shape	Rounded to Angular	Increase
	Size	Increase in maximum size	Increase
Bituminous Binder	Stiffness	Increase	Increase
Bituminous Mixture	Bitumen content	Decrease	Increase
	Air void content	Decrease	Increase
	VMA	Decrease	Increase
Loading & Environmental Conditions	Temperature	Decrease	Increase
	State of stress/load	Decrease in tyre contact stress	Increase
	Load cycles	Decrease	Increase
	Presence of water	Wet to dry	Increase

2.4.2.3. Laboratory Testing to Evaluate Rutting

Over the years, various testing programs have been used to predict the rutting in asphalt pavement structures. The tests can generally be classified as fundamental tests, and simulative tests (Wheel tracking test) (Zhang et al. 2005). Three of most commonly used fundamental tests are the static uniaxial compression test (Flow time test), repeated/cyclic uniaxial compression test (Flow Number test), and repeated load triaxial (dynamic modulus) (Witczak 2005). Whereas, the common machines used for simulative tests include the Hamburg Wheel Tracking Device (HWTD), the French Pavement Rut Tester and Asphalt Pavement Analyzer (APA), (Williams and Prowell 1999). In this section, each test is discussed in turn.

a. Static creep (SC) uniaxial and triaxial test

The static creep (SC) test is the simplest test for assessing the permanent deformation response of viscoelastic materials such as bituminous mixtures. The test was developed by the Shell company to evaluate bituminous materials in the early seventies (Hills, 1973). During the test, a constant load is applied on cylindrical bituminous mix samples, which are commonly 100 mm in diameter and 50 mm in height and can be obtained from field cores or laboratory compacted mixes (Witczak et al. 2002).

The static creep (SC) test should be carried out at a relatively low-stress level; otherwise, premature failure could occur (Zhang et al. 2005). The test can be performed in unconfined, confined or triaxial conditions. The unconfined creep test is considered low-cost and simple

to perform. However, due to its unconfined and static type load conditions, which do not precisely simulate real field conditions, the capability of this test to predict bituminous performance is still unclear (Roberts et al. 1991). The typical stress levels range from 70 to 200 kPa for the unconfined SC test. To closely simulate the actual field conditions, the confined or triaxial static creep test is usually performed by applying a confining pressure of 130 kPa and a vertical pressure of 800 kPa or higher. Confinement is also required for some mixes to prevent the specimen's early failure from occurring (Brown and Foo 1994).

The output of the static creep (SC) test is commonly reported as cumulative permanent deformation as a function of time during creep loading (Rushing et al. 2014). For a large range of materials, such as polymers and metals, cumulative plastic deformation has been classified into three stages: primary, secondary, and tertiary (Oeser et al. 2008, Al-Qadi et al. 2009), as displayed in Figure 2.8 for a typical creep data set. The primary stage is defined as the portion in which strain rate decreases transiently due to toughening or repacking of the aggregate skeleton in the mixture, whereas, in the secondary stage, the strain is at a steady-state rate with time. The strain rate starts to accelerate in the tertiary stage due to instability and this is usually associated with a reduction of air voids to near-zero and a decrease of aggregate dilation (Witczak et al. 2002).

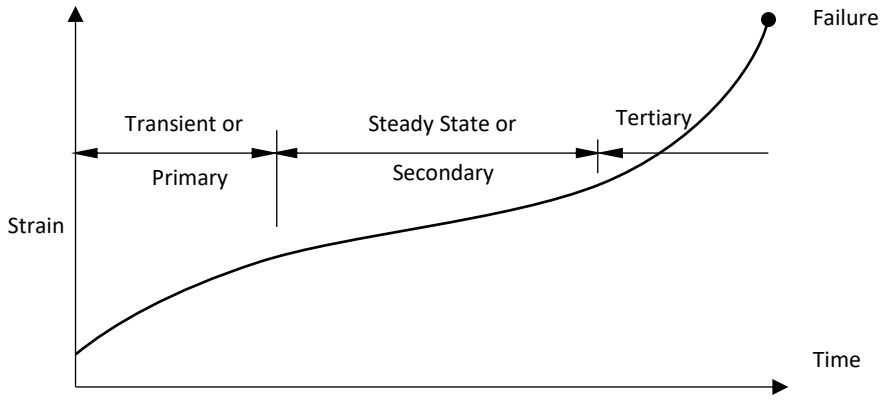

Figure 2.8 Stage of creep (Little et al. 1993)

The key parameter usually derived from SC tests is the Flow time (FT). The FT is defined as the time at which a minimal rate of strain change occurs during the SC tests. The FT usually takes place close to the starting point of the secondary flow stage previously defined. The FT can be measured by fitting the creep data set to a Francken model (Equation (2.1)) and

acquiring the second derivative (Equation (2.2)) to identify the time at which minimal rate of strain change occurs (Rushing and Little 2014).

$$\varepsilon_p = At^B + C(e^{Dt} - 1) \tag{2.1}$$

$$\frac{d^2\varepsilon_p}{dt^2} = AB(B-1)t^{B-2} + CD^2e^{Dt} \tag{2.2}$$

where ε_p is the permanent strain (%); t is the time; and A, B, C and D are fitting coefficients. Another typical approach for analysing SC test data set is by plotting the strain data versus time on a logarithmic scale. Since the secondary stage of the creep curve commonly has a nearly straight line, these data can be fitted to Equation (2.3) for a model creep behaviour of materials under a constant load, where ε_p is the accumulated axial strain, t is the creep time, and a and m are the intercept and slope, respectively (Rushing et al. 2014). Figure 2.9 displays a creep test data set plotted on a logarithmic scale. In general, reducing the value of a and m will increase the permanent deformation resistance (Leahy 1989).

$$\varepsilon_p = a \times t^m \tag{2.3}$$

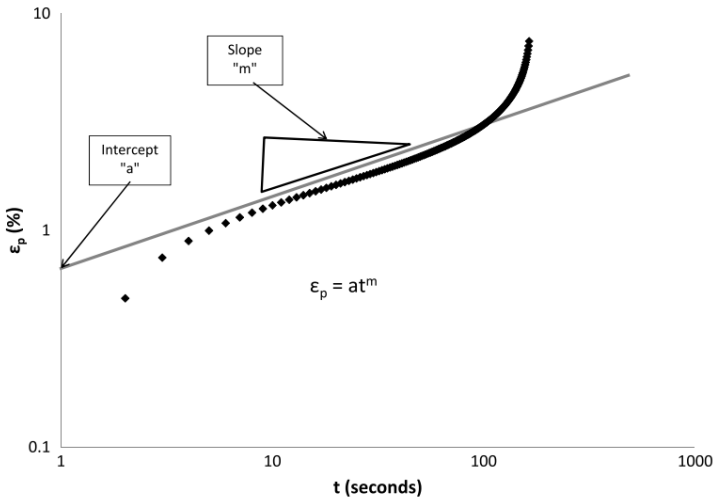

Figure 2.9 Slope and intercept determination (Rushing and Little 2014)

b. Cyclic uniaxial and triaxial test

As an improvement to the SC test, the cyclic creep test also known as repeated load axial test (RLAT) or cyclic compression test was developed to evaluate the behaviour of bituminous materials under a real field loading conditions. During the test, the load is

repeatedly applied on cylindrical samples for a specific loading period followed by an unloading period. The test is continued for typically 10,000 load cycles or until the sample fails (Witczak et al. 2002). The output of the cyclic compression test is usually reported as cumulative permanent deformation as a function of the number of applied axial load cycles (Rushing and Little 2014).

The cyclic creep test can be performed in three different loading modes: triaxial cyclic, uniaxial cyclic with confinement and unconfined uniaxial cyclic, see Figure 2.10. For the triaxial test, a sample 100 mm in diameter and 150 mm in height is suggested by NCHRP Report 547 (Witczak 2005) (Figure 2.10a), whereas for the uniaxial test, the recommended specimen dimension is 150-mm diameter by 60-mm height for the test with confinement (within the specimen) (BSI 2016) (Figure 2.10b), and 100-mm diameter by 60-mm height for the test without confinement (BSI 1996), see Figure 2.10c. All three tests are conducted using a friction reduction system (usually using graphite powder) between the specimen and loading plates to ensure the samples are subject to shear rather than flexural rupture (White 2015a).

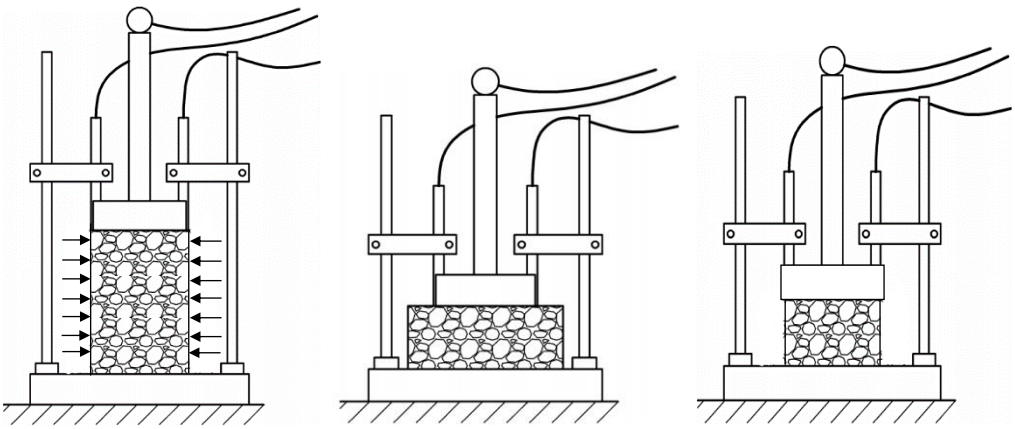

(a) Triaxial cyclic (b) Uniaxial cyclic with confinement (c) Uniaxial cyclic

Figure 2.10 Triaxial and uniaxial cyclic compression test

Several studies (Brown and Foo 1994, Hofko and Blab 2014, Gayathri et al. 2016, Santagata et al. 2017) have underlined the importance of the triaxial cyclic creep test since it is more representative to simulate in situ loading conditions. The importance of the confinement was most obvious in tests performed at high temperature and under high load pressure (Gayathri et al. 2016). Although the cyclic test in an unconfined condition does not closely

simulate traffic loading, Gibb (1996) suggested that it provides more reliable permanent deformation response than static creep (SC) test when used to compare different bituminous mixtures.

Various loading and unloading pulse durations during cyclic creep tests have been adopted to represent the field loading condition. A loading period of 0.1 s followed by a rest time of 0.9 s is recommended by NCHRP 465 report (Witczak et al. 2002), whereas in the UK, 1s of loading time followed by 1s of unloading time is commonly adopted (BSI 2016). The test loading can also be performed in various waveforms/loading pattern such as square form, triangular, sinusoidal and trapezoidal. In general, a sinusoidal (haversine) waveform (Witczak et al. 2002, Zhou et al. 2002) and square (block) wave (BSI 2016) have been recommended by many standards as the optimal loading waveforms in a cyclic creep test. The loading specifications of these standards are displayed in Table 2.4.

Table 2.4 Cyclic creep loading forms in different standards (Mansourkhaki and Sarkar 2015)

Standard	Reference	Loading options			
		Waveform	Loading time (ms)	Recovery time (ms)	Deviator stress (kPa)
BS EN 12697-25:2016	BSI (2016)	Block pulse	1000	1000	100
		Haversine pulse	200	1500	Max. 350 Min. 80
British: DD 226:1996	BSI (2012b)	Block pulse	1000	1000	100
NCHRP 465	Witczak et al. (2002)	Haversine pulse	100	900	69
VESYS manual	Zhou and Scullion (2004)	Haversine pulse	100	900	138

A typical test result for loading and unloading phases for block pulse waveform is shown in Figure 2.11. In a typical loading-unloading cycle it can be seen that at time t_o, when the load is applied, a strain, ε_o, consisting of elastic (ε_e) and plastic (ε_p) parts, occurs immediately. As the sample exhibits creep, viscoelastic (ε_{ve}) and viscoplastic (ε_{vp}) strains are then developed. When the load is released, the elastic strain disappears; at the same time, a portion of the viscoelastic strain (ε_{ve}) is partially restored. At the end of the rest time, the residual strain contains the permanent (ε_p) and viscoplastic (ε_{vp}) strain parts that have not been recovered.

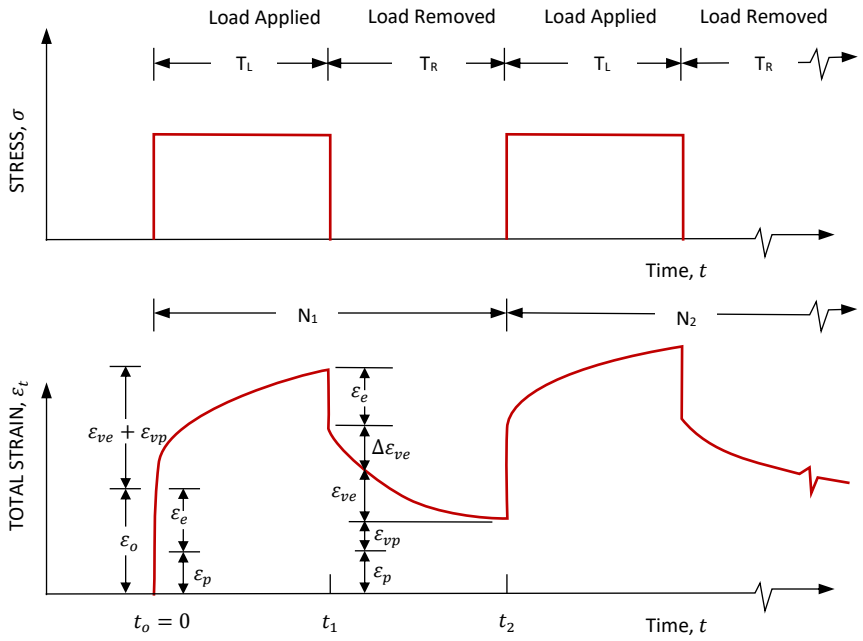

Figure 2.11 Typical cyclic creep stress and strain relationships (Perl et al. 1983)

The key parameter commonly extracted from cyclic creep tests is the Flow number (FN). The flow number (FN) is defined as the number of cycles at which a minimal rate of strain change occurs during the cyclic load test. Similar to FT, the FN can be determined by fitting the test data series to the Francken model (Equation (2.1)) and taking the second derivative (Equation (2.2)) to define the number of cycles at which the change in strain rate turns from negative to positive.

The results of cyclic creep stress can also be mathematically modelled using the power-law model in Equation (2.4), where ε_p is the accumulated irrecoverable strain, N is the number of load cycles, and a and b are the regression coefficients. As discussed before, the secondary stage of the strain curve commonly displays a linear section on a logarithmic scale.

$$\varepsilon_p = a \times N^b \tag{2.4}$$

c. *Dynamic Modulus (DM) Test*

Test Procedure – The dynamic modulus (DM) test, also known as the complex modulus test (AASHTO TP62-03), is conducted by applying sinusoidal axial loads on cylindrical samples and measuring the corresponding vertical strain (Figure 2.12). DM tests are different from cyclic creep tests in terms of loading cycles and frequencies. While in cyclic creep tests, the

same load level is applied for several thousand cycles at the same frequency, in DM tests, a load is applied over a wide range of frequencies for 30 to 45 seconds (Brown et al. 2001). The stress levels are applied to result in 50–150 microstrain. The samples are commonly tested at five different temperatures and six frequencies, hence a total of thirty combinations of temperature and loading frequency have to be carried out. The recommended testing temperatures are –10°C, 4°C, 21°C, 37°C, and 54°C, while the recommended testing frequencies are 25, 10, 5, 1, 0.5, and 0.1 Hz (Rushing et al. 2014). The test can be performed with and without confinement. The typical sample dimension is 100mm in diameter and 150mm in height. The vertical deformations of the samples are measured through two linear variable differential transformers (LVDTs) located vertically on opposite sides of the samples (Figure 2.12). Moreover, a study by Huang et al. (2017) suggested that the DM test can also be performed on trapezoidal beam samples.

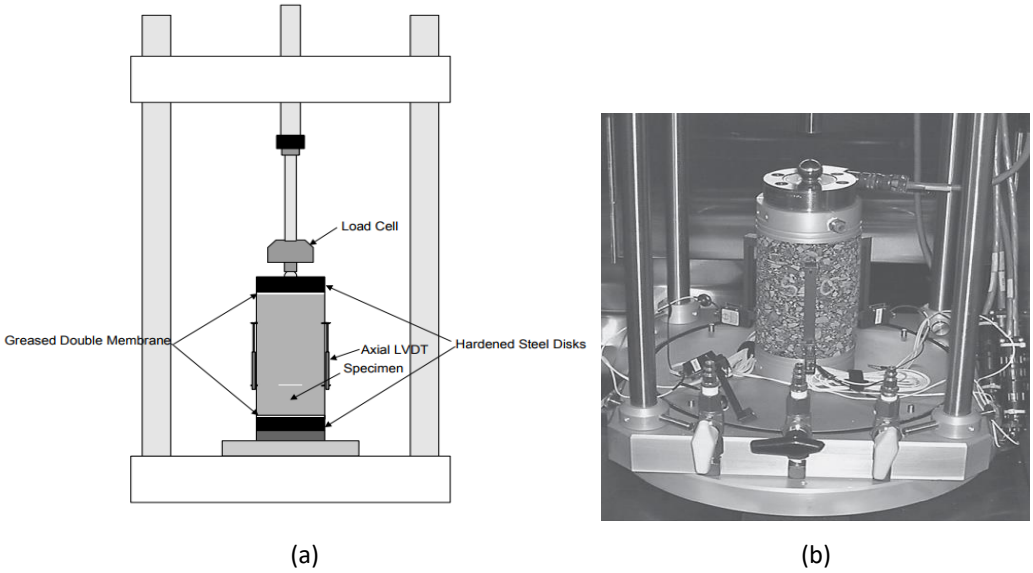

(a) (b)

Figure 2.12 Dynamic modulus test in uniaxial compression: (a) Test schematic (Dougan et al. 2003); (b) Test setup (Loulizi et al. 2006)

A bituminous mixture is a viscoelastic material that exhibits both viscous and elastic components when subjected to loading (Rahman et al. 2018). Under a DM test, stress and strain responses of pure elastic materials will be in the same phase (phase angle = 0°), whereas for pure viscous materials, a 90° phase lag will be observed. For viscoelastic materials, the behaviour is between pure elastic materials and pure viscous materials (Figure 2.13).

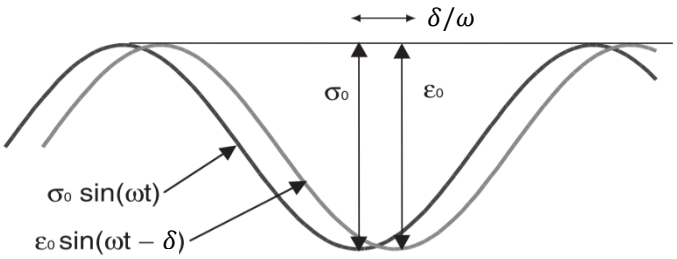

Figure 2.13 Dynamic modulus test schematic of strain-stress relationship (Zhu et al. 2011)

Upon applying the sinusoidal cyclic stress (σ), the corresponding cyclic strain (ε) can be defined as $\varepsilon = \varepsilon_0 \sin(\omega t + \delta)$, where ε_0 is the strain amplitude, ω is the angular velocity, in degrees per second ($2\pi f$), t is time, δ is the phase angle by which ε_0 lags behind σ_0, and can be expressed as $\phi = \frac{\Delta t}{t} 360^{o}$, where Δt is the time lag in seconds. The applied stress (σ) is then $\sigma = \sigma_0 \sin \omega t$, where σ_0 is the stress amplitude.

The DM test measures the specimen's stress-to-strain relationship under a continuous haversine loading. For linear viscoelastic materials, this is defined as complex dynamic modulus (E^*), as shown in Equation (2.5) below (Witczak et al. 2002):

$$E^* = \frac{\sigma}{\varepsilon} = \frac{\sigma_0 \sin(\omega t)}{\varepsilon_0 \sin(\omega t + \delta)} \tag{2.5}$$

The complex modulus consists of two components, the storage and loss modulus. The storage modulus (E') describes the stored energy and represents the elastic behaviour of the samples, while the loss modulus (E'') describes the energy dissipated in the form of mechanical work, heat generation or damage (Rowe 1996) and represents the viscous behaviour of the samples. The E' and the E'' can be mathematically expressed as follows:

$$E' = \frac{\sigma_0}{\varepsilon_0} \cos(\delta) \tag{2.6}$$

$$E'' = \frac{\sigma_0}{\varepsilon_0} \sin(\delta) \tag{2.7}$$

The complex modulus (E^*) is the sum of the E' and E'' where the E'' is multiplied with i, the imaginary unit. It can be expressed as follows:

$$E^* = E' + iE'' \tag{2.8}$$

The absolute value of the complex modulus is:

$$|E^*| = \sqrt{E'^2 + E''^2} \tag{2.9}$$

Dynamic Modulus (DM) Master Curve Development – The temperature dependency of bituminous materials can be described by the time-temperature superposition principle because bituminous materials have been historically proved as thermo rheologically simple (TRS) materials (Nguyen et al. 2009). This behaviour allows for shifting of the DM curve vertically, as well as horizontally (on time or frequency axes) to develop a single DM master curve as a function of reduced frequency or reduced time (Equation (2.10)) at a targeted reference temperature (Figure 2.14). The master curve provides for the prediction of mechanical characteristics of bituminous mixes over a large range of loading conditions (Zhao et al. 2012).

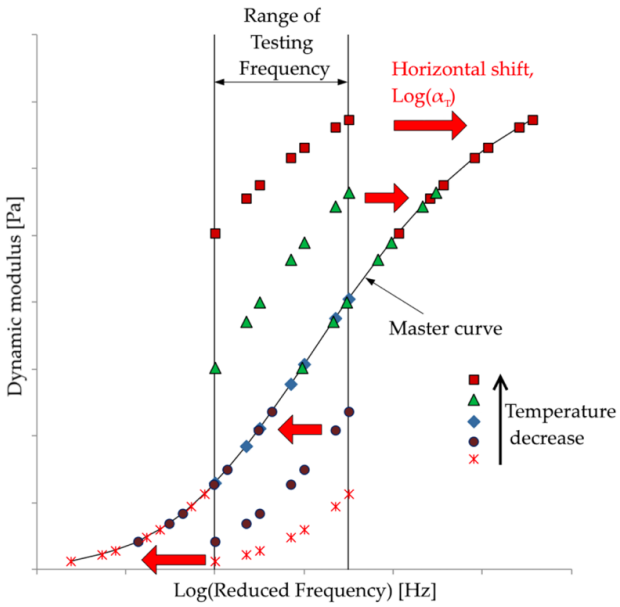

Figure 2.14 Concept of time-temperature superposition principle and master curve development (Hasheminejad et al. 2019)

The amount of horizontal shifting is determined by the time-temperature shift factor, a_T, shown in Equation (2.10). One of the functions that can be used to approximate the shift factor for given temperatures is the Williams-Landell-Ferry (WLF) function (2.11).

$$t_r = t/a_T \tag{2.10}$$

where t is the original time before shifting, for a particular temperature; t_r is the reduced time at the desired reference temperature; and a_T is the time-temperature shift factor for a particular temperature.

$$\log a_T = -\frac{C_1(T - T_s)}{C_2 + (T - T_s)} \tag{2.11}$$

where C_1 and C_2 are constants to be determined experimentally.

Typically, the DM master curve can be mathematically expressed by a sigmoidal function (Pellinen et al. 2003), shown in Equation (2.12).

$$\log|E^*| = \delta + \frac{\alpha}{1 + e^{\beta + \gamma \log t_r}} \tag{2.12}$$

where $|E^*|$ is the dynamic modulus (MPa), α, β, γ and δ are the fitting coefficients, and t_r is the reduced time (s).

Development of Phase Angle Master Curves. The same temperature-frequency shift factors for the $|E^*|$ master curve can be used to develop the phase angle (ϕ) master curve. The resulting phase angle (ϕ) master curve is expected to be a single smooth curve. To fit the phase angle (ϕ) master curve, the following expression is used:

$$\phi(t_r) = \lambda_1 + \lambda_2 \log(t_r) - \lambda_2 \frac{\pi}{2} \alpha\gamma + \frac{e^{\beta + \gamma \log t_r}}{(1 + e^{\beta + \gamma \log t_r})^2} \tag{2.13}$$

where $\phi(t_r)$ is the phase angle (in radians), α, β and γ are the fitting regression coefficients obtained by fitting the $|E^*|$ function using Equation (2.12), and λ_1 , λ_2 and λ_3 are fitting parameters.

d. Wheel tracking test

The wheel tracking test is widely adopted to simulate bituminous pavement rutting performance under conditions close to those in the field. The test has been commonly used for many years around the world because of its simplicity and reliable results. Different types of wheel tracking apparatus have been developed with various configurations and capabilities, such as the Georgia loaded wheel tester (base model for APA), French Pavement Rut Tester (FPRT), Hamburg Wheel-Tracking Device (HWTD), Asphalt Pavement Analyser (APA), Model Mobile Load Simulator (MMLS3), Nottingham pavement testing facility, etc. The test can be performed at full-scale in an Accelerated Pavement

Testing facility (APT), such as the National Airport Pavement Test Facility (NAPTF), medium scale such as in the Nottingham Pavement Test Facility (PTF), or small scale like the APA, HWDT and small size wheel tracker. The specimen can be loaded by different tyre types, including a small-scale pneumatic tyre, a metal tyre, or a solid hard rubber tyre. The selection depends on the scale of the test.

In the laboratory small-scale test, the specimen is repeatedly loaded by moving back and forth under the loaded tyre. As an illustration, a typical schematic of a laboratory wheel tracker is presented in Figure 2.15. To assess the pavement resistance to rutting, the test is usually performed to 8000 cycles when tested in the APA (Mohammad 2006) and 20000 cycles when performed in the HWTD (Aschenbrener 1995).

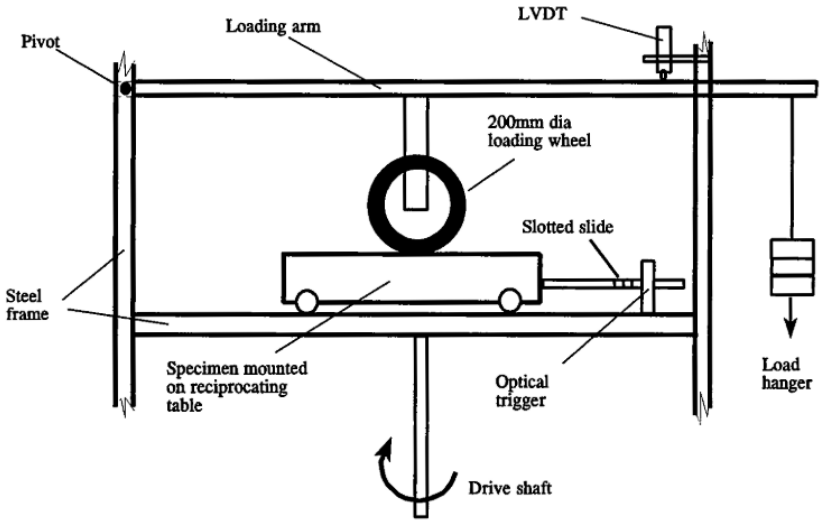

Figure 2.15 Schematic of Wheel tracking apparatus (Gibb 1996)

In the UK, the wheel-tracking test is conducted using a Cooper wheel tracker following BS EN 12697-22 (BSI 2013a). A solid hard rubber tyre with an outside diameter of 200 mm and width of 50 mm is fitted to the wheel, see Figure 2.16. The standard frequency of the moving load as specified in BS EN 12697-22 is 26.5 load cycles per 60 s and the travel length is 230 mm. A summary of the test criteria and device configurations of the small-scale wheel tracker in the UK along with other commonly used devices (APA, HWTD, and FPRT), is presented in Table 2.5. It can be seen that each device provides different features, such as testing multiple samples simultaneously, testing in a wet (immersed) condition, and simulating field-like wheel configuration.

Figure 2.16 Cooper's Wheel Tracker Machine in University of Nottingham (Al-Mosawe 2016)

Table 2.5 Wheel tracking test criteria and device configuration, reproduced from (Williams and Prowell 1999)

Parameters	**FPRT**	**APA**	**HWTD**	**Cooper's wheel tracker**
Test temperature (°C)	60	Range from 40.6 to 64	60	60
Environmental condition	Dry	Dry or submerged in water	Wet (immersed) or dry	Dry
Specimen size, mm	500 x 180 x 20-100	150mm diameter and 75mm tall (cylindrical) 300 x 125 x 75 (Slabs)	320 x 260 x 40-80	302 x 302 x 40-100
Number of samples tested at the same time	Two samples at the same time	Six samples at the same time	Six samples at the same time	Only one sample
Wheel type	Pneumatic (600 kPa)	An aluminium wheel on pressurize hose (830 kPa)	Steel	Solid rubber
Wheel size	400mm diameter, 90mm wide	Maximum hose diameter of 29mm	204mm diameter, 47mm wide	200mm diameter, 50mm wide
Load, N	5000	534	685	700
Wheel speed	1.6m/s	0.6m/s	Sinusoidal with a max. of 0.33 m/s at the centre of sample	0.23 m/s
Standard	BS EN 12697-22	AASHTO TP63	AASHTO T32	BS EN 12697-22

Rushing et al. (2014) recommended the APA to assess the rutting potential of airport bituminous materials because it provides several advantages. The test can be carried out in two hours or less and can test up to 6 samples simultaneously. The test can also be modified to achieve higher tyre pressure and it is also compatible with testing field cores obtained from the pavement layer for quality control tests. Emery and Mihaljevic (2008) suggested

that the APA test has similar features to the Cooper wheel tracker, which is widely used in the UK.

As a conclusion, there are several tests that are widely available and commonly used to evaluate the rutting potential of airport bituminous materials, including static uniaxial compression, repeated/cyclic uniaxial compression, dynamic modulus, and wheel tracking tests. Rushing et al. (2014) performed the above-mentioned four performance tests on twenty-six bituminous mixtures and found that each test was able to identify the airport bituminous mixture that showed lowest resistance to rutting. Since each test shows a similar degree of accuracy, other variables such as the cost to conduct the test, the time needed to complete the test, the simplicity of the test setup, efforts for the data analysis, and the test variability are usually used as the determining factors to select the rutting performance test (Rushing et al. 2014). In Table 2.6, a summary of the advantages and drawbacks of each of the tests is displayed.

2.4.2.4. Early Works on Asphalt Rutting Prediction

Extensive research efforts have been performed on deriving mechanistic relationships to predict rutting development since the early 1960s, (Fwa et al. 2004, Ji et al. 2016). In the earliest considerations of rutting in road design, the approaches were based on restricting the axial compressive elastic strain on the top of subgrade (Monismith 1976, Archilla and Madanat 2000). Dormon and Metcalf (1965) developed rut limiting criteria in the form of relationships between the vertical compression strain on the top of the subgrade and the number of load repetitions. The method gained popularity amongst researchers as an alternative to purely empirical design methods. Following this approach, researchers have developed more advanced rutting predictions by incorporating laboratory tests, observed field data, and the mechanistic response of bituminous materials. In this section, three methods to compute the strain at a point within the pavement structure for rutting prediction: the layer-strain method, the viscoelastic approach and the linear-viscous approach are discussed. For any of these methods, strains are computed at each point using a layered elastic analysis or a finite element analysis. Making use of the computed strain value at the centre of each layer of the pavement, multiplying by the layer thickness and summing from bottom to top, the surface rut depth then can be calculated.

Table 2.6 Summary of advantages and drawbacks of different rutting performance tests, reproduced from Zhang et al. (2005) and Rushing et al. (2014)

Test Method	Test parameters	Sample Condition	Advantages	Disadvantages
Uniaxial or triaxial static	Intercept Slope FT	100 mm diameter × 200 mm height & others	• simple to carry out • Test apparatus is uncomplicated and commonly available • Well known and has been used throughout the world • Provide more technical parameters • Likely low-cost	• Restricted testing temperature and stress levels • Does not simulate field dynamic phenomena • In triaxial mode, a triaxial chamber is required • In triaxial mode, the confinement setup adds the test complexity
Uniaxial or triaxial cyclic load	Intercept Slope FN	100 mm diameter × 200 mm height & others	• Simulates traffic and environmental conditions well, due to realistic tests temperature and load levels	• The apparatus is more complex and expensive • In triaxial mode, a triaxial chamber is required
Dynamic modulus	$\|E^*\|$	100mm in diameter and 150mm in heigh	• Master curves are available for rutting prediction • Generally unconfined	• Requires coring and sawing of specimens • Multiple days are required to complete the test • The LVDTs system is complex to set up
Asphalt Pavement Analyzer	Number of cycles to achieve 10-mm rut depth	150mm dia. and 75mm height (cylindrical) 300 x 125 x 75 (Slabs)	• Simulates realistic field loading and temperature conditions • Short test duration • 3-6 samples can be tested at the same time • Ability to test field cores • Unified specifications are available • Can test both cylindrical and beam specimens	• The apparatus is relatively expensive • The fundamental properties of materials are not measured

a. Layer-Strain Method

Many of the rutting prediction approaches established in the 1960s were based upon the Layer-Strain approach (Khanzada 2000). This approach is formulated on the use of elastic theory and the results of permanent strain derived from cyclic compression laboratory tests on bituminous materials (Hu et al. 2011). The approach was originally proposed by Heukelom and Klomp (1967). Since then, more studies have been carried out by other researchers such as Romain (1969), Barksdale (1972), Morris and Haas (1972), Monismith (1973), and McLean and Monismith (1974) for different pavement materials, including soil subgrade, unbound granular materials, and bituminous materials. The basic concept of this approach is that it assumes the permanent strain ε_p is proportional to the elastic strain

portion of material response and number of load cycles. This constitutive approach is assumed to be applicable for any type of material and at any point and location within the pavement structure.

The permanent deformation behaviour of different materials is determined from the results of laboratory tests for loading condition, test temperature, stress level, moisture, mixture volume, and other factors that are predicted to take place in the field. Since the permanent deformation properties are known and provided, elastic theory is then adopted to calculate the predicted stress state within the pavement structure. By dividing each pavement layer or sub-layer into suitable thicknesses Δz_i and calculating the average stress state in each pavement layer, the total rut depth (RD) or permanent deformation, may be found by adding up the permanent strain at the mid-thickness of each pavement layer and multiplying the strain by its layer thickness, by using the following equation:

$$RD = \sum_{i=1}^{N} (\varepsilon_p)_i \, \Delta z_i \tag{2.14}$$

where RD is the total rut depth, N is the number of layers or sub-layer, $(\varepsilon_p)_i$ is the permanent strain at the centre of layer-i, and Δz_i is the thickness of layer-i.

Many researchers have tried to develop rutting models as the correlation of load cycles, plastic strain and resilient strain based on regression analysis of laboratory tests and observed field data. Leahy (1989) developed a model based on uniaxial repeated load tests on over 250 bituminous mixture samples. The correlations including test temperature, some volumetric properties of mixes (i.e., VMA, air voids content) and bituminous binder viscosity were incorporated into the model. Leahy's rutting model was further improved by Kaloush (2001) by utilizing a large quantity of cyclic compression test results. Kaloush's rutting model was the initial step in the AASHTO Mechanistic-Empirical Pavement Design Guide (MEPDG) (Carvalho 2012). The model was calibrated against field data in NCHRP Project 1-37A as part of the MEPDG rutting model development (ARA Inc. ERES Division 2004). The final MEPDG HMA rutting model is displayed in the equation below:

$$\frac{\varepsilon_p}{\varepsilon_r} = k_1 \times 10^{-3.4488} \, T^{1.5606} \, N^{0.479244} \tag{2.15}$$

where, ε_p is the permanent strain, ε_r is the elastic strain, T is the temperature (F°), N is the number of load cycles and k_1 is the coefficient depth adjustment.

Since the majority of laboratory repeated load tests were performed on the unconfined condition, depth adjustment coefficient was introduced in MEPDG to adjust the calculated permanent strain as a result of confining pressure at various depths:

$$k_1 = (C_1 + C_2 \times D) \times 0.328196^D \quad (2.16)$$

$$C_1 = -0.1039h_{ac}^2 + 2.4868h_{ac} - 17.342 \quad (2.17)$$

$$C_2 = -0.0172h_{ac}^2 - 1.7331h_{ac} + 27.428 \quad (2.18)$$

where D is the depth beneath the pavement surface (in.) and h_{ac} is total bituminous layer thickness (in.). It is noted that the rutting models expressed in Equation (2.14) - (2.18) can be used for any bituminous mix types.

The layer-strain approach is considered to be a “reliable" method for rutting prediction in bituminous mixes because of its adaptability to incorporate linear or non-linear elastic theory for the analysis. However, there are a few limitations of this method such as the use of observed experimentation (empirical) instead of a purely mechanistic approach and, as such, it might not suitable for field conditions that are considerably different from those used for model calibration (Carvalho 2012). It is also suggested that the approach depends only on the elastic properties of the materials and does not directly use the viscous properties of the materials (Khanzada 2000).

b. Viscoelastic Method

The viscoelastic approach is used to describe the behaviour of polymeric materials. Mechanical behaviour of viscoelastic materials has been commonly modelled as an arrangement of a finite number of linear Hookean springs (purely elastic) and Newtonian dashpots (purely viscous) (Widyatmoko 1998). The stress-strain relationships of Hookean springs and Newtonian dashpots are expressed in Equation (2.19) and (2.20), respectively.

$$\sigma_s = E\varepsilon \quad (2.19)$$

$$\sigma_d = \eta\dot{\varepsilon} \quad (2.20)$$

where E_s is the elastic modulus of the spring, η is the viscosity of the dashpot, and ε and $\dot{\varepsilon}$ are the strain of the spring and strain rate of the dashpot, respectively. By connecting these two elements in series, a Maxwell model is constructed (Figure 2.17a), and by connecting them in parallel, a Kelvin-Voigt model is formed (Figure 2.17b). In the case of Maxwell's model, since the spring and dashpot are in series, after some mathematical operations, the creep-recovery response $\varepsilon(t)$ (subject to constant stress) and the stress relaxation function $\sigma(t)$ (subject to constant strain) can be expressed by:

$$\varepsilon(t) = \sigma_0 \left(\frac{1}{\eta} t + \frac{t}{E}\right) \tag{2.21}$$

$$\sigma(t) = \varepsilon_0 \, E e^{-t/T_0} \tag{2.22}$$

where $T_0 = \frac{\eta}{E}$ is called the relaxation time.

In the case of Kelvin-Voigt's model (Figure 2.17b), since the spring and dashpot are in parallel, after some mathematical operations, the creep-recovery response $\varepsilon(t)$ (subject to constant stress) and the stress relaxation function $\sigma(t)$ (subject to constant strain) can be expressed by:

$$\varepsilon(t) = \frac{\sigma_0}{E}\left(1 - e^{-E\frac{t}{\eta}}\right) \tag{2.23}$$

$$\sigma(t) = \frac{1}{E}(1 - e^{-t/T_0}) \tag{2.24}$$

where $T_0 = \frac{\eta}{E}$ in contrast to the Maxwell model, is called the retardation time.

Figure 2.17(a) and (b) also illustrate the creep and recovery response of the Maxwell and Kelvin-Voigt models as compared to the realistic response of bituminous mixtures. As seen in the figure, neither element could exactly model the realistic response of the bituminous mixtures. The Maxwell element could not represent the retarded viscoelastic strain, whereas the Kelvin-Voigt element could not capture unrecoverable/plastic strain of the bituminous mixtures. The accuracy of model response prediction can be improved by adding more elements in the models (Monismith et al. 1966). On the other hand, as more elements are added, the mathematical formulae become more complex. Hence, the mechanical model to predict the behaviour of bituminous materials needs to be selected by considering the accuracy of the model and simplicity of the formulation.

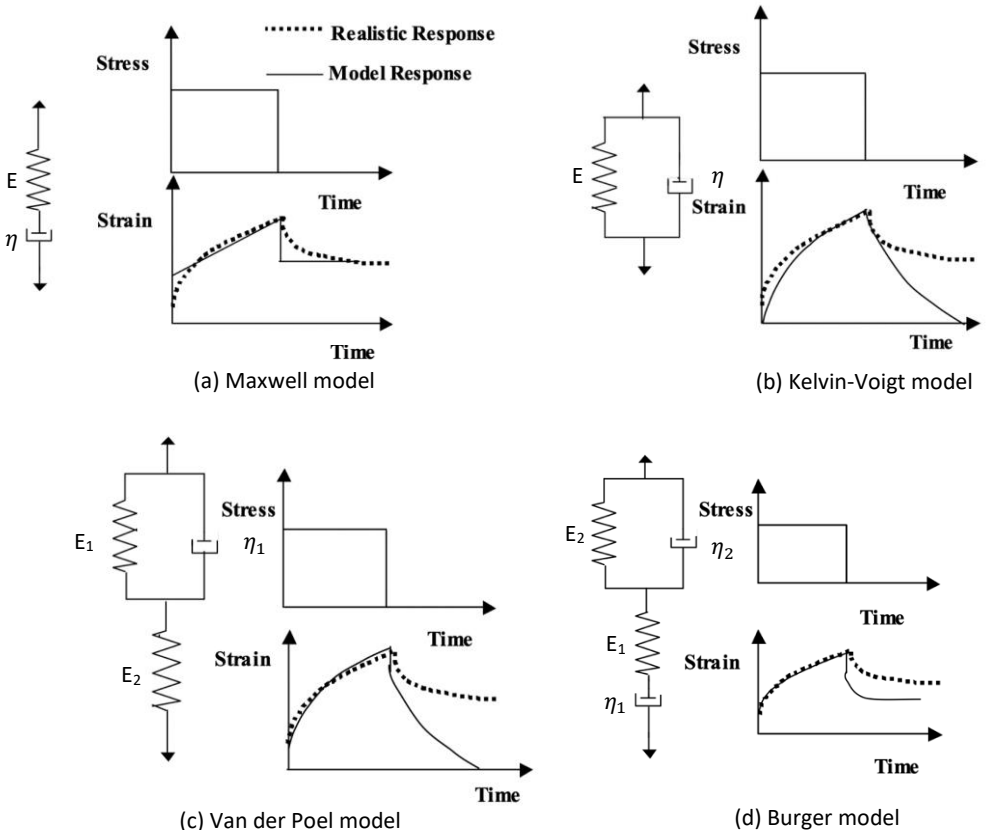

Figure 2.17 Viscoelastic models - comparison of the model and real response (Taherkhani 2006)

Figure 2.17 also presents the creep and recovery response of the Van der Poel model (Kelvin-Voigt element in series with the addition of a spring), and the Burger's model (Kelvin-Voigt element in series with the addition of a Maxwell element). As seen in the figure, the Burger's model can represent the creep-recovery response of the bituminous mixture well. To even better simulate the realistic response of bituminous materials, Generalised models, as seen in Figure 2.18, are commonly used as feasible options.

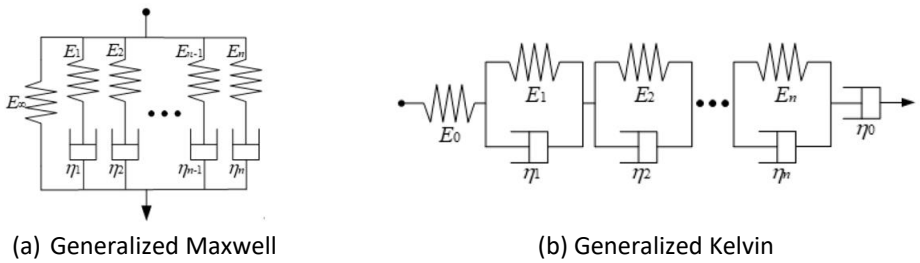

Figure 2.18 Illustration of a generalized solid model (Wang et al. 2020)

The generalized Maxwell model (Figure 2.18a) consists of a number of Maxwell units in parallel. For relaxation modulus, $E(t)$, the generalized Maxwell model can be expressed in the following equation (Tarefder and Rahman 2016):

$$E(t) = E_e + \sum_{i=1}^{n} E_i e^{-(t/\rho_i)} \tag{2.25}$$

where E_e is the equilibrium or long-time modulus, E_i are the relaxation strengths and ρ_i is relaxation time. E_e, E_i and ρ_i are Prony series parameters.

The generalized Kelvin model contains a number of Kelvin-Voigt elements in series. An additional spring – or a dashpot – is added as well. For creep compliance in a time domain $D(t)$, the generalized Kelvin model is expressed in the following form (Kim et al. 2008):

$$D(t) = D_e + \frac{1}{\eta}t + \sum_{i=1}^{n} D_i(1 - e^{-\left(\frac{t}{\tau_i}\right)}) \tag{2.26}$$

where D_e, D_i, and η are Prony series parameters; and τ_i are retardation times. Equation (2.25) and (2.26) is also known as a Prony or a Dirichlet series expansion (Elseifi et al. 2006).

The bituminous mixtures response can be characterised as linear or non-linear viscoelastic. In the linear viscoelastic (LVE) approach, the relationship of stress and strain is a function of temperature and time but not a function of stress level (Rahimzadeh 2002). LVE models have been adopted by many researchers (Thrower 1977, Monismith and Secor 1962, Huschek 1977, Huang 1967, Nunn 1986, Collop et al. 1995), to characterise bituminous mixture response, stress and strain analysis, and rutting/permanent deformation prediction because its simplicity. Meanwhile, a few attempts have been made by researchers to enhance linear viscoelasticity by incorporating non-linear effects, e.g. Sousa et al. (1993), Collop et al. (2003b) and Pei et al. (2016). However, due to its complexity and the number of constants needed for the models, nonlinear viscoelastic models have not been extensively used for characterizing bituminous material response.

The viscoelastic properties of bituminous materials are commonly obtained from the complex modulus test, the creep compliance test, and relaxation modulus test. However, direct testing of relaxation modulus is difficult to carry out and generally time- and cost-consuming, because it is difficult to control the constant strain in the laboratory tests (Zhang et al. 2018, Forough et al. 2017). Moreover, the relaxation modulus (usually as a Prony

series) is the key input for constitutive modelling or finite element application for rutting and prediction (Asifur Rahman et al. 2017). To solve this issue, researchers commonly convert the relaxation modulus from creep compliance and complex modulus test results through an interconversion procedure (Park and Schapery 1999).

Elseifi et al. (2006) employed a relaxation modulus represented by a generalized Kelvin solid model (Prony series), see Equation (2.26) to model hot mix asphalt (HMA) mixtures as viscoelastic materials in a FE (finite element) program, ABAQUS. The relaxation modulus was interconverted from the laboratory indirect creep compliance test after the measured creep compliance had been fitted to a master curve for a reference temperature. The results of the developed FE viscoelastic model were in agreement with the in-situ-measured pavement response. Elseifi et al. (2006) also compared the FE elastic model against field measurement pavement response and found that the use of elastic properties of HMA underpredicts the pavement response to traffic loading, as compared to the viscoelastic model.

Using the same technique, Wang and Al-Qadi (2011) used the relaxation modulus (represented by the generalized Maxwell, Equation (2.25)) as the viscoelastic input of airfield HMA pavement for a three-dimensional FE model in ABAQUS to evaluate the effect of non-uniform tyre pressure of aircraft on airport pavement response. The relaxation modulus parameter was derived from the laboratory complex modulus test through the interconversion procedure. The use of viscoelastic properties of HMA for FE analysis by employing relaxation modulus converted from complex modulus or creep compliance has also been carried out by other researchers: Liao (2007), Al-Qadi et al. (2008), de Araújo et al. (2010), Wang et al. (2016), (Zhang et al. 2016). In general, the use of the viscoelastic model provides better pavement response prediction as compared to the elastic model.

c. Linear-Viscous Approach

The fundamental concept of the linear-viscous approach is similar to the linear elastic approach, other than that the elastic properties (Elastic modulus) are displaced by the corresponding viscous properties (viscosity) (Thrower 1977). Nunn (1986) developed a viscous approach for rutting prediction in bituminous mixtures. The approach was based on the use of the viscous portion of the bituminous material response. The procedure of the viscous approach for rutting prediction was as follows:

- A creep test was performed to obtain the plot of mixture stiffness ($S_m(t)$) against loading times
- The bituminous binder properties (softening point and penetration) were employed to determine binder stiffness ($S_b(t)$) against loading time by using the Van der Poel Nomograph
- The two plots were then merged to make a plot of $S_m(t)$ versus $S_b(t)$
- The corresponding equivalent number of traffic loads for a given loading time was then computed at the desired temperature and used to determine the $S_m(t)$, and the axial viscosity. The axial viscosity of the bituminous mixture ($\eta_m(t)$) was calculated as follows:

$$\eta_m(t) = \frac{\sigma}{\dot{\varepsilon}} = \frac{1}{\frac{d}{dt}\left(\frac{1}{S_m(t)}\right)} \tag{2.27}$$

Nunn (1986) then employed the axial viscosity parameter with the Poisson's ratio parameter in a viscous approach to calculate the average rate of plastic strain and the accumulated rutting within the pavement structure. The rutting prediction results demonstrated an accuracy of approximately 30% in comparison to the measured rutting.

A new modified method developed as an improvement to this approach was proposed by Al-Mosawe et al. (2018). The axial pseudo viscosity of the bituminous mixture was estimated indirectly from the uniaxial cyclic test/ repeated load axial test (RLAT). The strain rate ($\dot{\varepsilon}$) for each load cycle was computed using the following formula:

$$\dot{\varepsilon} = \frac{\varepsilon_2 - \varepsilon_1}{t_2 - t_1} \tag{2.28}$$

where ε_2 and ε_1 are strains corresponding to time, t_2 and t_1 (in seconds), respectively. The nonlinear axial pseudo viscosity of the material can be obtained by dividing the test stress (σ) by the permanent strain rate ($\dot{\varepsilon}$), as shown below:

$$\eta = \frac{\sigma}{\dot{\varepsilon}} \tag{2.29}$$

The results of the modified method were compared by Al-Mosawe et al. (2018) against wheel tracking test results and field data. In general, the results provided a reasonable rutting prediction. However, to be able to predict the rutting accurately, the samples under the RLAT test should reach high deformation/tertiary stage of creep. Furthermore, the

effects of moving traffic loads were examined indirectly from the pulse loading in the cyclic compression test/ RLAT. To obtain more precise rutting estimation, the frequency of the RLAT test should be designed to be consistent with the design speed; otherwise, adjustment, such as time-temperature superposition (shift factor) should be applied. For the purpose of this research, the linear viscous approach was used for the rutting prediction. The detail of the approach for this study will be discussed later in Chapter 5.

2.4.2.5. Rutting in Airfield Pavement

Bituminous mixture is extensively used for surfacing layers of airfield pavements in many countries (Xiao et al. 2020). Unlike typical highways, the bituminous layer used in airport pavements is subjected to comparatively greater loading intensity that can lead to higher levels of rutting (Rushing et al. 2017, Darabi et al. 2019). Rutting in airfield pavement is usually observed in areas where aircraft are required to slow down for turning and braking after landing (Wensel et al. 2002). A study by Vallerga et al. (2000), reported the issue of severe rutting occurring on taxiways subject to slow traffic movements and sharp turning of B747 at San Francisco International Airport in 1995. It was determined that the bituminous binder was too soft to produce sufficient shear resistance. Excessive rutting in airfield pavements in slow-moving areas was also documented by Wensel et al. (2002) in two Canadian air force bases. The deficiency in the mix design and material performance was the main cause of the distress.

It is also expected that most of the rutting takes place during summer periods when pavement temperatures are extremely high. Nepal (2014) reported premature damage on a newly laid asphalt surface at Tribhuvan International Airport (KTM), Nepal, in 2011 during night-time resurfacing work. After opening to traffic in the morning, several pavement distresses were observed, including rutting (see Figure 2.19), causing numerous flying delays, cancellations and missed connecting flights. A number of airports have also reported excessive rutting during the hot summer season: Fukuoka Airport (FUK), Japan (Hachiya et al. 2008), San Francisco airport (SFO) (Monismith et al. 2000), Dubai airport (DXB), UAE and Kuala Lumpur Airport (KUL), Malaysia (Rodway 2009).

Figure 2.19 Premature damage and rutting after trafficking newly laid asphalt (Nepal 2014)

White (2017b), however, suggested that rutting failure is not a commonly recorded type of distress in airfield asphalt pavement surfaces. Rutting does not normally occur on General Aviation airport pavements (Moses et al. 2009), as long as materials and construction standards are followed carefully, rutting failure has rarely been found (Rodway 2016). However, where rutting does occur, free water is retained in the rut depth on the runway surface. It unfavourably affects skid resistance of airside pavement and may result in a loss in aircraft braking ability and lack of directional control during aircraft take-off and landing due to hydroplaning. This may lead to a veer off or runway-overrun accidents (Pasindu et al. 2016). Skid resistance is an important feature of airfield asphalt surfaces and is crucial for flight operations (White 2017b).

2.4.3. Interface Shear Bond of Asphalt Overlays

Pavement structures consist of several layers with different materials. The pavement strength does not depend only on the mechanical properties and stiffness of each individual layer, but it is also affected by the bond strength between layers (Collop et al. 2003a). The bond is crucial to assure that the layers act as a monolithic system to resist traffic and thermal loading (Muslich 2010). In the monolithic case, the highest tensile strain develops at the base of the asphalt structure (Figure 2.20a). In a no-bonding case, layers start to act independently (Figure 2.20b). In this instance, tensile strains occur at the bottom of each layer, whereas compression strains are observed at the top of the layer. This redistribution of strains and stresses causes overstressing areas in the pavement and reduces its performance (Shahin et al. 1986).

To ensure a monolithic structure is achieved, a light application of bituminous binder (called a “tack coat”) is commonly applied at the interface. Studies performed on interface shear bonding pavements have indicated that strong interlayer bonding is critical to distribute stress/strain into the entire pavement structure (Uzan et al. 1978, Shahin et al. 1987) and to

preserve the pavement life (Romanoschi and Metcalf 2001a, Khweir and Fordyce 2003). On the other hand, insufficient bond strength of interlayer may cause slippage between the layers, and consequently, this can generate pavement distress such as top-down cracking, slippage cracking, fatigue cracking, delamination, and even potholes (Hu and Walubita 2011).

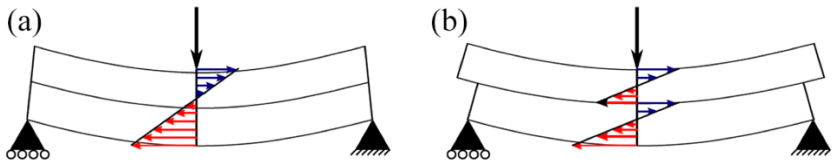

Figure 2.20. Illustration of a double-layer system under a bending moment: (a) monolithic case; (b) debonding case (Leischner et al. 2019).

Pavement failure cases associated with poor interface bonding between the newly laid asphalt overlay and the existing pavement in airfield pavement facilities have been reported by many studies (Hachiya et al. 1997, Tashman et al. 2008, Tsubokawa et al. 2007, Horak et al. 2009, Cook et al. 2016). Details regarding premature shear failures in airfield pavements are presented in section 2.3.3.5 of this Chapter.

2.4.3.1. Contributing Components in the interface bond strength

Uzan et al. (1978) stated that interface shear bond in multilayer pavement systems is affected mainly by the combination of friction or grain interlock and adhesion. Canestrari and Santagata (2005) proposed residual friction, cohesion, and dilatancy as the three components contributing to the interface shear bond. It is noted that both approaches are coherent with each other. The term 'adhesion' proposed by Uzan et al. was cited as 'cohesion' by Canestrari and Santagata (White 2016c).

The relationship of each component can be shown diagrammatically as a failure envelope in Figure 2.21. The interface friction mechanism follows a mechanical principle in which interface shear failure occurs if the shear stress at the interlayer is greater than the normal stress and the interlayer surface roughness (Leischner et al. 2019). Canestrari and Santagata (2005) indicated that the interface friction component can be directly measured by performing a test on a multi-layered sample that is manufactured individually and stacked together without any tack coat treatment, while the other two components are difficult to quantify directly from an experimental test.

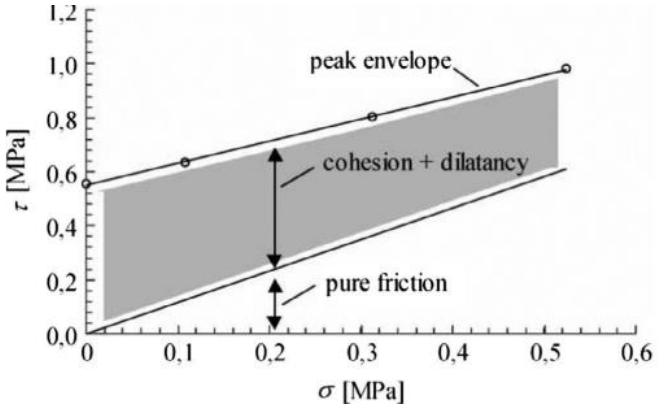

Figure 2.21 Shear failure envelope as a function of shear Strength (τ) and normal Stress (σ) (Canestrari and Santagata 2005)

Dilatancy is also an important factor contributing to the interlayer shear resistance. Dilatancy is defined as the volume change in a granular material due to disengagement of macrotexture (Collop et al. 2003a, Tozzo et al. 2016b). It is suggested that dilatancy is greatly affected by the applied normal stress. The normal stress prevents the volumetric increase (Tozzo et al. 2016a), thus when normal stress increases the dilatancy contribution to interface bond strength is likely to reduce (Canestrari et al. 2005). Dilatancy is also significantly affected by the particle shape and gradation of the material (Vangla and Latha 2015).

The cohesion component is related to the viscous behaviour of the bonding /tack coat material. Besides, the cohesion component is also highly affected by the application rate of the tack coat (in litres per meter square). Insufficient or excessive tack coat application rate could cause interface shear failure, which may contribute to reduced pavement service life (Muench and Moomaw 2008).

Several studies (Uzan et al. 1978, West et al. 2005) have shown that as the axial traffic load increases, the interface shear stress at failure also increases. The relationship between interface shear stress and normal stress has been typically assumed as a straight line using the Mohr-Coulomb envelope principles. This approach was first determined by Uzan et al. (1978) and has been widely used by many others to predict the shear failure of pavement interfaces (Mohammad et al. 2002, Canestrari et al. 2005, Canestrari and Santagata 2005, Mohammad et al. 2009, Chen and Huang 2010, Mohammad et al. 2012, D'Andrea et al. 2013a). The linear Mohr-Coulomb envelope for interface shear stress is displayed in Equation (2.30).

$$\tau_{\text{failure}} = c + \sigma \times \tan(\phi) \tag{2.30}$$

where τ_{failure} is the shear stress at failure (kPa), c is the cohesion (kPa), σ is the normal stress at failure (kPa) and ϕ is the internal friction angle (degrees).

2.4.3.2. Shear Failure Mechanism

Several researchers have tried to study the mechanism of interface shear failure in pavement layers. Muslich (2010) classified the interface shear failure into three separations modes (Figure 2.22): Mode A (shear separation), Mode B (tensile separation) and Mode C (the combination of shear and tensile). He also noted that this failure mode/ classification is only a simplification approach and does not correlate to the standard terminology used in classic fracture mechanics (Muslich 2010). Mode A is caused by traffic loading and temperature-induced interlayer shear stress (De Beer and Maina 2011). Tensile separation (mode B) is caused by the vertical tensile strain developed at the pavement interlayer induced by the tyre suction such as blisters (Bernhard et al. 2005). In a real pavement structure, however, the incidence of bond failure associated with this significant tensile strain (mode B) has rarely occurred (Raab et al. 2009) and has neither been confirmed nor reported. A combination of shear and tensile separation (Mode C) could occur at the interface beneath a surfacing layer. Raab and Partl (2004) demonstrated a simple schematic explanation of the induced-stresses in a surfacing layer by a tyre load (Figure 2.22 Mode C). When a tyre load travels on a thin bituminous layer, the transverse loads are concentrated in the surfacing course and lead to buckling of the area in front of the wheel (Muslich 2010). Moreover, the mechanism of interface shear failure is complex, thus the results and conclusions from previous studies are not universally applicable.

In general, it is suggested that interface shear failure and debonding occurs when the interlayer bond cannot resist the applied shear forces (Mohammad et al. 2009). Failure at the layer interface may occur monotonically due to a single wheel load. However, it is more expected that the failure occurs due to cyclic loading and a fatigue failure mechanism (Hakimzadeh et al. 2012). While extensive studies have been carried out on the interface shear strength (ISS) through monotonic tests, comparatively fewer studies (Romanoschi and Metcalf 2001a, Diakhaté et al. 2008, Tozzo et al. 2014a) can be found in the literature in regard to the interface shear fatigue resistance through dynamic/cyclic tests. Until now, most researchers have simply employed the fatigue analysis approaches commonly used for bituminous mixture for the interface shear bond. Yang et al. (2020), however, suggested that these approaches cannot be applied directly to determine the interlayer fatigue properties.

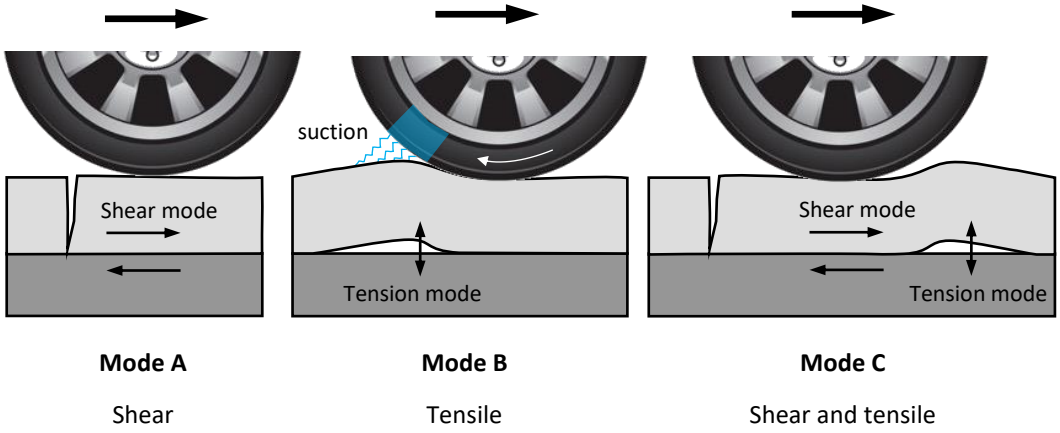

Figure 2.22 Shear bond separation mode, re-produced from Raab and Partl (2004), Muslich (2010)

2.4.3.3. Laboratory Testing of Pavement Interface Bonding

In the past few years, many studies have developed testing apparatus and methods to evaluate pavement interface shear bond (Raab et al. 2009). Regardless of these attempts, no universally recognized testing apparatus and method have been confirmed until now. The test methods and protocols are different in terms of test apparatus, stress and loading levels, specimen dimension, testing temperature and specimen preparation. Because of this wide range of variables, the results of the tests from different studies are generally not comparable (Roffe and Chaignon 2002).

In evaluating the interface shear strength, laboratory tests are more commonly used than field tests (White 2016c). A laboratory test using field core samples is expected to be more economical and reliable than a field test. The laboratory test procedures are typically categorized into four main load systems; direct shear (shear), torsional shear (torque), axial tension (tensile), and wedge splitting. The working schemes of these four interlayer shear tests are displayed schematically in Figure 2.23. A comprehensive list of interlayer shear test procedures is displayed and summarised in Table 2.7 (Mohammad et al. 2012, White 2016c, Canestrari et al. 2013).

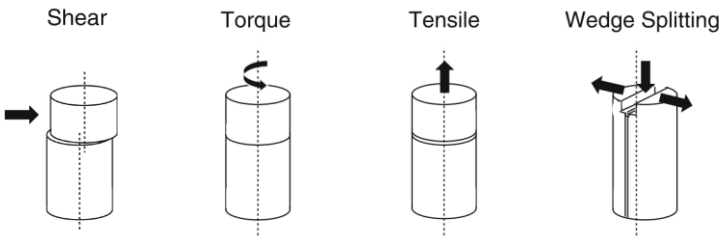

Figure 2.23 Working schemes of destructive interlayer tests after (Canestrari et al. 2013)

Table 2.7 Laboratory test of pavement interface bonding

No	Test Method	Measured Variable	Remarks	References
1	Pure direct shear test (without normal load):			
	Leutner test	(1) maximum shear force at failure (2) Corresponding maximum displacement	no normal load, the displacement rate is 50 mm/min at 21 °C	Sangiorgi et al. (2002a) Collop et al. (2003a) Kruntcheva et al. (2005) Muslich (2010)
	LPDS (Layer Parallel Direct Shear)	maximum shear force at failure	without normal confining load, A constant displacement rate (50.8 mm/min, in standard condition) is applied through a semi-circular shear yoke	Raab and Partl (2004) Canestrari et al. (2005) Santagata et al. (2008)
	Florida shear test	maximum shear force at failure	no normal load, the specimen is deformed at a constant rate of 50 mm per minute at 25 °C until failure occurs.	Sholar et al. (2002) Tashman et al. (2008)
2	Shear tests (with normal load):			
	Dynamic Shear Box (University of Nottingham)	maximum shear force at failure	With normal load	Kruntcheva et al. (2005)
	ASTRA interface shear test	maximum shear force at failure	Fixed normal load of any value. A horizontal force is applied at a constant rate of 2.5 mm per minute	Canestrari et al. (2005) Canestrari and Santagata (2005)
	Superpave Shear Testing (SST)	maximum shear force at failure	The shearing equipment is fitted into the SST chamber and the sample is loaded with a constant rate of 222.5 N/min. until it failed	Mohammad et al. (2002) Tayebali et al. (2004)
	Louisiana Interlayer Shear Strength Tester (LISST)	maximum shear force at failure, horizontal and vertical displacement	Can be fitted into any universal testing machine, normal stress of 207 kPa was also applied	Bae et al. (2010), Mohammad et al. (2012)
	Sapienza horizontal shear test (SHST) machine	maximum shear force at failure	Normal load applied in monotonic and cyclic load modes. Constant displacement rate of 1.27 mm/min at 20 °C	D'Andrea et al. (2013b) D'Andrea et al. (2013a)
	NCAT shear test	Bond shear strength	Constant displacement rate of 51 mm/min at 25 °C. Can be fitted into any universal testing machine or a Marshall apparatus	West et al. (2005)
3	Torque tests	Peak shearing torque at failure	a steel plate is clamped or glued on top of the sample. A torque force is applied until the sample failed	Buchanan and Woods (2004)
4	Tensile tests (pull-off tests)	Maximum load registered at failure	The top surface of the specimen is glued to a steel plate that is pulled off in axial direction until the interface failure	Tashman et al. (2008) BS EN 13863-2:2003 BSI (2003b)
5	Wedge splitting tests	(1) Maximum horizontal force (2) Specific fracture energy	Specimens prepared in different shapes, a double-layered specimen with opening crack was loaded until a complete separation	Tschegg et al. (1995)

Pure direct shear tests (without the addition of normal load) are the most commonly adopted tests because they are simple to perform. The most accepted pure direct shear test equipment is the Leutner test which was developed in 1979 (Canestrari et al. 2013). The main test procedure involves applying a constant shear deformation across a shear plane. During the test, the resulting applied force and the corresponding deformations are monitored. The Leutner testing frame can be fitted into a universal testing machine, see Figure 2.24a. The equipment allows for testing of specimens with a diameter of 150 mm, obtained either from field cores or samples manufactured in the laboratory. A displacement rate of 50 mm/min is normally applied as for the Marshall test (Sangiorgi et al. 2002a).

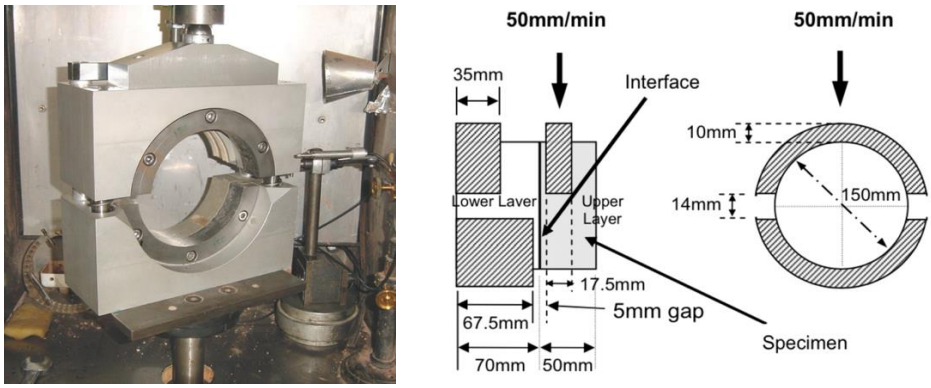

(a) Photograph (b) Cross section (c) Shear ring

Figure 2.24 Leutner shear testing frame: (a) photograph (Choi et al. 2005); (b) cross section; (c) shear ring (Collop et al. 2009)

As an improvement to the Leutner test, the Layer-Parallel Direct Shear Test (LPDS), was proposed by the Swiss Federal Laboratories for Materials Science and Technology – EMPA (Raab and Partl 2004, Raab et al. 2009) to address the Leutner test's limitations such as the absence of a gap between the shear ring and the interface and non-uniform stress generated on the interface plane. The improvement of the Leutner test by adding a gap of 5mm has also been proposed in the UK by Choi et al. (2005) and Collop et al. (2009), see Figure 2.24b and c. The output from the direct shear test is usually the maximum shear stress, obtained at failure condition known also as interface shear strength (ISS). This can be easily computed by dividing the ultimate load by the cross-sectional area at the interface (discussed later in section 2.3.3.4).

As an alternative, direct shear tests with normal (confinement) load have been adopted to highlight the relationship between the interlayer shear strength and normal stress. The direct shear test with influence of normal stress was first developed by Uzan et al. (1978) et al. Other apparatus of similar configuration to that commonly used are the ASTRA apparatus from the Polytechnic University of Marche (Figure 2.25), the Louisiana Interlayer Shear Strength Tester (LISST), the Superpave Shear testing Machine (SST), Sapienza horizontal shear test (SHST) machine and NCAT shear test. As for the pure direct shear test, the ISS parameter at different applied normal stress is the typical output of the test.

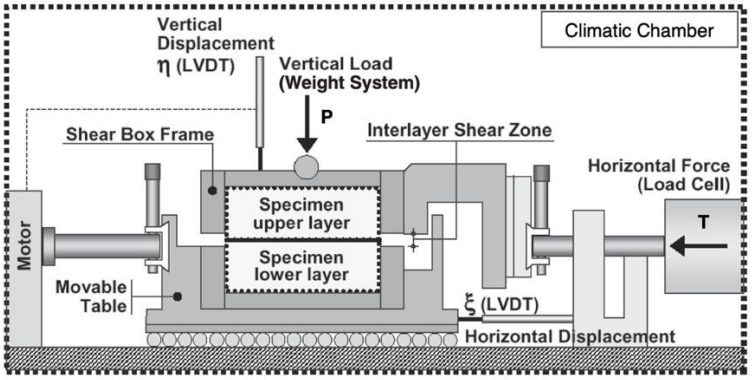

Figure 2.25 Ancona shear testing research and analysis (ASTRA) device (Canestrari et al. 2005)

Different normal/vertical loads have been adopted by researchers to closely represent the actual stress state in pavements. Canestrari et al. (2005) applied three different normal pressures; 0, 0.2, and 0.4 MPa using the ASTRA device, while 0, 0.25, and 0.70 MPa were used by Ai et al. (2017). By performing the direct shear test with a normal load, it is feasible to determine the shear failure envelope in a Mohr plane (Figure 2.26). To obtain this shear failure envelope, a regression technique is usually performed on the sample data set (ISS versus normal stress from the test). The method has been widely used to predict the shear failure of pavement interfaces (Wang et al. 2016, Ozer et al. 2013, Suddeepong et al. 2020, White 2016b). The Mohr-Coulomb theory assumes that interface failure is controlled by the envelope of a combination of interface shear stress and normal stress as presented in Equation (2.30).

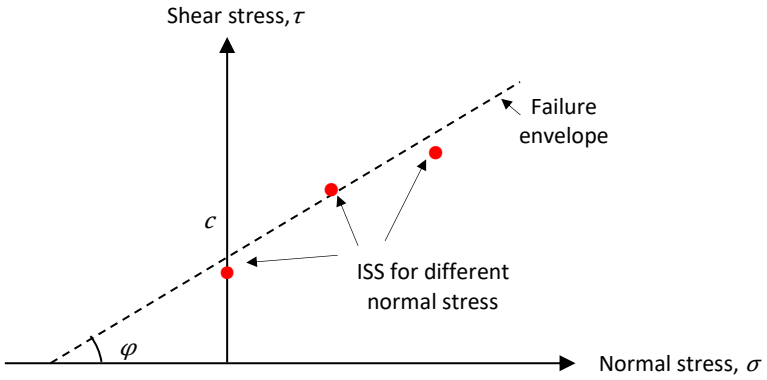

Figure 2.26 Example of ISS data set for different normal stress and development of shear failure envelope in the Mohr plain

The second type of test is the interface torque test. The test procedure consists of applying torque forces on cored specimens and measuring the ultimate torque force that causes the de-bonding of a surfacing layer from its underlying layer. In principle, a shearing torque is

applied to a steel plate glued/clamped to the top of the surfacing layer. The adoption of the torque test is, however, not frequently reported. A commonly available handheld torque wrench was originally developed in Sweden and has been adopted in the United Kingdom by the British Board of Agrement (BBA) (Figure 2.27a). The test can be performed on either 100 or 150 mm diameter core specimens (British Board Agrement 1998). Other similar torque test devices include the University of Texas-EI Paso (UTEP) (Eedula and Tandon 2006), ATacker™ device (Buchanan and Woods 2004), and Oregon Field Torque Tester (OFTT) (Mahmoud et al. 2017). Several limitations of these test have been addressed by researchers. Canestrari et al. (2013) stated that non-uniform stress occurs during the test. The torsional forces vary from zero at the centre of the specimen to the highest value at the outside of the specimen. White (2016c) suggested the difficulty of the test to limit the deformation location only at the interface. The failure could also occur within the asphalt layer because the torsional stress is applied to the top of the layer which is relatively far away (50–60 mm) from the interface. Despite these limitations, White (2016c) suggested that torque test results correlate fairly well with the results from the direct shear test.

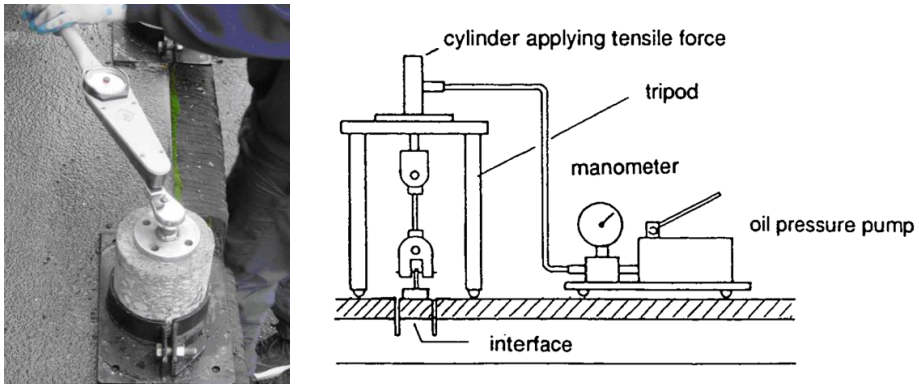

(a) (b)

Figure 2.27 Asphalt interface shear bond tests: (a) Torque test (Tashman et al. 2008), (b) Schematic of Schenck-Trebel pull-off device (Litzka et al. 1994)

The axial tension (pull-off) test evaluates the strength of adhesion between two layers. During the test, the top of the surfacing layer is glued to a metal plate that is pulled in an axial direction until the interface fails. The output of the test is the ultimate load recorded during the test. Moreover, the test only measures the adhesion level between two layers and does not involve any contribution from the grain interlock or friction and dilatancy elements (Canestrari et al. 2013, White 2016c). The direct tension test is therefore suitable for studies that focus on the evaluation of the quality of tack coat materials and the optimum application rate. The test

can be performed either in a laboratory or in-situ. Pull-off test devices commonly used include the Schenck-Trebel (Litzka et al. 1994) (Figure 2.27b), Switzerland Pull-Off Test (Raab and Partl 1999), and the Louisiana Tack Coat Quality Tester (LTCQT) (Mohammad et al. 2012).

The interface wedge splitting test, proposed by Tschegg et al. (1995), consists of a groove or opening of a crack at the interface of a double-layered sample and it is tested until the two layers are completely separated. The output of the test is a force-displacement plot that can be used to evaluate the fracture mechanics properties of the interlayer. Many studies (Harmuth 1995, White 2016c, Jamaaoui et al. 2017) however suggest that the interlayer wedge splitting test is more suitable to measure the fracture or crack propagation than to assess the pavement interlayer bond.

Similar to the mechanisms of other pavement distress types, interface shear and slippage failure are not likely to occur due to a monotonic single high-pressure load event; rather, they are expected to occur after repeated load. In many cases, the actual traffic loads/stresses are relatively low as compared to the peak ISS, but they are applied repeatedly over the service life of the pavement. To better evaluate the interface stress behaviour, several studies (Donovan et al. 2000, Romanoschi and Metcalf 2001b, Diakhaté et al. 2011, Wellner and Hristov 2015, Isailović et al. 2017, Isailović and Wistuba 2018, Ragni et al. 2019) have suggested repeated/cyclic shear tests rather than monotonic direct shear tests. Such tests are complex, time-consuming and difficult to operate. Therefore, the monotonic shear test is usually preferred for studies that are interested only in the comparison of different tack treatments (Tozzo et al. 2014b).

Recently, Ragni et al. (2019) employed direct shear test devices currently available, such as the ASTRA and Leutner tests, for cyclic interface shear testing by installing the devices into a servo-pneumatic universal testing machine, NU14. From the cyclic ASTRA test results, the typical three stages of a fatigue/creep test were observed on the deformation-number-of-cycles curve. During the Leutner test, however, the curves did not display the typical three stages of a fatigue test result. This is likely due to the absence of the normal stress in the Leutner test. Moreover, future research in regard to interface shear bond is expected to be focused on shear fatigue behaviour through the cyclic shear test; however, significant effort is needed before interface shear fatigue is properly understood. In the cyclic approach, the interface shear stiffness/modulus and shear fatigue life are introduced as useful parameters to investigate the interface bond characteristics.

For the purpose of this study, the direct shear tests with normal load was selected to assess the interface shear resistance of asphalt layers as it is likely to be most representative of field conditions with friction, grain interlock and adhesion which contribute to the resulting ISS. The testing load is also applied in a more realistic condition and direction to that closely simulate the actual field conditions. Finally, by using this method, it is feasible to determine the shear failure envelope in a Mohr plane to predict the shear failure of pavement interfaces.`

2.4.3.4. Measurements of Asphalt Interface Bonding

In the monotonic test, the interface shear strength (ISS), which is the ultimate shear stress achieved during the test, is generally used by the majority of studies to measure the shear bond strength. The interface performance in shear can also be measured by the interface shear modulus (ISM) and interface shear work (ISW) (White 2016c). The three measures (ISS, ISM and ISM) are displayed using a typical shear force versus displacement curve obtained from an actual shear test with normal load in Figure 2.28. The ISS is computed by dividing the ultimate force (F_{ULT}) by the cross-sectional area at the interface (A) (Equation (2.31)), while the ISM is calculated by dividing the ultimate shear stress (F_{ULT}/A) by the corresponding displacement at failure (d) (Equation (2.32)) from the force-displacement plot (see Figure 2.28) (Uzan et al. 1978). ISW is the area under the load versus displacement curve until a specific shear displacement occurs (White 2016c), as displayed in Equation (2.33)) and presented in Figure 2.28.

$$ISS = \frac{F_{ULT}}{A} \tag{2.31}$$

$$ISM = \frac{(\Delta F/A)}{\Delta d} \tag{2.32}$$

$$ISW = \sum(F \times \Delta d) \tag{2.33}$$

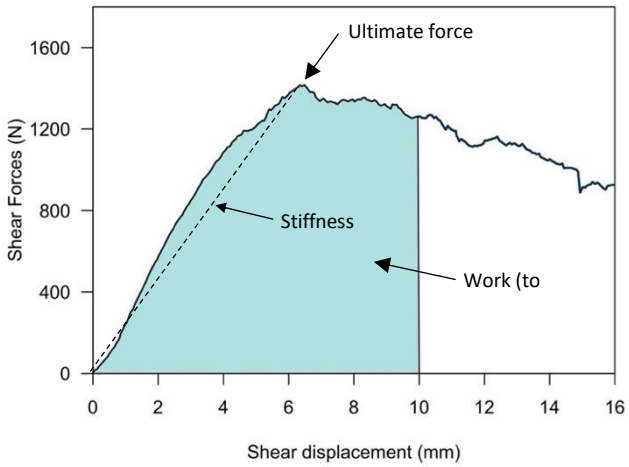

Figure 2.28 Example of a plot of force versus displacement plot and the parameters, reproduced from White (2016c)

Many studies (Canestrari et al. 2005, Mohammad et al. 2002, Collop et al. 2003a) have used the ISS as a parameter to compare different tack coat materials and investigate the optimum tack coat application rate under different conditions. The linear relationship between ISS and applied normal stress from the direct shear test is also often used to develop the Mohr-Coulomb type failure envelope. This is a useful technique to predict the shear failure of pavement interfaces (as discussed in section 2.3.3.3.) and has been adopted for airfield pavement application (Wang et al. 2016, White 2016b).

Similar to ISS, ISM is a useful measure to characterize interlayer shear strength and differentiate between good and poor bonding. Additionally, with suitable calculation tools, it is feasible to model the different interface conditions represented by different values of ISM (Ortiz-Ripoll et al. 2020). In particular, Shell's linear elastic pavement analysis program, BISAR, is applicable for this purpose. To characterise fully or partially bonded interfaces, a parameter known as shear spring compliance (AK) was proposed in BISAR. AK is defined as the ratio between the horizontal deformation and the shear stress acting on the interface (Crispino et al. 1997) which is the reciprocal of the ISM defined in Equation (2.32). Several studies (Wu et al. 2017, Zhang et al. 2014, Shuangxi Li et al. 2020) have tried to investigate the influence of different interface bonding conditions on the stress and strain distribution within the pavement using this parameter.

The ISW is a valuable parameter to evaluate the behaviour of a layer interface (such as residual strength) after the ultimate load has been reached for specimens with comparable *ISS*

and *ISM* parameters. Despite this, very few studies have used ISW to measure interface shear resistance. Santagata et al. (2009) adopted the energy to the ultimate stress to determine the corresponding shear strain. Romanoschi and Metcalf (2001a) and Santagata et al. (2009) suggested that the residual strength after the ultimate force is controlled by the friction element of the layer interface.

2.4.3.5. Factors Affecting Interface Shear Failure

The actual aspects causing de-bonding and interface layer shear failure are not thoroughly recognized yet, but it is feasible to determine several factors that seem to play an important role in increasing the risk of interface shear failure occurrence. In general, factors affecting the resistance of bituminous mixtures to interlayer shear failure, from various studies, are outlined in Table 2.8.

Table 2.8 Factors affecting bituminous mixtures resistance to interlayer shear failure

	Factor	**Transition in factor**	**Effect of transition in factor on resistance to interlayer shear**	**References**
Tack coat	Softening point [a]	Increase	Increase	(White 2016c)
	Application rate	Optimum to excessive	Decrease	Mohammad et al. (2010)
	Modifier	Presence of polymer	Increase	Rabiot and Morizur (1996), Hachiya et al. (1997), Canestrari et al. (2005), Recasens et al. (2005), Moreno-Navarro et al. (2015)
Asphalt Upper layers	Gradation	Gap to continuous	Increase	Chen and Huang (2010) Collop et al. (2009)
	Aggregate shape	Rounded to Angular	Increase	Tran et al. (2012)
	Aggregate -tack coat surface chemistry	Opposite charges	Increase	Zhang (2017)
Interface condition	Interface texture/ roughness	Increase	Increase	Mohammad et al. (2010), Tashman et al. (2008)
	Presence of water	Wet to dry	Increase	Sholar et al. (2002)
	Cleanliness	Dusty to clean	Increase	Hachiya et al. (1997), Sangiorgi et al. (2002b), Raab and Partl (2004)
Construction process	Curing time [b]	Increase	Increase	Sholar et al. (2002), Tashman et al. (2006), Chen and Huang (2010), Tran et al. (2012)
	Tack coat spread uniformity	Increase in surface coverage	Increase	Mohammad et al. (2010),
	Compaction level	Increase in density	Increase	Canestrari et al. (2005).
Loading & Environmental Conditions	Temperature	Increase	Decrease	Canestrari and Santagata (2005), Bae et al. (2010), Mohammad et al. (2012) Diakhate et al. (2006)
	Braking/horizontal load stress	Increase in braking forces	Decrease	(Wang et al. 2016) (White 2016b)
	Load cycles	Increase	Decrease	Diakhaté et al. 2008

[a] at high temperature condition, [b] for emulsion tack coat,

Based on the literature, it can be concluded that tack coat properties and the application rates are of great importance to the interface shear bond strength of pavement. Many studies (Rabiot and Morizur 1996, Hachiya et al. 1997, Canestrari et al. 2005, Recasens et al. 2005, Moreno-Navarro et al. 2015) have shown that the ISS significantly improves when polymer-modified emulsions are used as tack-coat when compared to neat bitumen emulsions. This is expected because the polymer-modified emulsion generally has higher stiffness than the neat emulsion at the same temperature. Moreover, the tack application rate also plays important role on the interface bonding, insufficient tack-coat application may cause weak bonding, while excessive tack coat application could lead to a slippage failure.

Moreover, it is also generally recognized that aggregate properties (such as aggregate gradation, surface texture, shape and size) of the bituminous mixtures being paved play an important part in the achieved interface shear resistance. Tran et al. (2012) suggested that the use of naturally rounded shape aggregate and/or water-sensitive aggregates could increase the likelihood of poor interlayer shear bond. Chen and Huang (2010) assessed the ISS of asphalt interfaces by using various aggregate gradations and found that interfaces with dense graded asphalt exhibit higher ISS as compared to mixes with open and gap-graded gradation. It is also noted aggregates used for pavements are differ widely in terms of their morphology and chemical properties. If tack coat and aggregate possess the same charge, the interface may not have sufficient adhesion. For example, cationic tack coat emulsions (positive charge) provide good adhesion when applied on a surface with negative-charge aggregates like gravel, granite and siliceous rock. In contrast, anionic tack coat emulsions (negative charge) typically provide good adhesion on mixes with positive-charge aggregates like limestone (Zhang 2017).

With regard to interface texture and roughness, several studies (Mrawira and Damude 1999, Santagata et al. 2008, Raab et al. 2012) have suggested that the micro and macrotexture of the underlying layer surface appears to have an important effect on the interface bonding condition. Mohammad et al. (2012) and Tashman et al. (2008) suggested that for similar testing conditions, the ISS of asphalt milled surfaces is dramatically greater than that of non-milled surfaces. This is likely because of the improved roughness through the grooving generated by the milling machine. Furthermore, the interface condition (cleanliness and dryness) also plays an important role in obtaining strong interface bonding. Soaked or contaminated surfaces are likely to have lower ISS. Sholar et al. (2002) found that paving an asphalt overlay over a tack-coated

interface that has been affected by rain is likely to be disadvantageous to the interface shear resistance, possibly causing immediate or future slippage or delamination.

In addition, many studies have consistently agreed that the ISS decreases with the increase of test temperature. High temperatures contribute to shear failure by escalating the plastic deformation of asphalt and decreasing the interface bonding strength between the upper layer and lower layers (Collop et al. 2009). The ISS in the pavement interface tends to decrease with the increase of temperature (Canestrari and Santagata 2005, Bae et al. 2010, Mohammad et al. 2012). However, no research has been found about the ISS of newly laid asphalt pavement at significantly higher temperature (more than 60°C) for the purpose of deciding on traffic opening.

Lastly, many studies (Sholar et al. 2002, Tashman et al. 2006, Chen and Huang 2010, Tran et al. 2012) have suggested that a slight increases in ISS is measured by allowing improved tack coat curing time. Tack coat curing time is the time window after emulsion tack coat is spread on the interlayer surface to ensure that the tack coat materials are fully broken before the newly laid asphalt is paved. For conventional emulsion tack coat, Hasiba (2012), Salinas et al. (2013) recommended 2 hours as the optimum tack coat curing time. In Europe, however, water-based emulsion tack coat is frequently used on the interlayer surface without allowing the tack coat to cure. It is assumed that the tack coat emulsion will break instantaneously once it is in contact with the loose hot bituminous mixture (Cross and Shrestha 2005, Chen and Huang 2010). It can be concluded that, in many cases, the curing time may still be important to ensure the tack coat breaking/setting is achieved. However, a shorter curing time to shorten the construction period, in a busy road or airport, can be achieved by using rapid setting emulsion or pure bituminous binder as a tack coat (Medeiros et al. 2012a, Zhang 2017).

2.4.3.6. Shear Failure in Airfield Pavement

Airside pavements encounter regular aircraft ground movement operations, such as taxiing, acceleration during take-off, braking during landing, and sharp turning in rapid exit taxiways (Wang et al. 2016). These movement operations could likely generate high shear forces at the pavement surface and interlayer. Slippage failure or delamination of asphalt surfaces has often been recorded (Mohammad et al. 2012). A number of instances of slippage failures occurring during take-off operations have been reported. Tsubokawa et al. (2007) reported slippage failures between asphalt layers at Nagoya Airport in 2000. A pavement section with an area of 4m x 8m

was completely ripped up, resulted in airport closure for several hours. The failure was reported to have occurred in the summer during aircraft take-off operation and evaluated as a de-bonding failure. The main cause of the failure, however, was not reported. Horak et al. (2009) investigated serious a slippage failure between the asphalt surface and the lower asphalt layers at an international airport in southern Africa in March 2007. It was reported that slippage cracking, such as crescent-shaped crack types, initially developed due to the insufficiency of bond strength between bituminous layers. During take-off, the opened crack was then blown into by the considerable jet blast, which was capable of lifting a large 'slab' area of new asphalt surface off. Slippage failure poses the significant hazard of Foreign Object Damage (FOD) and loose material and which can damage aircraft and cause injury. FOD of asphalt layer pieces was found inside an aircraft body when debonding failure occurred in Surabaya (SUB) airport in Indonesia in 2017 (Figure 2.29d).

Figure 2.29 Slippage failure in new asphalt overlay layer at the runway in Indonesian airport: (a) Jakarta (HLP) airport, (b) Yogyakarta (JOG) airport, (c) Lampung (TKG) airport, (d) FOD found in aircraft body in Surabaya (SUB) airport (Courtesy of Indonesia Airport Authority).

A significant number of premature interface bond failures that occurred shortly after completion of newly laid asphalt overlay in the hot summer were reported in Indonesian airports

during 2017 and 2019. Slippage failure was observed in HLP airport in Jakarta on July 28, 2017 (Figure 2.29a). It was reported that failure occurred after the take-off operation of a wide-body aircraft, B777. It is noted that the airport pavement was previously designed for narrow-body type aircrafts such as A320 and B737. The airport authority suggested that the heavier loads and higher braking stress of the new infrequent aircraft combined with poor bonding condition were the main factors that caused the failure. A similar failure was also recorded in Adisucipto (JOG) airport in Yogyakarta on November 29, 2019 (Figure 2.29(b)). The airport was shut down for eight hours for the section repair work, causing extensive flight delay.

Recently, rapid exit taxiway (RET) usage has been increased considerably as an effort to improve runway capacity by reducing runway occupancy times during landing operations (White 2014b). It is expected that aircraft manoeuvring, turning and braking, at RETs could cause high shear stresses at the pavement surface. Several studies have reported horizontal deformation distress (shoving) of asphalt in high shear areas of airports (Bognacki et al. 2007, White 2014a, Jones et al. 2012). In 2002, slippage failures were reported to have occurred at a rapid exit taxiway on a landing runway (4R- 22L) at Newark International Airport during the summer months (Bognacki et al. 2007). Asphalt shoving and tearing distress was observed at heavy braking and turning areas such as landing zones and rapid exit taxiways at Houston George Bush International Airport (Jones et al. 2012). Similarly, White (2014a) identified horizontal surface deformations concentrated in high shear force areas in Melbourne Airport. It was reported that the main cause of the deformation failure was not related to the lack of interface bond strength between asphalt layers, rather, it was the result of a lack of asphalt mixture resistance to repeated shear load under heavy braking aircraft traffic.

In summary, shear related pavement failures have commonly only been observed in high-shear and high-speed areas of airports, such as rapid exit taxiways and landing and take-off runway zones. The majority of the failures were observed to take place during the hot summer period. This suggests that high pavement temperatures have also contributed to slippage failures in asphalt pavements. In many cases, the failures were assessed to be related to interface debonding due to lack of interface shear strength. However, it is suggested that horizontal deformation failure can also be caused by inadequacy of the upper layer of asphalt to resist shear creep under aircraft braking and turning forces and not related to interface shear resistance (White 2016b). Nevertheless, when slippage failures and delamination occur, they can adversely

affect airport operations and air traffic systems due to possible closure for removing and replacing the affected layer(s) (Shahin et al. 1986). For a busy airport, this can cause several issues, including flight cancellations, excessive air traffic system delays, high rehabilitation costs and loss of airline revenue.

2.3. Warm Mix Asphalt (WMA)

Warm mix asphalt (WMA) is an emerging new technology which allows the production, placement and compaction of bituminous mixes at considerably lower temperatures than that of conventional Hot Mix Asphalt (HMA) (Kandhal 2010). The technology can reduce the asphalt production temperatures by 20 to 55°C (D'Angelo et al. 2008). WMA commonly uses the same aggregates, bitumen and mix design procedure as HMA, thus there is no additional requirement for mix design of WMA (White 2013).

WMA was first initiated and developed in Europe (Germany and Norway) between 1995 and 1999 and was adopted in the US in 2002 (Prowell et al. 2011, D'Angelo et al. 2008). It was primarily developed in response to the need for reduced greenhouse gases under the Kyoto protocol (Kandhal 2010). In recent years, WMA production has increased considerably in many European Countries and the United States (EAPA 2017) due to promising initial laboratory results that showed WMA has comparable performance to conventional HMA (Jamshidi and White 2020). In the United States, based on NAPA surveys, a nearly nine-fold increase of WMA use between 2009 and 2018 was observed. In 2018 157.7 million tons or 40.5 % of total asphalt mixtures were produced using WMA technologies (Williams et al. 2019).

Currently, more than 30 WMA products are available (Mejías-Santiago and Rushing 2018). Different WMA products claim different temperature reduction techniques and additives. In general, the approach to lower asphalt mix temperature is achieved by reducing the viscosity of binder (flow improver) at reduced mixing, placing and compaction temperatures, improving the workability of the mixture by reducing surface or interfacial tension between aggregate and bituminous binder, increasing mixture flluidity and promoting adhesion (anti-stripping agents). In the following sub-sections, a review of various WMA technologies is presented. Furthermore, the advantages and drawbacks corresponding to WMA applications in airfield pavements are highlighted.

2.3.1. WMA Technologies

There are generally three types of WMA technologies to date: organic additives, chemical additives and asphalt foaming technologies (West et al. 2014a, Su et al. 2009, Kheradmand et al. 2013). Some technologies require temporary or permanent changing of the bitumen characteristics, such as reduced viscosity. Other technologies are based on enhancing the covering ability of bitumen to aggregates by chemically promoting the adhesion between aggregates and bitumen or providing surfactant to enhance the aggregate wettability (Zaumanis 2014). Examples of WMA additives and their descriptions are presented in Table 2.9.

2.3.1.1. Organic or Wax Additives

Waxes or fatty amides are usually used as organic WMA additives. These materials are added to the bituminous binder to reduce the viscosity and increase the lubricity of bitumen, thus, allowing coating of the aggregates at lower temperatures, in the mixing process (D'Angelo et al. 2008). The organic wax has longer hydrocarbon chains than crude oil or paraffin wax and exhibits low viscosity (very fluid) at higher temperatures or above its melting point (98°C) and high viscosity (malleable) at lower temperatures, upon cooling down of the mix. It is also noted that the wax additives must be selected carefully in order to ensure that the melting points are higher than the expected in-service temperature so that rutting or plastic deformation does not occur (Prowell et al. 2011).

2.3.1.2. Chemical Additives

Chemical additives are the newest WMA technologies. A number of WMA technologies using chemical additives have been developed in the United States and Europe. Substantial information on the products, such as the effect of additives on the mixes, is generally available and provided by the manufacturers. However, specific information on the chemicals they used in these processes and precise mechanisms of how these additives work is generally either unclear or classified by the manufacturers (Jalali 2016, Caputo et al. 2020). In general, chemical additives do not lower the bitumen viscosity (West et al. 2014b). As surface-active agents, surfactants, the additives work at the microscopic interface to reduce surface or interfacial tension in a thin film between aggregate and bituminous binder (Raghavendra et al. 2016). Chemical technologies are usually a combination of surface-active agents, emulsification agents, anti-stripping agents, polymer modifier and wax additives to enhance covering, workability, and compactability of the

mixture. Chemical additives can be used either in emulsion form or can be blended with bituminous binder in the terminal and later mixed with heated aggregates. Usually, slight modifications are required to the mixing plant (Chowdhury and Button 2008).

Table 2.9 List of commonly used WMA technologies, reproduced from Diab et al. (2016) Jalali (2016), and Kheradmand et al. (2014)

Technology or additive	Manufacturer	Asphalt temperature reduction ranges (°C)	Description and (dosage)
Organic (wax) Additives			
Sasobit	Sasol Wax International (Germany)	20-30	Fischer-Tropsch wax (2.5–3.0% of bitumen weight in Germany 1.0-2.0% of bitumen weight in US)
Asphaltan B	Romonta GmbH (Germany)	20-30	Refined Montan wax with fatty acid amide (2.0–4.0% by bitumen weight)
Licomont BS 100	Clariant (Switzerland)	20-30	Fatty acid amide (3.0% by bitumen weight)
Chemical Additives			
Evotherm ET and DAT	MeadWestvaco (USA)	35-50	Chemical packages with water (0.5% by bitumen weight)
Evotherm 3G	MeadWestvaco (USA)	35-50	Chemical packages without water (0.25-0.75% by bitumen weight)
Rediset	Akzo Nobel (Netherlands)	15-30	Cationic surfactants and organic additive (0.4-0.6% by bitumen weight for LQ 1-2% by bitumen weight for WMX)
Cecabase	Arkema Group (France)	20-40	Chemical-based (0.2–0.5% by bitumen weight)
REVIX	Mathy-Ergon (USA)	33-40	Surface-active agents, waxes, processing aids and polymers (0.2–0.5% by bitumen weight)
Foaming (Water-bearing Additives)			
Aspha-Min	Eurovia GmbH (Germany)	20-30	Water-bearing additive using zeolites (0.3% by bitumen weight)
Advera WMA Zeolite	PQ Corporation (USA)	20-30	Water-bearing additive using zeolites (0.25% by bitumen weight)
Foaming (Water-based Processes)			
WAM Foam	Shell (UK) and Kolo-Veidekke (Norway)	20-40	Initial coating with soft bitumen and followed by foamed hard bitumen (2–5% water by bitumen weight)
LEA—Low Energy Asphalt	LEA-CO (France)	50-60	Hot coarse aggregate blend followed by wet sand (3–4% water by bitumen weight)
LT Asphalt	Nynas (Netherlands)	60-80	Foam bitumen with hydrophilic additive (0.5–1.0% by bitumen weight)
Double—Barrel Green	Astec Industries (USA)	10-30	Water foaming technology (~2% water by bitumen weight)
Ultrafoam GX	Gencor Industries Inc. (USA)	20-40	Water foaming technology (1.25–2% water by bitumen weight)

2.3.1.3. Asphalt foaming Additives

Foaming technology can be considered as the first developed temperature reduction technique. It is suggested that the technology was invented in 1956 to reduce construction temperature

(Kristjansdottir 2006). However, WMA foaming technology in its present forms was first proposed in Europe in the mid-1990s. It uses a small volume of water injected into the hot bitumen or additives. This can be achieved through the use of a water-based process (nozzles), water-bearing additives (zeolite), or some of the wet aggregates (Zaumanis 2014).

Water-bearing additives are commonly synthetic additives (zeolite) that carry water and discharge it when exposed to the heated mixing temperatures through the evaporation process during mixture production (Diab et al. 2016). As a result, the bitumen volume will be expanded and the viscosity will be reduced temporarily due to the foaming effect (Masson et al. 2001). The viscosity reduction will improve the coating between bitumen and aggregate and enhance mixture workability. The water-based foaming process produces foamed WMA by adding a small volume of cold water into the hot bitumen to produce microscopic bubbles. and more stable foams (Kheradmand et al. 2014).

2.3.2. Possible Benefits and Drawbacks of WMA

2.3.2.1. Benefits of WMA

Although the degree/level of benefits is dependent on the kind of WMA technology adopted, the benefits of WMA can be generally categorised as follows:

a. Reduced plant energy requirement / less fuel costs

   The most recognized advantage of WMA is the reduced energy consumption utilized to dry the aggregate and heat bituminous binder. Studies (Wang et al. 2018a, Olard et al. 2007) have demonstrated that lower production temperatures resulting from adopting WMA can reduce energy consumption by as much as 40%. Based on other research, energy costs can be reduced by about 12-14% when using WMA technology (Mohammad et al. 2015). As an illustration, energy consumption as a function of the production temperature of asphalt is presented in Figure 2.30.

b. Reduced carbon dioxide emissions

   EAPA (2004) suggested that the major part of CO_2 emissions from bituminous pavements occurs within the initial construction stage from the burning of fossil fuels for pavement production. WMA significantly lowers the consumption of fossil fuels, compared to HMA, due to its lower temperature production (Kristjansdottir 2006, Hamzah et al. 2010, Kandhal 2010). A study by Mallick and Bergendahl (2009) indicated that the use of WMA with 10-

30°C temperature reduction is estimated to provide 30-40% reduction of CO_2 emissions. This may allow asphalt mixing plants to be situated in or nearby urban areas that have air quality restrictions.

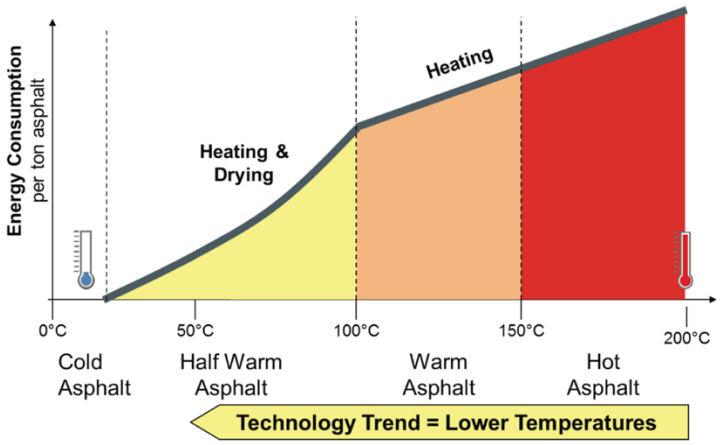

Figure 2.30 Illustration of WMA and HMA energy consumption (EAPA 2014)

c. Increased paving crew comfort and safety

WMA technologies generally enable a reduction in the production and placement temperature of bituminous mixes, therefore improving worker's health and safety (McCarthy et al. 2012) and increasing the paving crew's comfort by working with cooler materials. Additionally, WMA produces less fumes (see Figure 2.31) and odours both at the paving location and the asphalt plant compared to HMA. This would also lead to enhanced working conditions which is beneficial to the paving crew's health.

Figure 2.31 Emission demonstration of WMA (on the right) compared to HMA (the left). Photo by NAPA, 2004

d. Improved workability during placement

WMA additives and processes may be utilized as a compaction aid to improve the compactibility of stiff mixes (polymer-modified, SMA, high RAP content) while producing asphalt at the same temperature as or closer to typical HMA production temperatures (Jamshidi and White 2020). Alternatively, mixes that would have a conventional viscosity at typical HMA temperatures can be provided with the same response to compaction at a lower temperature by the use of such WMA additives. The benefit of improved workability would allow the contractor to potentially reduce the number of compactors and compaction effort required on the job site (Bennert et al. 2010). There are comprehensive experiences with the adoption of particular kinds of WMA with Stone Mastic Asphalt (SMA) in Europe (Mazurek and Nowakowski 2015). The use of WMA with SMA has been recorded in several airfield surfacing projects including Frankfurt airport in 2005 for runway overlay, and Johannesburg airport, South Africa in 2005 for taxiway surface repair (Sasol Wax 2016).

e. Extended paving seasons and haul distance

Producing WMA at regular HMA temperatures may be feasible to extend the paving season. In this case, WMA technologies are used as compaction aids, therefore the temperature window for asphalt compaction can be extended. By extending this time window, it will allow longer haul distances during colder months of the year or where the asphalt plant is considerably far away from the project site and requires longer haul times.

f. Increased percentages of reclaimed asphalt pavement (RAP) in the mix

Studies (Mallick et al. 2008, Doyle et al. 2011, Guercio and McCarthy 2015) have demonstrated that the portion of reclaimed asphalt pavement (RAP) can be significantly higher mixed with WMA instead of HMA. It is well known that one of the primary issues concerning RAP application is the secondary ageing of RAP bitumen during the heating and mixing operation with new hot asphalt mixes. This ageing can cause the bituminous pavement to be more susceptible to cracking. The lower production temperatures with the addition of WMA technology will reduce the secondary ageing of RAP bitumen. Moreover, the use of RAP in WMA could result in improved rutting resistance of mixtures due to increased ageing of the mixture with the addition of aged stiffened RAP bitumen. The combination of RAP and WMA is beneficial to overcome the natural drawbacks of WMA and RAP individually (Hettiarachchi et al. 2019).

g. Early opening of newly laid asphalt for operational use

The lower production and compaction temperatures of WMA as compared to HMA cause less cooling time before the paving section can be opened to traffic. This is beneficial for pavement overlay projects in typical busy airports and congested highways since the pavement section cannot be closed for a long time from an economic perspective (Su et al. 2009). For the purpose of this project, WMA offers rapid opening of new pavement to traffic during airport pavement rehabilitation. In this research, the potential benefit of WMA for overlay/resurfacing material, in terms of quick trafficking, is investigated and presented in Chapter 6.

2.3.2.2. Drawbacks of WMA

Although each WMA technology has its own drawbacks, there are several general challenges and inherent drawbacks regarding the performance and application of WMA, as follows:

a. Increased rutting susceptibility

Short-term ageing of bituminous binder occurs when it is heated and mixed with the hot aggregate. This ageing process is as a result of the loss of lighter oils from the bituminous binder during high temperature mixture production (Kandhal 2010). Moreover, when WMA is added to the conventional bituminous binder and produced at a lower temperature, the ageing or hardening effect of the bitumen during the production process may be reduced, contributing to a higher rutting susceptibility (Aho et al. 2016, Julaganti et al. 2019). Several studies (Buss et al. 2014, Mogawer et al. 2011a, Doyle et al. 2011) have indicated that the design of WMA incorporating RAP could enhance the mix rutting resistance.

In the case of organic additives such as Fischer–Tropsch (F–T) waxes, however, many studies (Perkins 2009, Pasquini et al. 2015, Merusi and Giuliani 2011) have suggested that the organic additives may be capable of offsetting the rutting issue since at in-service temperatures they solidify (crystallize) and thus improve stiffness and rutting resistance of the mixture. Furthermore, at midrange and low temperatures, waxes may increase fatigue susceptibility of the mixtures (Medeiros et al. 2012b, Petit et al. 2012).

b. Increased moisture damage susceptibility

The moisture damage susceptibility of WMA comes as a result of incomplete aggregate drying in the drum due to a decrease of mixing temperature of WMA or when water is added in the production process, such as with mechanical foaming (Goh and You 2011, Yin et al. 2016).

However, this problem can be minimized by utilizing an anti-stripping agent such as hydrated lime (Diab et al. 2013, Cheng et al. 2011, Hesami et al. 2013).

c. Reduced plant production

The complexity of adopting WMA additives and/or foaming processes may lead to reduced plant production. The production cost of WMA can also be slightly higher than that of HMA due to the cost of additives and/or initial investment in foaming equipment (Aho et al. 2016).

d. Lack of long-term performance data for evaluation

It is essential to ensure that pavement constructed using WMA exhibits identical or even better mechanical properties and long-term performance as HMA. Currently concerns still exist over the long-term performance of WMA pavements. This is primarily because WMA is reasonably new, and the in-situ performance evidence is insufficient.

2.3.3. WMA Use in Airfield Pavement

Warm mix asphalt (WMA) has more commonly been adopted for highway pavement works than for airfield facilities (Aho et al. 2016). The adoption of WMA for airfield pavements has been limited to date (shown in Table 2.10). One of the causes is insufficient available construction specifications.

The first use of WMA for airport pavements was reported during night-time runway rehabilitation work at Fukuoka Airport in 2002 (Hachiya et al. 2008). The water-bearing additive (zeolite) was used to produce the foamed WMA at 30°C lower than the production temperature of conventional HMA. The WMA was used to allow a quicker asphalt opening to aircraft traffic in the morning. The allowable time to carry out the rehabilitation work was from 11 pm to 6 am. WMA was used to achieve an asphalt surface temperature less than 50°C when the first aircraft operated in the morning. The WMA mixture showed a rapid temperature drop of asphalt surface during construction. In addition, polymer-modified bitumen was also employed in conjunction with the WMA additive to improve the rutting performance of mixtures. A survey and inspection performed after the construction showed that no excessive initial rutting was observed in the newly laid section. Impact acoustic tests carried out in 2006, four years after construction, also demonstrated that the overlay section showed excellent pavement condition (Hachiya et al. 2008).

Table 2.10 Use of WMA for airfield overlay projects

Airport	Year	Location	WMA Technology
Fukuoka Airport (FUK), Japan [b]	2002	Runways, Taxiways	Foamed bitumen
Johannesburg Airport (JNB), South Africa[d]	2005	Apron and taxiway	Sasobit (wax)
Frankfurt Airport (FRA), Germany [a,d]	2005	Runway	Sasobit (wax)
Svalbard Airport (LYR), Norway[d]	2006	Runway and Taxiway	Sasobit (wax)
Boston Logan Airport (BOS), Massachusetts[a]	2006 – 2015	Taxiways/Runways	Sasobit (wax) + RAP
Gelendzhik Airport (GDZ), Russia[d]	2007	Runway and Taxiway	Sasobit (wax)
West Bend Airport (ETB), Wisconsin [a]	2008	Runway	-
O'Hare Airport (ORD), Chicago[a]	2012	Taxiway (low use)	Rediset LQ
Anchorage Airport (ANC), Alaska[a]	2012	Aircraft Parking Area	Evotherm 3G
Seward Airport (SWD), Alaska[a]	2013	Runway/Taxiway	-
Adelaide Airport (ADL), Australia [c]	2013	Taxiway	Double Barrel Green
Barrow Island Airport (BWB), Australia [a]	2013	Runway, Taxiway, Apron	Double Barrel Green
John F. Kennedy *(JFK), New York [e]	2015	Runway Shoulder	Evotherm 3G

[a] Aho et al. (2016), [b] Hachiya et al. (2008), [c] White (2015b) [d] Sasol Wax (2016) [e]Butt et al. (2019)

Several airports have used organic WMA technologies (Sasobit) on runways, taxiways, and aprons (Sasol Wax 2016). For example, Gelendzhik Airport (GDZ), Russia, Svalbard Airport (LYR), Norway and Johannesburg Airport (JNB), South Africa adopted WMA technologies to reduce the compaction effort required for very stiff and low air void content asphalt mixes. WMA technologies have also been used at Frankfurt Airport (FRA) in Germany, and Linz (LNZ) Airport to reduce the airport closure due to the lag time of asphalt cooling. In Frankfurt airport, Germany, in 2005, WMA was used for the main runway rehabilitation. The permitted work period was 8 hours per night each day, with normal aircraft operations on the runway during the remaining hours. The permissible temperature of the asphalt surface for trafficking was set to be less than 85°C by Lufthansa. The application of WMA generated a cooler temperature of asphalt placement compared to conventional HMA. The contractors were able to ensure the required temperature threshold for aircraft trafficking. More than 468,000 tons of WMA was placed. Until today, the runway pavement has shown good rutting performance (Aho et al. 2016).

In the United States, Boston Logan International Airport (BOS) was the first major airfield in the US to adopt WMA as the pavement materials for both runway and taxiway facilities. Aho et al. (2016) describe the 10-year experience of using WMA for movement areas at Boston Logan Airport (BOS). WMA was used at the airport for several projects between 2006 and 2015. The WMA additive product used was Sasobit (F-T wax). Some pavement sections were built with HMA to give a baseline for evaluation. During construction, it was reported that the

WMA provided several benefits to the construction process, including improved compactibility and potential thicker lifts of asphalt. PCI (Pavement Condition Index) was conducted regularly to investigate the pavement performance. After 10 years of usage, WMA showed comparable PCI performance to that of conventional HMA. An overview of the current condition of the runway in a turning area and excellent condition of grooves in the touchdown area are shown in Figure 2.32a and b, respectively (Mejías-Santiago et al. 2015). Moreover, in some cases, WMA even showed slightly better performance.

(a) (b)

Figure 2.32 Runway 15R-33L, Boston Logan Airport (BOS): (a) view of turning area and (b) zoomed view of the grooves at the landing area. (after Mejías-Santiago et al. (2015))

WMA application for airfield pavements was also reported for several airports in the US, including West Bend Airport (ETB), Wisconsin, O'Hare Airport (ORD), Chicago, Anchorage Airport (ANC), Alaska, and Seward Airport (SWD), Alaska. However, WMA application on airport pavements in the USA is still limited today. This is likely because the current construction specification (FAA AC 150/5370-10) does not incorporate specifications for Warm Mix Asphalt (WMA), thus only few airport agencies have adopted the technology (Mejías-Santiago and Rushing 2018, Garg et al. 2020).

In Australia, the use of WMA at Adelaide Airport and Barrow Island Airport has generally shown a good result (White 2015b). WMA has been used to repair a number of areas in runway and taxiways facilities. Material samples from the production plant and cores collected in-situ have generally shown identical performance of WMA to that of HMA (White 2015b). There was no statistically significant variation between the HMA and WMA moisture content after asphalt production (White 2013). The relative densities reached in the field of both WMA and the HMA were in compliance with the specification. Laboratory tests, including wheel tracking tests and resilient modulus tests on field cores demonstrated no statistically significant

differences in rutting performance for both WMA and HMA. WMA had slightly higher rut-depth and lower resilient modulus and Marshall stability. This is likely due to the reduced bitumen aging of WMA at reduced production temperatures. Furthermore, from visual inspection, the HMA and WMA sections were virtually indistinguishable.

It can be concluded that several airports around the world have embraced WMA as a surfacing material in runway and taxiway rehabilitation projects. In general, the main purpose of the WMA adoption is to reduce the environmental impact of pavement construction. Additionally, in some airports, the use of WMA is also aimed to aid the compaction process of stiff airport mixtures, and to reduce the cooling time of newly laid asphalt, hence the airport can be quickly opened to air traffic. Based on in-situ and laboratory tests as well as visual assessment, many researchers have identified no significant performance differences between HMA and WMA, indicating the WMA as a viable option for use on airport pavements. However, only a few usages of WMA in airport pavements have been recorded until now. This is likely due to the lack of long-term pavement performance data of WMA on airfields and lack of WMA construction guidance and specification for airfield application.

2.3.4. Research of WMA for airfield pavement

The empirical evidence of the use of WMA at several airports (discussed in section 2.3.3.) has indicated the WMA exhibited comparable performance to conventional HMA. Nevertheless, limited research has been performed to evaluate the potential of WMA as airfield pavement material (Rushing et al. 2013). Su et al. (2009) conducted a series of laboratory tests to evaluate the engineering properties (rutting and moisture resistance) of WMA for adoption in airfield pavement rehabilitation projects compared to a control HMA. The results showed that WMA prepared at a temperature 30 °C less than the HMA had significantly better performance than WMA with 50 °C temperature reduction. The results indicated that the HMA mixture generally performed better than WMA. The unacceptable WMA mixtures were probably due to the fact that the additive used was a low-cost WMA wax additive with a very low melting point (at in-service temperature).

A performance study of WMA mixture for airfield pavement with various types of additives was performed by Rushing et al. (2013). Eleven WMA mixtures (different additives) and one HMA mixture were included in the research study. Asphalts produced in the laboratory

and in an asphalt mixing plant were investigated. Tensile strength ratio (TSR) testing, asphalt Pavement Analyzer (APA) testing and Hamburg wheel tracking tests were performed to investigate the rutting and moisture damage susceptibility of WMA. It was concluded that most WMA mixes produced in the laboratory exhibited slightly poorer rutting and moisture damage performance than the HMA mixes. The plant-produced mixes also showed similar trends. However, the authors recommend the WMA as a feasible alternative to HMA for airfield surfacing course.

To validate previous laboratory test results of WMA performance, and as a continuation of a previous study, Mejías-Santiago et al. (2014) carried out a comprehensive investigation of WMA technology for airfield pavement. The study was divided into two phases. In Phase I, the WMA properties were assessed. The investigation performed included binder properties, rutting, moisture damage, low-temperature cracking, durability, and workability of both HMA and WMA. Phase II comprised investigating the procedures of WMA production and placement. Full-scale permanent deformation performance using a full-scale accelerated pavement testing (APT) facility, the heavy vehicle simulator (HVS-A), was also evaluated. The field full-scale test result suggested that WMA mixture had similar or slightly improved performance in comparison with HMA. It was concluded that WMA is viable for airfield pavement application.

Another series of extensive studies of WMA for airfield application was carried out at FAA's National Airport Pavement and Materials Research Centre (NAPMRC) (Garg et al. 2018a, Garg et al. 2018b, Kazmee et al. 2019, Garg et al. 2020). The studies were divided into two phases and designated as Test Cycle 1 (TC1) and Test Cycle 2 (TC2). The first phase of the study, TC1, involved accelerated pavement testing (APT) using special equipment: airport heavy vehicle simulator (HVS-A) on full-scale test lanes containing HMA and WMA with two different bituminous binder grades and one chemical WMA technology (Evotherm 3G) (Garg et al. 2018b). The test was performed at two different tyre pressures of 1.45 MPa and 1.75 MPa, and two constant test temperatures of 49 and 32°C. Furthermore, to investigate the moisture susceptibility of WMA, high temperature indirect tensile strength tests (IDT) and Hamburg wheel tracking tests were also performed to test the field cores. Both field and laboratory experiments suggested that WMA had identical performance to that of HMA, suggesting the WMA potential for use in airfield pavements (Garg et al. 2018b). A subsequent study, performed

by Kazmee et al. (2019), suggested the use of WMA with polymer modified bitumen for enhanced rutting resistance.

In test cycle (TC-2), Garg et al. (2020) evaluated three different WMA technologies: organic (Sasobit), chemical (Evotherm 3G) and hybrid (Advera). The utilization of WMA containing recycled asphalt pavement (RAP) was also investigated. A similar full-scale rutting test using accelerated pavement test (APT) facility was performed at NAPMRC. In addition, the pavement response using heavyweight deflectometer (HWD), and fatigue performance of both HMA and WMA were evaluated. The HWD result, so far, showed that HMA and WMA with organic additive exhibited identical performance and had better performance than WMA containing chemical and hybrid additives. Moreover, further stages of the research are currently in progress. In general, based on the above mentioned studies, it can be concluded that WMA could be a feasible alternative to HMA for airfield pavement. Moreover, insufficient evidence on the long-term field performances of WMA has been the main barrier to the acceptance of WMA in airfield pavements.

2.4. Spray Water Cooling on Newly Paved Asphalt

In tropical countries, where the ambient temperature is high (exceeding 30°C), the temperature drops slowly, so the cooling time would be very lengthy to reach a targeted temperature. Some contractors practice spraying water on the newly laid asphalt to speed up the cooling time. However, there is no specific research regarding the effect of water spraying on a new asphalt surface. It is not recommended by the Asphalt Institute (2009) as there is a concern that hot bituminous binder would experience a foaming effect (reduced viscosity) and this could affect the long term performance of the pavement. Spraying water on the asphalt is also predicted to be ineffective, it would only cool the asphalt surface temporarily, while the temperature inside the asphalt would not be much affected. In addition, Roads and Maritime Services (2010) of New South Wales Government (Australia) prohibits the water application during asphalt construction for rapid cooling because the risk of moisture damage.

There are limited research and guidance related to water spraying application for asphalt cooling. It is hypothesized that the water spraying would lead to particular detrimental impact, including long term durability of asphalt and asphalt moisture damage/stripping. Based on the above mentioned background, it is still questionable whether forced cooling of the newly laid mat using spray water will adversely affect the performance of the pavement. It is also arguable

whether the spray water will effectively reduce the cooling time of new asphalt. Currently, there has been no investigation into the use of water spray on a new asphalt surface. Therefore, more specific research could usefully be done to investigate the impact of water spraying onto freshly laid asphalt. The finding of such research could help agencies and authorities to evaluate the treatment of newly laid asphalt.

2.4.1. Previous Studies on Spray Water Cooling

Spray water cooling, which reduces heat from a hot object by spraying droplets of water onto the surfaces, has been widely adopted in a broad variety of engineering applications, such as metal production, nuclear safety, emergency cooling systems, electronic component cooling and aerospace engineering (Lee et al. 2010, Al-Ahmadi and Yao 2008). Spray water cooling plays a critical role in the industrial processes of steel production in controlling the rates of heat transfer and obtaining desired distributions of surface temperature (Zhou et al. 2013). It reduces the surface temperature, leading to the improvement of steel strength through grain refinement (Chen et al. 2015) and the required surface condition and mechanical properties (microstructure) of the rolled steel (Chen and Tseng 1992).

The most acceptable method of quantifying the heat transfer process, such as spray water cooling, is to determine the convective heat transfer coefficient, which allows the calculation of thermal flux using the basic Newton's law of cooling (Cebo-Rudnicka et al. 2012). Several studies ((Bamberger and Prinz 1986, Wendelstorf et al. 2008, Zhou et al. 2013) have tried to quantify the heat transfer coefficient of forced spray water cooling in metal casting. This coefficient is essential to estimate the cooling rate and to model heat transport during the spray water process.

Several factors affect the rate of spray water cooling which include: (1) the temperature of the water, (2) the temperature of the surface and (3) the water flow/ intensity (Wendelstorf et al. 2008). An empirical equation (Equation (2.34)) to determine heat transfer coefficients (h_{wc}) during water cooling of materials was developed by Bamberger and Prinz (1986) based on a cooling experiment with various types of metal and cooling methods.

$$h_{wc} = 0.69 \log \frac{V_w}{0.0006} \left[1.4 \sqrt{(k\rho C) \exp\left(0.32 \frac{T_s - T_e}{T_w - T_e}\right)} + h_v \right] + h_{rad} \qquad (2.34)$$

where k = thermal conductivity of the material (W/m K); ρ = density of the material (kg/m^3); C= specific heat of the material (J/ kg K); T_s= surface temperature of the material (K); T_e= evaporation

temperature of water (K); T_w= initial bulk temperature of the water (K); T_A= ambient temperature (K); h_v= heat transfer coefficient for stable film evaporation at high surface temperature (≈ 750 W/m²K); h_{rad}= heat transfer coefficient for radiation (W/m²K); σ = Stefan–Boltzmann constant (5.67×10^{-8} W/m² K⁴); ε= emissivity; V_w= water flux density (m³/m² s); and h_{rad} as given by:

$$h_{rad} = \sigma\varepsilon \frac{T_e^4 - T_A^4}{T_e - T_A} \tag{2.35}$$

Based on this formula, the heat transfer coefficient of spray water cooling reduces with the increase of initial temperature of water and increases with the increase of the spray flow rate. Other heat transfer coefficient formulae for spray-hot steel surface systems from various experimental works reported by Nozaki et al. (1978) and Ishiguro (1974) in Morales et al. (1990) are presented in Equation (2.36) and (2.37), respectively.

$$h_{wc} = 1.57V_w^{0.55}(1 - 0.0075T_w)\left(\frac{1}{\alpha}\right), \alpha = 4 \tag{2.36}$$

$$h_{wc} = 0.581V_w^{0.451}(1 - 0.0075T_w) \tag{2.37}$$

where T_w= water temperature (°C) and V_w= water flow rate, (L/m² ·s).

In asphalt pavements, there has been no investigation into the use of water spray onto the new asphalt layer to accelerate the asphalt cooling and its effect on pavement performance. White (2016a) evaluated the effect of an unexpected moderate rain event that occurred during and before asphalt paving in two runway construction cases. Field cores were taken from the affected new asphalt sections and the density and interface shear strength (ISS) of the field cores were evaluated. The laboratory tests showed that there was no evidence that the rainfall during the asphalt paving had any detrimental effect on either the density or the ISS. It is noted that in this case, the rain/spray water occurred during and before the paving operation, hence the situation is slightly different from forced cooling using spray water applied immediately after the paving operation is completed.

2.5. Previous studies on cooling simulation of freshly laid asphalt

Practitioners and researchers have worked on developing programs and tools to estimate the cooling response of newly laid asphalt pavement using different techniques. Cooling curve fitting techniques using a general form of exponential and logarithmic functions have been adopted to estimate the cooling of asphalt (Chen et al. 2008, Miller et al. 2011, Vasenev et al. 2012). These

techniques rely on the measurement data from trial sections or in situ projects. The measurement data, including asphalt temperature data from infrared and thermocouple sensors, the compactor machine movements from global positioning system (GPS) tools, and weather condition of the locale, are utilized to develop empirical curve models to predict asphalt cooling trends. This technique has limited flexibility as it requires re-calibration of curve functions when it is used in different project weather conditions and different asphalt mixtures (Zhu et al. 2019).

To overcome the limitation of the experimental based technique, several model improvements using numerical methods have been made by researchers. Chadbourn et al. (1998) developed a computer program, PaveCool, based on one-dimensional heat transport theory to estimate the pavement cooling rate of single layer asphalt pavement. The program calculates the cooling rate of the new asphalt and determines the ideal beginning and completion time for compaction in cold temperatures. The PaveCool program was then improved by Timm et al. (2001) by considering multi-lift asphalt paving operations and projects in warm climate using a finite-difference model called Calcool, also well known as MultiCool. However, there are still some important feature limitations in the program (Wang et al. 2014b), including the estimation of internal pavement profile temperature, and the consideration of detailed climatic conditions such as duration of sunshine and wind speed.

The majority of past research on asphalt prediction has been associated with studies concentrating on determining the temperature range of newly laid asphalt which provides the window time for compaction. Several studies, however, developed a cooling prediction to predict the performance of asphalt mixtures, such as rutting and thermal cracking, due to the temperature effect (Diefenderfer et al. 2006, Sun et al. 2006, Jia et al. 2007, Chen et al. 2008, Alavi et al. 2014, Taamneh 2016). Diefenderfer et al. (2006) established a model to predict the pavement temperature at the desired depth derived from measured data from the Virginia smart road project. The model is beneficial to determine the pavement temperature profile in order to calculate the viscoelastic properties of asphalt materials. Alavi et al. (2014) provided a Windows-based program to predict the temperature within the asphalt pavement using the finite control volume method (FCVM). The program is used to define the viscoelastic performance of an asphalt layer under traffic and thermal loading.

More recently, with the growth of advanced computers and numerical software, researchers have used the finite element method (FEM) to simulate the cooling response of newly

laid asphalt layers based on the principles of thermodynamics and heat transport theory (Zhu et al. 2019). The use of FEM supports the complex two- or three-dimensional geometric features of a pavement structure and fluctuating weather condition input features which is often not available in other techniques. Table 2.11 displays a comparison between the FEM model and the cooling program, MultiCool (Kassem et al. 2014) to highlight the advantages and challenges of FEM for cooling estimation.

Table 2.11 Comparison of MultiCool and finite element method based prediction, Kassem et al. (2014).

Items	MultiCool	FEM based prediction
Thermo-physical properties (k, C, ρ and ε)	Built-in material properties	Input is provided by user, can be selected from past studies or laboratory measurement
Solar radiation	Determined based on geographic coordinate and the beginning time of the cooling simulation	Input is provided by user, can be selected from meteorological databases or from in situ measurement. The value can be varied over the simulation time
Underlying layers	The user can input the type and the temperature of the underlying layers	Allows defining multiple underlying layers, including the type of material, temperature, and moisture content
Ambient air temperature	Fixed, at the beginning time of the cooling simulation	The value can be varied over the simulation time
Wind speed	Fixed, at the beginning time of the cooling simulation	The value through convection coefficient can be varied over the simulation time
Model Geometry	Only the layer's thickness can be input by the user	The user can create any 2D or 3D geometry model, but the process is time-consuming
Output	The spatial average of asphalt overlay temperature	Graphic and tabular output of the temperature at any points/ nodes of the pavement structure
Computation time	Speedy	Depends on complexity of the model, dimension and number of elements

Several general-purpose-FEM programs are used as numerical tools. For instance, Yinfei et al. (2015) developed a two-dimensional (2D) heat-transport model of a pavement structure using the ABAQUS program to predict the cooling of asphalt pavement with low thermal conductivity material. Wang et al. (2014b) used the ANSYS program to predict the cooling response of newly paved asphalt road pavement in an urban area by 2D FEM analysis. Various weather parameters including hourly solar radiation and wind speeds were set in the program. Kassem et al. (2014) adopted FEM for asphalt pavement simulation using a program called the Automated Dynamic Incremental Nonlinear Analysis (ADINA). Making use this tool, several scenarios, including different asphalt pavement types: hot mix asphalt (HMA), Porous HMA

(PHMA) and warm mix asphalt (WMA), layer thickness, sets of weather conditions and paving times were investigated to see their effect on the cooling time.

Recently, Chu et al. (2019) developed a cooling simulation using ABAQUS to predict the cooling time required, before the multi lift newly laid asphalt section can be opened to traffic. The model was capable of estimating the temperature of a multi-lift asphalt mixture. Using the same model, He et al. (2020) investigated the suitable location of temperature measurement within a newly laid asphalt layer for determining the time for new asphalt to be trafficked. In general, the use of FEM in asphalt cooling modelling provides an accurate prediction, as validated against in-situ data. The FEM also offers a more convenient and versatile tool than other methods.

2.6. Summary

This Chapter has presented some context around the problem being investigated as well as a summary of existing knowledge applicable to the planning and execution of the research. A range of test methods and investigation techniques has been summarised and a number of important findings from previous relevant investigations presented.

Major themes included asphalt pavement rutting and interface shear bond performance at high temperature, current specification on traffic opening temperature, common practice of airfield pavement resurfacing, the use of WMA for airfield pavement application and spray water cooling onto newly laid asphalt pavement. This will assist in forming the basis for the research methods adopted. A number of gaps in the existing knowledge were identified (Table 2.12). These gaps generally relate to current practice in airfield pavement rehabilitation and should be addressed in order to accomplish the aim of this research.

Table 2.12 Summary of existing knowledge gaps

No	Gaps	Actions
1	Asphalt pavement rutting performance at elevated temperatures (60°C - 85°C), during its early life	To understand the performance of newly laid asphalt pavement, in terms of rutting during its early life at the opening to traffic and determine construction practice that will result in satisfactorily constructed pavements
2	The impact of typical aircraft braking on interface shear bond condition of asphalt at high temperature	To understand the performance of newly laid asphalt pavement, in terms of interface shear bond condition of asphalt during its early life at the opening to traffic
3	Strategies for reducing the cooling time of asphalt to accelerate asphalt pavement rehabilitation/construction	To understand the strategies that can be adopted to reduce the cooling time of newly paved asphalt
4	The allowable asphalt temperature at the opening to traffic	To determine the allowable opening-to-traffic asphalt temperature for airport pavements
5	The use of warm mix asphalt (WMA) for airfield pavement rehabilitation.	To determine the effect of the use of WMA on the reduced cooling time of newly laid asphalt and to investigate the performance of WMA at an in-service temperature at opening to traffic
6	The potential use of spray water for cooling of newly laid asphalt to quickly open the pavement to traffic	To investigate the potential use of spray water onto newly paved asphalt, and to evaluate the effect of spray water on the mechanical performance of asphalt mixture

3. Material Properties and Experimental Program

3.1. Overview

This chapter briefly explains the materials used in this research and laboratory test program and its purposes for the study. The basis of selection of the materials is discussed. The results of the rheological testing of binder samples, including dynamic shear rheometer (DSR), Brookfield viscometer, multiple stress creep recovery (MSCR) tests were also presented. Furthermore, the chapter discusses the testing performed during the study, including the repeated load axial test (RLAT), interface shear test and water cooling measurement.

3.2. Materials in Use

3.2.1. Bituminous Binder

The control binders for the research were as follows:

- 40/60 penetration grade bitumen

  Unmodified bitumen was selected in this study as it is traditionally used for airport asphalt for many years (White 2017b). In addition, the 40/60 penetration grade bitumen (meets PG 64 requirement) was adopted as it is reasonably common to be used in airfield surfacing material in the UK (Hakim et al. 2014) and traditionally used for airport asphalt in many airports, including those in tropical countries. The conventional properties of the binder, including penetration, softening point and viscosity are shown in Table 3.1.

- Polymer (styrene-butadiene-styrene, SBS) modified binder

  The use of polymer modified binders (PMB) in airfield pavement work has been gaining popularity over the last decade (White 2017b). The use of the PMB generally improves temperature susceptibility and resists permanent deformation in bituminous mixtures

(Airey 2004). In this research, bitumen with elastomer styrene butadiene styrene (SBS) (meets PG 76 requirement), one of the most commonly used polymers for binder modification, was used. The binder is produced by crosslinking bitumen and thermoplastic elastomers. Typical properties of SBS binder used in this study are listed in Table 3.1.

Table 3.1 characterization of the control binders

No.	Property	Test method	Units	Neat binder 40/60 pen grade	Polymer modified bitumen, SBS
1	Penetration @25°C	BS EN 1426 (BSI 2015a)	dmm	53	45 - 80
2	Softening Point	BS EN 1427 (BSI 2015b)	°C	50	> 65
3	Viscosity at (135°C)	BS EN 13302 (BSI 2018a)	Pa.s	0.395	0.960
4	Viscosity at (165°C)	BS EN 13302 (BSI 2018a)	Pa.s	0.114	0.302

3.2.2. Warm Mix Additives

Two types of additives for WMA, organic and chemical, are respectively used: Sasobit®, one of the most used organic WMA additives available, and Rediset® LQ-1102CE, a popular chemical WMA additive. The Sasobit® concentration was selected at the rate of 2% of bitumen based on past research (Jamshidi et al. 2013). The Rediset® is added at 0.5% by weight of bitumen following a recommended dosage by Akzonobel® (Akzonobel® 2014). Both additives are shown in Figure 3.1. The two warm-mix technologies at selected dosage rates were blended with the control bitumen in the laboratory, based on British Standard BS EN 12594:2014 (BSI 2014b). A total of six bituminous binders are used for the tests. The bituminous binders' and mixtures' designations are presented in Table 3.2.

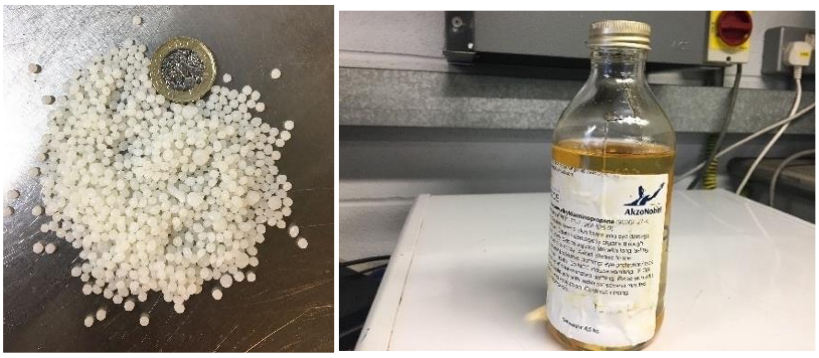

(a) Sasobit® (b) Rediset® LQ-1102CE

Figure 3.1. Warm mix additives for the research

Table 3.2. Bituminous binders used in this research

Terminology of bitumen and mixtures	Binder type	WMA Additives	State of additives	Additives dosage (% of binder weight)
B1	Polymer modified binder	-	-	-
B2	Polymer modified binder	Sasobit®	Prill form	2%
B3	Polymer modified binder	Rediset® LQ-1102CE	Viscous liquid	0.5 %
B4	Pen. grade 40/60	-	-	-
B5	Pen. grade 40/60	Sasobit®	Prill form	2%
B6	Pen. grade 40/60	Rediset® LQ-1102CE	Viscous liquid	0.5 %

3.3. Bituminous Binder Tests

3.3.1. Brookfield Viscometry Test

Rotational viscosity testing using Brookfield viscometry was performed on the binders at an elevated temperature (range from 115°C to 185°C). The test was intended to find out the correct production temperature of the binders. The results of the viscosity test for the neat binder, SBS modified binder, and both binders containing warm mix additives, are presented in Table 3.3. The temperatures for bituminous mixture production with additives were determined based on the results (Figure 3.2), and are listed in Table 3.3, with standard viscosities between 0.15 and 0.2 Pa·s for mixing, and between 0.25 and 0.3 Pa·s for compaction of bituminous mixture.

Table 3.3. Results of Brookfield viscometry test and predicted production temperature

Sample ID	Viscosity (Pa.s) at 135°C	Viscosity (Pa.s) at 165°C	Viscosity (Pa.s) at 185°C	Mixing temp. °C (viscosity 0.15 ~ 0.20 Pa.s)	Compaction temp. °C (viscosity 0.25 ~ 0.30 Pa.s)
B1	0.960	0.302	0.159	179 ~ 186	165 ~ 172
B2	0.769	0.253	0.139	174 ~ 182	159 ~ 165
B3	0.833	0.448	0.149	177 ~ 185	163 ~ 169
B4	0.395	0.114	0.057	152 ~ 160	142 ~ 147
B5	0.356	0.105	0.056	147 ~ 156	139 ~ 144
B6	0.418	0.116	0.058	151 ~ 160	142 ~ 147

In general, it was found that, based on the viscosity-temperature relationship from the testing, both warm mix additives were responsible for a reduction of only about 5°C in mixing temperature. The reduced production temperature of WMA based on the viscosity comparison was not as much as 15°C of reduction as found in Liu et al. (2011), or even 25°C of reduction as shown by NCAT Report 05-06. The unremarkable impact on the mix temperature of Sasobit-WMA mixtures when it is determined using the viscosity test is also found in other studies: Wasiuddin et al. (2007),Tasdemir (2009), Silva et al. (2010), Jalali et al. (2014) and Abed et al. (2019). Furthermore, in this research, the compaction energy index (CEI) and the traffic

densification index (TDI) approach suggested by Sanchez-Alonso et al. (2011) was used to determine the production temperatures of WMA, as will be discussed in the section 3.4.2.

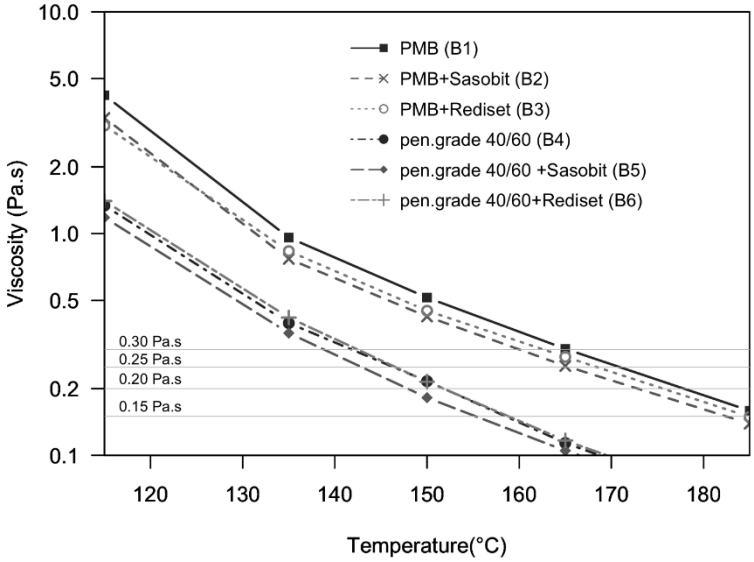

Figure 3.2. Viscosity of binders at high temperature

3.3.2. Dynamic Shear Rheometer (DSR)

In this research, the DSR was used to assess the rutting influence of the bituminous binder. The test was arranged following BS EN 14770 (BSI 2012a). In this research, to represent the temperatures during early life trafficking, all binders were tested in the temperature ranges from 52˚C to 82˚C in increments of 6˚C, following the Superpave performance grading system (Cominsky et al. 1994). The test results of G*/sinδ for (both unaged and short-term aged condition) neat binder, SBS modified binder, and both binders containing warm mix additives, are presented in Table 3.4 and sketched in Figure 3.3(a) and (b), respectively.

Table 3.4. Results of DSR test G*/sinδ (kPa) for each binder

Binders	DSR, G*/sinδ (kPa) at test temperature:							
	58˚C		64˚C		70˚C		76˚C	
	Unaged	Aged	Unaged	Aged	Unaged	Aged	Unaged	Aged
B1	4.76	7.45	2.78	4.15	1.74	2.46	1.16	1.49
B2	11.90	12.27	5.91	7.12	3.27	4.33	1.73	2.73
B3	5.07	6.44	2.90	3.74	1.81	2.33	1.21	1.39
B4	4.57	12.49	2.00	5.52	0.95	2.71	-	-
B5	8.59	15.83	3.83	7.06	1.91	3.29	1.01	1.62
B6	5.04	9.64	2.23	4.21	1.08	1.95	-	-

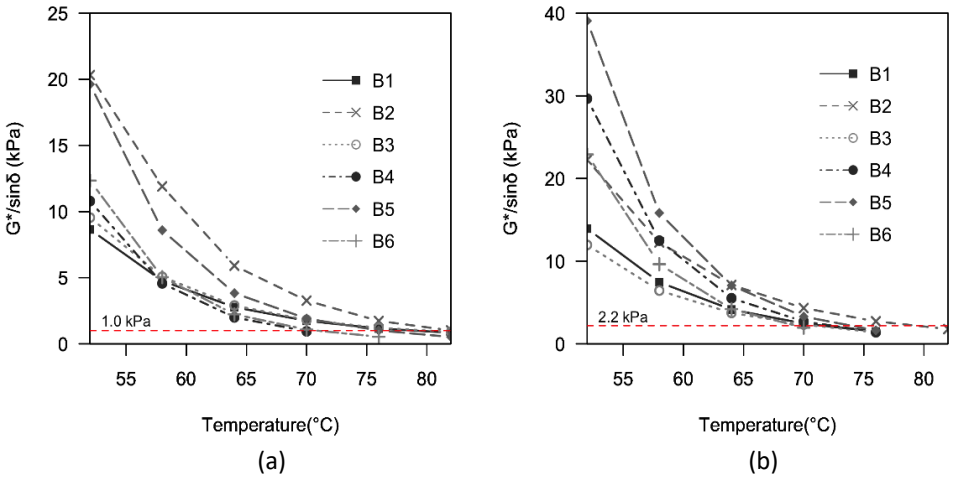

Figure 3.3. G*/sin δ of binders at high temperature: (a) unaged and (b) RTFO aged

In general, SBS modified binder (B1) has higher G*/sin δ values as compared to neat binder (B4). It can also be noted that, for both conditions (unaged and RTFOT-aged), the addition of WMA additives into the binders increased the G*/sin δ value. As an illustration, the G*/sin δ of binders at 64°C, for unaged and RTFOT aged condition, is shown in Figure 3.4 a and b, respectively.

In an unaged condition at 64°C, the addition of Sasobit® and Rediset® with the neat binder (B4) caused an increase in the G*/sin δ value, up to 92% and 12%, respectively. The SBS modified binder containing Sasobit® (B2) and Rediset® (B3) increased the G*/sin δ value to approximately 113% and 4%, respectively, as compared to the control binder (B1). The increase is more notable for binder with the addition of Sasobit® (B2 and B4). A similar finding was observed for RTFOT aged binders with the addition of Sasobit® (wax additives). However, in RTFOT aged condition, the G*/sinδ of binders containing Rediset® (B3 and B6) was found to be lower than the control binder (B1 and B4). Similar trends can also be found at test temperatures of 58˚C, 70˚C and 76˚C, as seen in Table 3.4. In general, it was found that the addition of Sasobit® with binders could make a significant difference in the G*/sin δ, indicating rutting performance improvement. This finding corresponds to the past published research studies (Wasiuddin et al. 2007, Liu et al. 2011, Oner et al. 2017).

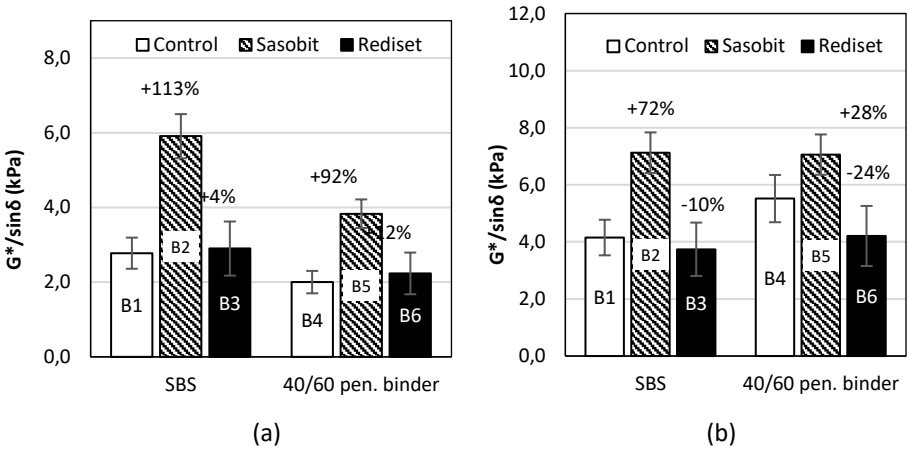

Figure 3.4. G*/sin δ of the binders at 64 °C: (a) unaged and (b) RTFO aged

3.3.3. Multiple Stress Creep Recovery Test (MSCR)

Many recent studies (Syed et al. 2019, D'Angelo 2009b, Salim et al. 2019) suggest that MSCR test of binders correlates better with rutting potential of asphalt than other parameters, particularly to assess the polymer-modified binder performance. In this study, MSCR tests were conducted on the six bituminous binders according to BS EN 16659:2015 (BSI 2015c). The MSCR test is performed at two stress levels (0.1 and 3.2 kPa). For each stress level, ten cycles of loading and unloading, as shown in Figure 3.5, are applied. The load is applied for 1s, the specimen is then allowed for 9s rest period.

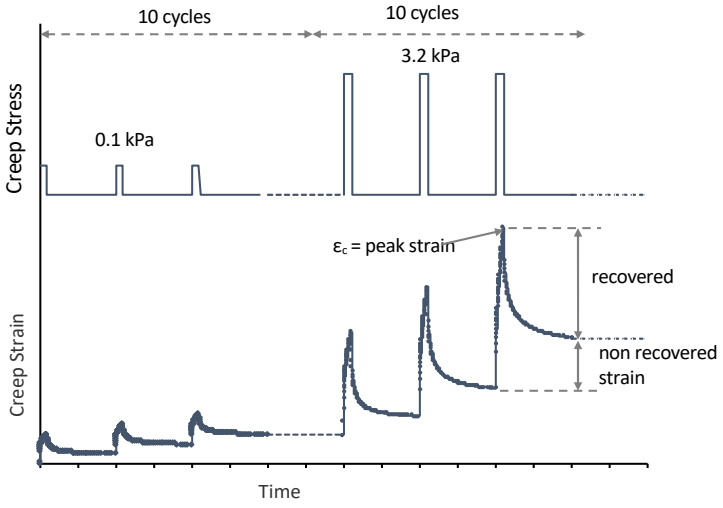

Figure 3.5. MSCR test

The output parameters of the test are the non-recoverable creep compliance (J_{nr}) and MSCR %recovery. The J_{nr} measures the proportion of permanent strain of binder specimen after periodic stressing and relaxation, relative to the amount of applied stress. The MSCR %recovery

is a proportion of how much the binder sample returns to its initial shape after being repeatedly loaded and unloaded. In this research, the MSCR test was performed on all bituminous binders at four different test temperatures: 52°C, 64°C, 76°C, and 82°C to represent the temperature during early life trafficking. Figure 3.6 and Figure 3.7 shows the MSCR tests at 3.2 kPa of SBS modified binders and neat binder with the addition of WMA additives, respectively. In general, it was found that, at high temperature, the binders modified with SBS (B1, B2, B3) showed much lower accumulated strain than the unmodified binder (B4, B5, B6), indicating lower rutting potential of the mixes with a polymer-modified binder.

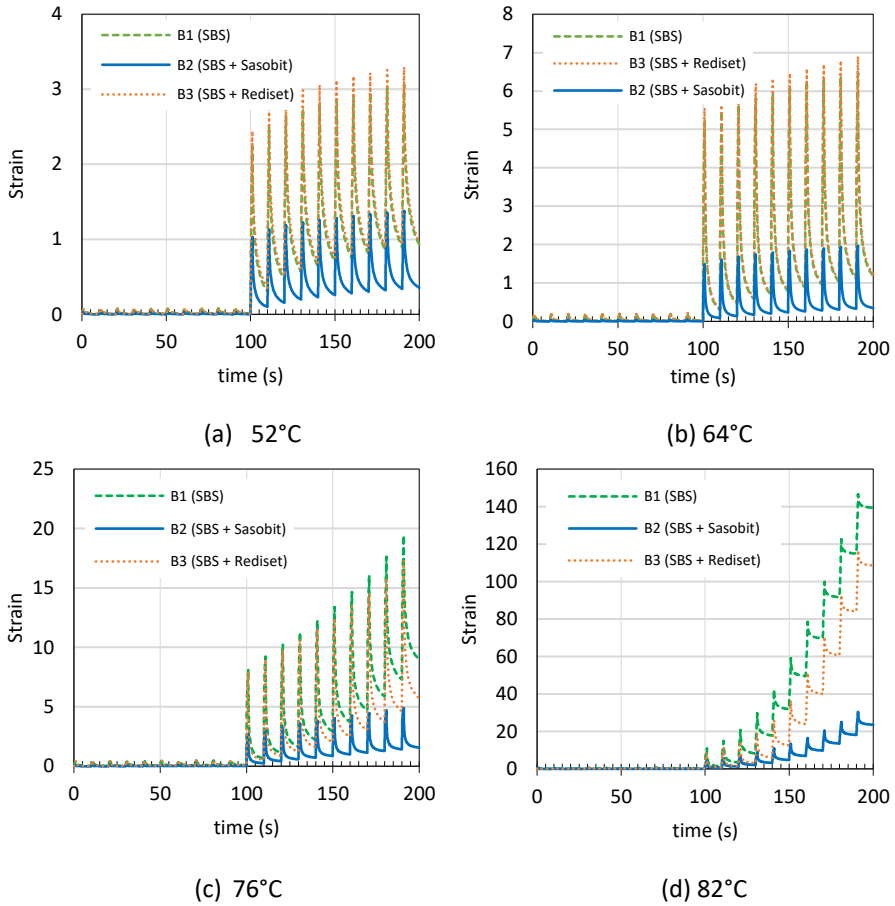

Figure 3.6. MSCR tests at 3.2 kPa at different temperature for SBS binder + WMA Additives

The addition of Sasobit® additives to the SBS modified binder (B2), as shown in Figure 3.6, improves the strain response of the unchanged binder (B1) drastically. This can be seen from the lower accumulated strains of B2 at the end of the test. A similar trend of a decreased accumulated strain of binder with the addition of Sasobit® (B5) was observed for neat binder (pen. grade 40/60), see Figure 3.7. The addition of Rediset® additives (B3 and B6) does not

significantly change the rheological behaviour of the binders. Thus the benefit of the Rediset additive appears to be in permitting lower mixing temperature but then delivering a virtually unchanged bitumen.

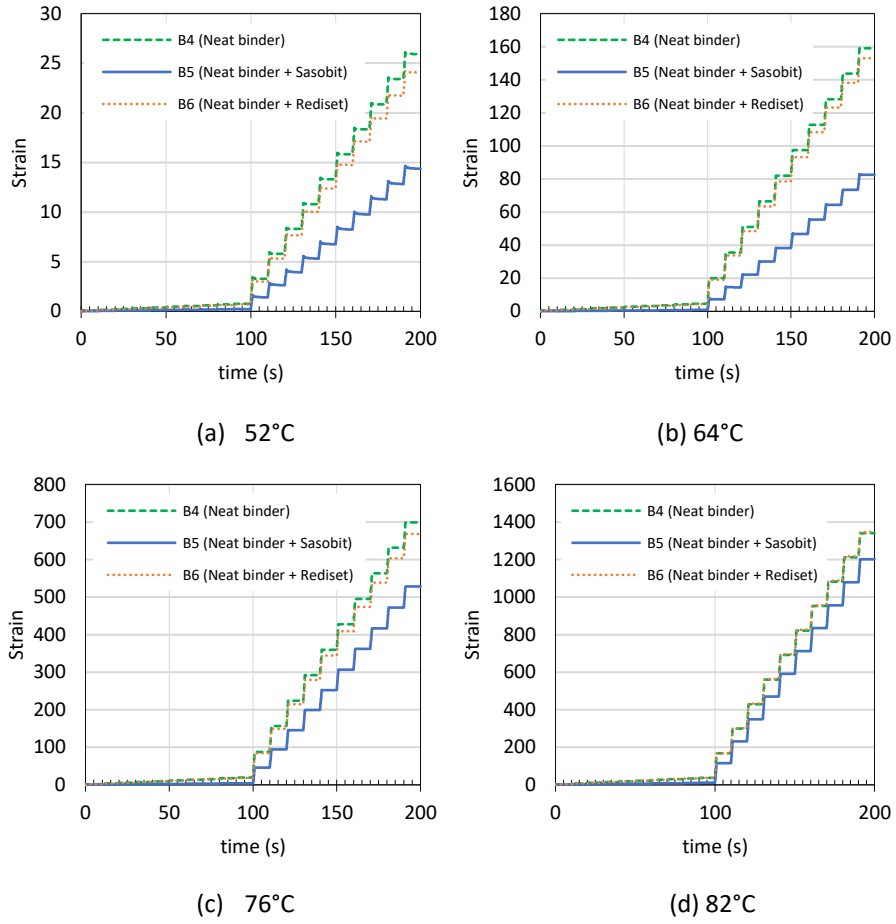

Figure 3.7. MSCR tests at 3.2 kPa at different temperature for Neat binder + WMA Additives

As mentioned before, the outputs of the MSCR test are the non-recoverable creep compliance (J_{nr}) and MSCR % recovery. The J_{nr} and %Recovery of the six binder specimens at all test temperatures (52˚C, 64˚C, 76˚C, and 82˚C) at 3.2 kPa stress level are presented in Table 3.5. Additionally, for illustration purposes, the test results for binder specimens at 76˚C are displayed in Figure 3.8. From Figure 3.8, it is apparent that at the test temperature of 76˚C, the J_{nr} value of binders with the addition of Sasobit (B2 and B5) was found to be significantly lower than that of the control binder (B1 and B4). Furthermore, a higher percentage of recovery of the B2 and B5 binders was observed. A similar trend can also be found at test temperatures of 52˚C 64˚C and 82˚C, as seen in Table 3.5.

Table 3.5. MSCR test data and analysis for the binders in unaged condition and RTFOT aged condition

Binders	Ageing condition	52˚C		64˚C		76˚C		82˚C	
		J_{nr} @ 3.2 kPa (kPa^{-1})	ε_r 3.2 kPa (%)	J_{nr} @ 3.2 kPa (kPa^{-1})	ε_r 3.2 kPa (%)	J_{nr} @ 3.2 kPa (kPa^{-1})	ε_r 3.2 kPa (%)	J_{nr} @ 3.2 kPa (kPa^{-1})	ε_r 3.2 kPa (%)
B1	unaged	0.029	95.76	0.036	97.75	0.280	91.59	4.349	48.30
	aged	0.040	90.02	0.076	94.13	0.374	87.24	2.842	50.70
B2	unaged	0.011	96.55	0.010	97.83	0.050	94.91	0.735	74.60
	aged	0.015	92.43	0.032	93.76	0.500	73.96	0.883	73.19
B3	unaged	0.030	96.02	0.041	97.59	0.180	94.64	3.390	60.00
	aged	0.059	87.01	0.107	92.87	0.676	81.25	3.868	44.10
B4	unaged	0.786	5.01	4.322	0.35	21.230	-1.12	40.706	-1.99
	aged	0.237	17.65	1.588	2.84	8.186	-0.10	15.809	-0.72
B5	unaged	0.442	16.02	2.984	2.24	16.370	-0.80	37.199	-1.99
	aged	0.158	26.38	1.081	7.72	7.568	0.20	20.634	-0.96
B6	unaged	0.730	5.75	4.463	0.31	20.290	-2.23	40.918	-2.20
	aged	0.271	15.64	1.954	2.14	9.572	-0.25	19.137	-0.95

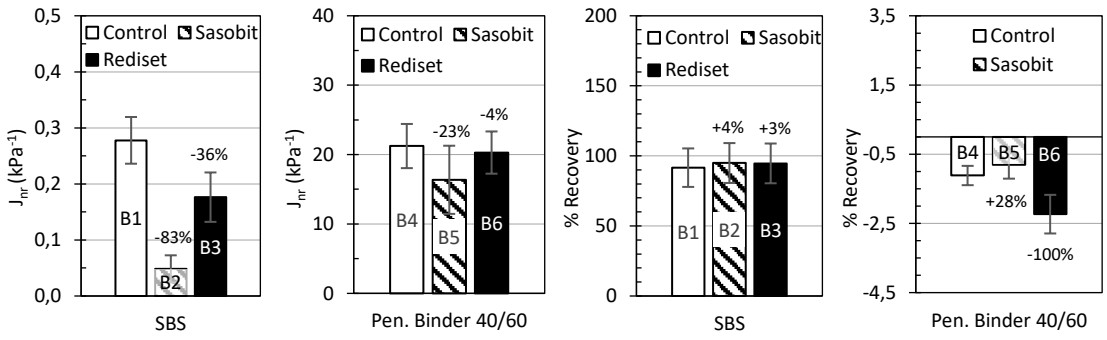

(a) J_{nr} (b) % Recovery

Figure 3.8. Variations in creep compliance (J_{nr}) and percent recovery of binders with WMA additives at 76°C (unaged condition)

The reduction of J_{nr} and improvement of %Recovery of binders with the addition of Sasobit indicates a lower potential of the bituminous binder to rutting. Similar impacts of Sasobit® supplement on lower non-recoverable compliances of binders can also be found from other researches: Morea et al. (2012), Ziari and Babagoli (2015), Ali et al. (2018), and Julaganti et al. (2019). Additionally, in general, the binders with the addition of Rediset result in comparable J_{nr} and %Recovery to those of the control binder.

Effects of Aging Condition

Ageing of binders may cause great damage to pavements and lead to many distresses, such as rutting, fatigue cracking and potholes (Yu et al. 2011). The effect of ageing can be evaluated by measuring the change in the rheological properties of the binder in unaged and aged condition (Singh et al. 2017). In this research, short-term ageing of bituminous binder during mixing,

transportation, laying and compaction of the asphalt mix was simulated in the laboratory by the rolling thin film oven test (RTFOT) according to BS EN 12607-1:2014 (BSI 2014a). Furthermore, the MSCR test was performed on RTFO-aged binders and compared to the unaged binders. The results of the tests performed on RTFO-ageing condition at different temperatures are shown in Table 3.5. As an example, the test results for unaged and aged binder at 76˚C are displayed in Figure 3.9.

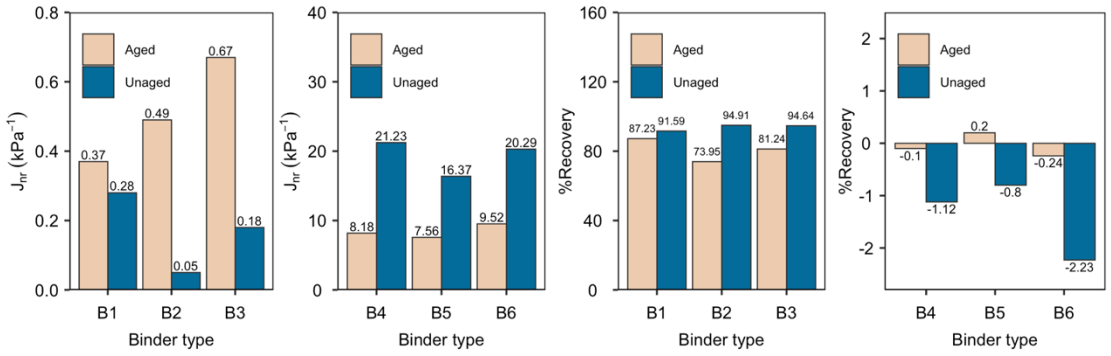

(a) J_{nr} (b) % Recovery

Figure 3.9. Variations in creep compliance (J_{nr}) and percent recovery of unaged and aged binders at 76°C at 3.2 kPa

The MSCR test results at 76°C show that, in the case of neat binders (B4, B5 and B6), the MSCR %Recovery increases with increased ageing. For instance, in the case of neat binder (B4), at 76°C, the average MSCR % recovery values under unaged and RTFO-aged conditions are -0.8 and 0.2%, respectively. In addition, in an aged condition, the value of J_{nr} decreased, indicating improvement in rutting resistance. A similar trend was also observed in binder B5 and B6. The increase of the MSCR %Recovery and the decrease of J_{nr} for the aged binders is likely due to the ageing process that makes the binder stiffer than the unaged binder. In contrast, in the case of SBS modified binder (B1, B2 and B3), the MSRC %Recovery decreased and the J_{nr} value increased with increased ageing. This is likely because ageing tends to degrade the polymer network (Airey 1997), which leads to degradation in rutting performance.

3.4. Asphalt Mixtures Specification and Manufacture

The asphalt mixtures for the research were arranged following the FAA Item P-401, Hot Mix Asphalt (FAA 2018) for ¾ in. (20 mm) and ½ in. (14 mm) maximum aggregate size (Gradation 2 and 3). The specification was selected because it has been popularly used for commercial airports around the world. The aggregates used were granite aggregates from Bardon Hill (Leicestershire,

UK) while the asphalt mix design is shown in Table 3.6, and Figure 3.10.

Table 3.6. The aggregate gradations for research

Sieve Size (mm)	Percentage by Weight Passing Sieves	
	20.0 mm max	14.0 mm max
20	100	--
16	95.5	--
14	89.6	100
10	76.9	83.4
8	66.5	73.3
6.3	58.9	65.6
4	47.8	53
2.8	40.4	44.5
2	33.9	37.3
1	23.4	25.7
0.5	15.5	17
0.25	10.3	11.3
0.125	6.9	7.6
0.063	5	5.4

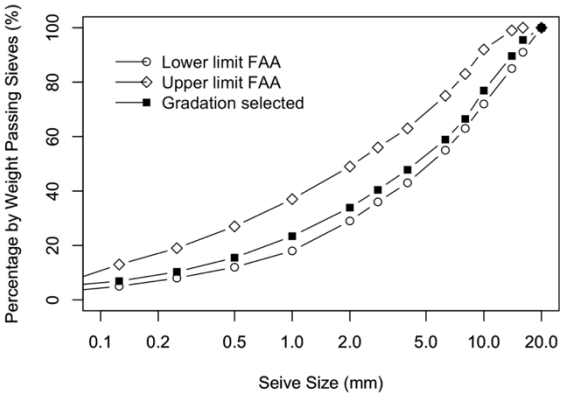

(a)

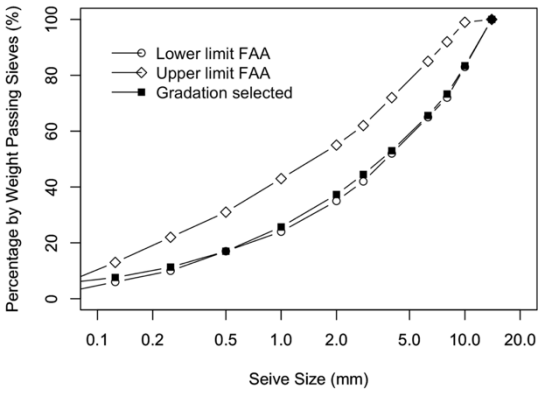

(b)

Figure 3.10. Aggregate gradation with: (a) 20 mm; (b) 14 mm max aggregate size

3.4.1. Determination of Optimum Binder Content

A 75-blow Marshall mix design criterion was used to obtain optimum binder content of pavements mixtures, as stated in the FAA AC 150/5370-10G (FAA 2018). Marshall mix design was performed by preparing two replicates at 0.5 increments of binder content percentage over a range of expected binder content. Two different aggregate gradations, displayed in Table 3.6, were investigated and the 40/60 pen. grade binder (B4) was used as the bituminous binder. The specimens were mixed and compacted with a Marshall hammer to produce cylindrical specimens 100 mm in diameter by 64 mm in height before being compressed with a loading rate of 50 mm/minute until fracture. The output of the test are the Marshall stability and flow values. The Marshall stability (in kN) measures the maximum load supported by the bituminous binder (Please 1961), while the flow value (in mm) refers to the vertical deformation when the maximum load is achieved. The results of the Marshall test performed in this study are presented

in Table 3.7 and displayed in Figure 3.11 and Figure 3.12. The results showed that binder contents of 5.3% and 5.8% for mixtures with gradations of 20 mm and 14 mm maximum aggregate size, respectively, were within the acceptable Marshall design criteria, and thus selected as the binder content of the asphalt mixes.

Table 3.7. Marshall results

	Maximum aggregate size					
	20 mm			14 mm		
Asphalt content (%)	5.0	5.5	6.0	5.5	6.0	6.5
Bulk density (Mg/m^3)	2.37	2.38	2.40	2.36	2.39	2.42
Stability (kN)	10.7	10.8	10.2	9.6	10.5	9.7
Flow (mm)	3.4	3.6	4.0	3.6	4.1	4.3

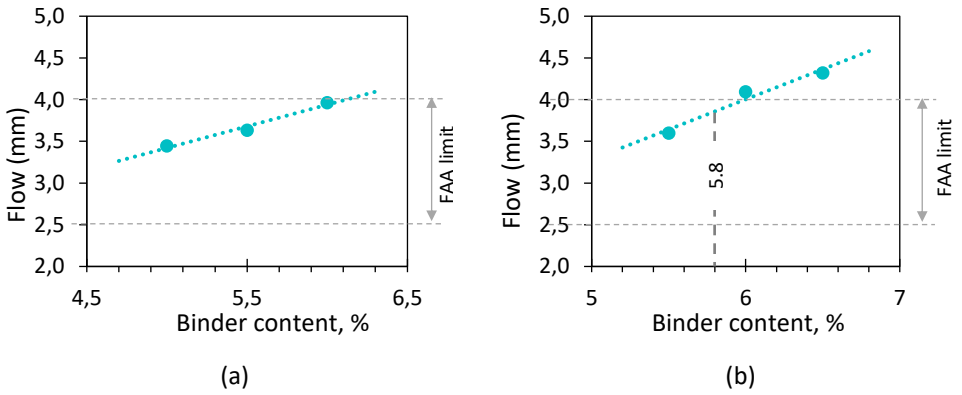

Figure 3.11. Flow: (a) for 20mm maximum aggregate size, (b) for 14mm maximum aggregate size

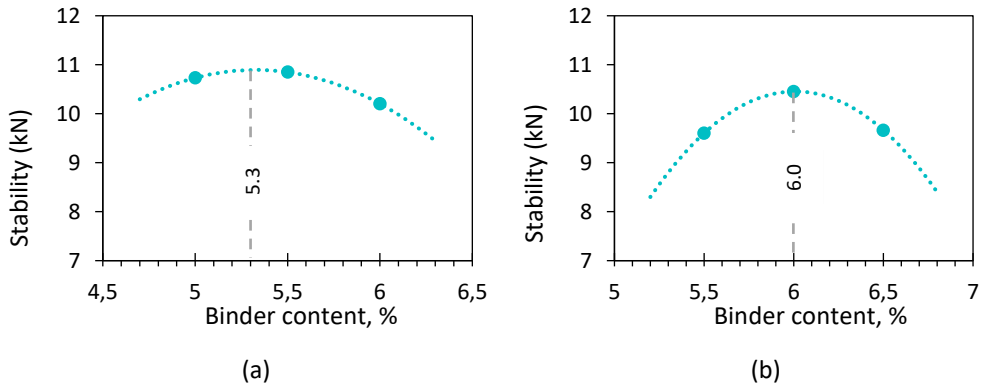

Figure 3.12. Marshall Stability: (a) 20mm maximum aggregate size, (b) 14mm maximum aggregate size

3.4.2. Selection of Mixing and Compaction Temperature

The behaviour of the compaction of the asphalt mixture during its compaction and its later densification under traffic loads can be predicted at laboratory scale, through the correlation between asphalt mixture compaction level and the gyratory compaction cycles (Sanchez-Alonso

et al. 2011). Some indices were developed in 1998 by Bahia et al. (2001), for estimating the energy of compaction, which is computed using data obtained from the densification curve as seen in Figure 3.13 (Mahmoud and Bahia 2004). These indices are the Compaction Energy Index (CEI) and the Traffic Densification Index (TDI).

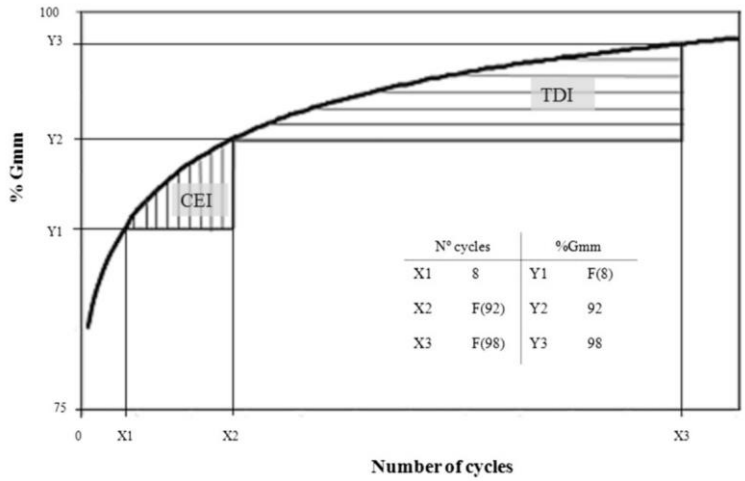

Figure 3.13. Densification curve (Mahmoud and Bahia 2004)

3.4.2.1. Compaction Energy Index (CEI)

The Compaction Energy Index (CEI) is referred to as the area under the densification curve, from the eighth gyration to 92% of G_{mm} (maximum density), as shown in Figure 3.13. It is assumed that CEI represents the compaction of an asphalt mixture by the roller during construction. The 8th gyrations is chosen as the start to simulate the work already applied by the asphalt paver during the paving process, while 92% of G_{mm} is the density after construction and during pavement traffic opening. The low values of CEI indicate better workability. However, if the value of CEI is too low, it could be a sign of a tender mixture and should be avoided (Sanchez-Alonso et al. 2011).

3.4.2.2. Traffic Densification Index (TDI)

The Traffic Densification Index (TDI) is referred to as the area from 92%, to 98% of G_{mm} under densification curve (see Figure 3.13). It is considered that the pavement continues to densify under traffic loads after opening to traffic at 92% of G_{mm}. The 98% of G_{mm} is assumed the constrained density, at which the mixture is reaching the plastic failure region. Mixtures with greater TDI values in this range are desired because they are predicted to bear more traffic load during their life span.

As discussed before in section 3.3.1 Brookfield Viscometry Test, the effect of warm mix additives on the asphalt mix temperature could not be determined using the viscosity test. As an alternative, in this study, the production temperature of WMA was determined by comparing the ease of compaction of HMA and WMA through these two indices from gyratory compaction data. The technique has been used in many studies to investigate the manufacture and compaction temperatures of WMA (Kanitpong et al. 2008, Sanchez-Alonso et al. 2011, Mo et al. 2012)

3.4.2.3. Results

The WMA mixes were manufactured with two different compaction temperatures, 20°C and 30°C below HMA compaction temperature. The CEI and TDI value was calculated by the densification curve obtained from the gyratory compaction result, as explained before. A maximum number of 750 gyrations and 800 kPa vertical stress was applied, with a compaction angle of 0.82° and a speed of 30 rpm. The data trends were modelled using logarithmic regression using Microsoft Excel tools. The area of CEI and TDI is calculated by performing a definite integral between two points. The CEI and TDI results are shown in Figure 3.14 and Table 3.8. In addition, as an example, the densification curves and CEI areas for mixes B1 (SBS control binder) as compared to B2 (control binder + Sasobit) are presented in Figure 3.14.

Table 3.8. CEI and TDI results

Type of mix	Compaction temp. (°C)	Regression Equation	R^2	CEI		TDI	
				Nº cycles	Value	Nº cycles	Value
B1	170	G_{mm} (%) = 77.734 $N^{0.0323}$	0.969	184	1124	1303	4354
B2	150	G_{mm} (%) = 78.045 $N^{0.0323}$	0.979	163	1132	1152	3847
	140	G_{mm} (%) = 77.203 $N^{0.0307}$	0.971	302	2127	2368	8124
B3	150	G_{mm} (%) = 78.744 $N^{0.0305}$	0.970	164	1129	1303	4487
	140	G_{mm} (%) = 77.413 $N^{0.0302}$	0.964	304	2564	2461	8516
B4	145	G_{mm} (%) = 81.908 $N^{0.0242}$	0.972	122	569	1656	6365
B4	125	G_{mm} (%) = 78.596 $N^{0.0320}$	0.979	137	890	988	2661
	115	G_{mm} (%) = 77.210 $N^{0.0317}$	0.977	252	2679	1848	6234
B5	125	G_{mm} (%) = 78.596 $N^{0.0328}$	0.981	133	869	913	3024
	115	G_{mm} (%) = 76.955 $N^{0.0309}$	0.979	323	3362	2499	8544

As seen in Figure 3.14 and Table 3.8, it was found that on a temperature reduction of 20°C, mixes with WMA additives result in a slightly lower CEI, which indicates the easiness of WMA to compact, as compared to HMA. However, it was found that reducing the mixtures' compaction temperature by 30°C indicates difficulties during compaction for both WMA additives. In general, reducing the mixing and compaction temperature by 20°C would result in

the same compaction workability of WMA compared to HMA. In this study, both WMA technologies were produced at 20°C below that of HMA.

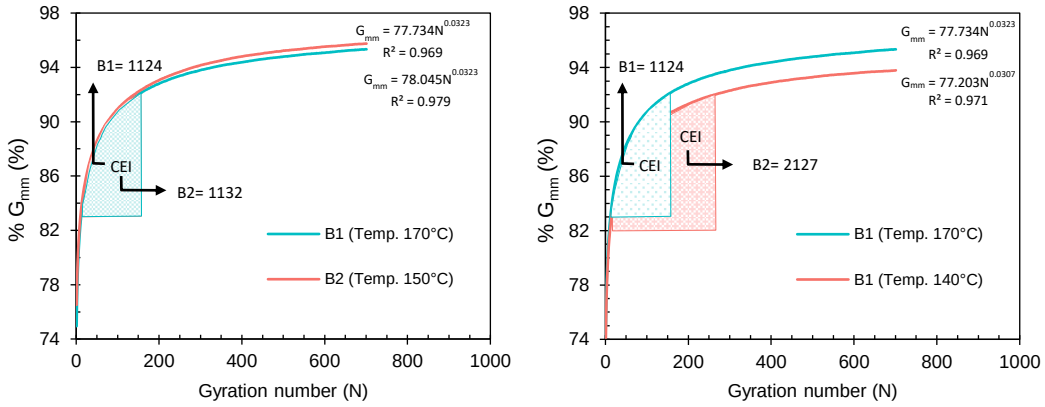

(a) WMA 20°C below (b) WMA 30°C below

Figure 3.14. Densification curve of B1 and B2

3.5. Portland Cement Concrete (PCC) Specification and Manufacture

In this research Portland cement concrete (PCC) slabs were prepared as the lower layer for the interface shear strength (ISS) test to study the effect of pavement surface texture on the ISS – which will be discussed in Chapter 5 and Chapter 6 of this thesis. The mixture of concrete was designed according to FAA P-501 Specification requirements for airport concrete (FAA 2018), see Table 3.9. The cement type employed in this research was Portland cement CEM I-42.5 following BS EN 197-1 (BSI 2011).

Table 3.9. Placement of concrete mix per cubic meter based on FAA P-501 (FAA 2018)

Material	Value
Coarse Aggregate, kg	875
Intermediate Coarse Aggregate, kg	291
Sand-Fine Aggregate, kg	727
Water, kg	136
Portland Cement, kg	297
Air, %	7
W/C Ratio	0.46
Total weight, kg	2326

To manufacture the PCC slab, the aggregates and cement were mixed for 1 minute using a concrete mixer as shown in Figure 3.15(a). Following that, water was added and the materials were mixed until a homogeneous mixture was achieved. The samples were prepared in steel rectangular moulds of 306 mm x 306 mm by 130 mm height. The roller compactor (originally

used for the asphalt slab), as seen in Figure 3.15(b), was used to compact the loose material so that it achieved the target air void content and density. The roller compactor compacted the mixture to an estimated height of 50 mm.

(a) (b) (c)

Figure 3.15. Preparation of concrete slabs by roller compactor: (a) concrete mixer; (b) roller compactor; (c) PCC slab before and after compacted

3.6. Experimental Program

The laboratory tests in this research were performed for two purposes: (1) to investigate the performance of hot mix asphalt (HMA) and warm mix asphalt (WMA) in terms of rutting resistance and interface shear-bond susceptibility at high temperature during an overlay's early life, so as to determine the allowable temperature at the opening to traffic, and (2) to investigate the effect of water spray for asphalt rapid cooling on the durability and moisture damage susceptibility of newly laid asphalt pavement. Laboratory tests, equipment and description of each test for this study are presented in Table 3.10.

3.6.1. Repeated Load Axial Test (RLAT)

The Repeated Load Axial Test (RLAT) or uniaxial dynamic creep test, was carried out to investigate the permanent deformation behaviour of asphalt mixtures under dynamic loads. The test consists of applying uniaxial repeated compressive stress to cylindrical asphalt specimens. In this research, an 8kN load is constantly applied for 1s followed by a 1s rest period (frequency of 0.5 Hz) in square waveform. All tests were performed on gyratory compacted specimens 100 mm in diameter by 60 mm high (Figure 3.16). The apparatus used for the experiment is a universal testing machine (NU14) available at the University of Nottingham, see Figure 3.18(a).

Table 3.10. Test and Equipment for the research

Test	Standard	Description	Apparatus	Settings
Determination of bulk density	BS EN 12697-6:2012 (BSI 2012c)	Test for determining the bulk density of a compacted bituminous specimen	-	-
Repeated load axial test (RLAT)/ uniaxial dynamic creep test	BS EN 12697-25:2016 (BSI 1996, BSI 2016)	Test for determining the performance of asphalt mixtures to rutting resistance subject to unconfined repeated loading	Nottingham Asphalt Tester /NU-14	Test temperature: 50,60,75, and 85°C Test stress: 1000 kPa Loading form: square Rest period: 1 sec Load pulse width: 1 sec Number of loads: 2000 Sample thickness: 60mm Sample diameter: 100mm
Wheel Tracking Test	BSEN 12697-22:2003 (BSI 2003a)	Test for determining the asphalt mixture susceptibility to permanent deformation under field-like load	Wheel-tracker	Test temperature: 60°C Contact area: 1196 mm^2 Tyre pressure: 620 kPa Load pass: 2000 Frequency: 26.5 loads/min
Interface Shear Bond Tests	BS EN 12697-48:2019	Test for determining the interface shear bond strength of asphalt mixture layers	Instron universal testing machine + shear frame	Test temperature: 60,70, and 80°C Sample dimension: 100mm x 100mm x height Loading rate: 50mm/min Normal load: 0, 0.15, 0.3 MPa
Cantabro Mass Loss Test	TxDOT: TEX-245-F And ASTM D7064 (ASTM International 2013)	Test to measure the mixture durability and its resistance to abrasion	Los Angeles abrasion machine	Sample dimension: ⌀150 mm × 110 mm Test temperature: 25°C Revolutions: 300
Indirect Tensile (IDT) Strength Test	ASTM D6931-17 (ASTM 2017)	Test for estimating the mixture potential for rutting, cracking and moisture susceptibility	Instron universal testing machine + ITS frame	Specimens: 100 mm × 65 mm Test temperature: 25°C Loading rate: 50mm/min

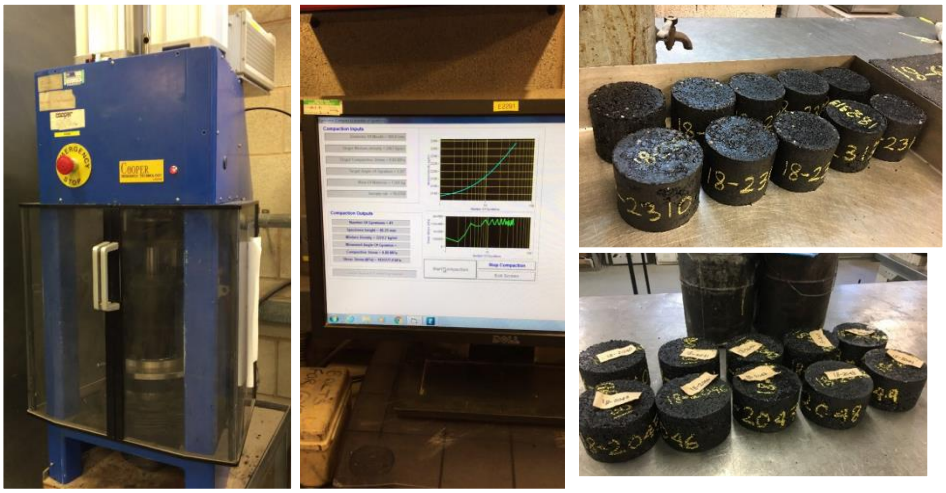

Figure 3.16. Gyratory compactor and produced specimens

The typical schematic cycle is shown in Figure 3.17. The RLAT was performed for 2000 load cycles or until the specimen failed (20mm of deformation). The result of the RLAT is presented as accumulated permanent deformation versus the number of cycles, as shown in

Figure 3.17. As illustrated in this figure, the total strain in each load cycle can be decomposed into recoverable and irrecoverable strain. The recoverable strain contains the strain in application phase, elastic strain (ε_e) and the strain in relaxation phase, viscoelatic strain (ε_{ve}). Meanwhile, the irrecoverable strain is represented as plastic strain (ε_p).

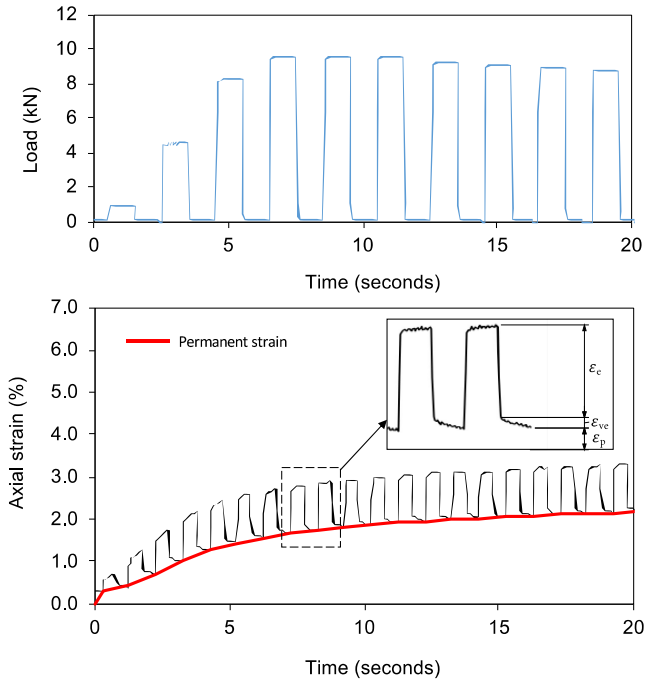

Figure 3.17. Typical load pattern of RLAT and Development of the axial deformation

3.6.1.1. Specimen conditioning at high temperature

To investigate performance at high temperature, all specimens were temperature conditioned in a separate oven or in the NU14 climate cabinet for 5 hours before testing. For RLATs performed at test temperatures of 50 and 60°C, the sample conditioning was carried out directly in the NU14 temperature cabinet (Figure 3.18a). However, for each RLAT with test temperatures higher than 60°C, the specimens were conditioned first in a separate high-temperature oven and were then quickly moved to the test cabinet just before the test. This is for safety reasons, as the test machine could only be operated at a maximum temperature of 60°C. In addition, for all elevated temperature tests (75 and 85°C), the testing temperature cabinet for the test was set to 60°C to minimize a specimen's temperature drop during the test. Furthermore, the specimen's temperature was monitored frequently using an infrared thermometer (see Figure 3.18c). In the separate oven, the temperature during conditioning was set 5°C higher than the targeted test temperature to anticipate the temperature drop when transporting specimens. The test was

commenced when the monitored temperature at the surface-centre of the specimen displayed the targeted temperature.

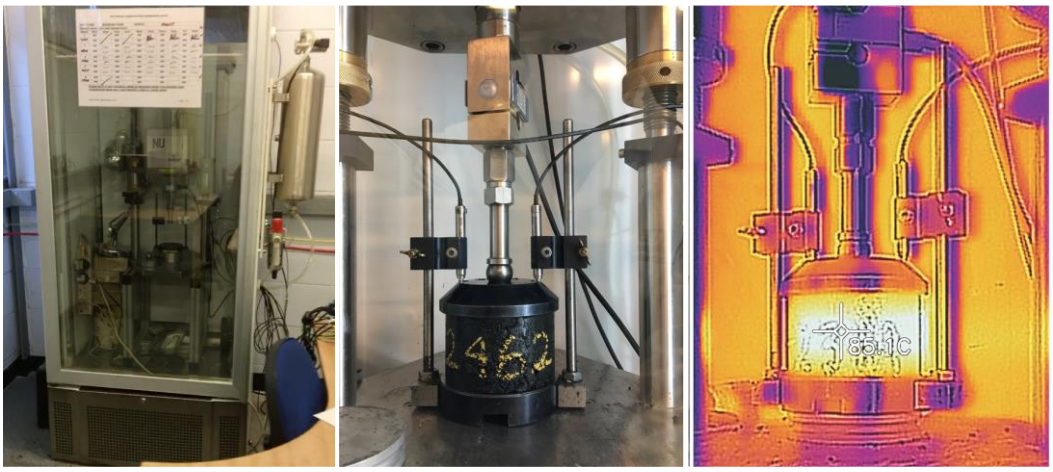

(a) (b) (c)

Figure 3.18. Configuration of RLAT: (a) NU14 equipped with temperature chamber, (b) RLAT setup, (c) temperature monitoring

However, infrared thermal can only measure the specimens' surface temperature. Thus, a two-dimensional heat transfer simulation was developed to predict the inner temperature of specimens during transporting and testing (Figure 3.19a). The predicted surface temperature from the model was compared to the infrared-gun measurement to evaluate the accuracy of the model. In this study, the typical thermal properties of asphalt mixtures and stainless steel plate are assumed. The ambient temperature of 60°C (inside the cabinet), low convection coefficient (0.5 $W/m^2 \cdot K$), and radiation are also considered.

It can be seen in Figure 3.19a that the temperature at the specimen surface and bottom-side drops rapidly. This is as expected, because of its direct contact with the stainless steel plate, which has a lower temperature (60°C). Furthermore, the result, as displayed in Figure 3.19b, shows a good agreement between the prediction (model) and infrared measurements hence it can be used for inner temperature prediction. It was found that the average temperature difference between the surface and the centre of the specimen was approximately 2.5°C. Based on this analysis, it can be concluded that the differences between surface and inner temperature are relatively low when the test started (after being transported from the oven), and thus the infrared thermometer can be considered a viable tool for the temperature monitoring. After 100 load cycles, the specimen temperature at every location dropped by about 5°C, where the centre of the specimen is the location with the highest temperature. Since only a few load cycles (during

traffic opening) is the interest of this study, the temperature drop is presumably acceptable to represent the cooling of newly laid asphalt in actual pavement field conditions.

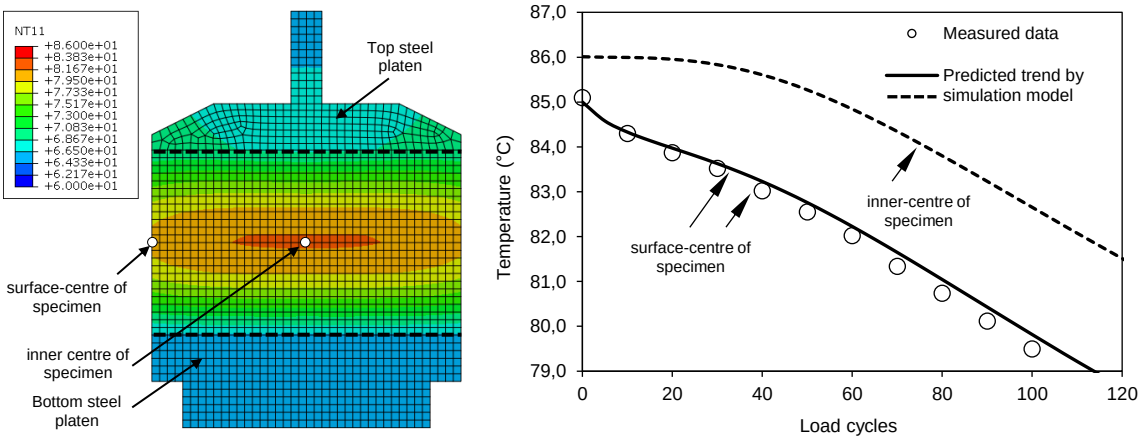

Figure 3.19. (a) Heat transfer model of RLAT specimen at 0 cycles; (b) data measurement and prediction trend of specimen's temperature

3.6.1.2. Test Program

To investigate the rutting performance of asphalt mixture at the elevated temperatures at the opening to traffic, asphalt mixtures containing six different bituminous binder (both HMA and WMA) as displayed in Table 3.2, were tested. Two different load levels: 8 kN and 5 kN, equivalent to axial stresses of 1020 kPa and 630 kPa were selected for the study. Furthermore, the RLAT was then performed at four different temperatures: 50°C, 60°C, 75°C and 85°C, for each specimen. The results and discussions of the RLAT test will be discussed in Chapter 5 and 6 of this thesis.

3.6.2. Wheel Tracking Test

Wheel tracking test was performed to investigate the rutting resistance of asphalt mixtures under elevated temperatures. In this study, only a small number of wheel tracking tests (2 asphalt slabs) were performed in the laboratory. The test was carried out only to validate the rutting analysis derived from RLAT data – discussed in Chapter 5. The test was performed conforming to BS EN 12697-22 (BSI 2013a). As shown in Figure 3.20, a solid tyre with outer diameter of 200 mm and width of 50 mm, moved back and forth in the middle of the 306mm x 306mm x 60 mm specimen at the speed of 26.5 loads/min (0.8Hz) with a travel length of 225 mm. The load applied was 742 N (0.62 MPa) and the test duration was 2000 passes. The asphalt slab was prepared by a roller

compactor and then conditioned in an environmental cabinet for a minimum of 6h to reach the temperature equilibrium. This test was performed at 60°C for 5000 cycles, and the total permanent deformation/strain was used to validate the rutting analysis, to be discussed in Chapter 5.

Figure 3.20 Wheel Tracker Machine (Al-Mosawe 2016)

3.6.3. Interface Shear Bond Tests

In this research, the interface shear bond test was carried out to study the ISS of a multi-layered pavement interface at high temperatures. A direct shear test was carried out using a universal testing machine on standard specimens of cubic-shaped double-layered samples. This test was performed following BS EN 12697-48 (BSI 2013b). The following section will discuss the specimen preparation, equipment design and procedure of the test.

3.6.3.1. Specimen preparation

The main test was conducted on block specimens (100 mm x 100 mm x h). Two types of existing layers (lower layers) were investigated in this study: asphalt concrete course and PCC slab. To produce the specimens, a slab consisting of a 50-mm asphalt concrete or a PCC topped with a 50-mm thick asphalt overlay layer was compacted inside a steel mould of 306 mm x 306 mm using a roller compactor (Figure 3.21a). The lower layers were left in moulds for 24 hours before a tack coat was applied (Figure 3.21b) and the upper layers placed (Figure 3.21c). After extraction (Figure 3.21d), the slabs were cut/ trimmed into the intended specimen size, as can be seen in Figure 3.21e and Figure 3.22.

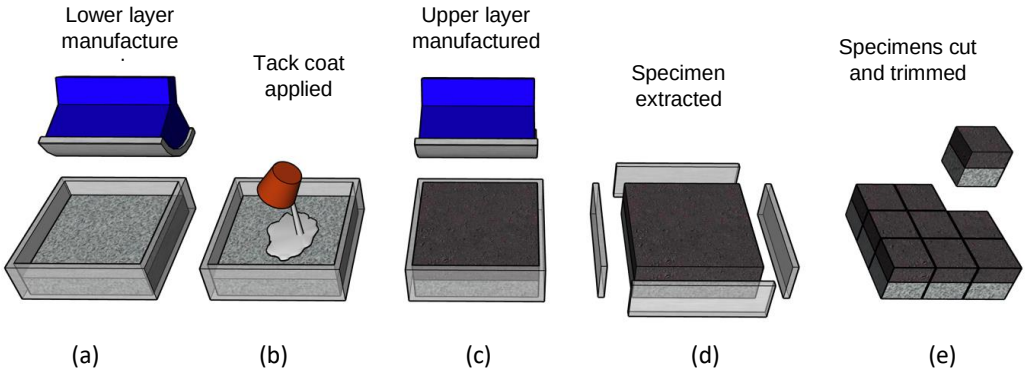

Figure 3.21. Specimens preparation for interface shear bond test

Figure 3.22. Specimens for interface shear bond test after the cut

3.6.3.2. Testing devices and procedure

The interface bond strength test was carried out by using a shear mould specifically developed for the test in this study, see Figure 3.23a. Shear was applied using a hydraulic machine at a rate of 50 mm/min. The test was ended when the interface ruptured. ISS was computed by dividing the peak load obtained from the test by the area of the sheared interface as shown in Equation (3.1.).

$$\tau = \frac{F_{max}}{A} \tag{3.1}$$

where τ is the interface shear strength (ISS), F_{max} is the peak load and A is the area of the sheared interface.

To reach the target testing temperature, the specimens were conditioned as for the RLAT, this time at 60, 70 and 80°C, a similar rapid transfer (as RLAT) between the oven and the test apparatus conditioning cabinet, and temperature monitoring (Figure 3.23b) was performed for the higher temperature specimens. It is acknowledged that the temperature of the interface can be quite different from that in the midle of asphalt layer. So, for example, the 80°C for rutting may not necessarily occur at the same time as 80°C for interface shear failure.

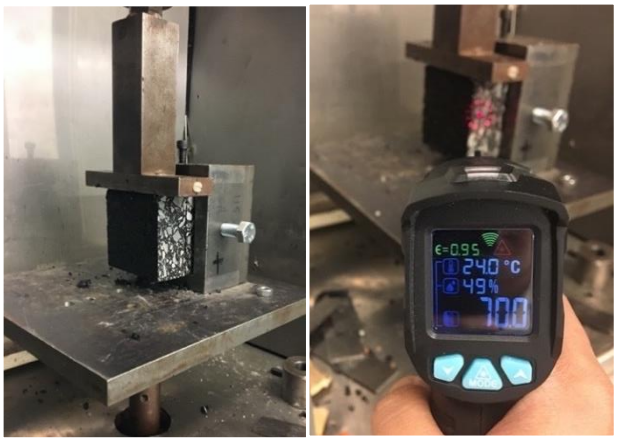

(a) (b)

Figure 3.23. interface shear bond test: (a) test configuration; (b) temperature monitoring

To simulate realistic pavement loading conditions and to obtain shear failure envelopes in the Mohr plane, a compression spring frame was developed to apply the normal load, as shown in Figure 3.24. To apply the normal stress, the compression spring is compressed by tightening the screw nuts. As the spring is compressed, it provides a force (push) to return the spring to its normal height (illustrated in Figure 3.25).

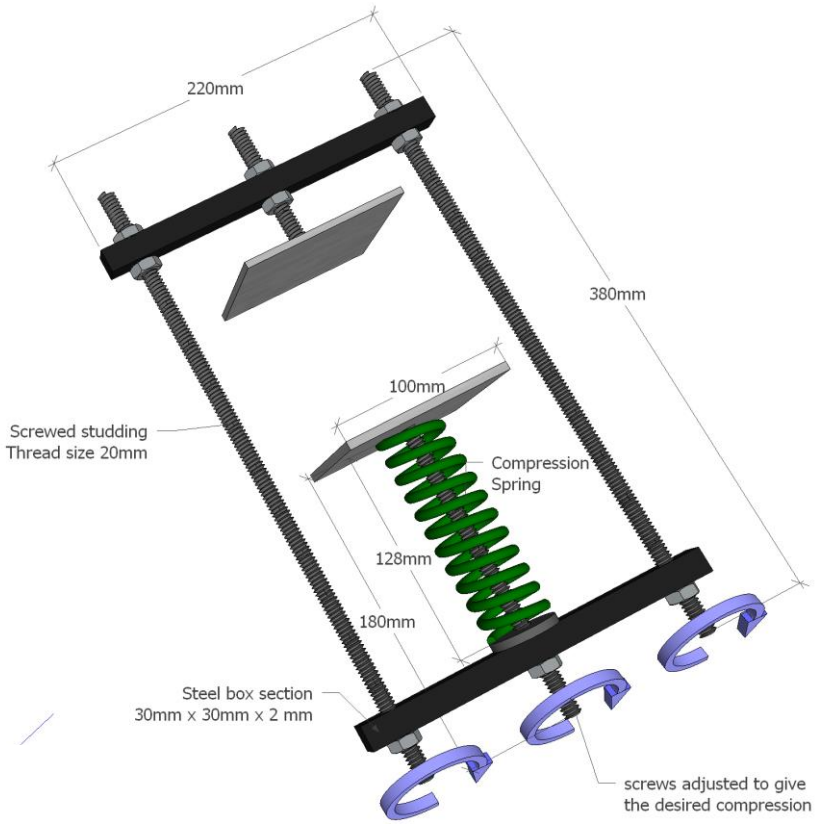

Figure 3.24. Compression frame for the test

Prior to the test, the spring is calibrated using a universal testing machine to investigate the stiffness of the spring, and the length of spring compression needed to generate the normal stress. The spring stiffness and distance needed to general the targeted normal stresses is displayed in Table 3.11. During the shear strength test, the spring is tightened to reach the targeted length. Three different normal stresses: 0, 0.15, and 0.3 MPa were considered in this research. The compression spring conditions at different stress levels are displayed in Figure 3.26.

Table 3.11. Compression springs for the frame

No.	Items	Value
1	D_H (mm)	50
2	D_d (mm)	25
3	L_o (mm)	115
4	Stiffness (N/mm)	81
5	Distance needed (mm) to generate 0.15 MPa	37
6	Distance needed (mm) to generate 0.3 MPa	18.5

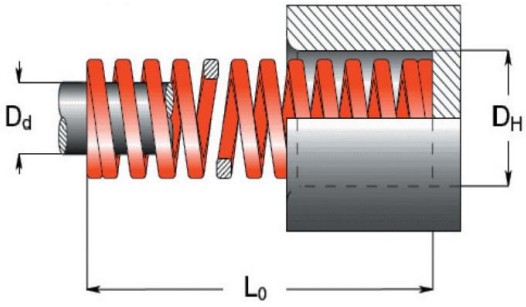

(a) Compression spring dimension

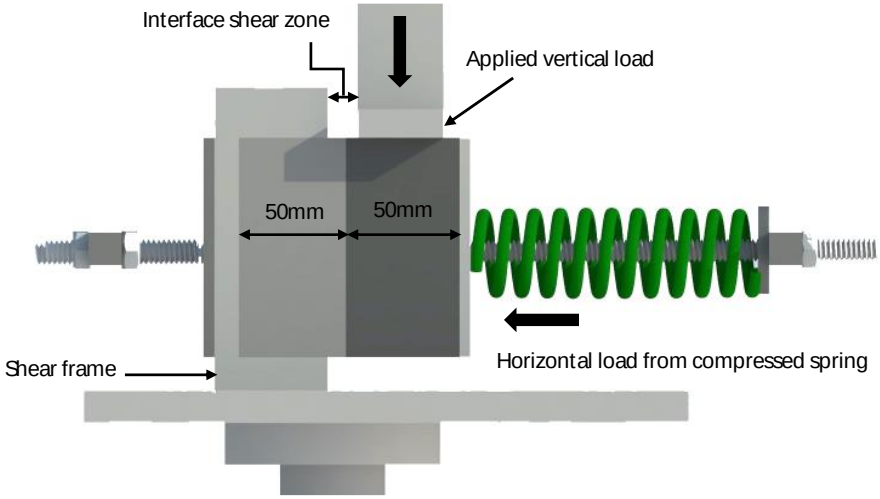

(b) Test schematics

Figure 3.25. interface shear bond test schematics

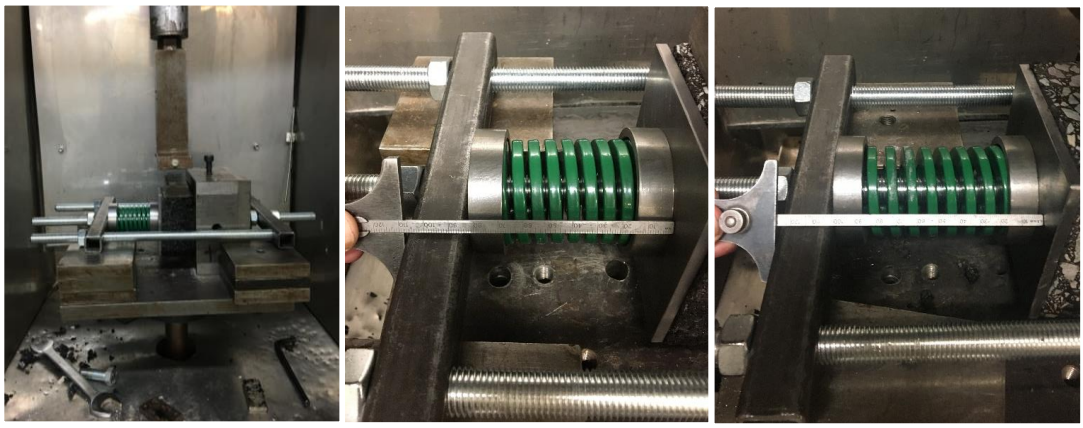

(a) Frame setup (b) 0.3 MPa of load (c) 0.15 MPa of load

Figure 3.26. Compression spring condition at different stress level

3.6.3.3. Test Program

To study the effects of tack coats on interface shear resistance, two different interface treatments were considered: conventional cationic emulsion (K1-40) and SBS polymer-modified bitumen (described in Table 3.12). The materials were selected to represent two different types of tack coats (asphalt emulsion and bituminous binder) commonly used in pavement application (Mohammad et al. 2012). K1-40 denotes rapid setting, cationic emulsion with 40% binder content, while the SBS modified binder consist of 100% bituminous binder without any added water or diluting material. Furthermore, two different pavement surface types: concrete and new HMA; and two different asphalt materials of the upper layer were also investigated its effect on ISS value. The interface condition investigated in this research is shown in Table 3.12. The results and discussions of the test will be discussed in Chapter 5 and 6 of this thesis.

Table 3.12. Experimental program of interface shear bond test

Interface designation	Pavement surface type (lower layer)	Upper layer	Tack coat type
A	PCC	HMA (SBS binder)	SBS binder
B	HMA (pen. 40/60 binder)	HMA (SBS binder)	SBS binder
C	HMA (pen. 40/60 binder)	HMA (pen. 40/60 binder)	SBS binder
D	HMA (pen. 40/60 binder)	HMA (SBS binder)	Emulsion K1-40
E	HMA (pen. 40/60 binder)	WMA (SBS binder+Sasobit)	SBS binder

3.6.4. Water Cooling Measurements

To measure the cooling response of asphalt forced by spray water, five small-scale asphalt slabs consisting of a 40-mm asphalt concrete course topped with a 70-mm thick asphalt overlay layer

were manufactured inside a steel mould of 306 mm x 306 mm using a roller compactor as shown in Figure 3.27. The five specimens represent different cooling strategies: natural cooling and water cooling with various temperature and flow intensities of water, as listed in Table 3.13.

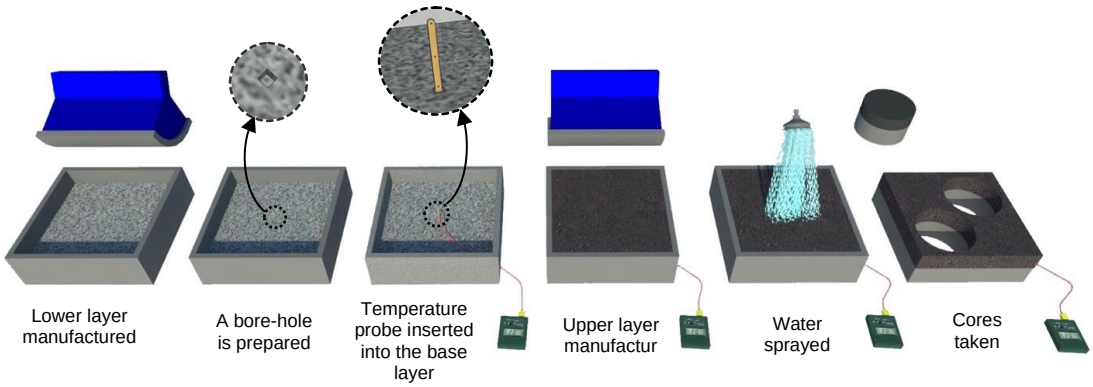

Figure 3.27. Sample preparation and temperature measurement of water cooling

Table 3.13. Spray water intensity and temperature for the test.

Designation	Water intensity (V_w)	Water temp. (T_w)
Normal cooling	None	None
WC1	Rate1 (64 L/ m^2·minute)	Temp1 (10°C)
WC2	Rate1 (64 L/ m^2·minute)	Temp2 (30°C)
WC3	Rate2 (30 L/ m^2·minute)	Temp1 (10°C)
WC4	Rate2 (30 L/ m^2·minute)	Temp2 (30°C)

For each specimen, the aggregates and bitumen were batched as determined in the asphalt mix designs and then heated up and mixed at the designed temperatures according to BS EN 12697-35:2016 (BSI, 2016). The lower layer (40mm) was initially manufactured as the base layer, and it was allowed to cool for 24 hours. A hole was then cut for the temperature probe to be inserted into this layer. The temperature probe consisted of three type-k thermocouples and steel tube support with a diameter of 8mm (see Figure 3.28(b)). The thermocouples were located in the centre of the slab and at various slab depths: one at the middle depth of the new asphalt layer (Z_2), and two at depths of 15 mm (Z_1) and 70 mm (Z_3) of the asphalt slab, see Figure 3.28(a). To protect the thermocouple wires, a groove was made on the base layer using a handheld cut-off saw (see Figure 3.28(b and c)). The thermocouple wires were then inserted into the groove and sealed with silicone sealant.

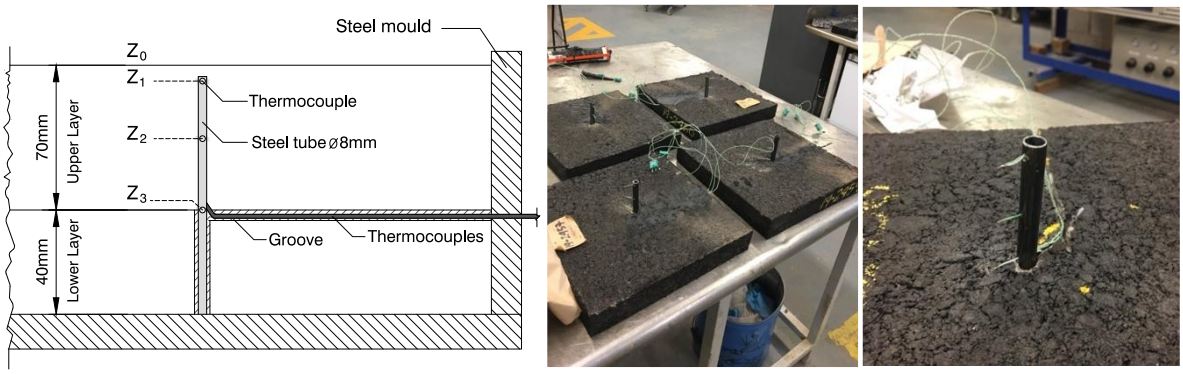

(a) (b) (c)

Figure 3.28. (a) Illustration of thermocouples position in asphalt mat, (b) temperature probe instalment and (c) thermocouple position

Before being overlaid with the upper layer, a tack coat (cationic K1-40) was applied on the lower layer surface at a rate of 0.5L/m^2 to ensure the bond between the upper and lower layers. Following that, the lower layer, the steel mould and thermocouple wires were conditioned at 35°C for 4 hours to represent a typical pavement temperature and condition in tropical countries. After completing this process, the upper layer was then laid and compacted above the lower layer. The specimen was moved into the prepared space/location and placed above a thermal insulation material to keep a thermally insulated boundary condition at the base of the steel mould, which later can simplify the solution of the heat transfer model. A heat loss by natural convection was assumed for the sides of the steel mould, since no side insulation was applied during the experiment. Temperatures were documented using a computer-based data acquisition system, once every one second (1 Hz), after the compaction and during the subsequent spray water cooling.

During the test, the air ambient temperature in the laboratory, as well as the temperature of the mould and the asphalt surface, was frequently recorded using an infrared thermometer. In addition, the exact start time of the mixing, compaction and temperature monitoring were also noted. The specimen manufacturing and temperature measurements were performed in the same location (room) with relatively constant room temperature, wind speed and heat flux (from a lamp bulb) to provide a consistent environmental condition. However, there were slight differences in ambient temperature (1-2°C) across the experiments. The average recorded air ambient temperature was 23.1°C, obtained from the thermocouple measurement. In this research, the water spraying was applied 20 minutes after asphalt compaction, or when the

surface temperature was in the range of 119 to 123°C, for a duration of 60 seconds. The spray water setup is shown in Figure 3.29 and Figure 3.30(b). Clean tap water was used throughout this work. The water flow rate value (as listed in Table 3.13) was selected to represent the actual water tank truck spraying system. Too high a rate of water intensity/flow rate may lead to high stress gradient at the pavement surface and consequently to cracks or fractures, while too low a value will result in slow temperature reduction.

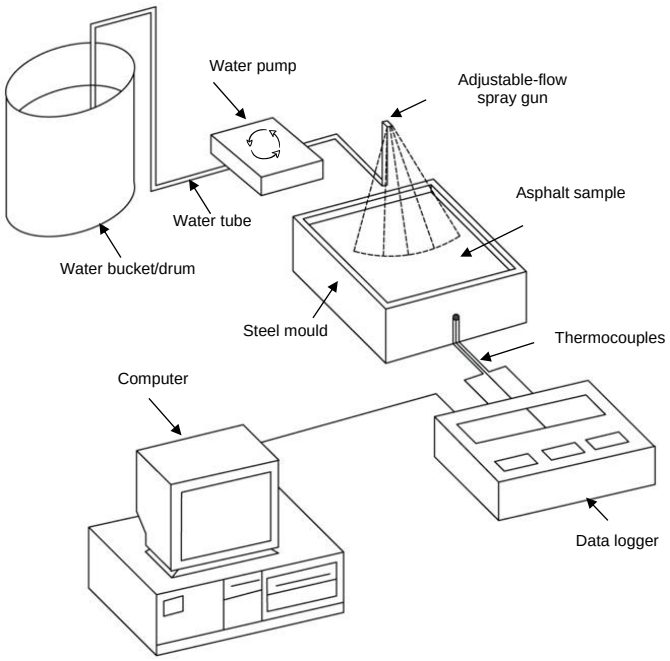

Figure 3.29. Sketch of the spray water cooling setup

(a) (b)

Figure 3.30. (a) Spray water cooling, and (b) Temperature monitoring configuration

To reach the target temperature of the spraying water, the clean tap water was conditioned in the environmental chamber for 4h and then quickly filled into the water bucket/drum before the spray water experiment was performed. To achieve the targeted water flow, a water pump and an adjustable-flow water spray gun (see Figure 3.30(a)) were used. To allow the water to flow off the surface of the asphalt, one side of the steel mould was removed before the spray water was applied. A wooden slat (with a height of 3.5mm) was used to raise the specimen, in order to replicate the pavement transverse slope/ drainage gradient (1%). Finally, to investigate the possible drawbacks of spraying water onto newly laid asphalt, cores were then taken from the affected slab and Cantabro tests and indirect tensile strength tests were performed. The results and discussions of the asphalt cooling response with the water spraying will be discussed in Chapter 7 of this thesis.

3.6.5. Cantabro Mass Loss (CML) Test

To investigate the potential durability drawback(s) of spraying cooling water onto hot asphalt pavement, the Cantabro Mass Loss (CML) test was performed. This test evaluates the breakdown of compacted asphalt specimens that are placed in a rotating drum (of the Los Angeles Abrasion machine). As the drum rotates the compacted specimen degrades by abrasion. The change of mass divided by the original mass of the specimen is specified as a mass loss (ML). Higher ML values suggest a mixture with lower durability and higher susceptibility to weathering and brittleness-related distress (Doyle and Howard 2016, Cox et al. 2017).

CML is commonly used for open-graded porous asphalt to examine its mixture durability as recommended by the ASTM International (2013) specification (D7064M-08). Recent studies (Cox et al. 2017, Doyle and Howard 2016) suggest the suitability of using CML for dense graded asphalt. Cox et al. (2017) investigated thousands of CML measurements on dense graded asphalt from three projects from the last few years. The results indicate the usefulness of the Cantabro mass loss (ML) values in predicting durability and brittleness of asphalt mixtures. Furthermore, Bazuhair et al. (2018) stated that CML results were able to reasonably predict various environmental effects on asphalt performance. The CML test is explained in detail in the following references (Texas Department of Transportation 2019, Cox et al. 2017, Doyle and Howard 2016, Doyle and Howard 2011).

For this research, CML testing was conducted on 150 mm ⌀ × 110 mm cored specimens conditioned at a temperature of 25°C for 24 hours in a temperature-controlled cabinet. The cored

specimens were taken from newly laid slabs affected by water spraying, see Figure 3.27. The asphalt specimens were exposed to 300 revolutions at 30 to 33 rpm in an AASHTO T96 (Los Angeles) abrasion drum (Figure 3.31(a)) without steel spheres. The large part of the asphalt sample was extracted from the drum, gently wiped off with a rag and weighed in the balance. Before and after the test, the mass of the asphalt specimen is noted and the mass loss of the specimen after the test is measured as a percentage of the initial mass. Before each test, any residual leftover from the previous test was cleaned from the Los Angeles drum to ensure that there would be no variability contributing to the tests. The mass loss (ML) values for the affected spray water slabs were compared to the ML of mixtures that had not received spray water to investigate the effect of spraying water onto newly laid asphalt on its durability.

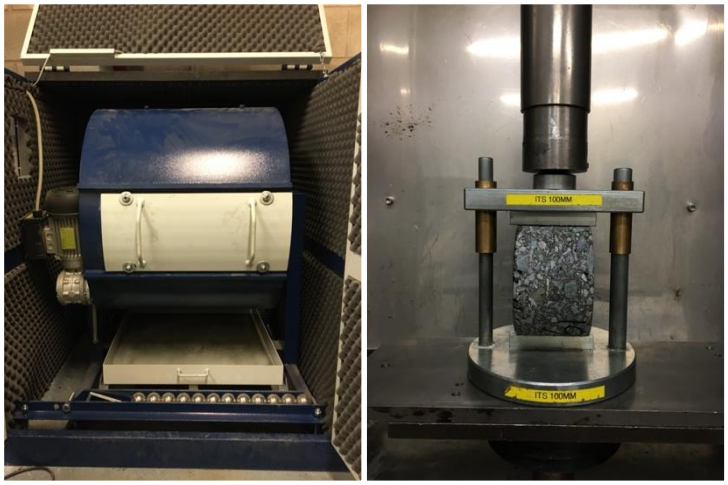

(a) (b)

Figure 3.31. (a) Los Angeles abrasion drum, and (b) Indirect tensile strength test configuration

3.6.6. Indirect Tensile Strength (IDT) Test

The application of spray water onto the newly paved asphalt may cause moisture damage to the asphalt mixture. Spray water may lead to stripping of bituminous binder from aggregates. The water on the pavement surface would be likely to migrate through the pavement layer and weaken the interface adhesion of mastic and aggregate. The indirect tensile strength (IDT) is one of the commonly used tests to assess the loss of adhesion and cohesion in asphalt mixtures, especially relating to moisture damage (Barman et al. 2018, Arepalli et al. 2019, Do et al. 2019). Greater IDT values commonly indicate the greater ability of a bituminous mixture to resist moisture damage (Xiao and Amirkhanian 2009). In this research, moisture susceptibility was evaluated following ASTM D6931-17 (ASTM 2017) by comparing the indirect tensile strength

(IDT) values of mixtures with natural and sprayed water cooling to examine whether the spray has a detrimental effect on mixture moisture damage. The specimens were prepared and divided into two sets. The first set of specimens, the control group, was intended to measure the tensile strength of specimens with dry/natural cooling. The second set of specimens was used to investigate the tensile strength of specimens with water spray. For all specimens, the IDT test was performed on 100 mm × 65 mm cored cylindrical specimens that had been conditioned at a temperature of 25°C in an environmental chamber for 4 h (Figure 3.31 (b)). A monotonically increasing load at a rate of 50 mm/minute was applied along the diameter using a servo-hydraulic testing system. The ultimate compressive load was recorded to calculate the indirect tensile strength using the following equation (ASTM 2017):

$$S_t = \frac{2000 \times P}{\pi \times t \times D} \tag{3.2}$$

where S_t is the IDT strength (kPa), P is the ultimate load (N), t is the height of the specimen before test (mm) and D is the diameter of the specimen (mm). The tensile strength ratio (TSR) was then computed as follows.

$$TSR = \frac{S_{t,water\ sprayed}}{S_{t,natural\ cooling}} \tag{3.3}$$

where $S_{t,water\ sprayed}$ is the IDT strength (kPa) of specimens sprayed with water and $S_{t,natural\ cooling}$ is the IDT strength (kPa) of specimens subjected to dry/natural cooling.

4. Cooling Response of Newly Laid Asphalt Pavement

4.1. Overview

This chapter reports the development of a simplified one-dimensional (1D) heat transfer model to simulate the cooling response of a newly paved asphalt pavement using general finite-element analysis program, ABAQUS. The cooling model was developed to investigate the cooling response of newly laid asphalt pavement for the purpose of traffic opening decision. Furthermore, factors affecting the cooling response of asphalt overlay were also investigated. The results are used to determine strategies for reducing cooling time of new asphalt to allow airport authorities to quickly open new asphalts to traffic. Eventually, this research phase is intended to answer the following question:

- How do the traffic-opening temperature, warm mix asphalt (lower initial laying temperature) and forced water spray cooling affect the required cooling time before trafficking and/or airport closure time and construction efficiency?

4.2. Thermodynamic Process of Newly Laid Asphalt Cooling

The cooling response of newly laid asphalt mixture is mainly dominated by the climatic conditions of the locale. This mechanism of heat transport in asphalt pavements is governed by thermodynamic principles (illustrated in Figure 4.1): conduction, radiation and convection. The heat flux at the top of the asphalt pavement comprises the fluxes from the air to the surface by radiation from the sun, convection, and heat diffusion (conduction) into the pavement layers underneath. Thermal flux on the surface of an asphalt pavement was described by Lytton et al. (2010):

$$\sum Q = Q''_{solar} + Q''_{rad} - Q_{conv} - Q_{cond} \quad (4.1)$$

where:

Q = the sum of heat flux (W/m²);

Q''_{solar} = thermal flux from total solar radiation (W/m²);

Q''_{rad} = thermal radiation (W/m²);

Q_{conv} = thermal convection between the pavement and the surroundings (W/m²);

Q_{cond} = thermal conduction at the surface of pavement (W/m²);

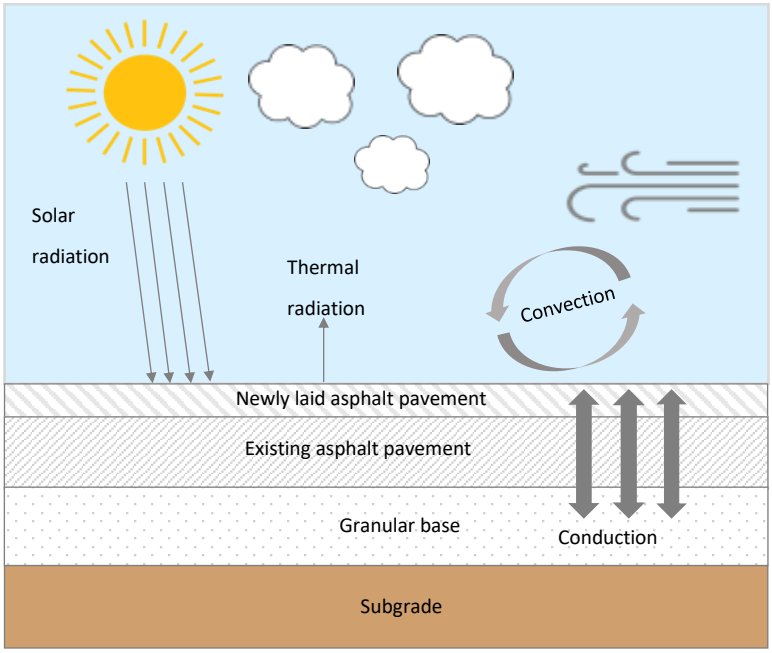

Figure 4.1 Heat transfer model of pavement and the surrounding environment.

4.2.1. Conduction

"Conduction is the transport of energy in a medium due to a temperature gradient, and the physical mechanism is one of random atomic or molecular activity" (Bergman et al. 2011). Whenever a temperature gradient exists in a solid medium, then heat is observed to flow from the hotter part to the cooler part of body (Kreith and Manglik 2011), see Figure 4.2. The conduction of heat within newly laid asphalt and its underlying layers is assumed to be governed by the Fourier law (Rohsenow et al. 1998):

$$Q_{cond} = -k\frac{\Delta T}{L} \quad (4.2)$$

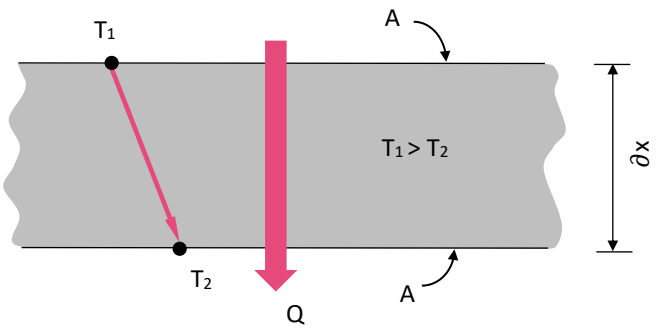

Figure 4.2 Heat conduction through a plane wall of thickness ∂x and area A (Yunus 2003)

Furthermore, the distribution of heat conduction over time and space for two-dimensional (2D) transient analysis is given by:

$$-\left(\frac{\partial Q_x}{\partial_x}+\frac{\partial Q_y}{\partial_y}\right)=\rho C_p\frac{\partial T}{\partial t} \tag{4.3}$$

$$Q_x=-k\frac{\partial T}{\partial x}=k\frac{T_2-T_1}{x_2-x_1} \tag{4.4}$$

and

$$Q_y=-k\frac{\partial T}{\partial y}=k\frac{T_2-T_1}{y_2-y_1} \tag{4.5}$$

where:

Q_x and Q_y	=	thermal conduction in the x and y directions (W/m^2)
ρ	=	material density (kg/m^3)
C_p	=	heat capacity of the material (J/kg.K),
k	=	thermal conductivity of asphalt mixture (W/m·K)
T	=	temperature (K)
∂T	=	temperature different (K)
x and y	=	coordinate direction in two-dimensional space

4.2.2. Convection

"*Convection is the energy transfer between a surface and a fluid moving over the surface*" (Bergman et al. 2011). In newly laid asphalt, the cooling primarily occurs by convection of heat flux between the asphalt surface and the air. The rate of heat transport by convection is defined by 'Newton's law of cooling' below (Rohsenow et al. 1998):

$$Q_{conv} = h_c(T_s - T_a) \tag{4.6}$$

where:

h_c = heat transfer coefficient (W/m^2 ·K)
T_s = pavement surface temperature (K)
T_a = air ambient temperature (K)

Lytton et al. (1993) suggested that the heat transfer coefficient in pavement cooling is a function of temperatures of ambient air and pavement surface along with wind speed. The value of heat transfer coefficient can be estimated using the empirical formula as shown below.

$$h_c = 698.24 \times a\left(0.00144\left\{\text{abs}\left[\frac{(T_{surface} + T_{air})}{2}\right]\right\}^{0.3} \times {v_w}^d + 0.00097(abs(T_{surface} - T_{air}))^{0.3}\right) \tag{4.7}$$

where:

v_w = wind speed (m/s);
a and d = empirical parameters equal to 1.4 and 0.5, respectively; and
abs = absolute value

In addition, there are also numerous empirical equations, as a function of wind speed (v_w), proposed by other researchers to estimate the heat transfer coefficient at the pavement surface. The models of several empirical equations are shown in Table 4.1.

Table 4.1. Previously published data to calculate heat transfer coefficient at the pavement surface

Equations		Model	References
$h_c = 5.8 + 4.1v_w$	(4.8)	Jurges	Dempsey and Thompson (1970), Solaimanian and Kennedy (1993), Hermansson (2004), Mrawira and Luca (2002), Palyvos (2008)
$h_c = 7.55 + 4.35v_w$	(4.9)	Nicol	
$h_c = 1.824 + 6.22v_w$	(4.10)	Kimura	
$h_c = 18.6 \times {v_w}^{0.605}$	(4.11)	ASHRAE	
$h_c = 5.7 + 6.0v_w$	(4.12)	Sturrock	
$h_c = 16.15 \times {v_w}^{0.4}$	(4.13)	Loveday	

4.2.3. Radiation

"*Radiation is the exchange of heat between surfaces, or between a surface and a surrounding fluid, by long-wavelength electromagnetic radiation.*" (Bejan and Kraus 2003).

4.2.3.1. Thermal Radiation

Thermal radiation, Q''_{rad}, is the electromagnetic radiation reflected from a surface due to its temperature. It contains the incoming (Q_{in}), and outgoing, (Q_{out}) long-wave radiation from the atmosphere to the asphalt surface and back. It is determined as follows (Solaimanian and Kennedy 1993, Hermansson 2004, Han et al. 2011):

$$Q''_{rad} = Q_{in} - Q_{out} = \varepsilon_a \sigma T_s^4 - \varepsilon_e \sigma T_a^4 \quad (4.14)$$

where:

Q_{in} = incoming wave radiation heat flow from the asphalt surface (W/m^2);
Q_{out} = outgoing longwave radiation heat flow from the atmosphere (W/m^2);
σ = Stefan–Boltzmann constant (5.67×10^{-8} W $\times$ m^{-2} $\times$ K^{-4})
ε_a = absorption coefficient of the surface;
ε_e = emissivity of the surface;

4.2.3.2. Solar Radiation

The solar radiation heat flux, Q''_{solar}, is the sum of solar radiation received by the surface of the asphalt and defined as follows (Bergman et al. 2011, Han et al. 2011):

$$Q''_{solar} = Q_{solar} - \tilde{\alpha} Q_{solar} = (1 - \tilde{\alpha}) Q_{solar} \quad (4.15)$$

where:

$\tilde{\alpha}$ = the albedo, a measure of how reflective a surface is;
$\tilde{\alpha} Q_{solar}$ = quantity of the solar radiation reflected by asphalt surface (W/m^2);

The intensity of the solar radiation, Q_{solar}, varies with time, and it is specified by geographic coordinate and the angle of incidence between the surface of pavement surface and the sunlight (Alavi et al. 2014). The albedo, $\tilde{\alpha}$, measures how much of the incoming solar radiation that strikes a surface is reflected without being absorbed. Its value ranges from 0 corresponding to a perfectly black body that absorbs all incident solar radiation and 1 corresponding to a perfectly white body that reflects all incident solar radiation. Typically, pavements with a higher level of albedo will absorb less solar energy and have cooler temperatures, whereas those with lower albedos will absorb more solar energy and have higher temperatures. Albedo levels of pavement surfacing materials are affected by several factors, including pavements age, surface colour, surface texture, coarse aggregate colour and environmental location. Many researchers (Alleman and Heitzman 2019, Richard et al. 2015, Li

et al. 2015) suggested that the albedos of aged bituminous pavement are higher than that of the new pavement. This might be associated with a gradual decrease in the surface appearance of the darker bituminous binder and a corresponding increase in the exposure of the coarse aggregate surfaces that has more reflective and lighter colour (Alleman and Heitzman 2019).

4.3. Thermal Properties of Asphalt Pavement Material

The cooling rate of newly laid asphalt pavement greatly depends on the thermo-physical properties of materials. Thermal conductivity, specific heat capacity, and density are the three most substantial properties of a material in a heat transfer analysis. In this sub-section, the typical values and factors affecting the thermo-physical properties of pavement materials are reviewed.

4.3.1. Thermal Conductivity

The thermal conductivity in Equation (4.2) is defined as a material property that indicates the amount of heat that will be transported per unit time across a unit area (Kreith and Manglik 2011). Materials with high thermal conductivity can effectively transfer heat easily (conductor), while materials with a low thermal conductivity will resist heat flow (insulator).

4.3.1.1. Factors Affecting Thermal Conductivity of Asphalt Pavement

a. Aggregate type

   A large proportion of an asphalt mixture is comprised of aggregate; consequently, it has a considerable effect on the thermal properties of asphalt mixtures. Kavianipour and Beck (1977) reported that the wide range of thermal conductivity values of asphalt mixes was caused by variation of aggregate and bituminous binder. Dawson et al. (2012) studied the effect of replacing limestone aggregates with quartzite for asphalt mixtures. It was concluded that the use of quartzite can improve thermal conductivity by about 135%. This finding is in agreement with Côté and Konrad (2005) who showed a superior thermal conductivity of quartzite aggregate as compared to other unbound materials.

b. Additions and admixtures

   Admixtures are the ingredients in asphalt mixtures other than aggregate and bituminous binder. An admixture is typically added to improve the asphalt performance such as workability, strength or durability. Dawson et al. (2012) studied the effect of copper slag, up to 80% of total aggregate volume, on the asphalt pavement thermal conductivity. The

outcome suggested that copper slag slightly improves the thermal conductivity of the asphalt concrete. The finding is consistent with those of other studies (Dehdezi et al. 2011, Cook and Uher 1974). Moreover, Shi et al. (2017) added two different additives: expanded polypropylene (EPP) beads and graphite powders to asphalt mixtures to improve the thermal properties of asphalt mixtures. The results of the study showed that the addition of EPP reduced thermal conductivity by up to 17%; conversely, the addition of graphite powder increased thermal conductivity by up to 43%.

c. Moisture content

Studies investigating the effect of moisture content on thermal conductivity of asphalt mixtures have been carried out by several researchers (Çanakci et al. 2007, Hall and Allinson 2009, Hassn et al. 2016). In general, it was found that thermal conductivity increased with increasing water content of asphalt mixtures.

4.3.1.2. Typical values of thermal conductivity

Typical values of thermal conductivity (k) for asphalt pavement from past studies are recapped in Table 4.2. Hall et al. (2012) presented the lowest value of k (0.6 W/m-K) and Kavianipour and Beck (1977) reported the highest value of k (2.88 W/m-K) for dense asphalt mixture. Jordan and Thomas (1976), Mrawira and Luca (2006), Gui et al. (2007), Zapata and Houston (2008), and Tan et al. (1997) reported intermediate values, see Table 4.2. For the purpose of this study, the selected values of thermal conductivity and specific heat capacity for the analysis are listed in Table 4.5 in the next section.

4.3.2. Specific Heat Capacity

Specific heat capacity is defined as a measure of a material's ability to store thermal energy (Yunus 2003). It refers to the amount of heat required to raise the temperature of a unit mass of a material by one degree (Mrawira and Luca 2006). The value of specific heat capacity is inversely proportional to thermal conductivity (Khan and Mrawira 2008). Typical values of specific heat capacity for asphalt pavement are summarized in Table 4.2.

Table 4.2 Typical thermal properties of pavement material from past studies

Source	Dry density, ρ_d (kg/m^3)	Thermal conductivity, k (W/m$^\circ$C)	Specific heat capacity, C_p (J/kg$^\circ$C)
Asphalt Pavement/HMA:			
Jordan and Thomas (1976)	–	0.80 – 1.06	850-870
Kavianipour and Beck (1977)	2242	2.28 – 2.88	921
Highter (1983)	–	0.80 – 1.60	879 – 963
Solaimanian and Bolzan (1993)	–	0.744 – 2.889	–
Tan et al. (1997)	2203 – 2275	1.32 – 1.49	–
Chadbourn et al. (1998)	–	2.00 – 2.50 (dense) 0.60 – 1.50 (SMA)	900
Mrawira and Luca (2002)	–	1.36 – 1.814	–
Luca and Mrawira (2005)	2295 – 2450	1.452 – 1.812	1116 – 1364
Mrawira and Luca (2006)	2308 – 2456	1.70 – 2.10	940 – 2000
Gui et al. (2007)	2238	1.21	921
Zapata and Houston (2008)	–	0.76 – 1.40	921 – 1674
Wang et al. (2014b)	2350 – 2450	1.5	850 – 860
Hall et al. (2012)	2360-2402 (dense) 1767-2322 (dense)	0.60 – 0.99 (dense) 0.39 – 0.57 (porous)	904 – 912 (dense) 897 – 911 (porous)
Warm mix asphalt/WMA:			
(Zhu et al. 2019)	2350	1.31	950
Granular Base			
Dempsey and Thompson (1970)	–	–	1000
Tan et al. (1997)	1483 – 1613	0.71 – 1.75 (dry) 1.12 – 2.46 (wet)	–
Côté and Konrad (2005)	–	1.99 – 3.39	–
Gui et al. (2007)	2238	1.21	921
Wang et al. (2014b)	2300	1.50	805
Subgrade			
Gui et al. (2007)	1500	1.00	1900
ASHRAE (2010)	1400-1500	0.30 – 2.00	800 - 1100
Wang et al. (2014b)	2200	1.79	1100

4.4. Development of Asphalt Pavement Cooling Model

4.4.1. Choice of modelling technique

A simplified one-dimensional finite element method (FEM) was adopted in this research to simulate the cooling response of a newly laid asphalt pavement during airfield pavement rehabilitation. Based on the literature studies presented before, the use of FEM provides a more versatile and convenient tool than other available methods. The use of FEM enables modelling of a wide variety of thermal properties of materials, multi lift paving operations, complex model geometry and enables prediction of both the surface and internal temperatures of a pavement structure. Additionally, the FEM model is capable of representing the changes in the environmental conditions over the simulation time through the convection coefficient. This

input feature is often not available in other techniques, which allow only constant weather condition input at the start time of the paving.

4.4.2. Finite Element Modelling

A simplified one-dimensional heat transport model of the asphalt pavement structure was developed in ABAQUS (BS Simulia 2016), a general-purpose finite element (FE) software. Thermal transient analyses are carried out to investigate the temperature change of newly laid asphalt overlay for different climatic conditions, construction times and material properties. The multi-layered pavement structure, including asphalt overlay, existing asphalt, granular base course and subgrade are modelled by 4-node linear heat transfer quadrilateral elements (DC2D4). Model geometry, including layer thicknesses and boundary conditions, is presented in Figure 4.3.

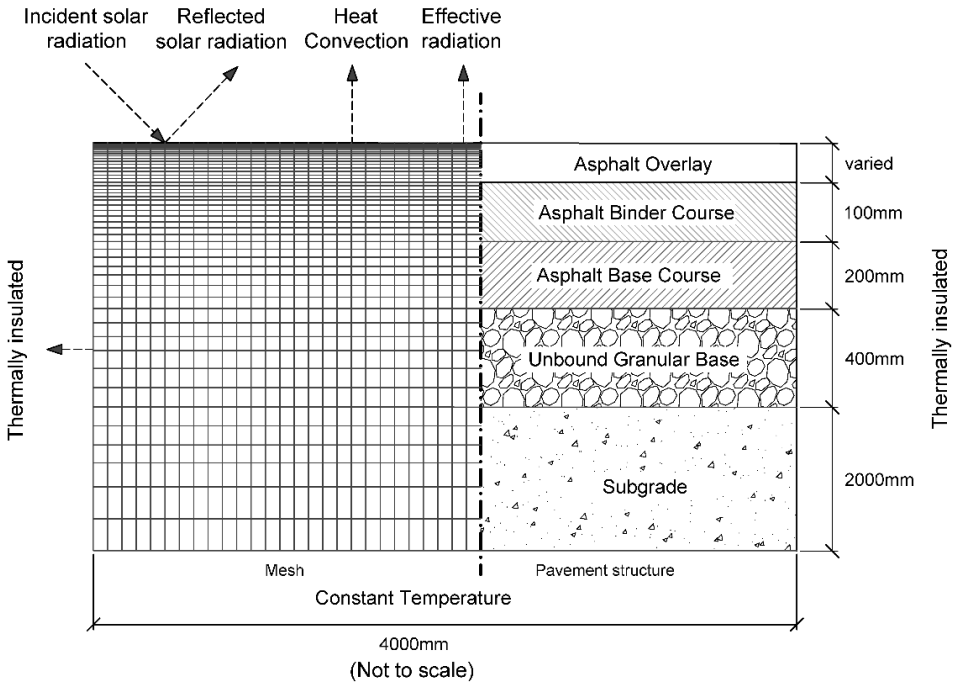

Figure 4.3 Pavement structure diagram used for heat transfer calculation.

The thickness of each layer is based on the typical pavement structure commonly used at airports. The absorbed radiation (including atmospheric and solar radiation), emitted radiation and convective heat transfer at the surface of the asphalt pavement are considered. The bottom boundaries are far from the asphalt. Hence its boundary condition is assumed to be a constant temperature; whereas the right and left boundaries are assumed to be thermally insulated. In

addition, it has been verified that the finite element mesh with a minimum element size of 5mm x 5mm in the freshly compacted asphalt was sufficiently fine to obtain computation convergence.

4.4.3. Model Validation

4.4.3.1. Comparison of FEM Simulation and MultiCool

MultiCool is widely adopted by practitioners as a pre-construction tool to help to estimate the cooling time of asphalt and the suitable temperature range of compaction during paving works. To investigate the efficiency of the presented FEM model, the cooling time results of the FEM model are compared with MultiCool. A typical tropical climatic condition (see the data on the Figure 4.4) was assumed for the analysis. The sky condition was selected to be overcast (night-time construction) and a dense-graded asphalt mix was selected, while the thermophysical properties for the FEM model is tabulated in Table 4.5. The results shown in Figure 4.4 indicate that the predicted temperature matched the result from MultiCool fairly well, especially in the first 30 minutes. After 120 minutes, the asphalt temperatures from the MultiCool analysis (see dotted red line) tend to be higher than the results from the FEM model. The difference is likely to be due to different assumptions of the thermal properties of materials and surface input parameters such as moisture transfer, albedo, asphalt pavement absorptivity and asphalt pavement emissivity (listed in Table 4.5 and Table 4.6).

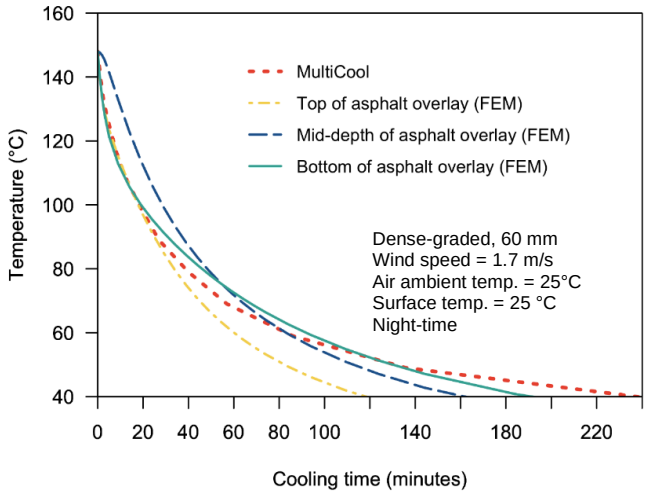

Figure 4.4 Cooling curve of newly laid of asphalt pavement

4.4.3.2. Comparison of FEM Simulation and Field Measurements

To validate the accuracy of the model, the heat transfer model was validated against temperature data from multiple thermocouple sensors inserted in the asphalt course, compiled from four

projects in Minnesota, USA, by Chadbourn et al. (1998) between 1996 and 1997. Table 4.3 presents the project locations and date of data collected. The temperature measurements were made using between four and six thermocouples embedded in the asphalt overlay at various depths (Chadbourn et al. 1998). A typical cooling curve and density reading from the field data are shown in Figure 4.5 for the Highway 52 project, while the asphalt paving conditions for various projects, including the air temperature, wind speed, lift thickness and sky conditions, are presented in Table 4.3.

Table 4.3 Asphalt paving conditions (Chadbourn et al. 1998)

Input	Site A	Site B	Site C	Site D
Location	Highway 52. Rosemount, MN	Ipava Avenue, Lakeville, MN	Ipava Avenue, Lakeville, MN	2nd Avenue, Waite Park, MN
Date and Time	12 July 1996, 9:45 am	13 October 1995, 10:30 am	14 October 1995, 12:15 pm	16 October 1995, 9:30 pm
Air temperature	19.4 °C	16.4 °C	15.4 °C	3.8 °C
Wind speed	16 km/h	16 km/h	3 km/h	2 km/h
Existing surface	HMA (dense)	Aggregate Base	HMA (dense)	HMA (dense)
Existing surface temp.	22.7 °C	19.4 °C	17.8 °C	3.1 °C
Cloud cover	50%	0%	100%	100%
Lift thickness	64 mm	50 mm	50 mm	60 mm

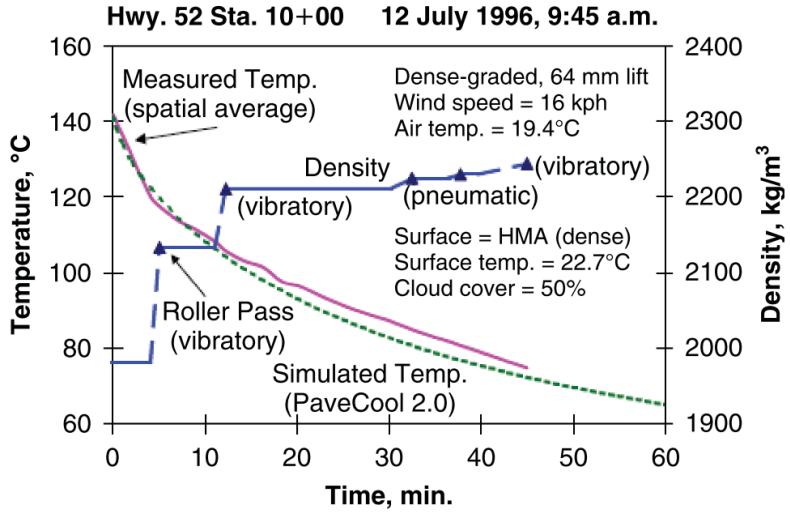

Figure 4.5 Site A. Blue line = density; red line = measured temperature; dotted green line = simulated temperature ((Chadbourn et al. 1998, Vargas-Nordcbeck and Timm 2011)

Using the paving condition data in Table 4.3, analyses were performed to confirm the accuracy of the heat transfer model. Comparisons of the heat transfer model and field data are displayed in Figure 4.6 for temperatures at middle points of the asphalt overlay. The results show a good agreement between the developed heat transfer model and site cooling measurements, confirming the suitability of the developed model.

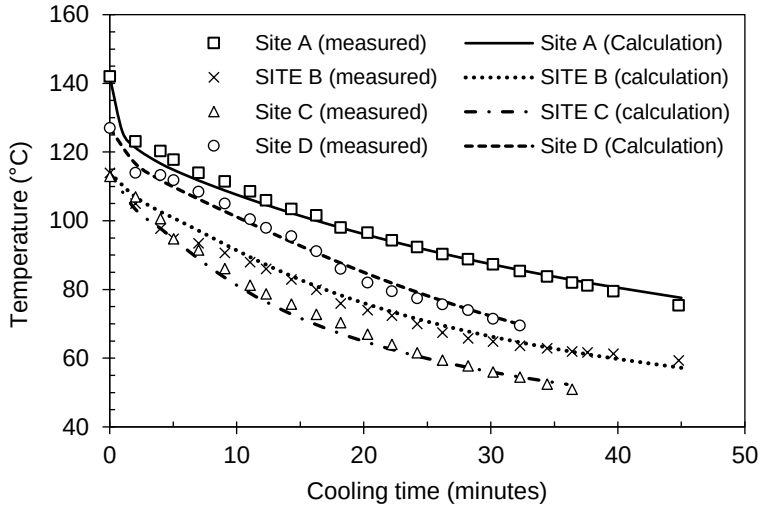

Figure 4.6 Summary of the comparison of the measured and calculated temperature changes at the mid-depth of new HMA layer

To examine the heat transfer model results more objectively, the root-mean-square error (RSME) of the model was used as the objective parameter (Wang et al. 2014b).

$$RMSE = \sqrt{\frac{1}{n}\sum_{i=1}^{n}(T_{i,measured} - T_{i,calculated})^2} \tag{4.16}$$

where:

$T_{i,measured}$ = measured temperature at a specific time point i

$T_{i,calculated}$ = calculated temperature at the same time point

n = number of data

A summary of the RMSE assessment results is presented in Table 4.4. It can be seen that the differences between the measured and predicted temperatures are reasonably small, suggesting a general correspondence between the field measurement and prediction. In summary, the presented model validation analyses have shown that the proposed heat transfer model is sufficiently trustworthy for further analysis of the cooling time prediction of newly paved asphalt pavement. The errors of the numerical model were within the allowable range for cooling prediction of asphalt pavement.

Table 4.4 RMSE results in the comparison of calculated and measured temp.

Comparison	Location			
	SITE A	SITE B	SITE C	SITE D
Number of comparisons	23	23	20	18
RMSE (°C)	4.32	5.03	4.45	2.54

4.4.4. Typical Result of Asphalt Cooling Trend

Figure 4.7 shows graphical screenshots of the output of the FE simulation presenting the temperature variation within the pavement depth at different times for asphalt mixture with a thickness of 70mm under the scenario of a wind speed of 2 m/s in a tropical location during night-time construction, as an example. The predicted temperature distributions in newly laid asphalt in the vertical direction and at different depths and instances, shown in Figure 4.7, were extracted and plotted in Figure 4.8.

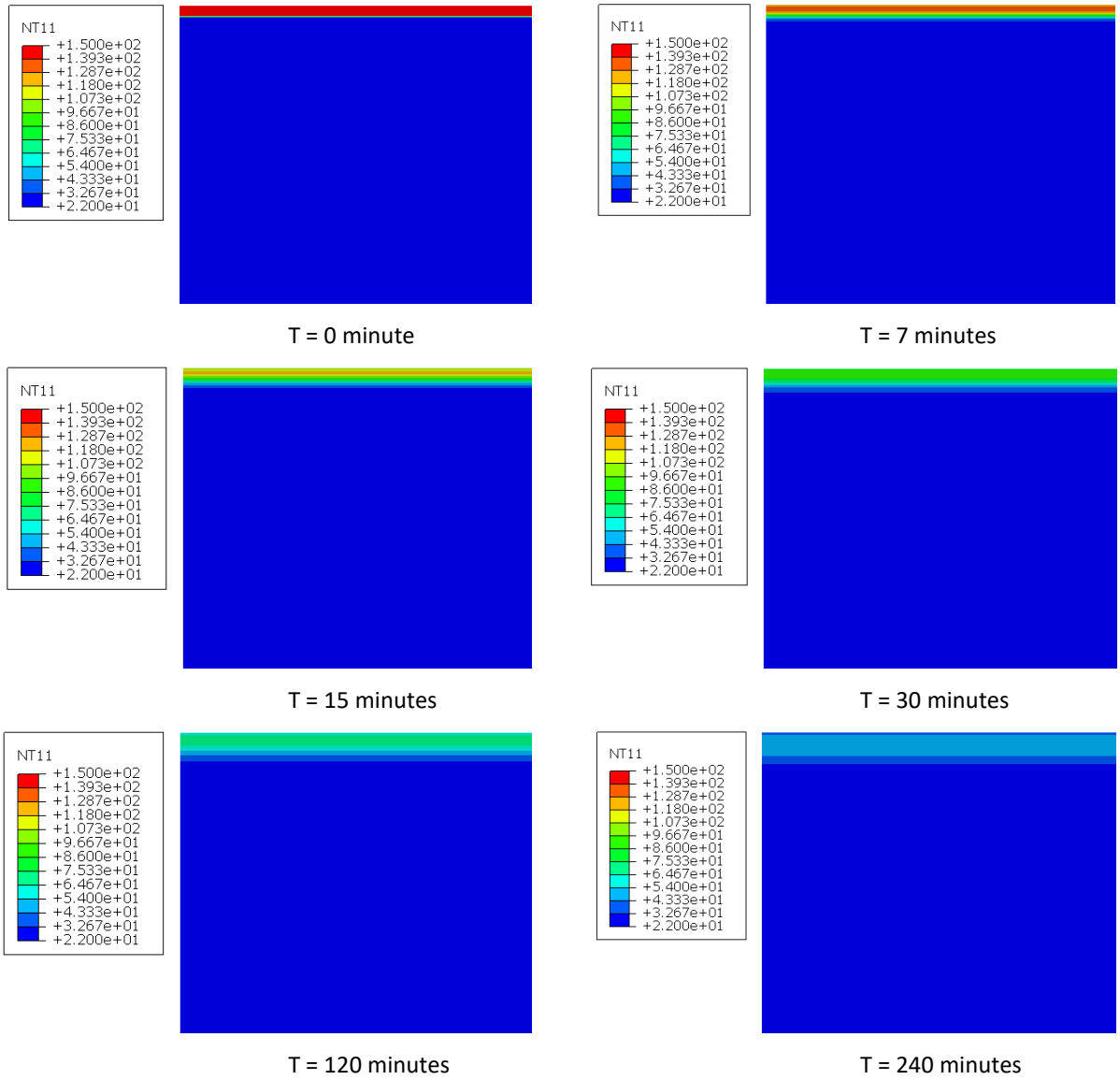

Figure 4.7 Distribution of surface temperature at various time

As can be seen in Figure 4.8, in the first few minutes, the temperature at the bottom of the layer declined rapidly, which is due to its direct contact with the underlying surface. However, after about one hour, the temperature at the base/ bottom quarter of the layer was higher than that at the asphalt surface. Therefore, using the surface temperature as the reference location for traffic opening time may underestimate the internal temperature of the newly laid asphalt. The findings of the current study are consistent with prior studies (Wang et al. 2014b, He et al. 2020). In this research, the temperature at the bottom quarter (3/4 depth) of the asphalt overlay was selected as the reference location for temperature measurement. Based on this finding, for practical implementation to avoid the mis-measurement of newly laid asphalt temperature, it is suggested for practitioners /airport authorities to use embedded thermocouple sensors to monitor the temperature changes within a new layer instead of using an infrared thermometer directed at an asphalt surface.

Alternatively, in the case where the embedded thermocouple measurement is not practical, surface temperature measurement using an infrared thermometer along with pre-determined asphalt cooling prediction can be used instead. The internal temperature of asphalt overlay for decision of opening to traffic can then be approximated using the actual surface temperature in the field and direct conversion using the estimated cooling curves (for different lift depths).

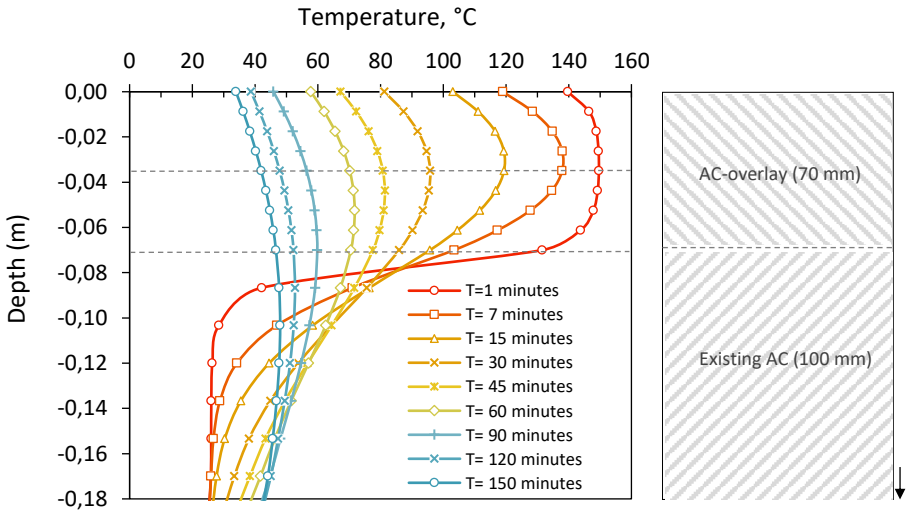

Figure 4.8 Temperature profile of pavement at various time

4.5. Effects of Various Parameters on Cooling Time

In this section, various parameters, including climatic conditions, construction time, wind

speeds, mixture types, initial laying temperatures and layer thicknesses are investigated through case studies to evaluate their effect on cooling response of newly laid asphalt pavement. The purpose of the analysis is to investigate strategies for reducing asphalt cooling time during overlay works to allow airport authorities to quickly open remediated pavements to traffic. Collectively, there were 52 different cases of cooling analysis performed in this research, as displayed in Figure 4.9.

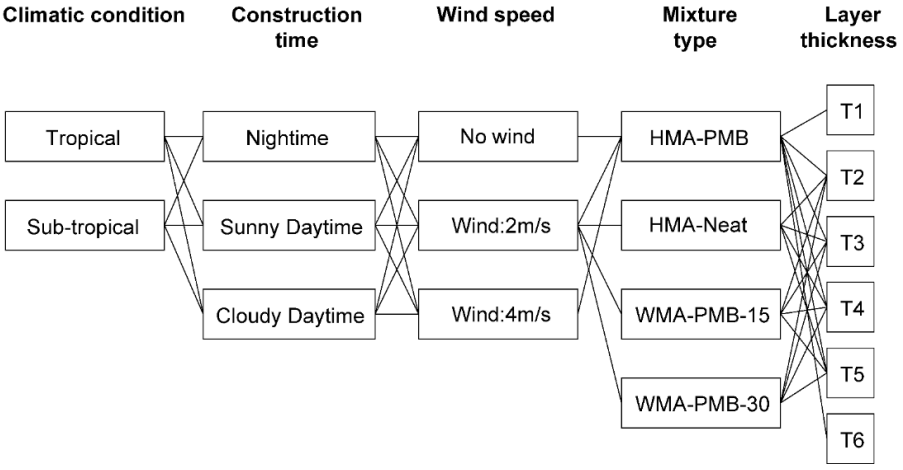

Figure 4.9 Cases studied in asphalt cooling response prediction

Table 4.5 lists the thermal properties and asphalt cooling parameters used in this study. The calibrated thermal properties of asphalt material from an earlier study by Zhu et al. (2019) and Wang et al. (2014b) were used for the cooling prediction. The values are within the range of typical thermophysical properties of pavement materials used by many studies, as presented previously in Table 4.2. The previous heat transfer structure model, displayed in Figure 4.3, was used in this analysis.

Table 4.5 Thermo-physical properties of materials, adopted from Zhu et al. (2019)

Materials types	Thermal conductivity, k (W/K.m)	Heat capacity, C (W.s/kg.K)	Density (kg/m^3)
Asphalt overlay, HMA	1.89	800	2400
Asphalt overlay, WMA	1.61	850	2400
Asphalt binder course	1.89	800	2400
Asphalt Base course	1.50	800	2200
Unbound granular base	1.13	805	2100
Subgrade	1.10	1100	1900

4.5.1. Effect of Environment Condition and Construction Time

In this study, two different climatic locations are studied. The main differences between the two

climatic locations are ambient temperature and existing underlying pavement temperature, see Table 4.6. Moreover, in this study, the wind speed was assumed as an independent factor. The three wind speeds considered: 0, 2, and 4 m/s and their corresponding heat transfer coefficients, are shown in Table 4.7. The wind speed of 2 m/s was selected, from a study by He et al. (2020), as an approximate annual average wind speed near the runway surface in a typical tropical climate. The heat transfer coefficient equation to represent the presence of wind from the Jurges model (Hall et al. 2012), Equation (4.8), was assumed for this study.

Furthermore, three different construction times were analysed: night-time, cloudy daytime and sunny daytime. In this study, night-time construction was assumed to have zero solar flux and the lowest environment temperature, while sunny daytime construction has the highest solar flux and ambient temperature. Cloudy daytime construction has values in between the other two construction times. The value of solar heat flux, ambient temperature and underlying surface temperature for each construction time condition is listed in Table 4.6.

Table 4.6 Parameters for cooling analysis of asphalt layer

Parameter	Values
• Construction time	Night-time and Daytime
• Wind speed (m/s)	Varied, see Table 4.7
• Ambient temp. (°C)	Tropical: 25°C (night-time) 30°C (cloudy daytime) 35°C (sunny daytime) Sub-tropical: 10°C (night-time) 15°C (cloudy daytime) 21°C (sunny daytime)
• Underlying surface temp. (°C)	Tropical: 26°C (night-time) 32°C (cloudy daytime) 38°C (sunny daytime) Sub-tropical: 8°C (night-time) 13°C (cloudy daytime) 19°C (sunny daytime)
• Solar flux (W/m^2)	Cloudy daytime: 500 W/m^2 Sunny daytime: 1000 W/m^2 Night-time: 0 W/m^2
• Asphalt pavement emissivity	0.8
• Pavement Albedo, $\tilde{\alpha}$	0.1
• Stefan-Boltzmann constant,	5.6704E-08 $W/m^2 . K^4$

Table 4.7. Heat transfer coefficient of different wind speed at pavement surface

Wind description	Wind speed (m/s)	Heat transfer coefficient $h = 5.8 + 4.1v_w$
No wind	0	5.8
Light breeze to gentle breeze	2	14
Moderate to fresh breeze	4	22.2

The cooling curves of the hot mix asphalt (HMA-PMB, initial laying temp. of 150°C) with a thickness of 70mm under two different climatic conditions, three different wind speeds and three different construction times are presented in Figure 4.10(a) to (f). Moreover, the cooling times required for all asphalt layers to cool down to 60°C are presented in Table 4.8. The following observations can be drawn from the cooling results:

- The graph reveals that the rate of cooling of the asphalt in a typical sub-tropical zone is higher than that in a typical tropical zone. This is as expected, as the lower ambient and existing pavement surface temperature in subtropical zones will increase the rate of heat loss from hot asphalt.
- The wind speed has a significant effect on the cooling curve. The lower the wind speed, the slower the rate of cooling of both surface and internal temperature of the new asphalt mat.
- The rate of cooling of the asphalt in night-time construction is higher than that in daytime construction. The cooling period of newly laid asphalt pavement during the daytime is significantly affected by solar radiation and relatively higher ambient temperature. It is observed, in Table 4.8, that the length of cooling time needed for asphalt overlay paved on a sunny daytime is more than two times the corresponding time required for night-time work.
- Based on the results, this study recommends that for rehabilitation projects in tropical climatic conditions: (a) night-time construction be adopted as the most ideal option, and (b) asphalt overlay work during sunny daytime should be avoided. However, in a cooler locale, sunny daytime overlay construction may be feasible.

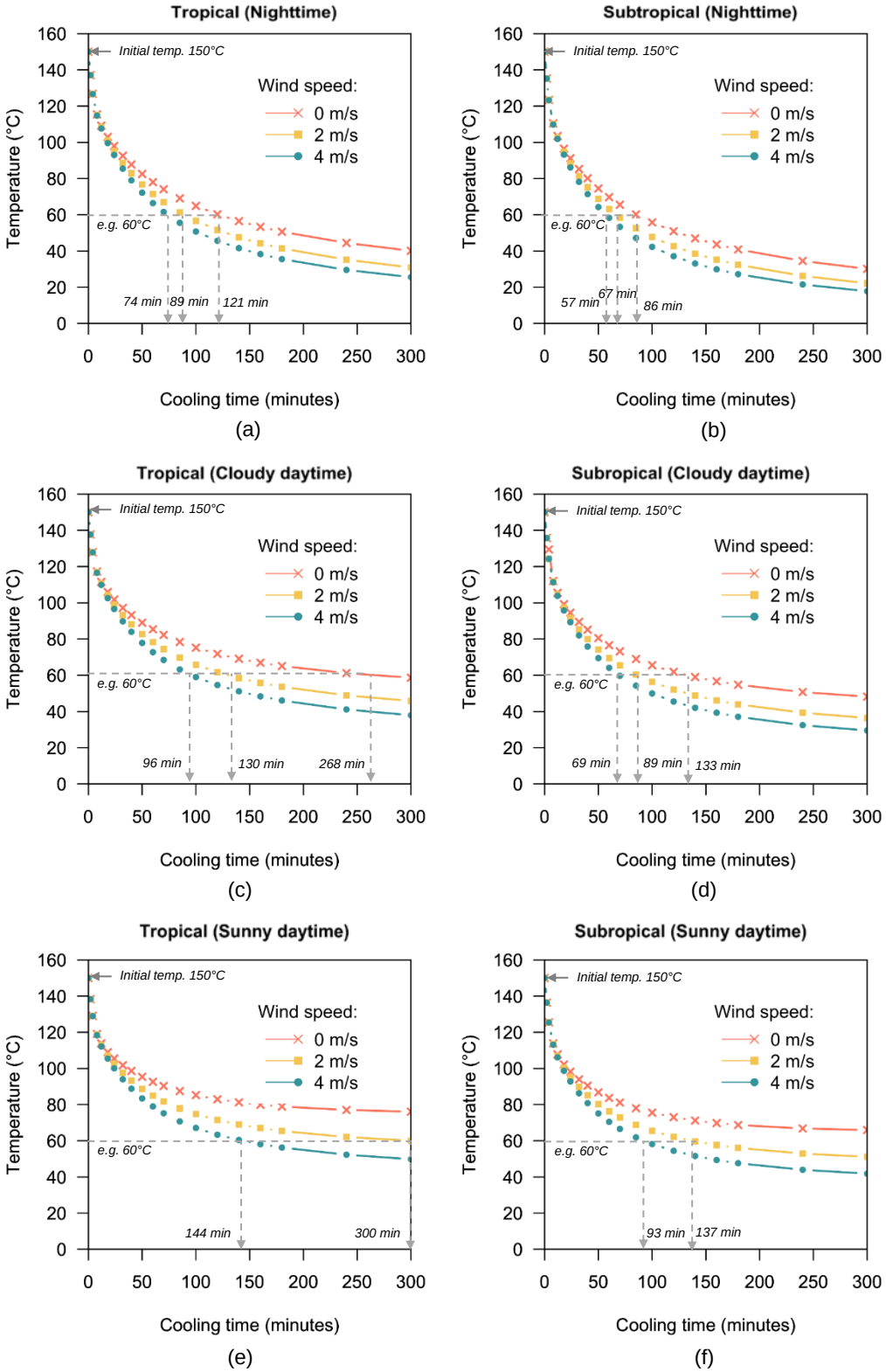

Figure 4.10 Predicted newly laid asphalt cooling in different climatic conditions and construction times for mixture HMA-SBS with a thickness of T1 (70mm)

Table 4.8. Asphalt cooling times needed to reach 60°C for different climatic conditions

Wind speed (m/s)	Cooling time (minutes) needed for asphalt mixtures to reach 60°C, for:					
	Tropical climate condition			Subtropical climate condition		
	Night-time	Cloudy daytime	Sunny daytime	Night-time	Cloudy daytime	Sunny daytime
0	121	268	>720	86	133	>360
2	89	130	300	67	86	137
4	74	96	144	57	69	93

4.5.2. Effect of the Thickness of the Layer (lift)

To investigate the effect of overlay thickness on the cooling rate, six different overlay thicknesses and lift paving operations presented in Table 4.9 were considered. A typical tropical climate during night-time construction under a wind speed of 2 m/s was adopted for the next analysis as it is likely to provide a conservative cooling estimation. In the case of multi-lift paving operation, it is assumed that the first lift is laid and compacted. The next lift is then placed immediately after the first lift reaches 85°C as suggested by Corlew and Dickson (1968). The cooling curves of the four asphalt overlay thicknesses are presented in Figure 4.11(a) to (d).

For the cases studied, it was observed that the greater the overlay, the longer the time needed for the pavement to cool. For instance, as seen in Figure 4.11, the cooling times required for HMA-PMB mixture with a thickness of 70 mm (T2) to reach 60°C is 89 minutes, whereas 144 minutes are needed when the overlay thickness is 100mm (T3). The difference in cooling periods is relatively greater for those cases with multi lift pavement operation. For instance, for the same total thickness of overlay, the required cooling time for single lift 100mm-overlay to reach the traffic-opening temperature of 60°C is 144, whereas the cooling time needed for two lifts (50mm + 50mm) is 150. Based on the results, in the case of the limited construction time available, to reach a rapid cooling, it is preferable to (a) select a thinner total lift depth of the asphalt overlay, and (b) avoid multi lift paving operations.

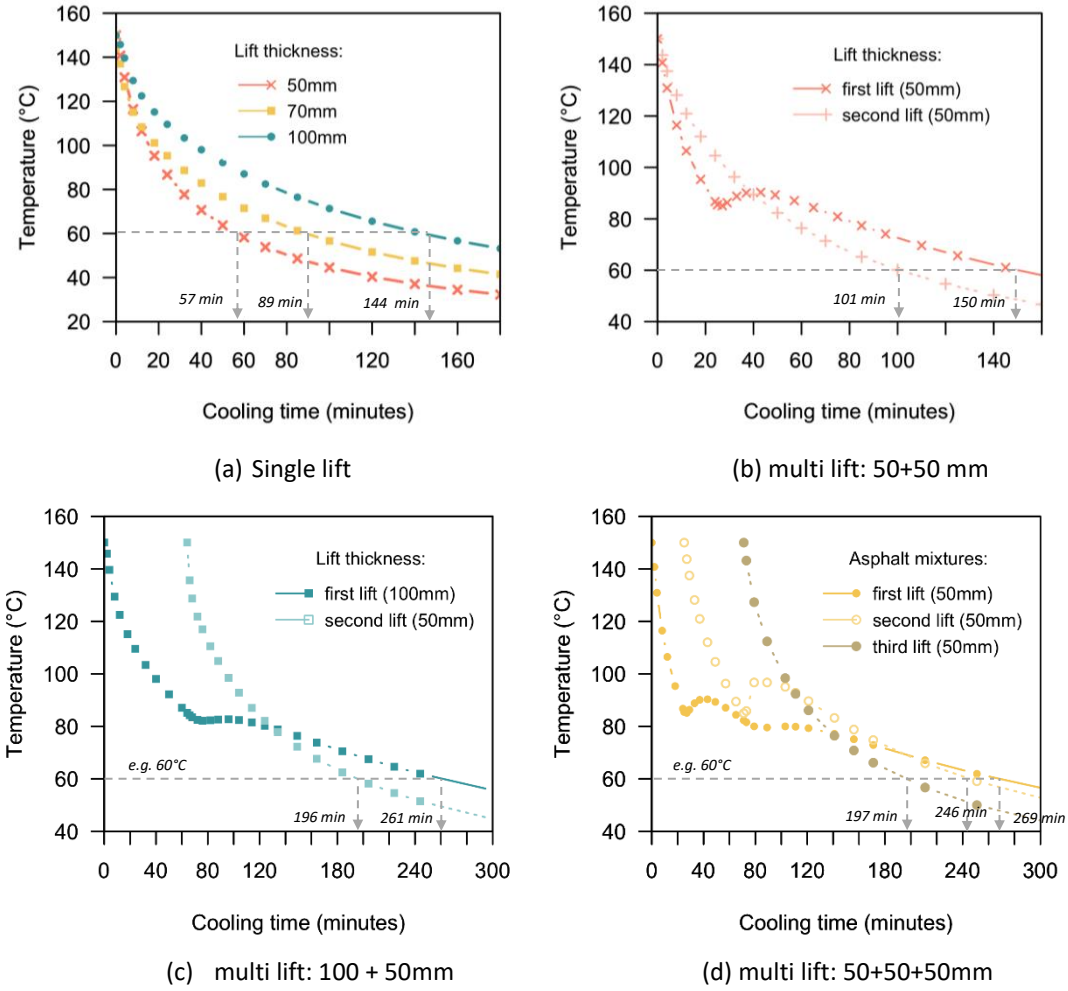

Figure 4.11 Predicted newly laid asphalt cooling with different overlay thicknesses

Table 4.9. Variations of asphalt overlay thicknesses for analysis

Designation	Overlay thickness	Description
T1	50mm	Single lift
T2	70 mm	Single lift
T3	100 mm	Single lift
T4	100 mm	2 lifts. A 50 mm lift and 50 mm lift
T5	150 mm	2 lifts. A 100 mm lift and 50 mm lift
T6	150 mm	3 lifts. 50mm each

4.5.3. Effect of the Initial Temperature (HMA and WMA Mixtures)

Four different asphalt mixes: (a) Hot mix asphalt, HMA with polymer modified binder (PMB), initial temperature of 150°C (b) HMA with neat/unmodified binder, initial temperature of 130°C (c) Warm mix asphalt, WMA-PMB with 15°C temperature reduction and (d) Warm mix asphalt, WMA-PMB with 30°C temperature reduction were analysed in this study to investigate the

effect of initial laying temperature on cooling time in a typical tropical climate. The initial laying temperature of HMA with PMB was assumed to be 20°C higher than that of HMA with neat binder (40/60 pen. grade), as supported by West et al. (2010) and Priyadharshini et al. (2013). It is well known that the addition of polymer increases the viscosity of the binder (Nicholls 1999), and thus requires a higher production temperature for adequate compaction.

The thermal properties for HMA-PMB and HMA-neat were assumed to be the same; however, different thermal properties of WMA and HMA were adopted in this study. A study by Zhu et al. (2019) suggested a lower thermal conductivity and higher specific heat for WMA, compared to HMA, see Table 4.5. In the case of Sasobit/wax-based additive, the reduced thermal conductivity of WMA is likely due to the addition of paraffin wax that has relatively low thermal conductivity. The predicted cooling curves of different asphalt mixes with different initial laying temperatures and lift thicknesses are shown in Figure 4.12(a) to (d). Moreover, the cooling times required to cool down to traffic-opening temperature are tabulated in Table 4.10. From the results, it was found that due to the lower initial temperature, WMA has shorter cooling times as compared to HMA. For instance, in the case of an overlay thickness of 100mm, the HMA-PMB needs 144 minutes to reach 60°C, whereas, only 136 and 111 minutes (8 and 33 minute reductions) are needed for WMA-15 and WMA-30, respectively. The WMA cooling time reductions were greater for those cases with greater overlay thickness (see Table 4.10).

Furthermore, it is also observed that the cooling time differences between HMA and WMA were not only affected by the lower initial laying temperature of WMA but also by the different thermal properties of WMA assumed in this study. It can be seen from the tails of the WMA cooling curves that they get closer and closer to the HMA cooling curve as time goes by. In general, it was observed that the use of WMA, compared to HMA, shortened the closure time of the airport during night-time construction by 6-65 minutes (5-35% reductions), depending on the asphalt overlay thickness, traffic opening temperature, and WMA production temperature. When the WMA is produced at a lower temperature, the airfield closure can be further reduced.

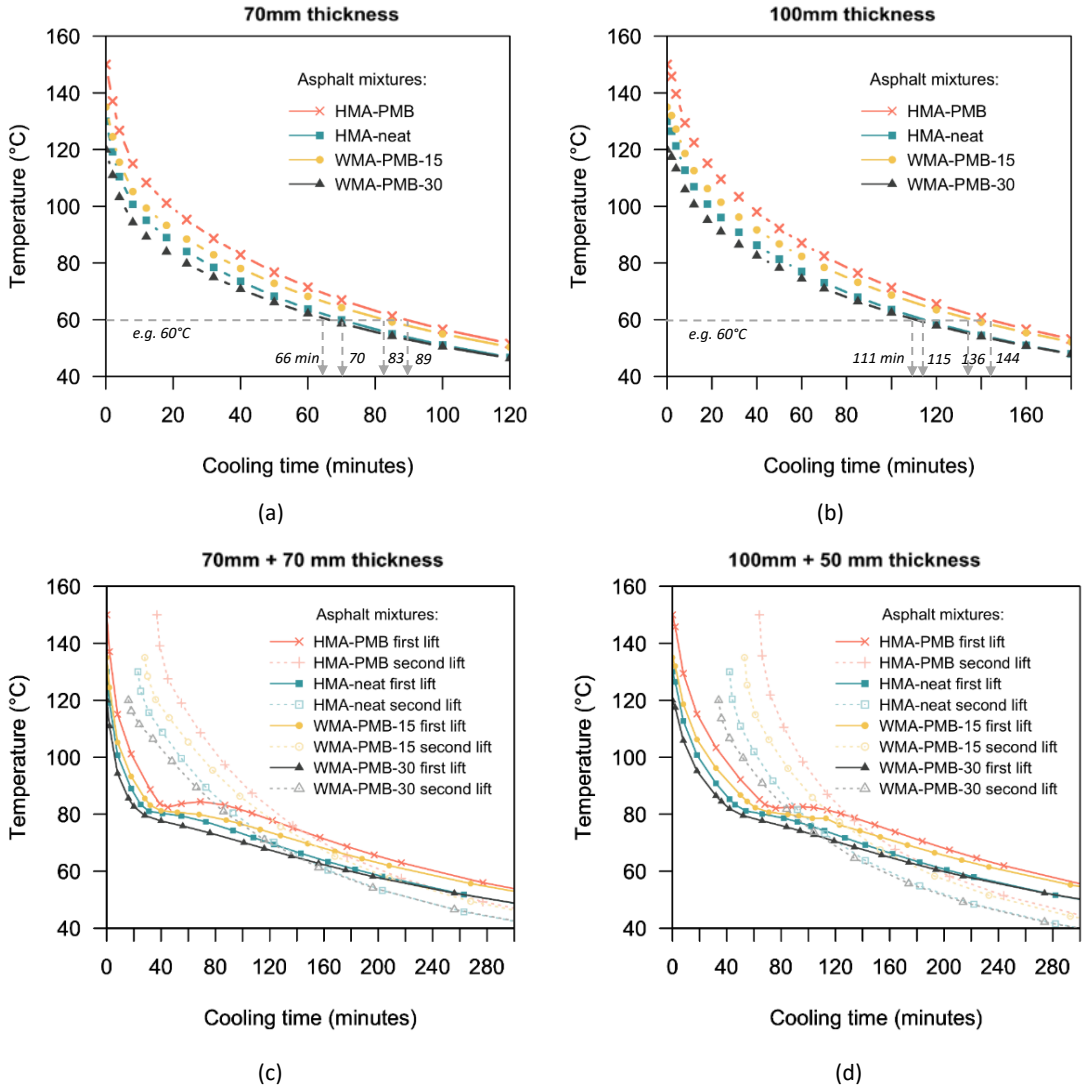

Figure 4.12 Predicted newly laid asphalt cooling; different overlay thickness and mixtures

Table 4.10. HMA and WMA cooling times needed and time saving with WMA during night-time construction

Overlay thickness	Cooling time needed for asphalt mixtures to reach traffic opening temp.:						WMA time saving (minutes) for traffic opening temp.:			
	60°C			70°C			60°C		70°C	
	HMA-PMB	WMA -15	WMA -30	HMA-PMB	WMA -15	WMA -30	WMA -15	WMA -30	WMA -15	WMA -30
70	89	83	66	63	56	42	6	23	7	21
100	144	136	111	105	96	73	8	33	9	32
70+70	243	227	179	169	148	120	16	64	21	49
100+50	261	247	199	188	167	123	14	62	21	65

4.5.4. Effect of Asphalt Temperature at Opening to Traffic

Opening a newly placed asphalt overlay to traffic at higher temperature is expected to reduce the cooling time. In this case, three different asphalt temperatures at opening to traffic: 60°C,

70°C and 80° C were reviewed to study the effect on the asphalt cooling time. The cooling trends of the newly paved asphalt layer for various mixes and thickness in a typical tropical climate, presented earlier in Figure 4.12, were used for the analysis. The times needed for all asphalt mats to cool down to 60°C, 70°C and 80 °C are presented in Table 4.11. From the results, it was found that raising the critical traffic-opening temperature reduced the cooling times needed for asphalt overlay. For the cases studied, compared to the traffic-opening temperature commonly set by many agencies (i.e. 60°C), opening at 70°C and 80°C could reduce the airport closure during night-time construction by 23-73 minutes (27-34% reductions in time to reach 60°C), and 40-132 minutes (47-57% reductions), respectively, depending on the asphalt mixture type, and lift thickness.

Table 4.11. HMA cooling times needed from its laying temperature to various traffic-opening temperature

Overlay thickness	Cooling time needed at the time of opening to traffic (minutes) for:						Reduced cooling time (minutes), compared to traffic-opening of 60°C:			
	HMA-PMB			HMA-Neat			HMA-PMB		HMA-Neat	
	60°C	70°C	80°C	60°C	70°C	80°C	70°C	80°C	70°C	80°C
70	89	63	45	70	47	30	26	44	23	40
100	144	105	76	115	79	53	39	68	36	62
70+70	243	169	126	188	124	94	74	117	64	94
100+50	261	188	129	206	137	96	73	132	69	110

4.5.5. Effect of Surface Input Parameters

A sensitivity analysis is performed in this study to investigate the effect of various surface input parameters, including albedo, emissivity and moisture transfer, on the cooling of newly laid asphalt pavement. Three different values (low, medium and high) of each surface input parameter from the literature (shown in Table 4.12) were used for the analysis. The typical weather condition in a tropical country during cloudy daytime construction (as presented in Table 4.6) and wind speed of 2 m/s was used. Furthermore, asphalt with a lift thickness of 70mm was selected.

Table 4.12. Surface input parameters

Surface input parameter	Values (Low, Medium, High)	Sources
Albedo, $\tilde{\alpha}$	0.05, 0.1, 0.15	Richard et al. (2015), Wang et al. (2014b), Alleman and Heitzman (2019)
Emissivity, ε_e	0.7, 0.8, 0.9	Wang et al. (2014b), Chu et al. (2019), Kassem et al. (2014)
Moisture transfer (heat transfer coefficient)	0, 5, 10 W/m^2	Mieczkowski and Budziński (2019)

The cooling results for different surface input parameters are displayed in Figure 4.13. For the albedo parameter, as seen in Figure 4.13(a), the lower the albedo, the slower the asphalt to cool down because more solar radiation is absorbed by the pavement. However, the effect of albedo on asphalt cooling is considered insignificant. For instance, 149 minutes are required for asphalt with a 0.05 albedo to reach a temperature of 60°C, whereas 140 minutes are needed for asphalt with a 0.15 albedo. It is also noted that the asphalt albedo will not affect the cooling of newly laid asphalt during night-time construction due to the absence of sunlight.

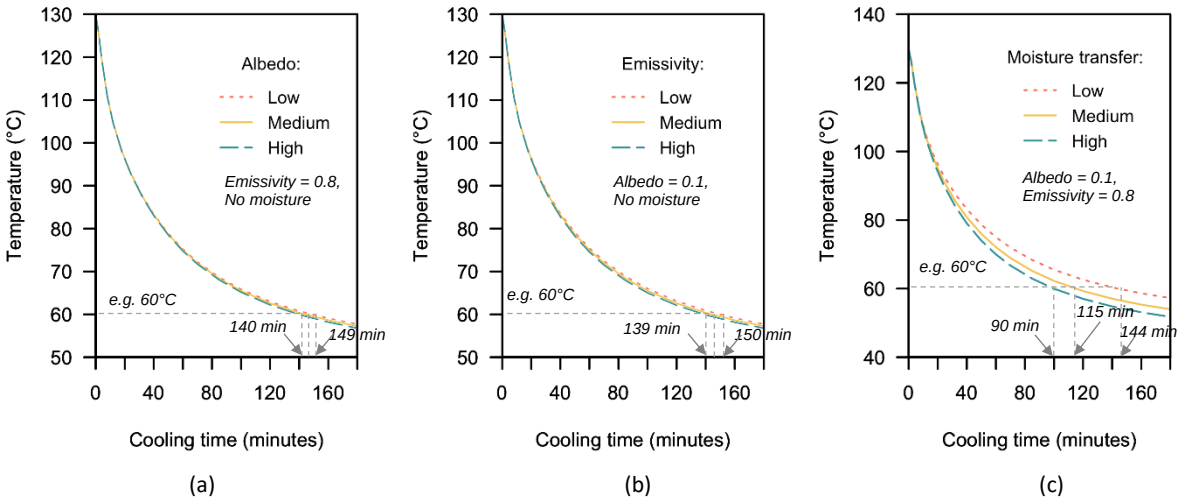

Figure 4.13. Temperatures at the bottom quarter (3/4 depth) of newly laid asphalt, (a) for various albedo values; (b) for emissivity values, and (c) for various moisture transfer.

The emissivity parameter, as seen in Figure 4.13(b), shows the trend of faster asphalt cooling time with the increase of the emissivity value. A high emissivity asphalt has the ability to emit more thermal energy than a low emissivity asphalt, thus, would enable faster cooling. However, the influence of emissivity on asphalt cooling is relatively minor. For the cases studied, the cooling time reduces by 11 minutes for asphalt with high emissivity (0.9), as compared to that with low emissivity (0.7).

The study also investigated the effect of moisture presence on the heat loss of newly laid asphalt. During asphalt construction, the moisture can appear from precipitation or from the wetting system of the compactors wheel to prevent sticking. In this study, the moisture is represented by the convective heat transfer coefficient on the asphalt surface. The heat transfer coefficient values were obtained from an empirical experiment carried out by Mieczkowski and Budziński (2019). Higher values of heat transfer coefficient indicate more moisture/water. The

results, presented in Figure 4.13(c), shows that the asphalt cooling is notably affected by the presence of moisture. For the cases studied, the high moisture content can reduce the asphalt cooling time by as much as 54 minutes. However, it is likely that the high reduced cooling time is largely a consequence of the assumption of a constant value of moisture and associated heat transfer coefficient throughout the analysis whereas, in practice, the presence of moisture is likely to fluctuate across the time of the construction thereby reducing the likely impact.

4.5.6. Effect of Thermal Properties of Pavement Material

It is hypothesized that the more conductive the asphalt mixture, the quicker the cooling will be due to the high rate of heat flow. Conversely, a higher specific heat (C_p) of an asphalt material will result in slower cooling as more energy is stored and must be removed to lower the temperature. In the case of newly laid asphalt, a material with high thermal conductivity and low specific heat will enable a quick opening to traffic. In this study, three different levels of thermo-physical properties of asphalt material from various sources (shown in Table 4.13) were analysed to investigate their effect on asphalt cooling. The typical weather condition in a tropical country during night-time construction (as presented in Table 4.6) was used and kept constant throughout.

Table 4.13 Thermal properties of pavement material

Level	Thermal material properties			
	Conductivity, k (W/K.m)	Sources	Specific heat, C_p (W.s/kg.K)	Sources
Low	0.6	Hall et al. (2012)	850	Wang et al. (2014b)
Medium	1.5	Wang et al. (2014b)	1400	Zapata and Houston (2008)
High	2.8	Côté and Konrad (2005)	2000	Mrawira and Luca (2006)

The cooling results are sketched in Figure 4.14. The analysis in Figure 4.14(a) indicates that cooling of asphalt is significantly affected by thermo-physical properties of the material. Approximately 142 minutes are needed for an asphalt overlay with low thermal conductivity (k) to reach a temperature of 60°C, whereas 84 minutes is needed for asphalt with medium thermal conductivity and approximately 61 minutes when using high thermal conductivity asphalt material. The cooling of asphalt is also considerably influenced by the specific heat (C_p) of asphalt material as shown in Figure 4.14(b).

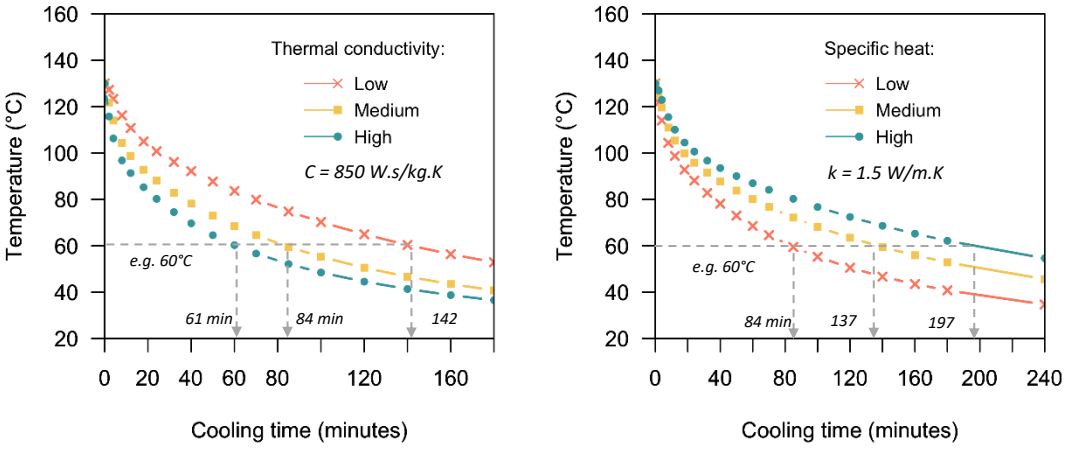

(a) (b)

Figure 4.14. Temperatures at the bottom quarter (3/4 depth) of newly laid asphalt, (a) for various thermal conductivities; (b) for various specific heat coefficients.

Several strategies, presented by past studies, can be used to enhance the thermal properties of asphalt mixture: (1) by using quartzite aggregate and adding copper fibres to asphalt mixtures (Dawson et al. 2012), (2) increasing the mixture density (Côté and Konrad 2005), (3) avoiding using porous friction asphalt mix (Wills 1982), and (4) replacing the traditional mix filler with conductive filler, such as graphite powder (Shi et al. (2017) and Bai et al. (2015)). Some modifications to mixes may be practical, whilst others seem to be of little value and/or uneconomic. It should be noted that engineers must also consider the effect of the selected materials on the mechanical performances of the asphalt pavement and choose the materials (with enhanced thermal properties) without compromising the long-term performance of the asphalt pavement.

4.6. Discussion and Summary

A simplified one-dimensional finite element transient heat transfer model was developed for simulating the cooling response of newly laid asphalt overlay. The model was well validated against field data, taken from four pavements in Minnesota, between the summers of 1996 and 1997. Using the validated finite element simulated model, various parameters affecting the cooling time of newly laid asphalt were investigated through case studies. The purpose of the analysis was to investigate strategies for reducing asphalt cooling time during overlay works. Reduced cooling time is expected to help airport authorities to quickly open new pavements to traffic and/or to reduce airport closure in the case of busy airports and 24-hour airport operations.

The following remarks on practical aspect of asphalt overlay work may be made from the results obtained:

- For practical implementation, to avoid the mis-measurement of newly laid asphalt temperature, it is suggested for practitioners /airport authorities to avoid using an infrared thermometer directed at an asphalt surface. Instead of using the temperature of the asphalt top surface, it is recommended to use embedded thermocouple sensors to monitor the temperature changes at the bottom or 3/4 depth of asphalt layer. Where this is not possible, a calibrated 1D heat transfer model can be used to predict internal mat temperature from the surface temperature reading.
- Based on the heat transfer simulation result, the study recommends that for a rehabilitation project in tropical climatic conditions: (a) night-time construction be adopted as the most ideal option, and (b) asphalt overlay work during sunny daytime should be avoided.
- The cooling analysis presented in this study showed that, in comparison to HMA, the use of WMA could shorten the closure time of an airport during night-time construction by 6-65 minutes (5-35% reductions in time to reach 60°C) depending on the asphalt overlay thickness, specified traffic opening temperature and WMA production temperature.
- For the cases studied, raising the critical traffic temperature reduced the closure of a runway to allow night-time construction in a typical tropical climate by 23-132 minutes (27-57% reductions), depending on the asphalt mixture type, lift thickness and traffic-opening temperature.
- In the case of the limited time available for asphalt overlay work, it is preferable to (a) select a thinner total lift depth of the asphalt overlay, and (b) avoid multi lift paving operation.
- Enhancing the thermal properties of asphalt mixture could reduce the cooling time needed for asphalt overlay to reach the traffic opening temperature. Several strategies from past studies such as using quartzite aggregate and adding copper fibres to asphalt mixtures, replacing the traditional mix filler with conductive filler, such as graphite powder and avoiding using porous friction asphalt mix can be adopted.

- The following strategies: (1) defining and selecting the warmest permissible asphalt temperature at opening to traffic, (2) reducing the cooling time by using warm mix asphalt (WMA), (3) increasing the cooling rate of asphalt by using high thermal conductivity material, can be adopted to obtain rapid cooling of new asphalt and to reduce airport runway closure time.

5. Analysis of The Allowable Asphalt Temperature at Opening to Traffic

5.1. Overview

Newly laid asphalt must be adequately cool before it can be trafficked to prevent the development of costly premature damage. Selecting an appropriate traffic-opening temperature of newly laid asphalt airport runway overlay would avoid early damage – while also minimizing the disruption to the airport service due to prolonged runway closure in a busy airport. In this chapter, the permissible temperature of newly paved asphalt at opening to traffic is investigated through a series of laboratory tests and analyses with regard to rutting and interface shear failure potential of newly paved asphalt at high temperature and high load.

5.2. Aim of Research Phase

The research questions to be answered in this research phase are as follows:

- What is the acceptable temperature for the opening of asphalt overlay to traffic?
- To what extent do the binder type, tack coat type and aggregate gradation of asphalt mixtures influence the decision of opening asphalt overlay to traffic?

A series of laboratory testing with regard to rutting performance and interface shear bond at high temperature was performed. A simple linear viscous approach was then used to predict the rut depth and cycles-to-failure of newly laid asphalt pavement at high traffic-opening temperature by using data derived from the repeated load axial test (RLAT). To study the interface shear failure potential of new asphalts, an interface shear bond analysis was conducted using the BISAR programme with data obtained from laboratory direct shear testing. The multi-axial stress states at the asphalt layer interface were modelled using the Mohr–Coulomb failure relationship applied to a normal-shear stress plane. The permissible asphalt temperature at trafficking was selected based on the temperature which shows acceptable asphalt performance.

Furthermore, an analysis was carried out to investigate the effect of selected traffic-opening temperature on airport closure time and overlay project productivity.

5.3. Rutting Performance of Asphalt at Traffic Opening Temperature

5.3.1. Laboratory RLAT Results

The Repeated Load Axial Test (RLAT) as detailed above in Chapter 3 was performed to study the permanent deformation behaviour of bituminous mixtures at high temperatures during early life trafficking. The test consists of applying uniaxial repeated compressive stress to cylindrical asphalt specimens. In this research, an 8kN load (1020 kPa) and a 5 kN load (630 kPa) were constantly applied for 1s followed by a 1s rest period (frequency of 0.5 Hz). The replication of the high contact stresses typical of commercial aircraft tyres (more than 1400 kPa) was not achieved due to the limitations of the laboratory equipment. However, in this research, the RLAT primarily aimed to capture the viscous properties of asphalt mixtures at high temperature for rutting analysis (discussed later in Section 5.4.2.). The actual tyre pressure of aircraft was applied in the rutting analysis. In addition, since the RLAT specimen was uniaxial and unconfined, the test was performed at relatively low stress levels, relative to actual aircraft tyre pressures, to avoid the sample failing prematurely which would have prevented the viscous properties of material from being obtained. As discussed in Chapter 3, the RLAT was performed for 2000 load cycles or until the specimen failed (see Figure 5.1b) or 20mm of deformation was achieved. Different types of bituminous binders, including different design air voids and RLAT load levels, were also examined. The apparatus used for the experiment was a universal testing machine (NU14). All tests were performed on gyratory compacted specimens 100 mm in diameter by 60 mm high.

5.3.1.1. Effect of Bituminous Binder Type on Rutting Performances

Two different bituminous binders were compared in this study: conventional 40/60 penetration grade and Styrene-Butadiene-Styrene (SBS) polymer-modified binder. As discussed before in Chapter 3, based on the rheological investigation, it can be noted that the mixtures with SBS modified binders demonstrate a superior rutting resistance at elevated temperature as compared to conventional penetration-grade 40/60 binders. Therefore they have potential to be trafficable at higher temperature, hence earlier, than conventional asphalts.

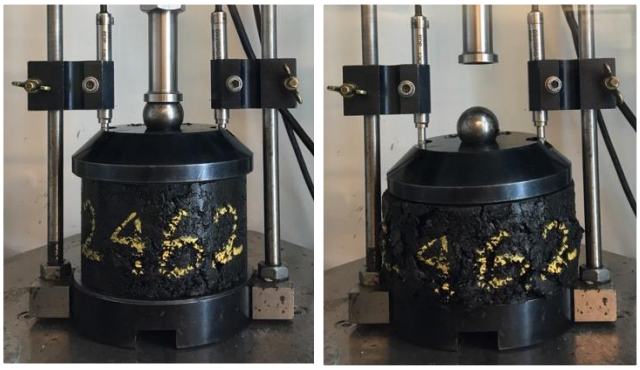

(a) (b)

Figure 5.1. RLAT specimen: (a) at the start of the test, (b) failure at the end of the test

Figure 5.2 displays the profile of unrecovered deformation of the bituminous mixture specimens containing both bituminous binders at 50°C, 60°C, 75°C and 85°C from RLATs. Overall, the results clearly show greater plastic deformation with increasing test temperature. This is consistent with previous studies (Hussan et al. 2019, Tarefder et al. 2003), where the temperature was found to be one of the most significant factors affecting the rutting of bituminous mixtures. In the case of the test temperature of 85°C, it was found that specimens with unmodified binder survived only a few cycles of loading. In addition, it is observed that the bituminous mixtures with SBS modified binders show improved rutting performance at high temperatures relative to that of the 40/60-penetration grade binder. Even at 85°C, a mixture containing SBS polymer had excellent rutting resistance under few load cycles. The results from the RLAT will be used for rut depth prediction in the next subsection.

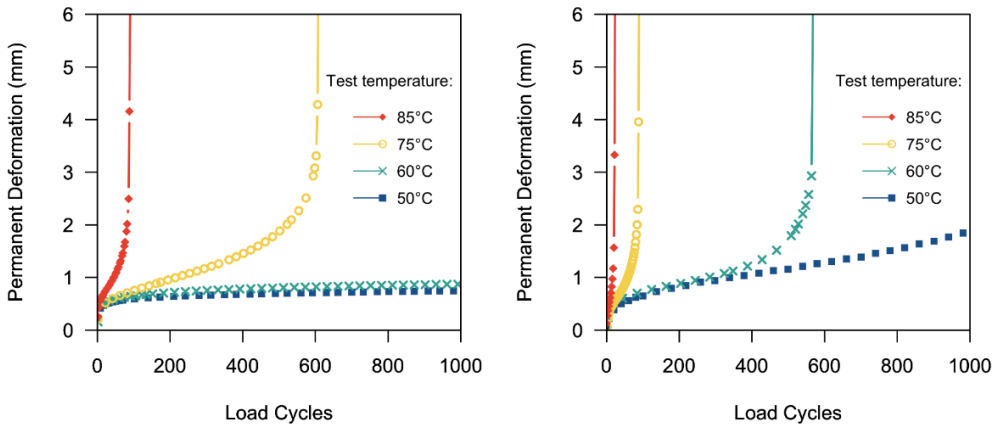

(a) (b)

Figure 5.2. RLAT results for mixtures with: (a) SBS modified binder, (b) 40/60 pen. grade

5.3.1.2. Effect of Load on Rutting Performances

Different axial loads of the test were considered in this section to accommodate different load during aircraft ground manoeuvring. To investigate different loading condition on rutting of asphalt, RLAT was performed under two different load levels: 8 kN and 5 kN, equivalent to axial stresses of 1020 kPa and 630 kPa. The axial stress pattern of both stress levels is displayed in Figure 5.3. It can be seen that the test apparatus required a few seconds to reach the target load level.

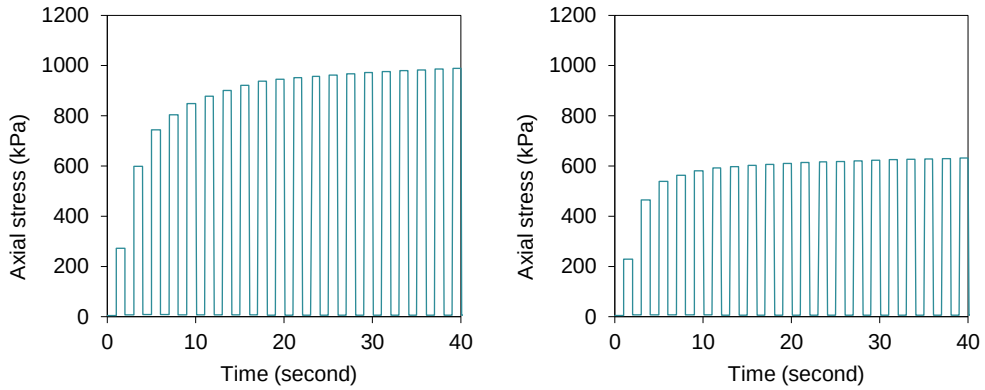

Figure 5.3. RLAT axial stress pattern: (a) 1000 kPa, (b) 630 kPa

Figure 5.4(a) and (b) shows the profile of plastic deformation of the bituminous mixture specimens under axial stress of 1020 kPa and 630 kPa, respectively. The figures show that load cycles to failure decrease significantly with increasing the RLAT axial load. This finding suggested that airport authorities could consider limiting slow aircraft movement with full weight on the new asphalt overlay to avoid premature rutting damage during the asphalt early life. During this time, the aircraft could use other runway or taxiway facilities.

5.3.1.3. Effect of Degree of Compaction on Rutting Performances

The effect of degree of compaction on the rutting potential during the early life of opening to traffic were investigated in this section. It is well known that insufficient level of compaction can cause a decrease in mixture density and an increase in air voids, thus, the asphalt material becomes less stiff leading to increased rutting potential (Witczak et al. 2002, Mogawer et al. 2011b). A high percentage of air voids caused by poor compaction may contribute to premature failure of the pavement (Tw Kennedy 1984).

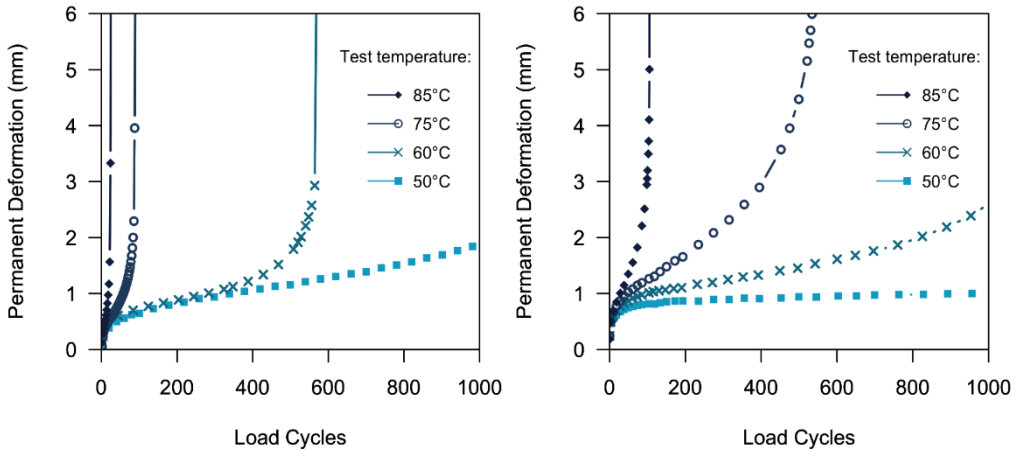

Figure 5.4. RLAT results for different axial stress: (a) 1000 kPa, (b) 630kPa

To simulate the effect of the degree of compaction, two different percentages of air voids of mixtures: high (~9%), and low (~4%) prepared using a gyratory compactor were investigated for this purpose. The low air void content was selected within the allowable design range in FAA specifications (FAA 2018) for airfield pavement: 2.8–4.2%, while the high air void content was selected to represent a potential poorly compacted asphalt mat. A neat binder of 40/60 pen. grade was used for all specimens.

Figure 5.5 (a) and (b) show the relationship between the permanent deformation and the repeated load cycles for mixtures with high and low air void contents, respectively. The results clearly indicate the importance of degree of compaction, as measured by air voids, for the asphalt resistance to deformation. It can be seen from Table 5.1 that the mixture with air voids of 9 % failed after only 4 load cycles at a test temperature of 85°C, while the mixture with low air voids survived 24 cycles of loading. Similar trends can also be found for other test temperatures: 50, 60 and 75°C. Reducing the air voids of bituminous mixture could result in less premature damage to the pavement during its early life of opening to traffic.

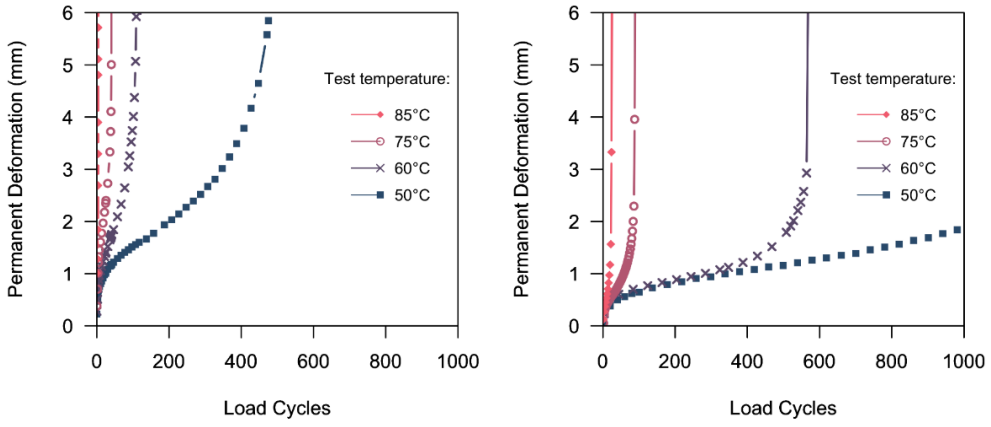

Figure 5.5. RLAT results for air void content: (a) High: ~9%, (b) Low: ~4%

Table 5.1. Load cycles to failure for different air void content and test temperature

Load	Air voids	Temperature (°C)	cycles to failure
High air void	9.3%	50	483
	9.3%	60	113
	9.0%	75	40
	9.6%	85	4
Low air void	3.9%	50	1383
	4.0%	60	584
	4.2%	75	92
	4.1%	85	24

5.3.2. Asphalt Rutting Prediction

A simple linear-viscous method as developed by Nunn (1986) and modified by Al-Mosawe et al. (2018) is adopted in this study for rutting prediction in newly laid asphalt pavement at various temperatures at opening to traffic. The approach employs a multilayer linear elastic program and inputs material axial viscosity instead of elastic modulus. The axial viscosity derived from previous RLAT data was used in an incremental linear-viscous analysis to predict the permanent strain rate for each increment, and ultimately the total rut depth.

5.3.2.1. Method of Rut Depth Prediction

The multilayer linear viscous approach method steps are explained as follows:

a. Manufacturing gyro cylindrical specimen

b. Performing RLAT in the laboratory at different testing temperatures

c. Calculating the strain rate ($\dot{\varepsilon}$) for each load cycle using the Equation (5.1). where ε_2 and ε_1 are strains corresponding to time, t_2 and t_1 (in seconds), respectively.

$$\dot{\varepsilon} = \frac{\varepsilon_2 - \varepsilon_1}{t_2 - t_1} \tag{5.1}$$

d. Determining the nonlinear axial viscosity of the materials, as a function of strain. Bituminous mixture axial viscosity (η) can be obtained by dividing the stress (σ) by the permanent strain rate ($\dot{\varepsilon}$), as shown in Equation (2.29) (Nunn, 1986):

$$\eta = \frac{\sigma}{\dot{\varepsilon}} \tag{5.2}$$

e. Producing a plot of mixture viscosity vs strain to obtain material properties for rutting analysis. An example of the viscosity-strain curve of a mixture showing three stages of creep (primary, secondary and tertiary) is displayed in Figure 5.6).

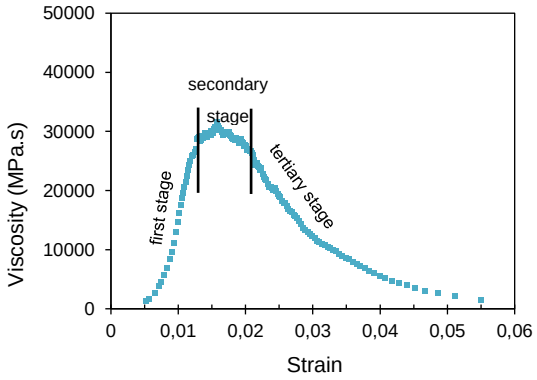

Figure 5.6 Example of the viscosity-strain curve for a bituminous mixture

f. Fitting a trend line to the data series to predict the viscosity at different strains. The first deformation analysis increment was performed using the initial material viscosity by extrapolating the trendline to zero strain.

g. Inputting material properties of the underlying pavement layers.

h. Performing the analysis and modelling of a typical airfield pavement structure using Shell's multi-layer linear elastic program: BISAR (Bitumen Stress Analysis in Roads) 3.0.

i. Performing a loop analysis to estimate the amount of permanent deformation after a given number of load applications. A permanent deformation increment of 0.2-0.5 mm at the asphalt surface was assigned. The number of load cycles to cause the deformation increment was calculated.

j. Following that, the axial plastic strain at the centre of each layer and sub-layer beneath the wheel load was calculated and used to determine the new corresponding viscosities from the viscosity strain curve for further deformation analysis.

k. The loop was continued until rutting failure was reached (in this case 20 mm rut depth).

A more complete review of this rutting prediction approach can be found in Al-Mosawe et al. (2018). In this method, the effects of moving loads were considered indirectly by using pulse loading in the RLAT. To simplify the above-mentioned methodology, see the flow chart in Figure 5.7.

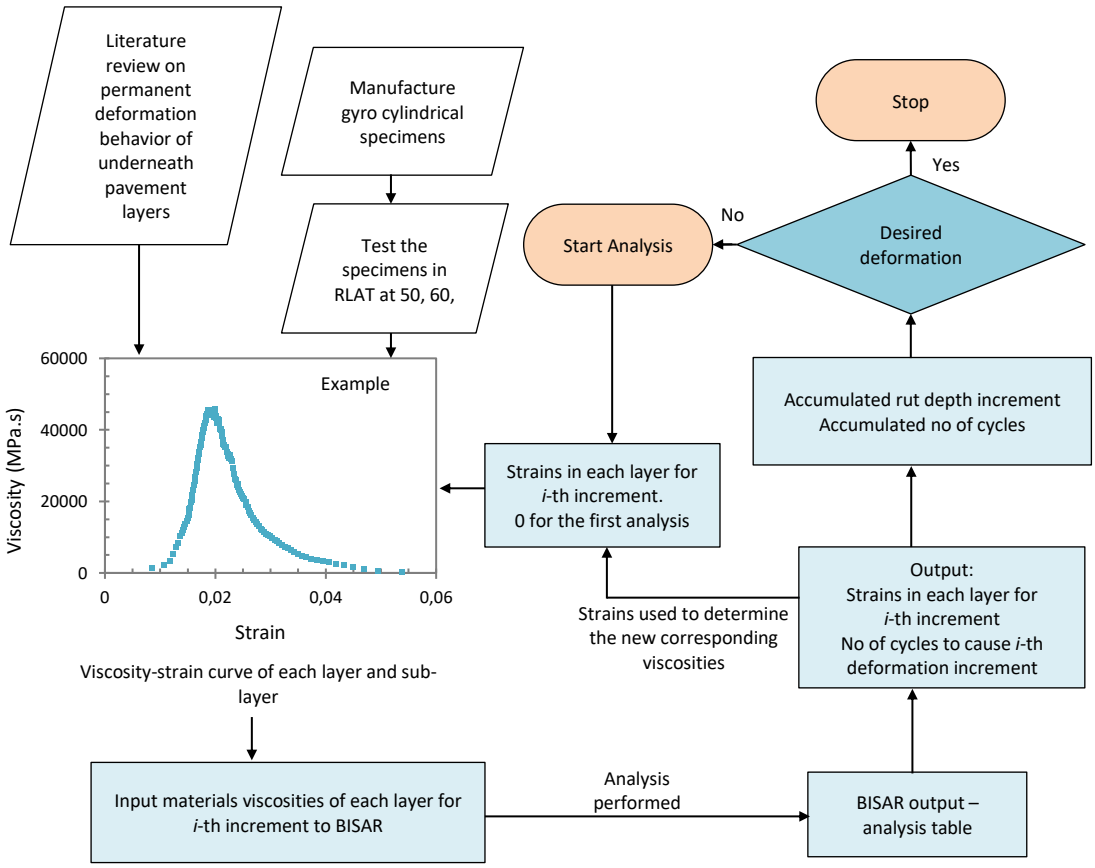

Figure 5.7 Flow chart of the rutting prediction methodology

5.3.2.2. *Validation against Wheel Tracking Test Result*

The application of the linear viscous approach for pavement rutting analysis was validated in this thesis by comparing the predicted rut depth with the result of the wheel tracking test in the laboratory. The wheel tracking test was performed at 60°C for 5000 cycles under a load pressure of 620 kPa on 306 x 306 x 50 mm compacted slabs. The validation process was carried out by

modelling the bituminous mixture slab in BISAR software and using the derived material properties from RLAT. For accuracy purposes, the slab was divided into three sub-layers with thicknesses of 10, 20 and 20 mm, see Figure 5.8. The load input data and coordinates of output points are shown in Table 5.3 and Table 5.2, respectively.

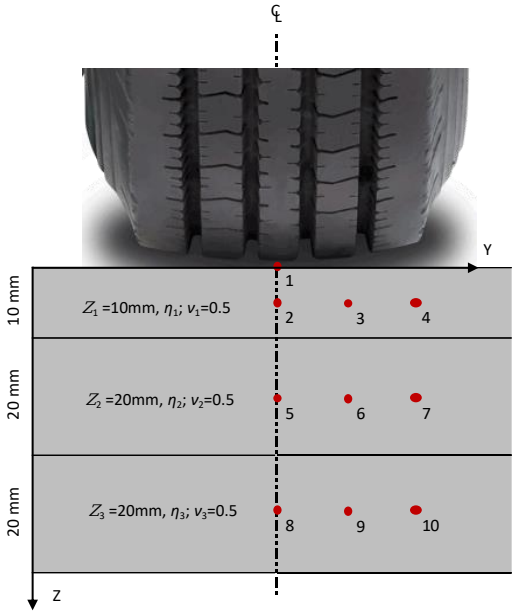

Figure 5.8 Slab Model Layers in BISAR

Table 5.2 the coordinates of selected positions where output is desired

Position Number	X Coordinate (mm)	Y Coordinate (mm)	Depth, Z (mm)
1	0	0	0
2	0	0	5
3	0	10	5
4	0	20	5
5	0	0	20
6	0	10	20
7	0	20	20
8	0	0	40
9	0	10	40
10	0	20	40

Table 5.3 Input data of the slab model analysis in BISAR

Input	BISAR
Load (N)	742
Load area (mm^2)	1257
Radius (mm)	20
Stress (kPa)	620

No adjustment was made to the time of loading because it was identical in both tests (RLAT and wheel track). The predicted rut depth along with the wheel tracking test result for mixtures with 40/60 pen. grade at 60°C showed in Figure 5.9. It was found that the rutting prediction showed higher rut depth and earlier failure cycles as compared to the wheel tracking test result. This is likely due to the absence of confinement pressure during RLAT experiments. As the test performed at high temperature, confinement pressure significantly affects the development of permanent deformation stages of bituminous mixtures (Gayathri et al. 2016). However, in general, the results showed reasonable compliance between the measured and predicted rut depth during the first few cycles. For the purpose of this study, as only a few early

aircraft passages are expected during opening to traffic, the model prediction is sufficiently realistic for further analysis of the rutting prediction of newly paved asphalt pavement.

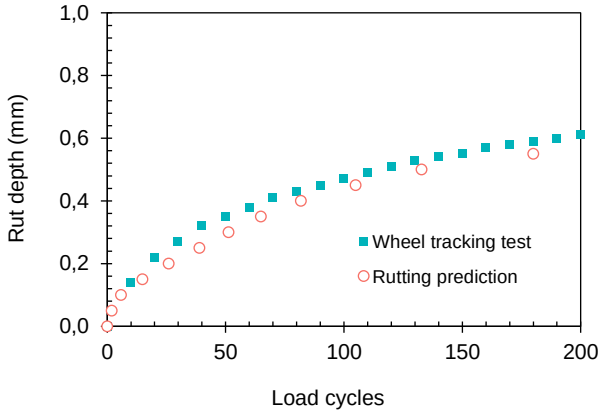

Figure 5.9 Rut depth from wheel tracking test vs prediction

5.3.2.3. Analysis of Asphalt Rutting During Opening to Traffic

a. Input Parameters

A multi-layered pavement structure, comprising asphalt overlay, bituminous binder course, asphalt base course, granular base course, and subgrade was represented as shown in Figure 5.10. The depth of each layer was adopted from pavement structures typically used for airfields.

For accuracy purposes, the newly laid asphalt overlay (70mm) is divided into four sub-layers with thicknesses of 10, 20, 20 and 20 mm. The viscosity-strain curves for different test temperatures derived from the RLAT are shown in Figure 5.11 and Figure 5.12 for mixtures with SBS modified binder and 40/60 pen. grade, respectively. A trend line was fitted to the data series to predict the viscosity at different strains. It was found that exponential regression provided excellent viscosity prediction with an average R^2 of 0.96. The Poisson's ratio of the all layers was assumed to be 0.5 (incompressible) so as to make sure that the predicted deformation is a result of viscous flow, not densification.

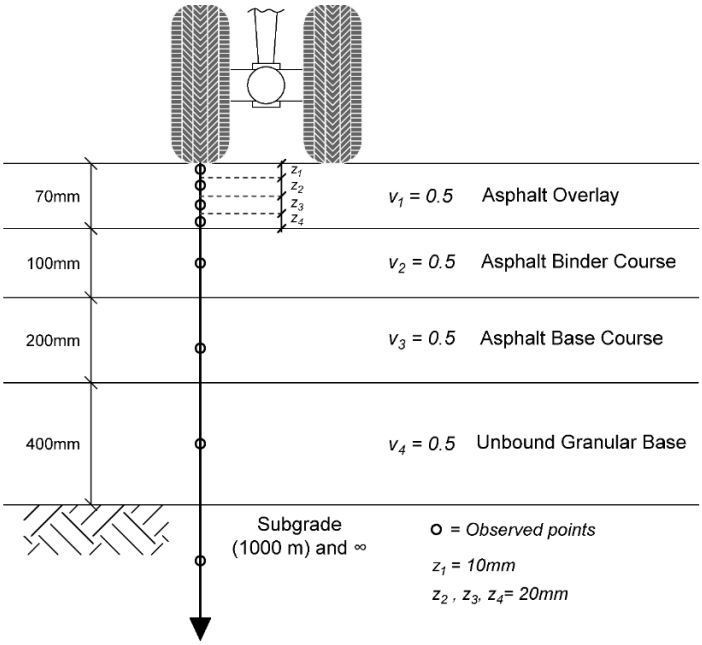

Figure 5.10. Model for rut depth analysis: pavement structure and properties of materials

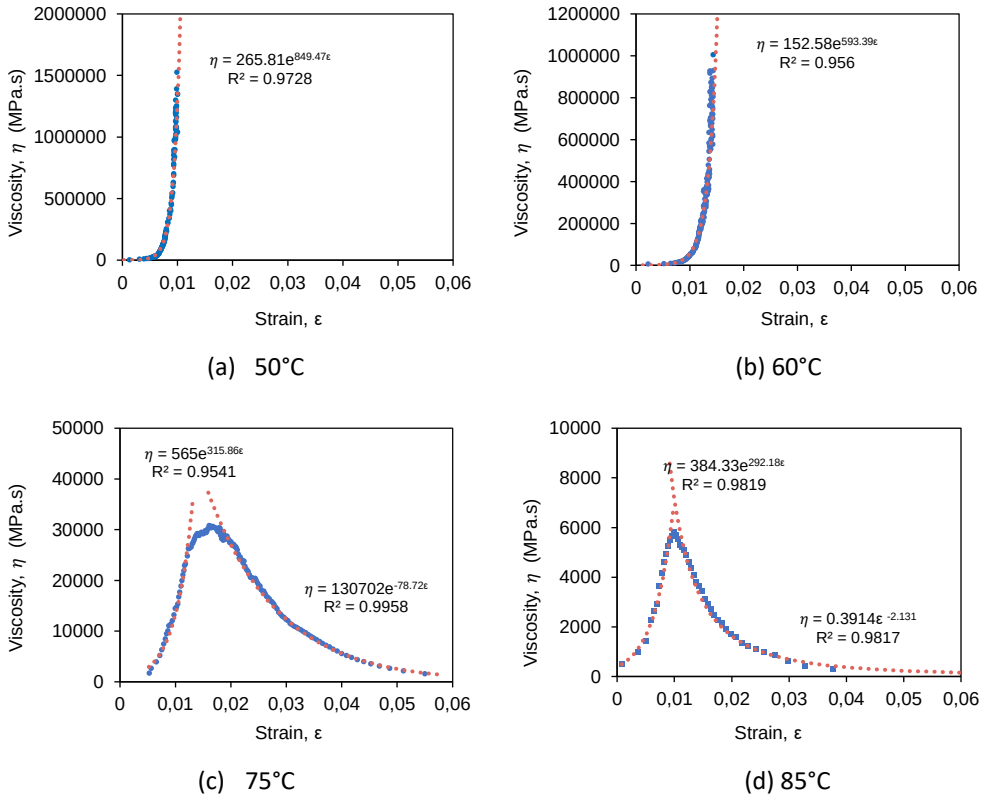

Figure 5.11 Viscosity-strain curve of mixtures with SBS modified binder

The material properties of the existing pavement layers were obtained from past research. The bituminous binder course viscous properties were obtained from RLAT testing of

asphalt concrete at 30°C conducted by Al-Mosawe et al. (2018). Using the previously-mentioned procedure, the viscosity-strain curves for bituminous binder and base course were produced and the fitting parameters are shown in Table 5.4. For unbound granular materials (UGMs) and subgrade layers, the 'pseudo-viscosity' is a constant unaffected by time of loading or temperature, which is different from that of asphalt materials. The 'pseudo-viscosity' for unbound granular base and subgrade were derived from repeated load triaxial tests performed by Lekarp and Dawson (1998) and Cong et al. (2011), respectively. The subgrade was silty soil with a resilient modulus (MR) of 50.5 MPa. The unbound granular base course was Sand and Gravel (S&G), which is commonly used as subbase material. In this research, a very high correlation between pseudo-viscosity and permanent axial strain was found with the exponential trendline equation as shown in Equation (5.3), as follow:

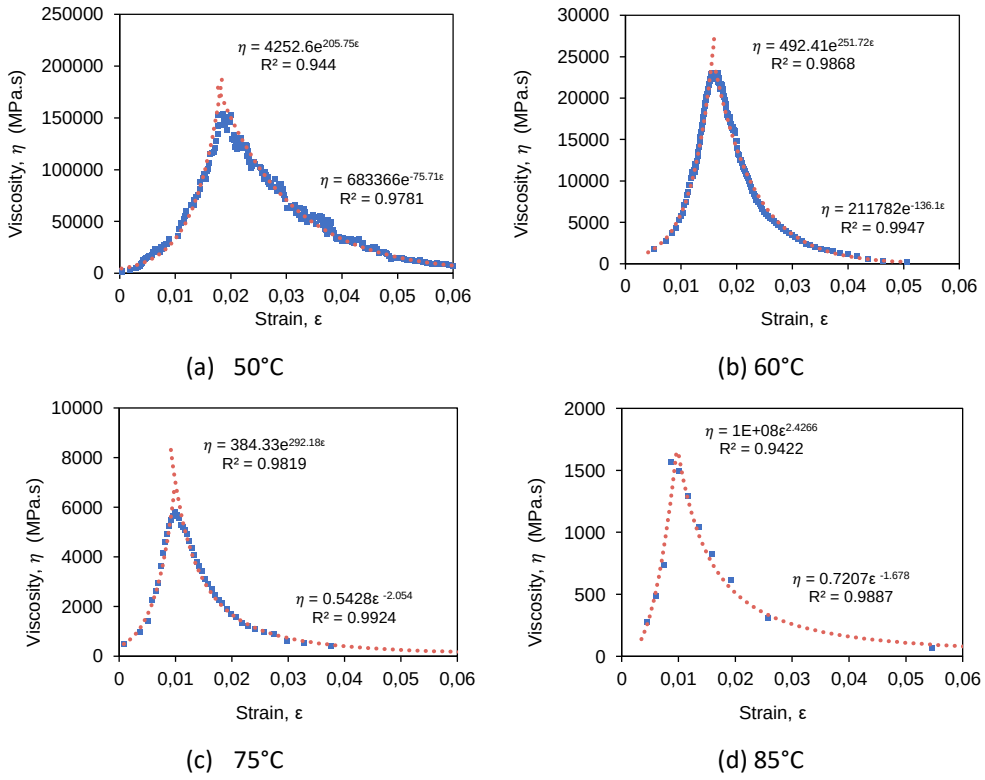

Figure 5.12 Viscosity-strain curve of mixtures with 40/60 pen. grade

$$\eta = A \times e^{B\varepsilon} \tag{5.3}$$

in which ε is additional permanent axial strain, and A and B are regression parameters. The calculated pseudo-viscosity-strain curve fitting parameter for the UGMs and subgrade layer materials are presented in Table 5.4.

Table 5.4. Viscosity curve fitting parameter for different materials

Materials	A	B	R^2	Sources
Bituminous binder course	1509.3	249.8	0.98	(Al-Mosawe et al. 2018)
Asphalt base course	323.4	245.9	0.94	
Unbound Granular Base	2620.9	806.8	0.99	(Lekarp and Dawson 1998)
Subgrade	5392.2	3281	0.99	(Cong et al. 2011)

During the aircraft operation, airfield pavements are subjected to different aircraft movements. In this study, in the term of rutting performance of asphalt pavement, the aircraft static or slow taxiing movement is assummed to be the most critical loading condition to be looked at. Impact loads during landing do not constitute a significant rutting problem for pavements. Having used up much of its fuel during flight, the aircraft is considerably lighter at landing than at take-off (Rowe 2012). A Boeing 777, for example, uses approximately 52 tons of fuel flying from London to Boston (Stewart 2014), therefore reducing its 340 tons take-off weight to 288 tons at landing. Furthermore, some portion of its remaining load is supported by the wing until a later stage of the landing. Therefore, in this study, the take-off/taxi weight of aircraft was assumed as the critical load for the investigation of rutting resistance of asphalt at traffic opening temperature. The tyre loading characteristics follow the specifications from the aircraft manual for a Boeing 737–800 (Boeing 2015). The aircraft was selected for the analysis, as it is one of the most used narrow-body aircraft in the world (Wang et al. 2016). Using the traditional approach, the landing gear wheel load was assumed to be uniform. Typical take-off weight of a single wheel load of 198.9 kN was considered. In addition, a tyre pressure of 1.42 MPa giving a contact area of 1401 cm^2 and radius of contact of 0.21 m was applied.

b. Rutting Prediction Results and Discussion

The prediction of number of load cycles to rutting failure for different mixtures and temperatures is summarized in Figure 5.13. Moreover, the predicted rut depth after a few load cycles (20 and 40 cycles) are presented in Table 5.5.

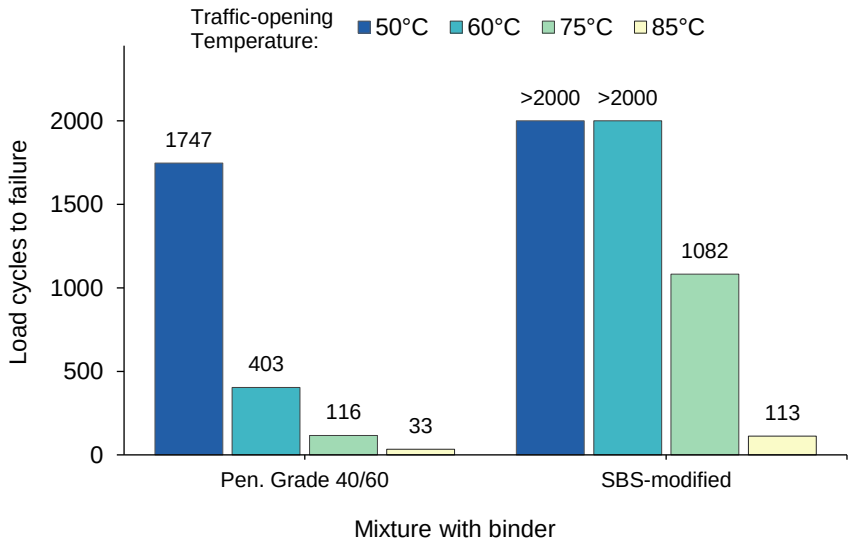

Figure 5.13. Predicted number of cycles to failure at various traffic-opening temperature for different bituminous mixtures

Table 5.5. Number of cycles to failure for various temperature and different binders

Mixture with:	Temperature (°C)	Rut depth (mm), after 20 cycles	Rut depth (mm), after 50 cycles	cycles to failure
Neat binder	50	3.141	4.914	1747
	60	4.004	5.740	403
	75	4.500	6.354	116
	85	6.157	failed	33
PMB	50	2.617	4.197	>2000
	60	3.309	4.930	>2000
	75	3.868	5.575	1082
	85	4.501	6.349	113

From the result, as expected, the mixtures with SBS binder showed a superior rutting resistance in comparison to that of conventional mixtures. In terms of rutting performance, it can be observed that a traffic-opening temperature of 60°C (or below), as recommended by many agencies, is reasonably tolerable for typical bituminous mixture with a conventional binder. At 60°C, for all bituminous binders, the newly laid asphalt has gained sufficient strength for trafficking. The predicted rut depth of the asphalt overlay with 40/60 pen. grade mixture at 60°C was as low as 4.00 mm and 5.74 after 20 and 50 cycles, respectively. The initial rut depth during asphalt opening to traffic at 60°C was considered acceptable and categorized as low rutting severity in airport pavement condition index, PCI (ASTM 2012). In this section, the rutting failure was defined as 12.5 mm (0.5-inch) depressions in the pavement based on the rutting prediction.

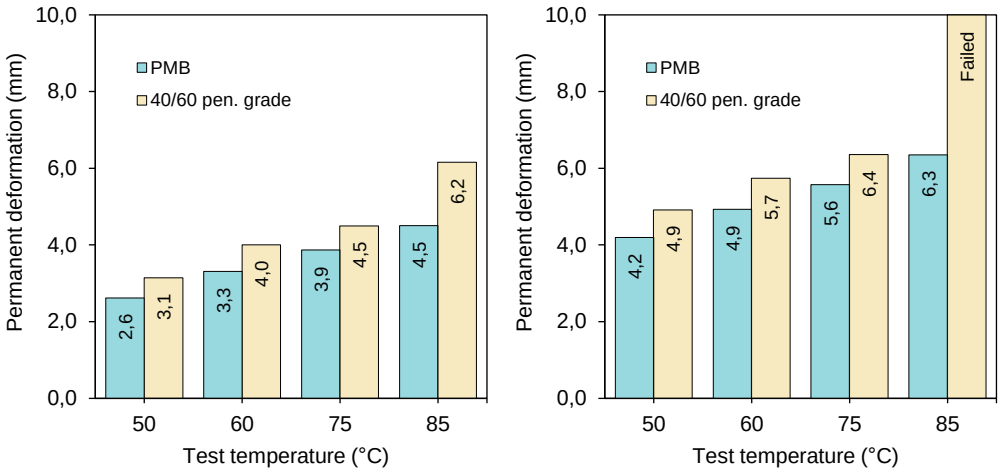

Figure 5.14. Predicted permanent deformation of newly laid asphalt pavement at different traffic-opening temperature

The analysis, however, suggests that the critical temperature can be raised as high as 85°C when binder improvement (such as polymer modification) is used. At 85°C, it is predicted that the SBS mixture would fail after 113 cycles under B737 load, but only a few aircraft passages can be expected at traffic-opening temperature. This is because less than 60 movements per hour (Roosens 2008) can be achieved at the busiest airports during which time the asphalt mat will gradually cool to a lower temperature and gain more strength.

A simple analysis was performed to compare the rutting damage of mixture containing PMB, assuming one hour after opening to traffic, under a temperature decreasing from 85°C and that of from 60°C. For this purpose, the cooling analysis results for asphalt (70mm) in typical tropical countries (a wind speed of 2 m/s) during night-time construction, obtained from Section 4.6.1, were used. To predict the rut depth, the linear viscous approach, that previously employed, was used by using different viscosity-strain curves (shown in Figure 5.11), instead of a single curve, depending on the asphalt temperature from the cooling analysis. The rutting damage for the first hour then can be predicted by doing a summation of damage due to load passes at different asphalt temperature. For example, the rutting damage is a combination of damages caused by A passes at 85°C + B passes at 75°C + C passes at 60°C + D passes at 50°C. In this study, the 40 aircraft passes / movements per hour was assumed. The result of this analysis is presented in Figure 5.15(a) and (b) for traffic-opening temperature of 85°C and 60°C, respectively.

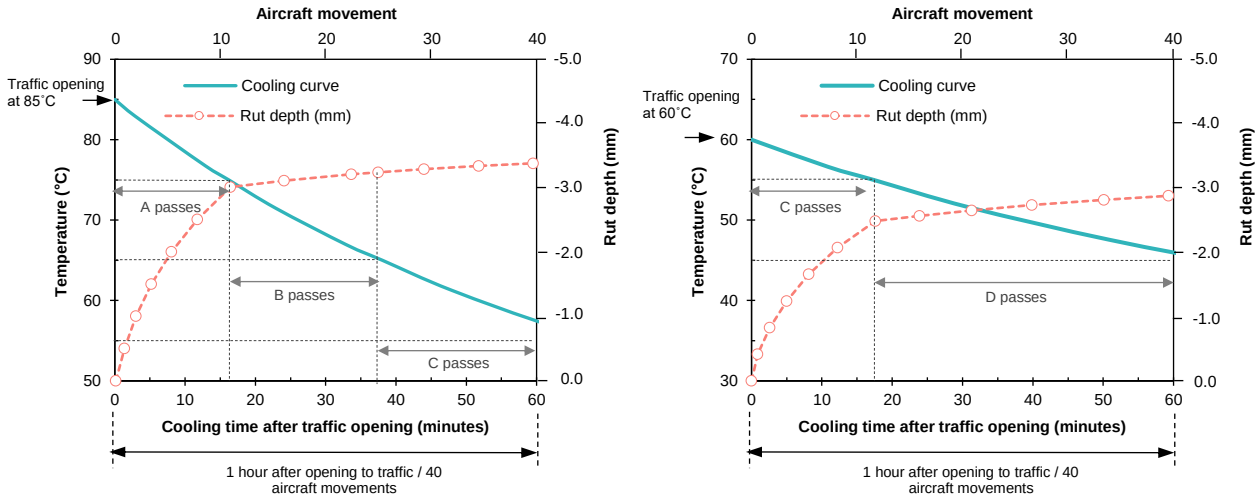

Figure 5.15. Rutting damage prediction for the first hour (of opening to traffic) under a temperature decreasing from: (a) 85°C and (b) 60°C

The results suggest that the predicted rut depth of mixture containing PMB under a temperature decreasing from 85°C in the first hour (of opening to traffic) (3.37 mm) is not significantly greater than that of under a temperature decreasing from 60°C (2.86 mm). This indicates that opening-to-traffic asphalt temperature at 85°C might not severely damage (in term of rutting) the new asphalt containing PMB, as it will only get a few passes at this high temperature, before the asphalt gradually cools and gain more strength. In addition, the analysis was carried out by assuming that the aircraft wheels pass along the same pavement strip during aircraft take-off and landing. In fact, the aircraft might not always pass the exact same pavement location due to aircraft wander distribution.

5.4. Asphalt Interface Shear Bond at Traffic Opening Temperature

5.4.1. Interface Shear Bond Test Results

A total of 135 sandwich-block specimens were prepared in the laboratory for interface shear bond (direct shear) tests at high temperature. The method discussed in Chapter 3 was used for this section. The typical shear load-displacement plot from the test is presented in Figure 5.16. In this research, the interface resistance is measured based on the ISS which can be calculated from Equation (5.4).

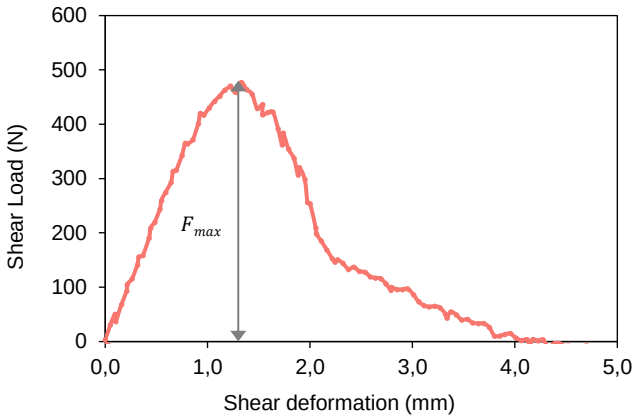

Figure 5.16 Typical load versus displacement plot of the test

$$ISS = \frac{F_{max}}{A} \tag{5.4}$$

where ISS is the interface shear strength, F_{max} is the maximum shear force and A is the cross-sectional area of a specimen.

In the next sub-section, optimum application rates for different pavement surface type and tack coat materials were investigated. Furthermore, various factors affecting the ISS including loading rate, test temperature, tack coat materials, pavement surface type and presence of normal stress were studied in the following subsections. Unless otherwise noted, each value of ISS in this research represents the average of two test specimens to anticipate variability of the results, as found in past studies (Romanoschi and Metcalf 2001a, Collop et al. 2003a).

5.4.1.1. Optimum Application Rate

An appropriate bond between asphalt layers is essential so as to give a monolithic asphalt pavement. Determination of an optimum application rate for tack coat is crucial in the development of this bond. Pavement surfaces with various conditions (e.g., new, old, or milled) require different tack application rates to accomplish adequate bonding. Excessive tack coats may develop shear failure at the interface (Mohammad et al. 2012).

To compare the application rates of different tack coat materials and pavement surfaces, the residual binder rate should be considered instead of total binder application rate (White 2016c). In this research, the optimum application rates refer to the residual bituminous binder rates (after setting or breaking). The optimum application rates of two tack coat materials: cationic emulsion (K1-40) and SBS polymer modified binder and two pavement surfaces: new

HMA and PCC were investigated. The surface preparation was performed with the method that previously explained in Section 3.5 and Section 3.6.3.1. Three different tack coat application rates based on past studies were adopted. Table 5.6 and Table 5.7 present the ISS test results for new HMA surface and PCC surface, respectively, with each tack coat material. At temperatures of 70°C and 80°C, some samples collapsed due to their own weights before the load was applied. This particularly occurred at the low tack coat application rate and for the K1-40. For this case, the ISS value was assumed to be the self-weight of the cubic specimen, see the star signs. In general, the ISS value of SBS polymer modified tack coat was superior to that of the K1-40 at high temperatures. It is also noted that new HMA surface provided higher ISS values than did the new PCC surface.

Table 5.6 ISS at various test temperatures and application rate for new HMA surface

Temperature (°C)	Interface Shear Strength (ISS), kPa					
	Cationic emulsion (K1-40)			SBS polymer-modified binder		
	0.30 L/m²	0.50 L/m²	0.70 L/m²	0.35 L/m²	0.70 L/m²	1.0 L/m²
60	21.0	22.9	8.8	36.1	53.4	49.0
70	10.6	14.0	6.0	19.0	19.2	31.5
80	1.64*	1.64*	1.64*	5.1	2.5	8.6

*Specimens failed due to their own weights before the load was applied

Table 5.7 ISS at various test temperatures and application rate for PCC surface

Temperature (°C)	Interface Shear Strength (ISS), kPa					
	Cationic emulsion (K1-40)			SBS polymer-modified binder		
	0.35 L/m²	0.70 L/m²	1.0 L/m²	0.35 L/m²	0.70 L/m²	1.0 L/m²
60	13.0	22.6	10.0	21.8	19.3	38.3
70	1.64*	5.8	1.0	9.7	7.7	17.1
80	1.64*	1.64*	1.64*	1.64*	5.1	3.0

* Specimens failed due to their own weights before the load was applied

Figure 5.17 (a and b) displays the variation of the ISS with tack coat application rates and test temperatures for asphalt emulsion material (K1-40). For HMA surface, for temperatures of 60°C and 70°C, it was observed that the optimum rate—at which the highest ISS was reached—is 0.5 l/m²; however, the application rate to the highest ISS values was measured at the rate of 0.7 l/m² for new PCC surface. This may be associated with the coarse PCC surface, which required greater tack coat application rates. For SBS modified binder tack coat, the variation of the ISS with tack coat application rates and test temperatures is presented in Figure 5.18 (a and b). For new HMA surface, the application rate of 0.7 l/m² was found to be the optimum rate. For new PCC surface, however, it was not possible to define an optimum tack coat application rate for the range of application rates from 0.35 to 1.0 l/m². Nevertheless, the application rate of 1.0/m² of

SBS polymer modified binder is used in further steps of this research. In general, the tack coat residual application rates are on a par with the recommended rates in previous literatures (Mohammad et al. 2012, Huang et al. 2015).

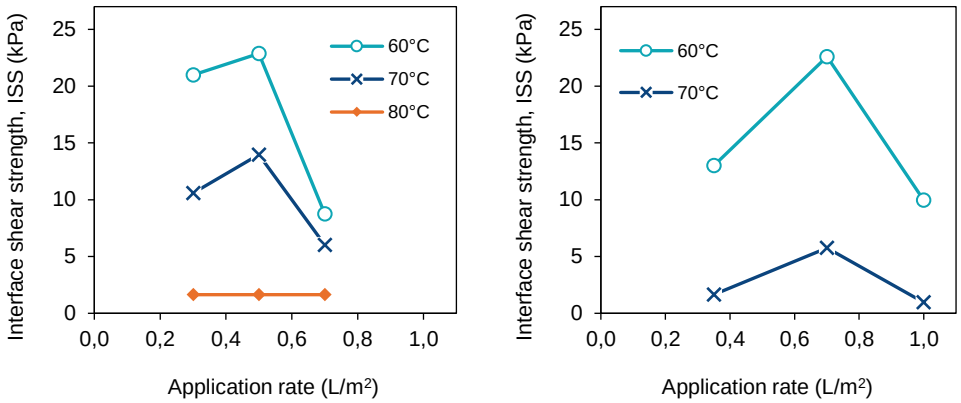

Figure 5.17 Variation of the ISS with application rate and test temperature for K1-40

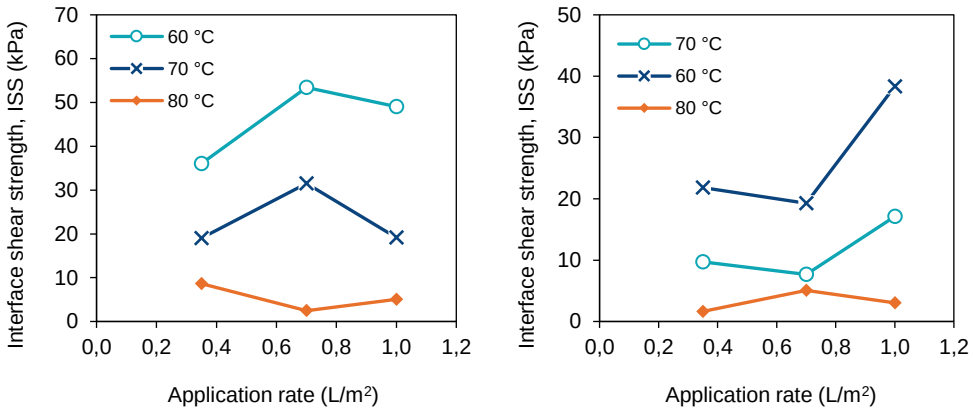

Figure 5.18 Variation of the ISS with application rate and test temperature for SBS binder

5.4.1.2. Effects of Loading Rate on ISS

It is essential to select an appropriate rate of loading or shear deformation of the test, since the loading rate critically affects the measured ISS (Mohammad et al. 2012). As the tack coats and bituminous binders are viscoelastic materials, they are dependent on temperature and rate of loading. It is expected that under slow loading rate, bituminous binders behave like viscous fluid and flow (Fwa 2005). A slower loading rate may result in a lower ISS due to a more plastic behaviour of asphalt and tack coat (White 2016c).

In this research, to study the effect of loading/shear deformation rate on ISS, four different loading rates: 5000, 50, 25 and 2.5 mm of deformation per minute during the interface shear test, were performed. The tack coat material used was SBS modified binder, while the lower layer /existing surface was asphalt. The test was performed in the laboratory at 50°C. Table 5.8 and Figure 5.19 present the ISS test results for different loading rates. Each ISS value represents the average of three test specimens.

Table 5.8 Effect of loading rate

Loading rate	Interface shear strength (ISS), kPa for replicate:			Average ISS, kPa	Test temp.
	1	2	3		
5000mm/min	279	291	-	285	50°C
50mm/min	178	191	118	162	
25mm/min	109	121	101	110	
2.5mm/min	65	73	67	69	

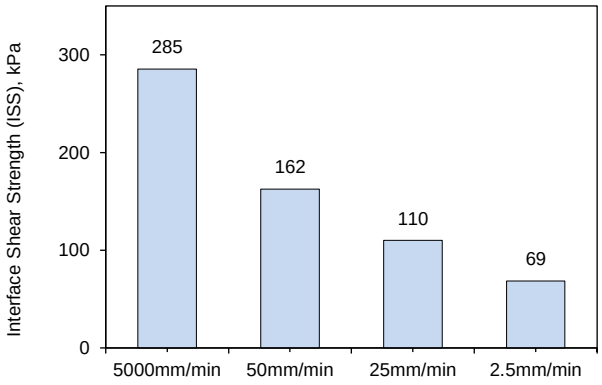

Figure 5.19 Effect of the loading rates on ISS

The results show that as the loading rate was greater, the ISS values increased. For instance, the ISS value increased by approximately 159% when the loading rate was raised from 25 mm/minute to 5000 mm/minute. In summary, the result indicates that the loading/shear deformation rate has a significant effect on the interface behaviour and the measured ISS. Nevertheless, the loading rate of 50mm/min was used for all further tests in this research. A loading rate of 50 mm/min is widely used in research of interface shear bond behaviour (Sholar et al. 2002). The loading rate of 50mm/min is often selected so that Marshall and CBR loading devices that are widely available can be used (Collop et al. 2009).

5.4.1.3. Effects of Test Temperature on ISS

Figure 5.20 displays the ISS values for SBS and K1-40 specimens at three different test temperatures 60, 70 and 80°C and two lower layer surface types without normal load. For both tack coat materials, a decrease in ISS was observed as a function of increasing test temperature. In general, it was observed that 58–87% reduction of the ISS was found when test temperature was raised from 60 to 80°C. Similar findings were found in past research (Uzan et al. 1978, Canestrari and Santagata 2005).

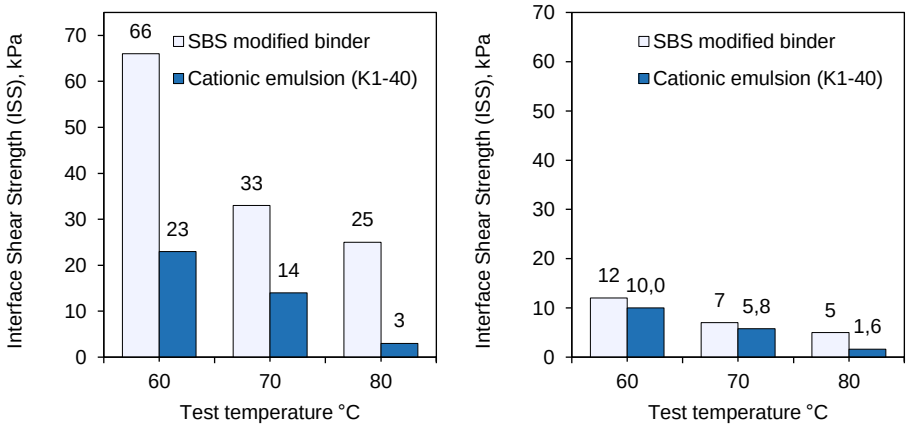

Figure 5.20 Effect of the test temperatures on ISS for: (a) HMA surface and (b) PCC surface

5.4.1.4. Effects of Tack Coat Type

From Figure 5.20 presented earlier, it was found that pavement interfaces with SBS modified binder as the tack coat have significantly higher ISS at all temperatures as compared to the conventional cationic emulsion (K1-40). The result highlights the significance of using a tack coat material to avoid poor bonding between new and existing layers. In general, it can be concluded that polymer-modified binder performs better than conventional emulsion. It is expected that these results indicate the effect of the presence of the polymer on improving the softening point of bituminous binder rather than any substantial enhancement in the adhesion or cohesion of the tack coat material (White 2016c).

5.4.1.5. Effects of Upper Layer Mixtures and Interlayer Surface

SBS modified binder tack coat was evaluated on two surface types: new HMA and PCC surface (Figure 5.21), and two different asphalt upper layer mixes: HMA with SBS modified binder and HMA with 40/60 pen. grade. Table 5.9 and Figure 5.22 display the variation of ISS with surface

type and asphalt upper layer mix at the test temperatures of 60, 70 and 80°C.

Table 5.9 Effect of bituminous mixture and Interlayer surface at different test temperature

Interface	Lower layer	Upper layer	Interface Shear Strength (ISS), kPa for test temperature:		
			60°C	70°C	80°C
A	PCC	HMA-SBS	12	7	5
B	HMA 40/60	HMA SBS	66	33	25
C	HMA 40/60	HMA 40/60	32	25	16

(a) (b)

Figure 5.21 Interlayer surface type: (a) PCC surface, (b) HMA surface

As shown in the Figure 5.22, the HMA surface provided greater ISS than did the PCC surface. This result was consistent with research conducted by Das et al. (2018). The research showed that, although the mean texture depth of the PCC surface was higher than the HMA surface, the HMA surface has better interface bonding than the PCC surface. This finding suggests that the different interface bonding behaviour between PCC and HMA surfaces was not only affected by the surface texture, but it is also likely affected by the chemico-physical interaction between the tack coat, aggregate and the bituminous binder.

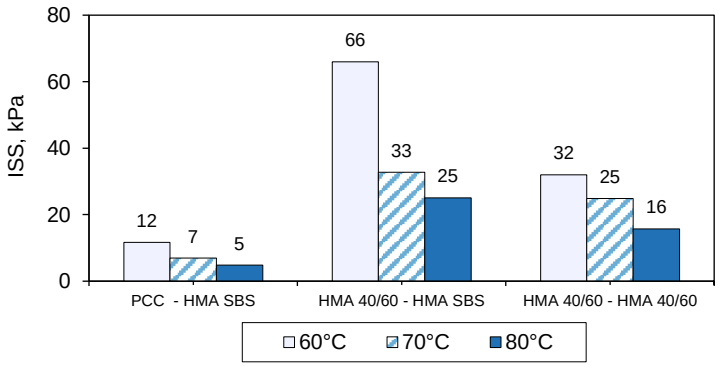

Figure 5.22 Effect of bituminous mixture and Interlayer surface on ISS

In this research, it is also observed that, for the same tack coat material, the ISS of interfaces whose upper layer comprised a bituminous mixture containing a polymer modified binder (PMB) is significantly higher than that in the case of neat bitumen upper layer mixes at all temperatures. The result indicates that the use of polymer modified mixtures for asphalt upper layer/overlay promotes interlayer adhesion and bond.

5.4.1.6. Effects of Normal Pressure on ISS

Four different interface conditions (A, B, C, D), three different test temperatures (60°C, 70°C, 80°C), and three different normal pressures (0 kPa, 150 kPa, 300 kPa) as presented in Table 5.10 were considered to investigate the effects of normal pressure on ISS. Figure 5.23 displays the load versus displacement plot for interface B at 60°C for different normal loads, as an example. An increase in interface shear resistance and higher resistance to deformation after peak load was observed as a function of increasing the normal load. The ISS of different interface conditions under different normal loads and test temperatures are presented in Table 5.10 and displayed in Figure 5.24.

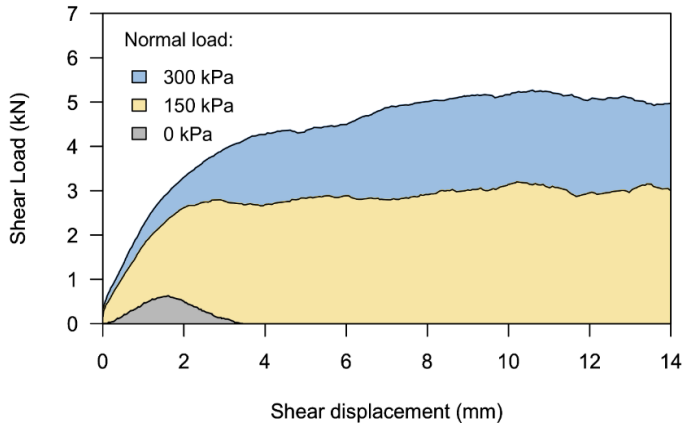

Figure 5.23 Comparison of different normal loads for interface B at 60°C

It is observed that the normal pressure effect is more evident at the higher test temperature. Take, for instance, the 300-kPa normal pressure on interface C, under temperatures of 60, 70, and 80°C, the corresponding ISS ratios (as compared to zero normal stress) are 7.8, 11.3, and 13.5 respectively, indicating a greater expected effect of normal pressure on ISS at high temperature. This is likely because the binder stiffness and viscosity is reduced and its adhesive behaviour diminishes; hence, the ISS is influenced predominantly by frictional resistance (West

et al. 2005, Ai et al. 2017) when, in accordance with Mohr-Coulomb theory, larger normal pressure induces greater frictional resistance (Ai et al. 2017).

Table 5.10 Effect of normal load on ISS at various test temperature and the failure envelopes

Test temp.	Interface	Pavement surface (lower layer)	Upper layer	Tack coat type	Interface Shear Strength (ISS), kPa for normal pressure:			Failure envelope criteria		
					0 kPa	150 kPa	300 kPa	*C* (kPa)	Internal friction angle, ϕ	R^2 (linear regression)
60°C	A	PCC	HMA-SBS	SBS binder	12	237	460	12.2	55.7°	1.00
	B	HMA-40/60	HMA-SBS	SBS binder	66	349	512	85.9	55.6°	0.98
	C	HMA-40/60	HMA-40/60	SBS binder	32	272	399	50.6	50.2°	0.97
	D	HMA-40/60	HMA-SBS	K1-40	23	194	315	31.3	43.7°	0.98
70°C	A	PCC	HMA-SBS	SBS binder	7	201	325	18.5	46.1°	0.98
	B	HMA-40/60	HMA-SBS	SBS binder	33	270	373	55.0	48.0°	0.95
	C	HMA-40/60	HMA-40/60	SBS binder	25	219	316	41.2	43.6°	0.96
	D	HMA-40/60	HMA-SBS	K1-40	14	154	261	19.4	38.9°	0.99
80°C	A	PCC	HMA-SBS	SBS binder	5	160	264	13.4	40.2°	0.98
	B	HMA-40/60	HMA-SBS	SBS binder	25	185	338	26.2	45.6°	0.99
	C	HMA-40/60	HMA-40/60	SBS binder	16	163	267	22.8	39.4°	0.99
	D	HMA-40/60	HMA-SBS	K1-40	3	123	187	12.2	31.1°	0.97

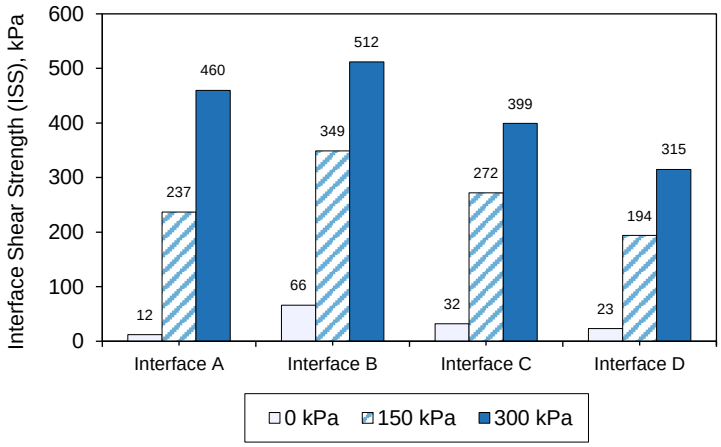

Figure 5.24 Effect of normal pressures on ISS at test temperature of 60°C

A linear relationship between the ISS and the associated normal stress is used by many studies as an approximation of the interface bond failure envelope in the Mohr-Coulomb plane (Wang et al. 2016, Ozer et al. 2013, Suddeepong et al. 2020, White 2016b). In this study, a trend line is fitted to the results of the laboratory direct shear test to obtain the failure envelope and its parameters (c and ϕ). The linear regression correlation coefficient R^2 with c and ϕ for all interface and test conditions is presented in Table 5.10 and displayed in Figure 5.25. The result

of the interface shear bond test and the failure envelope presented in this section is used for multi-axial stress state shear analysis in the next section to investigate the shear failure susceptibility of newly laid asphalt overlay during opening to traffic.

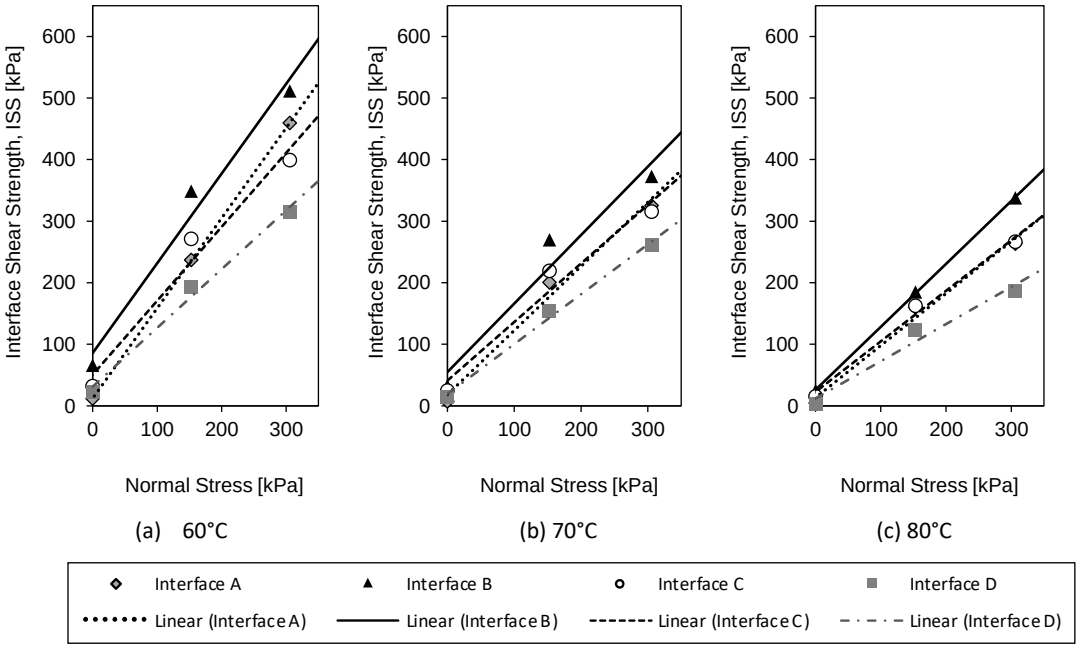

Figure 5.25 Failure envelopes for different interface condition and test temperatures

5.4.2. Analysis of Shear Failure at the Opening to Traffic

In this section, an analysis was performed to investigate the interface shear damage potential of newly laid asphalt pavement during the opening to air traffic for different aircraft ground movements. The shear failure in the bulk material is not investigated, as it is assumed that the most critical shear failure potential occurs at the layer interface (Wang et al. 2016).

5.4.2.1. Aircraft Loading under Various Ground Movements

During the aircraft operation, airfield pavements are subjected to different aircraft movements such as taxiing, landing, turning on rapid exit taxiway (RET), and full braking (Wang et al. 2016). A combination of loads and stresses of aircraft manoeuvring need to be considered in airfield pavement analysis.

The tyre loading parameters of an aircraft are commonly obtained from the aircraft manual published by the aircraft manufacturers. However, the information of the braking operation of aircraft at different manoeuvring conditions is limited to date. In this research, instantaneous /full braking operations were assumed equal to normal (vertical) load multiplied

by the coefficient of tyre-pavement friction, as seen in Eq. (5.5). In this case, a pavement coefficient of 0.8 was assumed for dry pavement conditions. In addition, the turning movement of aircraft at high speed into a rapid exit taxiway (RET) is expected to result in high shear stress on the pavement. The effect of the tangential stress caused by aircraft turning at an RET is represented by centripetal forces as seen in Eq. (5.6). The typical turning speed of aircraft of 90 km/h and radius of RET of 457 m was used for this research.

$$F_B = \mathrm{N} \times \mu \tag{5.5}$$

$$F_c = m \frac{v^2}{r \times 1000} \tag{5.6}$$

$$F_B = m \times d \,/1000 \tag{5.7}$$

where:

F_B = Braking forces (kN)
N = Vertical forces (kN)
μ = Coefficient of friction of tyre-pavement
F_c = Centripetal forces during turning at RET (kN)
m = Mass of aircraft on a single wheel (kg)
v = The aircraft velocity (m/s)
r = Turning radius of RET
d = The rate of airplane deceleration (m/s^2)

Another loading condition considered in this research is aircraft landing. After the landing, the aircraft brake is normally used to decelerate the aircraft speed until it is suitable for turning at a taxiway. Eq. (5.7) is used to calculate the braking force during the landing. However, the forces of aircraft on the pavement during the landing varies with time, as some portion of aircraft forces are supported partly by the wing which results in less aircraft forces on pavement.

White (2016b) interviewed an experienced pilot to understand the aircraft movement during landing. The interview highlights the use of the aircraft braking system, and typical aircraft speed during the aircraft movement. The interview results can be summarized as follow:

a. Regardless of aircraft size and the runway orientation, the aircraft lands at 250 km/h. The speed is restricted to 90 km/h when the aircraft starts to turn at an RET.
b. All aircraft have a braking system and airbrakes. There are 5 brake settings used during the landing. The braking systems target the following aircraft decelerations: 0.9 m/s^2, 1.2 m/s^2, 2.1 m/s^2, 3.0 m/s^2, and 4.3 m/s^2.

c. The brake setting selection is based on the slope of the runway and the speed of the prevailing winds.

d. During the landing, the airbrakes contribute up to 15% of the total braking effort. The airbrakes start to be ineffective at speeds below 150 km/h.

e. During the landing, some portion of the aircraft force is supported by the wings until a speed of approximately 150 km/h. Below that speed, the lift forces from the wings are assumed to become negligible.

f. The braking settings are chosen prior to landing and activated 1.5 seconds after touch down.

g. The brakes are continued until around 120 km/h, at which time, the braking system is manually released and gentle brake or natural aircraft slowing down are applied.

Based on the summarized interview, an illustration of the aircraft speed and forces on the pavement for a B737-800 aircraft and 3.0 m/s^2 deceleration have been created as shown in Figure 5.26. The purpose of the illustration is to understand the critical forces from the aircraft during landing. Furthermore, in calculating the aircraft loadings, the following assumptions were used:

a. Mass is equal to maximum design taxi weight for full braking (FB) and rolling during taxiing (T) movement. The information was obtained from the aircraft specification from Boeing (2015)

b. Mass is equal to the maximum design weight of aircraft for landing (L) and turning at RET (RET) movement.

c. Turning radius of rapid exit taxiway is 457 m, based on FAA (2014a).

d. Air brakes contribution was neglected. The input of wind resistance was also ignored.

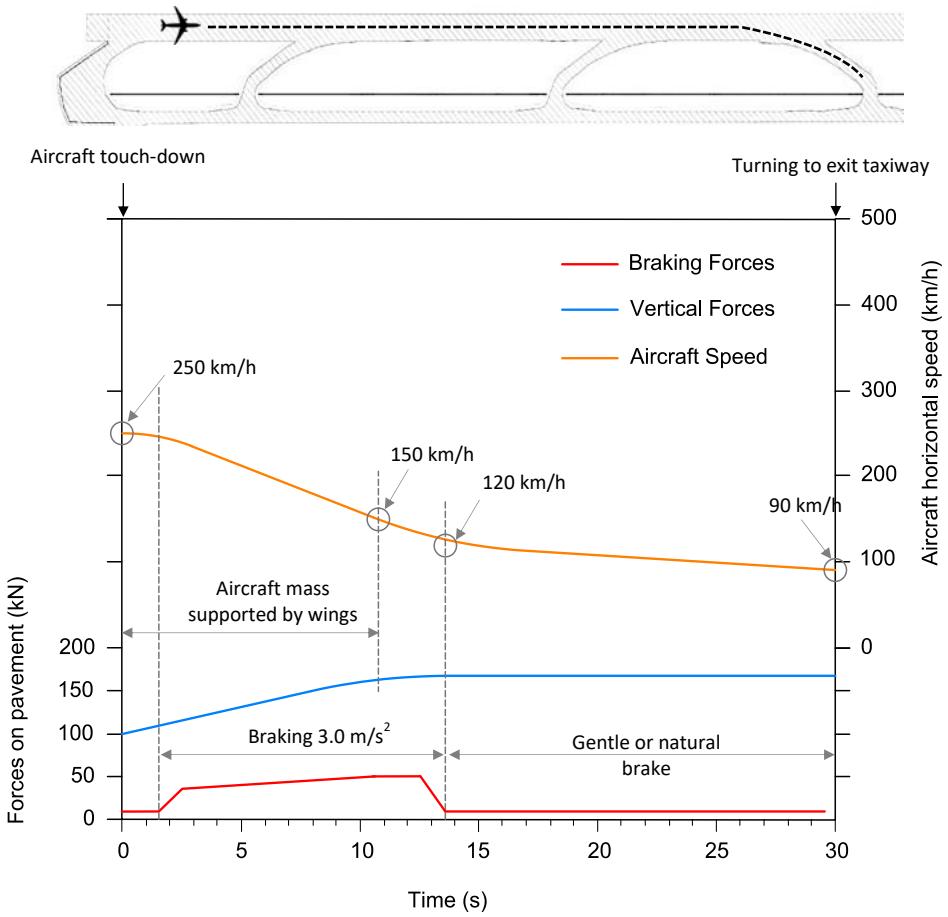

Figure 5.26 Forces on the pavement during the landing of B 737-800 (single wheel load)

5.4.2.2. Analysis Method

A multilayer linear elastic analysis using the BISAR program was carried out to investigate the stress state in the interface of newly laid asphalt overlay at three different traffic-opening temperatures: 60°C, 70°C, and 80°C. The pavement structure from the rutting analysis was used for this shear failure analysis (Figure 5.10). Different aircraft movements were simulated including taxiing (T), landing (L), turning on rapid exit taxiway (RET), and full braking (FB). The shear failure potential of newly laid asphalt pavement at the opening to traffic was examined by measuring the stress state point (from the analysis in BISAR) compared to the failure envelope by means of the Mohr–Coulomb failure relationship applied to a normal-shear stress plane.

a. Material Properties

The modulus of elasticity (E) of the newly laid asphalt pavement for the program input varies for each temperature. The modulus of elasticity was obtained from the repeated load axial test

(RLAT) as discussed in the rutting discussion before, using a technique proposed by Taherkhani and Collop (2008). The modulus of elasticity for each temperature for different bituminous mixtures is presented in Table 5.11.

Table 5.11 Modulus of Elasticity of asphalt overlay at different temperature

Bituminous Mixtures with binder:	Modulus Elasticity (MPa) of asphalt overlay at temperature at opening to traffic:		
	60°C	70°C	80°C
Pen. grade 40/60	454	316	142
SBS binder	626	460	324

b. Aircraft Loading Input

The B737-800 tyre loading parameters adopted for this analysis were similar to those used in the rutting analysis. Furthermore, the observation points for the interface shear analysis and tyre load footprint of the aircraft are shown in Figure 5.27. The estimated critical forces for four different B737-800 aircraft movements: full braking (FB), Rolling during taxiing (T), Landing (L) and Turning at RET (RET) are summarized in Table 5.12.

Table 5.12 Critical aircraft single wheel load of Boeing 737-800

Aircraft movement	Vertical forces (kN)	Braking forces (kN)	Centrifugal forces (kN)
Full braking (FB)	198.9	158.4	0
Rolling during taxiing (T)	198.9	0	0
Landing (L)	166.2	50.8	0
Turning at RET (RET)	166.2	0	25.3

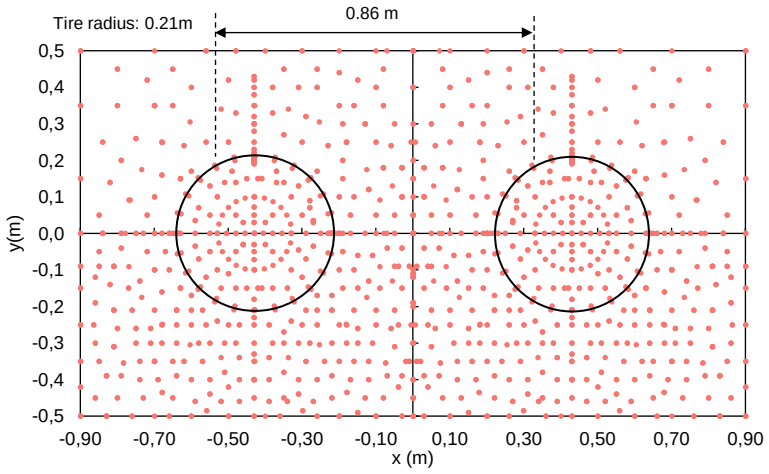

Figure 5.27 Tyre footprint of B737 for BISAR input and the observation points

c. Failure criteria

One of the methods to investigate the interface shear failure of asphalt pavement is by using the

Mohr-Coulomb criteria as displayed in Figure 5.28 (Mohammad et al. (2002), Canestrari et al. (2005), Chen and Huang (2010)). The method has been widely used to predict the shear failure of pavement interfaces (Wang et al. 2016, Ozer et al. 2013, Suddeepong et al. 2020, White 2016b). The Mohr-Coulomb theory assumes that interface failure is controlled by the envelope of a combination of interface shear stress and normal stress. The linear Mohr-Coulomb envelope for interface shear strength is displayed in Equation (5.8):

$$\tau_{failure} = c + \sigma \tan \phi \tag{5.8}$$

Where:

τ_{failure} = shear stress at failure, kPa
c = cohesion, kPa
σ = normal stress at failure, kPa
ϕ = angle of internal friction, degree

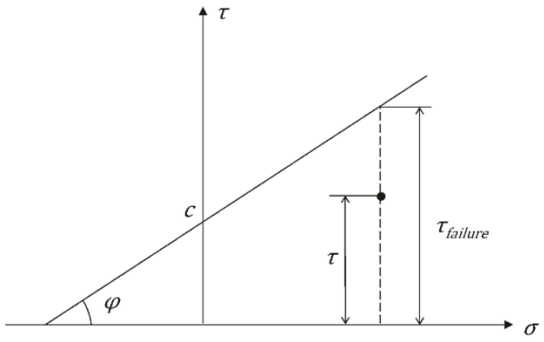

Figure 5.28 Representation of the Mohr-Coulomb failure criterion

The cohesion (c) is primarily affected by the properties of tack coat and binder, while the internal friction angle (ϕ) is determined by the interface texture, aggregate shapes and aggregate gradation. According to this criterion, the shear strength increases with increased normal stress on the failure plane. In this study, a trend line is fitted to the laboratory direct shear test data to obtain the failure envelope and its parameters (c and ϕ). The failure envelopes, as displayed previously in Figure 5.25, were used for the analysis. To measure how close the layer interface is to shear failure, the stress state points (from the analysis in BISAR) were examined against the failure envelope through a stress-to-strength ratio, as displayed in Eq. (5.9)(5.6). This ratio is also defined as a means of assessing the criticality of traffic-imposed stresses at the interface. The higher the ratio (closer to 1), the more likely shear failure becomes.

$$\text{Stress} - \text{to} - \text{strength Ratio} = \frac{\tau_{occ}}{\tau_{failure}} = \frac{\tau_{occ}}{c + \sigma \tan \alpha} \quad (5.9)$$

where:

τ_{failure} = Shear stress at failure, kPa

τ_{occ} = calculated shear stress, kPa

5.4.2.3. Typical Stress Distribution

The stress state data obtained from BISAR for each observation point was plotted in MATLAB using the contour function. X, Y and Z represent the transverse, longitudinal and vertical directions, respectively. The shear force was applied in the longitudinal direction for landing (L) and full braking (FB) conditions and in the transverse direction for turning at a RET (RET). No shear force was applied in the taxiing (T) movement. The peak shear stresses, as seen in Figure 5.29, were found to be at the front of the tyre over a depth range of 30 to 50 mm. The depth of peak shear stress matches those observed in earlier studies (Perdomo and Button (1991); Wang et al. (2014a); Su et al. (2008), and White (2016b)).

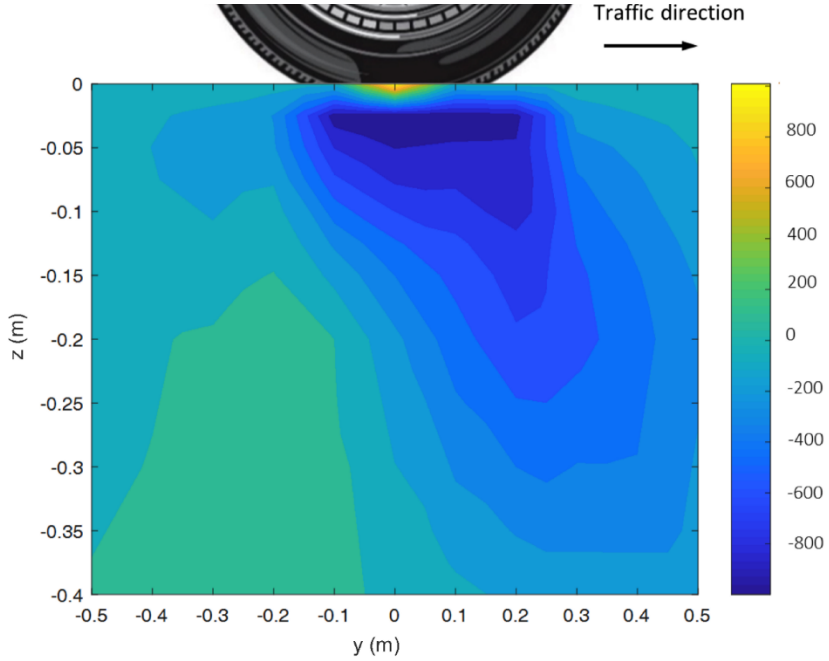

Figure 5.29 Shear stress Y-Z (kPa) with depth for full braking condition

The stress distributions along the width of the single tyre footprint at the layer interface (70 mm below the pavement surface) under the tyre centre area for various aircraft ground manoeuvring are plotted in Figure 5.30.

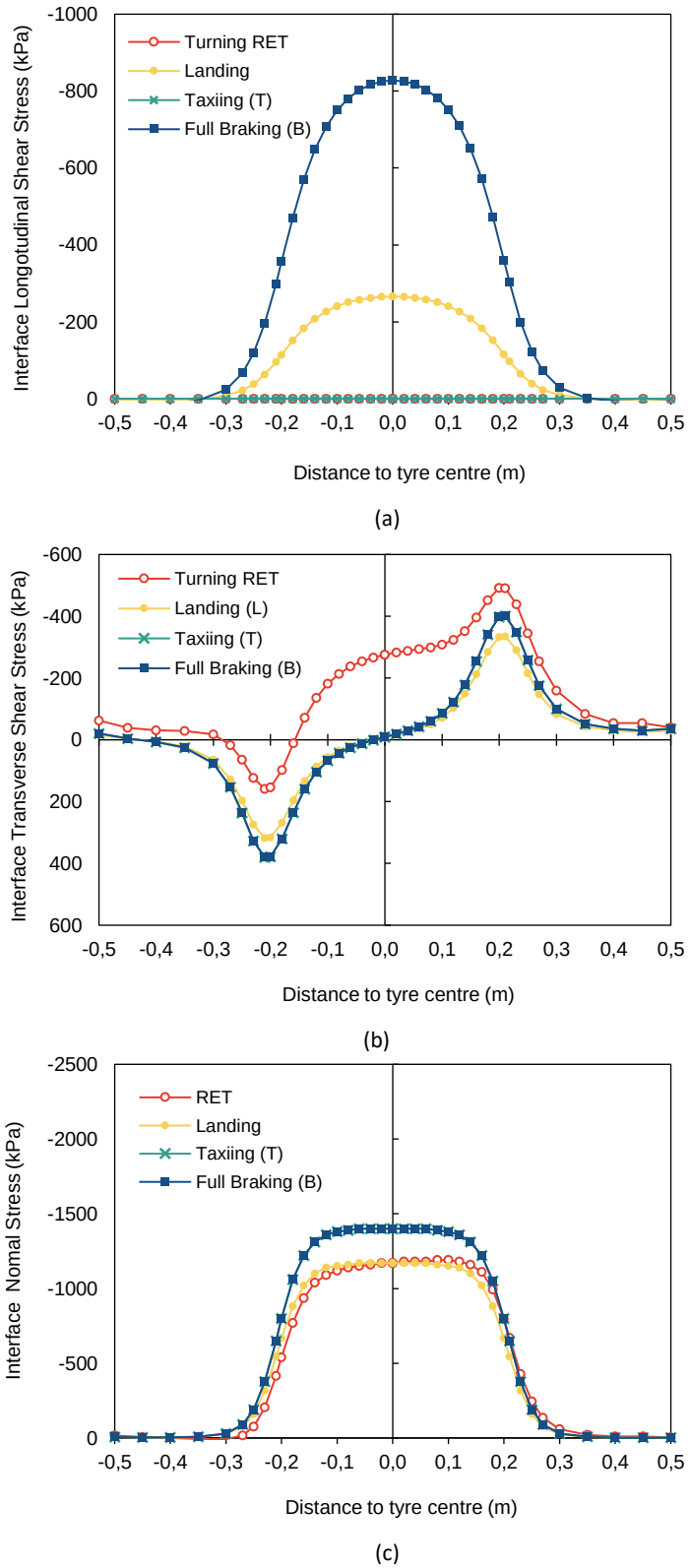

Figure 5.30. Distributions of (a) longitudinal shear stress; (b) transverse shear stress; and (c) normal stress at the interface along single tyre footprint at 60°C for interface C

The longitudinal shear stress (y-z) is parallel to the aircraft movement direction, while the transverse shear stress (x-z) is perpendicular to the aircraft movement direction. The results in Figure 5.30 show that the aircraft turning manoeuver at a RET produces much higher transverse shear stresses as compared to other aircraft movements. The transverse interface shear stresses were found to be concentrated towards one tyre side due to the centripetal force. Moreover, aircraft braking condition produces the greatest longitudinal shear stresses due to the highest horizontal load being applied parallel to the aircraft movement direction. The peak shear stress was 828 kPa, which is 60% of the vertical contact stress. This is similar to the values published by Wang et al. (2016) and White (2016b).

Variations in normal stresses at layer interfaces were not noticed among different aircraft movements with the same applied vertical loads on the pavement surface. For instance, it is found that taxiing and full braking caused similar interface normal stresses, even though different shear stresses were applied. Since the same vertical load was assigned on the asphalt surface, this suggests that applied shear stresses have no influence on the normal stresses at the asphalt interface. In addition, lower normal stresses at the asphalt interface were observed in aircraft turning at RET and landing operations, this is due to the lower vertical stress applied on the pavement surface.

5.4.2.4. Critical Stress Locations

Furthermore, the critical stress locations at which failure potential would be likely to occur were analysed. Figure 5.31 a and b shows the calculated normal stress and shear stress, respectively, at the pavement layer interface under B737 instantaneous/ full braking. As seen in Figure 5.31b, the maximum shear stress is concentrated at the front of the tyre. The shear stress directly under the tyre was found to be less than that at the front of the tyre. For comparison, the associated normal stress is presented in Figure 5.31a.

It is evident from the figure that within the tyre contact area, the normal stress was higher than the shear stress, which indicates high confinement. Figure 5.32 shows the calculated stress-to-strength ratio on the pavement layer interface under B737 instantaneous braking at 60°C for interface C. It can be seen that higher stress-to-strength ratios were found at the tyre contact edges or outside the tyre contact.

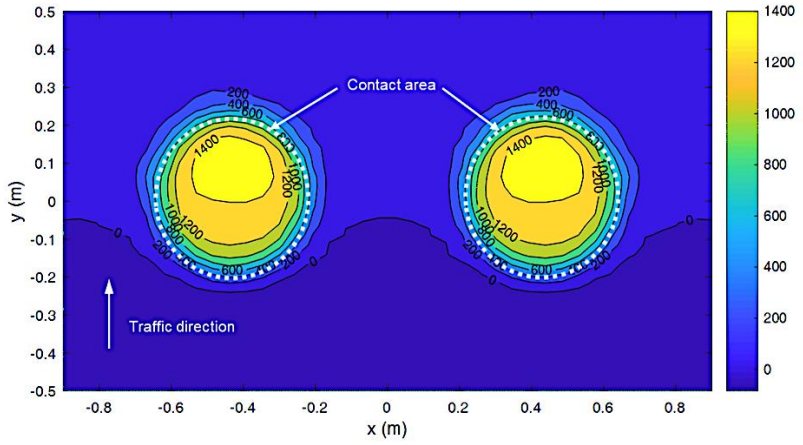

(a) Normal Stress (kPa) at layer interface

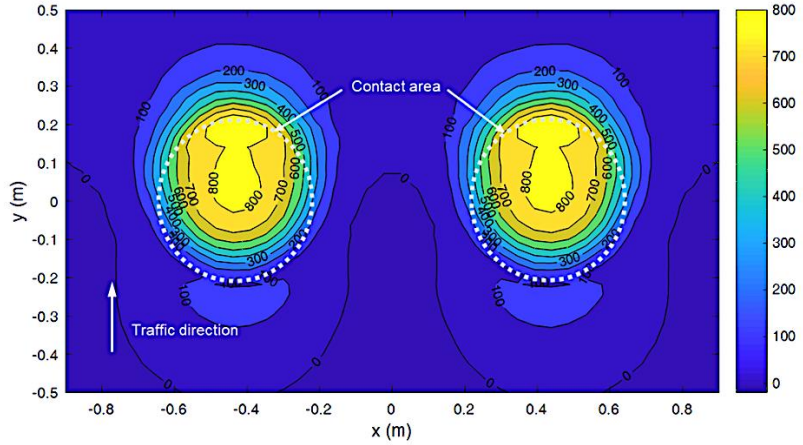

(b) Shear stress (kPa) at layer interface

Figure 5.31 Typical stress states (kPa) at the pavement layer interface

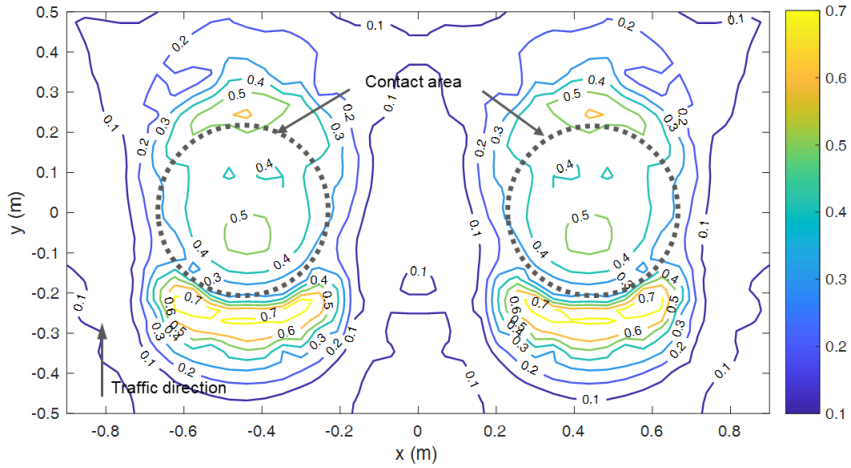

Figure 5.32 .Contours of calculated stress-to-strength ratio on pavement layer interface under B737 braking condition at 60°C for interface C

5.4.2.5. Shear Failure Analysis Results and Discussions

The critical stress-to-strength ratio for various aircraft movements with different traffic opening temperatures and interface types were calculated. For an illustration, the shear stress states for different aircraft movements at pavement temperatures of 60°C, 70°C and 80°C for interface C are shown in Figure 5.33. The failure envelope is presented along with the stress states to assess the shear failure potential of the layer interface. The interface cohesion strength and the friction angle of the failure envelope, obtained from the interface bond strength as presented before in Table 5.10, were used in the analysis. Furthermore, the maximum stress-to-strength ratio under various aircraft movements for each interface condition and instance is presented in Figure 5.33 and summarized in Table 5.13.

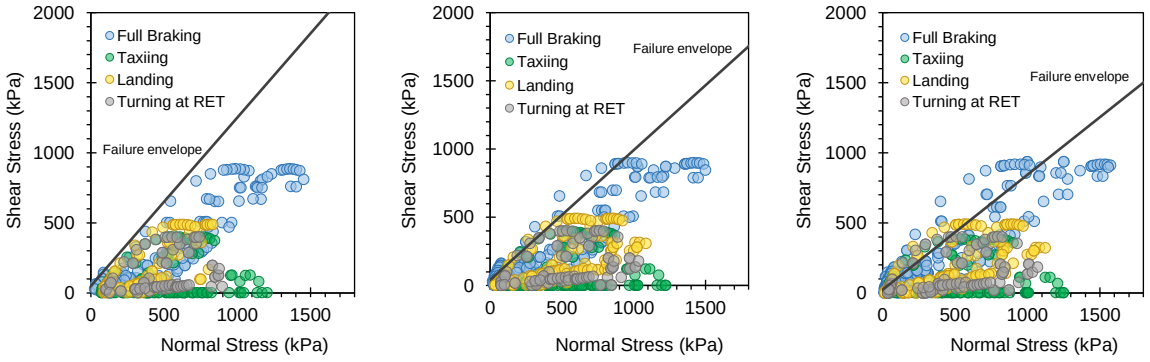

(a) 60°C (b) 70°C (c) 80°C

Figure 5.33 Critical stress at interface under B737 aircraft at different temperature at opening to traffic for interface C

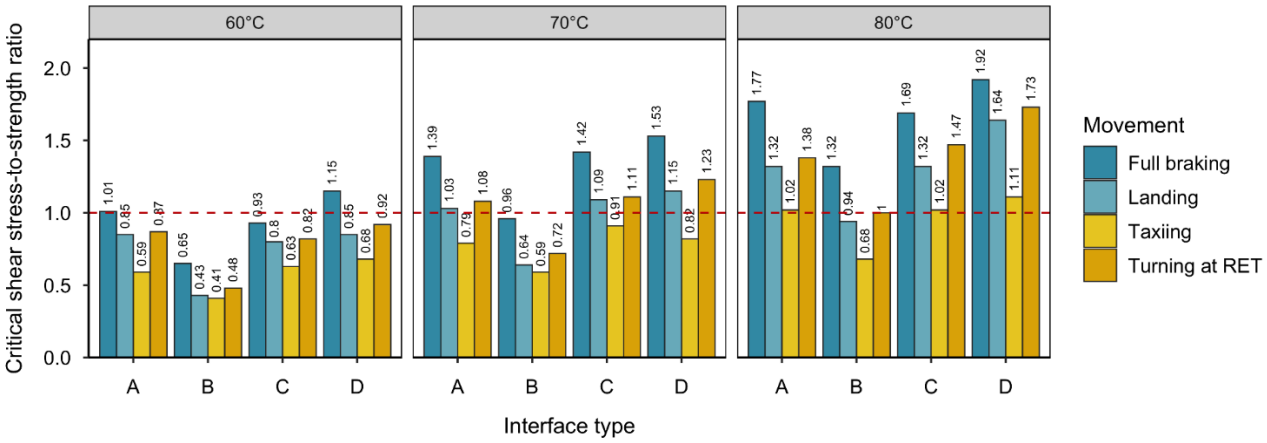

Figure 5.34 Critical stress-to-strength ratio for different B737 aircraft movement conditions at different temperatures at opening to traffic

These results show an increase in stress-to-strength ratio as a function of increasing temperature. In particular, it is observed that the stress-to-strength ratio at 80°C was higher than that at 60°C and 70°C. A high stress-to-strength ratio indicates the susceptibility of the asphalt interface to shear bond failure and a reduction of the shear fatigue life of the interface (Wang et al. 2017). It was found that at 60°C, the stress-to-strength ratios for almost all interfaces and aircraft load conditions were below 1, suggesting that the interface can still resist the forces applied. As expected, at 70°C and 80°C, the stress-to-strength ratio of the majority of the interface conditions under various aircraft movements exceeds 1. However, interface B still shows relatively acceptable shear resistance at the elevated temperatures.

Table 5.13 Critical stress ratio for different B737aircraft movement conditions

Test temp.	Interface	Pavement surface (lower layer)	Upper layer	Tack coat type	Critical stress ratio at layer interface for B737 aircraft movement:			
					T[a]	B[b]	RET[c]	L[d]
60°C	A	PCC	HMA-SBS	SBS binder	0.59	1.01	0.87	0.85
	B	HMA-40/60	HMA-SBS	SBS binder	0.41	0.65	0.48	0.43
	C	HMA-40/60	HMA-40/60	SBS binder	0.63	0.93	0.82	0.80
	D	HMA-40/60	HMA-SBS	K1-40	0.68	1.15	0.92	0.85
70°C	A	PCC	HMA-SBS	SBS binder	0.79	1.39	1.08	1.03
	B	HMA-40/60	HMA-SBS	SBS binder	0.59	0.96	0.72	0.64
	C	HMA-40/60	HMA-40/60	SBS binder	0.91	1.42	1.11	1.09
	D	HMA-40/60	HMA-SBS	K1-40	0.82	1.53	1.23	1.15
80°C	A	PCC	HMA-SBS	SBS binder	1.02	1.77	1.38	1.32
	B	HMA-40/60	HMA-SBS	SBS binder	0.68	1.32	1.00	0.94
	C	HMA-40/60	HMA-40/60	SBS binder	1.02	1.69	1.47	1.32
	D	HMA-40/60	HMA-SBS	K1-40	1.11	1.92	1.73	1.64

Notes: [a]Taxiing, [b]Full braking, [c]Turning at rapid exit taxiway, [d]Landing

These results indicate that the selection of bituminous mixtures and tack coat materials play an important role in allowing the opening of new asphalt to traffic. A modified binder used as a tack coat (interface B) resulted in a significantly better interface resistance to shear failure, compared to a conventional emulsion (interface D). Additionally, with the same tack coat, the overlay mixtures with the unmodified binder (Interface C) showed greater shear damage potential compared to mixtures containing SBS modified binder (interface B). It was also found that the PCC surface has a greater stress ratio than the HMA surface.

For all interface conditions, it was observed that aircraft instantaneous/ full braking (in the presence of a friction coefficient of 0.8) was the most critical loading condition for interface shear failure. It was also found that aircraft turning at RETs was more critical than typical aircraft landing (not hard landing). The aircraft taxiing/take-off, landing, and turning at a RET

movements caused significantly lower shear failure as compared to aircraft full braking (FB). These results suggest that to avoid premature shear damage during the early life of a new asphalt overlay, airport authorities should consider limiting aircraft extreme braking and turning activities. As the typical day-in-and-day-out braking condition in a major airport is expected to be the steady braking, 3.0 m/s^2 (O'Massey 1978), it is recommended that the occasional aircraft full braking operation (coefficient of friction of 0.8) should be restricted during the early life of newly laid asphalt to prevent premature interface shear failure.

Overall, in terms of rutting and interface shear bond performance, it can be concluded that a traffic-opening temperature of 60°C (or below), as recommended by many agencies, is likely to be acceptable for typical asphalt mixtures with conventional binder when an overlay is placed in compliance with the construction specifications. At 60°C, for all bituminous binders and tack coat materials, the newly laid asphalt has gained sufficient rutting and shear bond resistance for trafficking. This result suggests that some of the failure cases that occurred at airfields (see Chapter 2, section 2.3.2.5 and 2.3.3.6) are likely not induced by the decision to open the new asphalt at commonly adopted traffic-opening temperature (60°C), rather it is likely caused by other factors, such as deficiency in the construction process or non-compliance with specifications / low-quality of pavement material. Moreover, the results, suggest that different mixtures, particularly those containing polymer-modified bitumen (PMB), could be re-opened to air traffic at a considerably higher temperature (up to 80°C). This recommendation is based on laboratory performance test data. Nevertheless, this analysis result should encourage airport authorities and agencies to be more flexible with the traffic-opening temperature specification, particularly for mixtures incorporating PMBs.

The selection of traffic-opening temperature is bituminous binder-dependent, hence it is necessary to give the pavement designer the ability to establish opening temperature based on the bituminous binder type and its performance. Based on this study, polymer modifier bitumen (PMB) can be beneficial for asphalt mixture and tack coat materials to enhance resistance to rutting and interface shear bond performance at the selected traffic-opening temperature. Although not used as much as asphalt emulsion, using a polymer modified binder, such as PG binder, as tack coat would provide an added advantage of less construction time, due to no curing time being required for the tack coat (Zhang 2017). This could be of great benefit at busy airports. However, the PMB needs to be heated to a significantly higher temperature to ensure spraying

flowability, which requires more energy and, thus, greater environmental and economic demands.

Finally, Polymer Modified Bitumen (PMB) is intended to enhance pavement performance at high in-service temperatures (Airey 2004, Carrera et al. 2010). Based on the Superpave Performance Grading (PG) grading (Kennedy et al. 1994), high temperature grades of bitumen with modifiers can be as much as PG76 or PG82 to provide service where the average seven-day maximum pavement temperature is under 76°C and 82°C, respectively. Hence, the adoption of 80°C (when PMB is used) as a critical traffic-opening temperature should be considered with caution and only applied in emergency situations.

5.5. Effect of Allowable Temperature at Opening to Traffic on Construction Productivity

In the following section, an illustrative study on the basis of a runway resurfacing is performed to demonstrate the effect of temperature at opening to traffic on reducing the overall construction time during a night-time overlay project. During night-time construction in an active airport, it is expected that the asphalt construction productivity is highly affected by the cooling time of the newly paved asphalt. From the predetermined time window each night, at the end of the work time frame, contractors should allow several hours for cooling of newly placed asphalt before traffic opening. Raising traffic-opening temperature would reduce the asphalt cooling time. In the case of the closure of an airport each night, the reduced cooling time would potentially improve work productivity and allow contractors to place the maximum amount of HMA each night due to the increase in useful work time. With higher productivity, the overall contract can be shortened and the project can be finished faster.

There are many variables affecting the productivity of the asphalt construction process. Among those variables are the bituminous mixtures characteristics, asphalt overlay thickness, delivery temperature, equipment productivity and the environmental conditions at the time of placement (Arbeider et al. 2017). The relationships between each variable are illustrated in Figure 5.35. It is noted that greater night-time productivity can be achieved by many methods including additional asphalt mixing plants, asphalt paver and roller equipment and labor teams. The ability to open pavement overlays at higher-than-conventional temperatures adds another option for the contractor to improve the construction productivity.

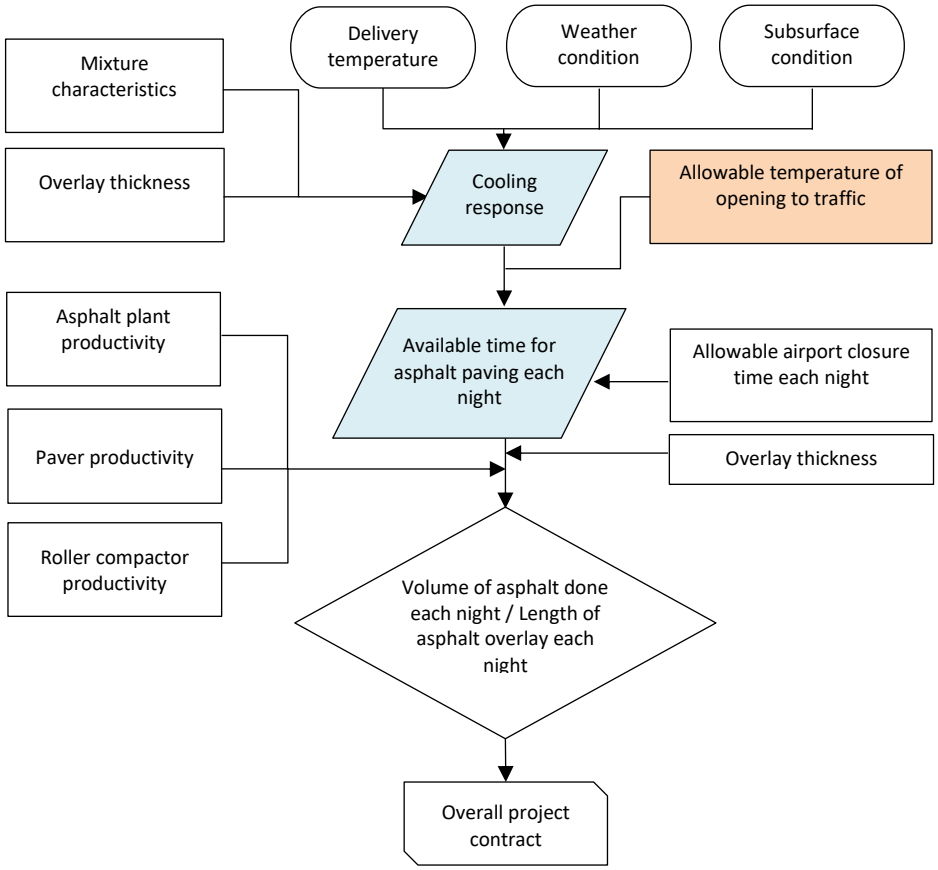

Figure 5.35 Relations between relevant variables

In this research, to reduce the number of independent variables in the analysis of construction productivity, these assumptions were adopted:

- A time window of seven hours is allocated per night
- A runway dimension of 3600 x 60 m was assumed
- Asphalt concrete overlay thickness: 70mm

5.5.1. Construction Stages

The asphalt overlay work stages were adopted from a real project at Fukuoka Airport, Japan (Hachiya et al. 2008) as illustrated in Figure 5.36. From the 7-hour available time window each night, 60 minutes are spent for trimming and cleaning the surface and 30 minutes for applying and setting the tack coat. The available time for asphalt placement and compaction for each mixture depends on the cooling time determined from the heat transfer analysis in Chapter 4. Moreover, at the end of the work period each night, before traffic-opening, approximately 60 minutes are required for re-installing the lighting system, painting the line-markings,

construction of temporary joints and cleaning.

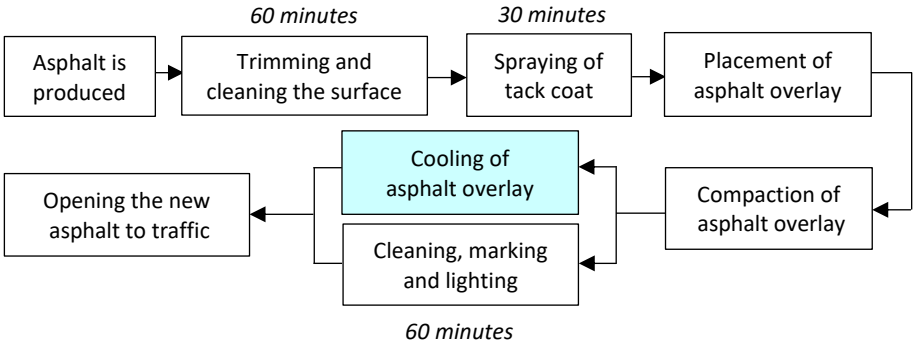

Figure 5.36. Construction stages of asphalt overlay (adopted from Hachiya et al. (2008))

5.5.2. Equipment Productivity

Empirical data on construction productivity adopted from Arbeider et al. (2017) and an airfield overlay project at Jakarta airport, Indonesia in 2019 were used in the analysis. The paver speed, roller speed, along with the number and production capability of each equipment are listed below:

- 2 asphalt pavers (speed of 4 to 7 m/min, depending on the thickness of pavement lifts) with screed width of 7.5 m and productivity of 212 ton/hour
- 8 tandem rollers (speed of 25 m/min) with a width of 1.5 m and productivity of 37 ton/hour each
- 4 pneumatic tyre rollers (speed of 45 m/min) with a width of 2 m and productivity of 80 ton/hour each. The 'distance' paver-to-roller-compactor is 15 minutes.

5.5.3. Cooling Time Estimation

As discussed in the previous chapter (Chapter 4), a one-dimensional (1D) heat-transfer model using a finite element (FE) solution was developed to investigate the effect of traffic-opening temperature on the cooling time of newly laid asphalt. For the purpose of this chapter, the predicted cooling times of 70mm asphalt overlay in typical tropical countries during night-time construction under different wind speed were used for the analysis. The initial laying temperature was assumed to be 150°C for HMA with SBS binder and 130°C for HMA with 40/60 pen. grade, as discussed in section 4.5.3 of this thesis. The cooling times needed for HMA to reach traffic-opening temperature obtained from Chapter 4 are as shown in Figure 5.37 for various mixtures.

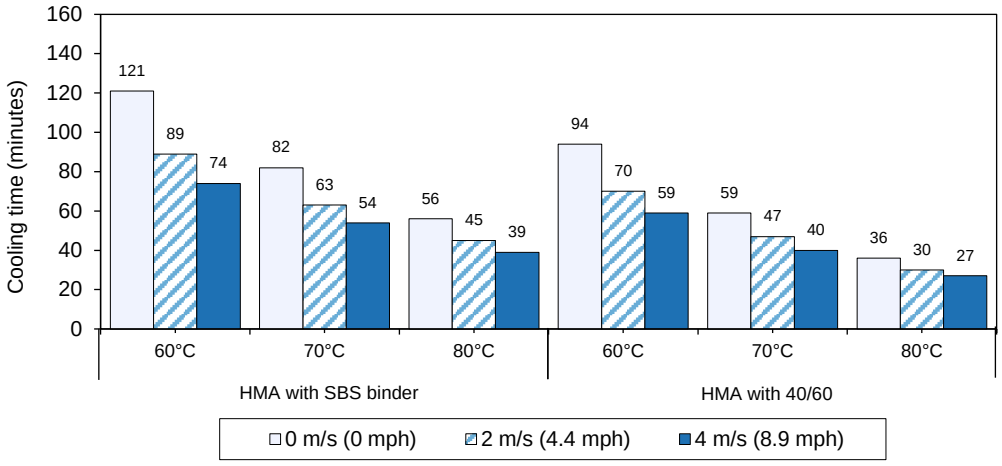

Figure 5.37 Cooling time needed for HMA to reach traffic-opening temperature

5.5.4. Construction Schedule

The total time available for the asphalt laying and compaction for each mixture and opening temperature strategy work can be calculated by subtracting the given closure time window (7 hours, in this case) with initial trimming and cleaning, setting up, and required cooling time, as well as the site clearing, marking and lighting installation time at the end of the resurfacing work. As an illustration, Figure 5.38 shows a typical construction schedule for each night for SBS bituminous mixture overlay with three different traffic-opening temperature strategies under a wind speed of 0 m/s. It is clear from Figure 5.38 that as a result of reduced cooling time, the available period for asphalt placement and compaction is extended. This indicates improved construction productivity can be achieved by opening the newly laid asphalt at a higher-than-conventional temperature.

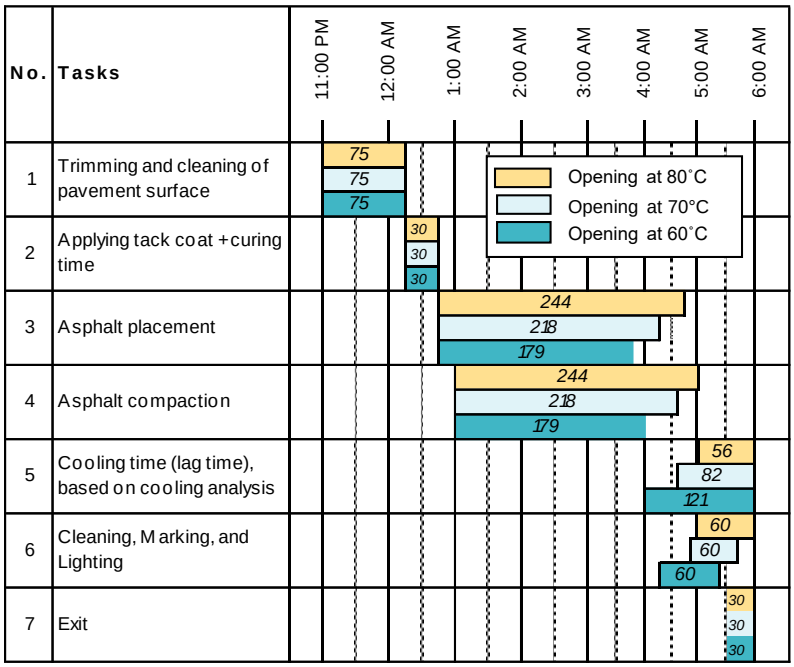

Figure 5.38. Schedule of asphalt overlay work per night (in minutes) for SBS mixture under a wind speed of 0 m/s for different traffic-opening temperatures

5.5.5. Construction Time Estimation

Making use of the available time for asphalt paving work and work productivity, the volume of asphalt produced each night was computed. Table 5.14 lists the estimated overall project nights for different overlay bituminous mixtures and wind speeds with different traffic opening strategies. For illustrative purposes, the work productivity, in terms of length of asphalt paved and work duration, for different mixtures under a wind speed of 0 m/s is displayed in Figure 5.39.

As displayed in Figure 5.39, for an asphalt overlay formed of an SBS mixture under a wind speed of 0 m/s, it is predicted that when traffic-opening temperature is set to 60°C, 42 nights are needed to finish construction, whereas 34 nights (a 19% reduction), and 31 nights (a 26% reduction), are needed when it is opened at 70°C and 80°C, respectively. Overall, for the cases studied, raising the critical traffic-opening temperature could reduce the overall construction time by 2-11 nights (see Table 5.15), depending on mixture type and wind speed. The reduction of asphalt overlay project period is more significant for mixtures with PMBs, see Table 5.15. From this, it can be concluded that raising the critical traffic-opening temperature is not effective for bituminous mixtures with unmodified binder for which the laying temperature is relatively low.

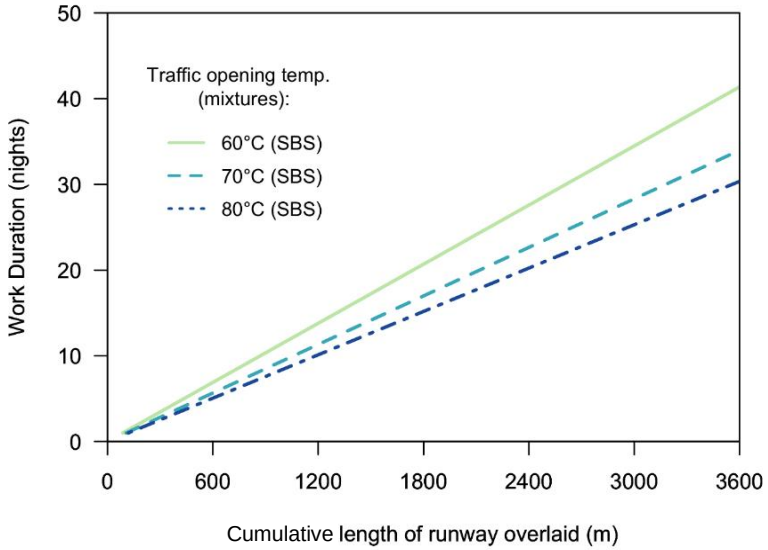

Figure 5.39. Work duration vs. length of runway overlay paved for different mixtures and traffic-opening temperature under a wind speed of 0 m/s

Table 5.14 Predicted construction duration of asphalt overlay project for different traffic-opening temperature, mixtures and wind speed

Night-time wind speed	Estimated total construction time (nights) on a-3600 x 60 m runway for different asphalt mixes and traffic-opening temperature:					
	HMA with SBS binder			HMA with 40/60 binder		
	60°C	70°C	80°C	60°C	70°C	80°C
0 m/s (0 mph)	42	34	31	36	31	31
2 m/s (4.4 mph)	36	32	31	33	31	31
4 m/s (8.9 mph)	33	31	31	31	31	31

Table 5.15 Construction savings nights as compared to traffic-opening temperature of 60°C

Night-time wind speed	Construction savings nights, compared to traffic-opening temperature of 60°C:			
	HMA with SBS binder		HMA with 40/60 binder	
	70°C	80°C	70°C	80°C
0 m/s (0 mph)	8	11	5	5
2 m/s (4.4 mph)	4	5	2	2
4 m/s (8.9 mph)	2	2	0	0

Moreover, the opening of newly laid asphalt pavement depends greatly on the time required for re-installing the lighting system, painting the line-markings, construction of temporary joints and cleaning at the end of each night. In the instance where this restoration period is longer than the asphalt cooling time, traffic-opening at high temperature, e.g. 70°C or 80°C, would be pointless. In this research, the restoring time was assumed to be 60 minutes. As

seen in Table 5.15, the overall number of construction nights for mixtures with cooling time less than 60 minutes was the same for all conditions: 31 nights. This is because the restoration time was the determining factor.

5.6. Results and Discussion

This chapter investigated traffic-opening temperature of newly laid asphalt through rutting and interface shear failure analysis. The effect of traffic-opening temperature selection on construction productivity was also examined. The following findings can be drawn from this study:

- Selection of bituminous binder, mixtures and tack coat materials play an important role to avoid premature rutting and shear failure of newly laid asphalt overlay during early life trafficking at high temperature.
- At 60°C, newly laid asphalt with typical conventional binder has gained sufficient strength to resist permanent deformation and interface failure caused by aircraft load and braking. The results demonstrated the suitability of the traffic-opening temperature set by many agencies.
- The results, however, suggested that different mixtures and tack coats, particularly those containing polymer-modified bitumen (PMB), could be re-opened to air traffic at considerably higher temperatures (up to 80°C) due to their superior rut resistance and interface bonding. This analysis result should encourage airport authorities and agencies to be more flexible with the traffic-opening temperature specification, particularly for mixtures incorporating PMBs.
- Selection of traffic-opening temperature is bituminous binder-dependent, thus it is necessary to give the pavement designer the ability to establish opening temperature based on the bituminous binder type and its performance at the selected traffic-opening temperature.
- The illustrative study presented in this study showed that raising the critical temperature could improve the construction productivity by shortening the overall project time (for a runway overlay) by 2-11 nights (6-26% savings time) for a PMB mixture, in the cases studied.

6. Analysis of Warm Mix Asphalt (WMA) for Airfield Pavement Overlay

6.1. Overview

Warm-mix asphalt (WMA) is commonly mixed and compacted 15°C to 30°C below that of conventional hot mix asphalt (HMA). The lower production temperature of WMA is expected to give an advantage of a lower cooling time of newly laid asphalt overlay before it can be opened to traffic during night-time airfield pavement construction. The reduced cooling time of WMA would allow a shorter airport closure time window and/or extend the time for the contractor for paving, and thus shorten the overall construction period due to more volume being done each night. This is a beneficial practical advantage to hectic airports where the typical off-peak period is as short as 6-8 hours. In this research, two different WMA technologies, Sasobit® and Rediset® (organic and chemical) were investigated through laboratory tests to see if there were notable differences in WMA rutting performance that could have considerable practical effects on the permissible temperature at opening to traffic as compared to HMA.

6.2. Aim of Research Phase

The research question to be answered in this research phase are as follows:

- How does the rutting and interface shear bond performance of WMA compare to HMA as the overlay to an airport pavement? Is there any notable difference in WMA performance, as compared to HMA, that could have significant practical effect on the permissible temperature at opening to traffic?

The same laboratory tests and analyses of rutting and interface shear bond performance of bituminous mixture carried out in Chapter 5 for determining traffic-opening temperature were repeated in this chapter in regard to warm mix asphalt material. Furthermore, an analysis

was also carried out to investigate the effect of the use of WMA on airport closure time and overlay project productivity.

6.3. Materials and Mixture Design

Two types of additives for WMA, organic and chemical, are used: Sasobit®, one of the most widespread organic WMA additives in commercial use, and Rediset® LQ-1102CE, a popular chemical WMA additive.

6.3.1. Sasobit

Sasobit is an organic warm mix additive that was first introduced in 1997 whose molecular formula is C_nH_{2n+2} (Sasol 2008). Sasobit is a synthetic hard wax, long-chain non-aromatic hydrocarbon produced from sustainable feedstock or natural gas using gas-to-liquids technology via the Fischer-Tropsch (FT) process (Jamshidi et al. 2013). Sasobit can be either in the form of a white powder or granules (prills) (Jalali 2016). Sasobit acts as a flow improver in the bituminous mixture which promotes aggregate coating with bituminous binder (Caputo et al. 2020). Modification with Sasobit alters the viscosity of bituminous binder, as seen in see Figure 6.1. When Sasobit becomes liquid over a temperature range between 90 and 110°C, it is completely soluble in a bituminous binder and thus the temperature of the bituminous binder at mixing viscosity can be reduced by 10-30°C (Diab et al. 2016). Conversely, at approximately 90-110 °C, Sasobit starts to crystallize and forms a microscopic crystal network structure in the bituminous binder which enhances stiffness and permanent deformation resistance of the bituminous mixture (Jalali et al. 2014), see Figure 6.1.

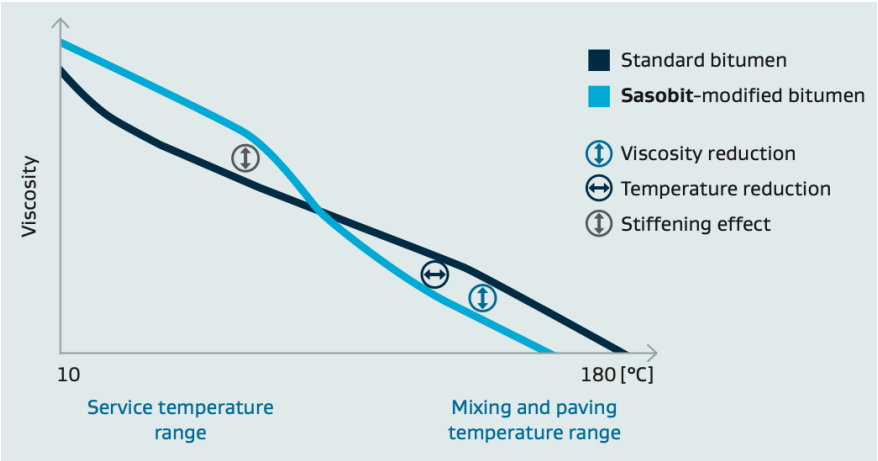

Figure 6.1. Viscosity curves of standard bitumen and Sasobit-modified bitumen (Sasol 2008)

The manufacturer claims that below the wax transition temperature, Sasobit could increase the rutting resistance of bituminous mixtures (Sasol 2008). This phenomenon is likely because Sasobit has long hydrocarbon chains that change the hydrocarbon chain length of the bituminous binder (Arabali et al. 2017) and thus modify the physical properties of the bituminous binder, such as stiffness and viscosity (Srikanth et al. 2018). Many studies (Capitão et al. 2012, Kheradmand et al. 2014, Das et al. 2012, Petit et al. 2012, Medeiros et al. 2012b), however, indicate that the addition of Sasobit may reduce fatigue and lower thermal cracking resistance of the bituminous mixtures at low service temperatures. Sasobit is typically added at 2% to 4% by mass of the bituminous binder. The Sasbobit prills can be added to the bituminous binder either by pre-mixing with the bituminous binder (ready-to-use binder) or in the plant supply tank. It can also be added to the mixture by pneumatically blowing them into the asphalt drum plant (D'Angelo et al. 2008).

6.3.2. Rediset

Rediset is a chemical warm mix additive that was introduced in 2007 (Bonaquist 2011). Rediset is marketed as an adhesion-promoting warm mix additive (Bonaquist 2011). It is a chemical (water-free) warm mix additive produced by AkzoNobel, Netherlands (Arega et al. 2011). It was first introduced in solid form and marketed with the name Rediset WMX. The liquid form, Rediset LQ, was then introduced in 2011 to simplify handling and metering at the plant (Akzonobel® 2014). In this study, only the liquid form of Rediset (LQ 1102 CE) was used for the laboratory tests.

Rediset is a combination of fatty polyamines, polymer and cationic components (Xiao et al. 2011, Xiao et al. 2012). The tail of this additive can be a long chain non-aromatic hydrocarbon structure and while its head can be an $-NH_3^+$ which has active adhesion promoters that react chemically with aggregate surfaces (Syroezhko et al. 2011). Rediset is a multifunction warm mix additive (Zhang et al. 2012) that lowers the production temperature of WMA based on the combination of surface active agent (surfactant) and rheology modifier (of organic nature) mechanisms (Prowell et al. 2011, Chowdhury and Button 2008, Kheradmand et al. 2014, Zhu et al. 2013). The surfactant component of Rediset reduces surface or interfacial tension of a bituminous binder (Banerjee et al. 2012), improves the coatability of aggregate with bituminous binder (Kassem et al. 2018), and improves moisture susceptibility and promotes adhesion of bituminous mixtures (Capitão et al. 2012), while the organic component lowers the viscosity of

bituminous binder and allows better lubrication for mixing and compaction of bituminous mixture (Tsai and Lai 2010, Kheradmand et al. 2013).

6.3.3. Material Designation and Rheological Properties

The two warm-mix technologies at selected dosage rates (explained in Chapter 3) were blended with the control bituminous binders of conventional 40/60 pen. grade and SBS polymer modified binder (Table 6.2) in the laboratory, based on British Standard BS EN 12594:2014. The bituminous mixtures with both WMA additives were produced approximately 20°C below that of HMA. A total of six bituminous binders were used for the tests. The bituminous binders' and mixtures' designations are presented in Table 6.2.

Table 6.1. Binders used in this research

Terminology of mixtures	Binder type	WMA Additives	State of additives	Additives dosage (% of binder weight)
B1	SBS modified binder	-	-	-
B2	SBS modified binder	Sasobit®	Prill form	2%
B3	SBS modified binder	Rediset® LQ-1102CE	Viscous liquid	0.5 %
B4	Pen. grade 40/60	-	-	-
B5	Pen. grade 40/60	Sasobit®	Prill form	2%
B6	Pen. grade 40/60	Rediset® LQ-1102CE	Viscous liquid	0.5 %

The conventional and rheological properties of bituminous binders used in this study are listed in Table 6.2. As discussed in Chapter 3 Section 3.3, it can be noted that the mixtures with SBS binders (B1, B2, B3) demonstrate a potential superior rutting resistance at elevated temperature as compared to conventional penetration-grade 40/60 binders (B4, B5, B6). This can be seen from the lower non-recoverable creep compliance (J_{nr}) and higher percentage recovery (% Rec) of SBS modified binder obtained from MSCR test. It was also observed that the addition of Sasobit (B2 and B4) improved rut resistance potential of bituminous binders as compared to the control binders at all temperatures, while the use of chemical additive, Rediset (B3 and B5), led to slightly higher permanent deformation.

6.4. Rutting Performance of Asphalt at Traffic Opening Temperature

6.4.1. Laboratory RLAT Results

Figure 6.2 (a) to (d) presents the permanent deformation profiles of the RLAT of all bituminous mixtures at 50°C, 60° C, 75°C and 85°C, respectively. In general, the results obviously show greater permanent deformation at the higher test temperature. This was predicted, as with

greater temperatures and load, the bituminous mixtures are more susceptible to plastic deformation. The specimens immediately failed after a few cycles, especially at 85°C.

Table 6.2. Rheological properties of the bituminous binders

Binder type	Viscosity (Pa.s)		DSR, G*/sinδ (kPa) at 64°C, unaged	MSCR at 64°C at 3.2 kPa		MSCR at 76°C at 3.2 kPa	
	135°C	165°C		J_{nr} (KPa^{-1})	% Rec	J_{nr} (KPa^{-1})	% Rec
B1 (SBS)	0.960	0.302	2.78	0.036	97.75	0.280	91.59
B2 (SBS+S)	0.769	0.253	5.91	0.010	97.83	0.050	94.91
B3 (SBS+R)	0.833	0.448	2.90	0.041	97.59	0.180	94.64
B4 (40/60)	0.395	0.114	2.00	4.322	0.35	21.230	-1.12
B5(40/60+S)	0.356	0.105	3.83	2.984	2.24	16.370	-0.80
B6 (40/60+R)	0.418	0.116	2.23	4.463	0.31	20.290	-2.23

Note: DSR = dynamic shear rheometer, Rec = recovery, J_{nr} = nonrecoverable creep compliance.

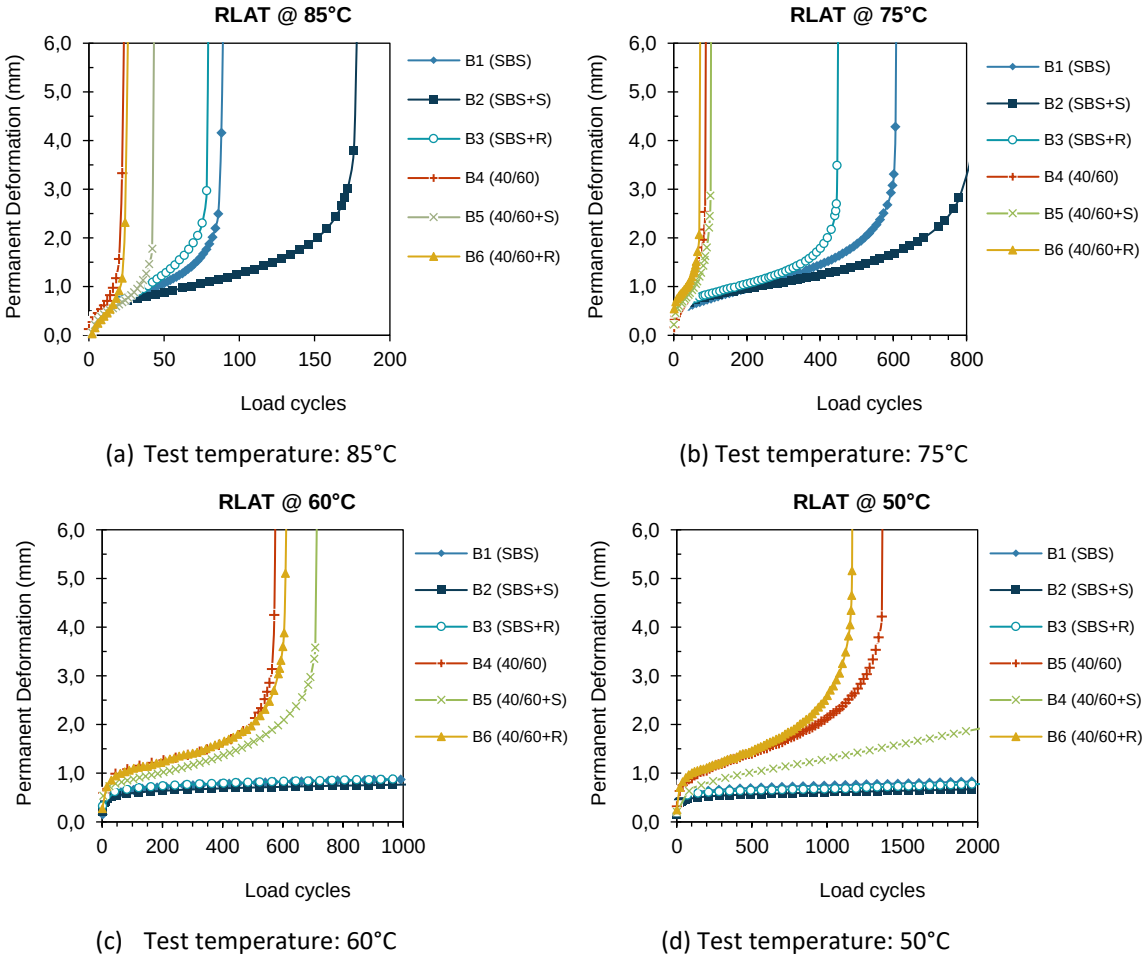

(a) Test temperature: 85°C (b) Test temperature: 75°C

(c) Test temperature: 60°C (d) Test temperature: 50°C

Figure 6.2. RLAT results

The results also revealed that the mixtures with SBS binders (B1, B2, B3) show much better rutting performance at high temperature than the conventional pen. grade 40/60 binders (B4, B5, B6). In addition, it was observed that the WMA Sasobit showed better rut resistance

than the WMA Rediset and HMA at all temperatures, while the use of chemical additives (Rediset) led to slightly higher permanent deformation. For instance, as summarized in Table 6.3, at 85°C, the RLAT cycles to failure of mixtures with SBS control binder (B1) were 90 cycles. The cycles to failure for mixtures with the addition of warm mix additives, B2 (Sasobit) and B3 (Rediset), were 176 and 79, respectively. In comparison, the RLAT cycles to failure at 85°C for mixtures with pen. grade 40/60 control binder (B4) were only 24 cycles. At the same temperature, the RLAT cycles to failure were 43 cycles for mixtures with B5 (Sasobit) and 26 cycles for B6 (Rediset).

Table 6.3. Test temperature, RLAT cycles to failure of mixtures and MSCR binder properties

Binder/mix with binder:	Test temp. (°)	RLAT cycles to failure	MSCR J_{nr} at 3.2 kPa^{-1}
B1 (SBS)	75	609	0.28
	85	90	4.35
B2 (SBS+S)	75	824	0.05
	85	176	0.74
B3 (SBS+R)	75	448	0.18
	85	79	3.39
B4 (40/60)	75	90	21.23
	85	24	40.71
B5 (40/60+S)	75	103	16.37
	85	43	37.20
B6 (40/60+R)	75	74	20.29
	85	26	40.92

6.4.2. RLAT Results vs. MSCR results

Figure 6.4 and Figure 6.3 shows a plot of the RLAT against the J_{nr} (non-recoverable compliance) extracted from the MSCR test at the high test temperature (Table 6.3), for SBS binders and pen. grade 40/60 binders, respectively. A linear relationship between the MSCR test results of neat binders and RLAT permanent deformation provided a good relationship with an R^2 of 0.913 (Figure 6.3). Additionally, for SBS modified binders, a power-law relationship provided an excellent correlation of J_{nr} to permanent deformation with an R^2 of 0.929 (Figure 6.4). Considering the mix variability from sample preparation, the J_{nr} of MSCR correlates well with the bituminous mixture permanent deformation assessed by the RLAT.

Based on the binder test (MSCR) and RLAT, the rutting performance of WMA is comparable with the HMA. Interestingly, the addition of Sasobit improved the mix rutting resistance significantly at fairly high temperature. This is likely because based on the Brookfield viscometry test results performed previously in Chapter 3 (Figure 6.5) after the asphalt

temperature drops to the Sasobit's wax transition temperature (95-115°C), the Sasobit begins to solidify (crystallize) and thus improves the stiffness, viscosity and permanent deformation resistance of the bituminous mixtures. The results indicate that the addition of Sasobit would enable new asphalts to be opened to traffic at higher temperatures than HMA or WMA with added Rediset.

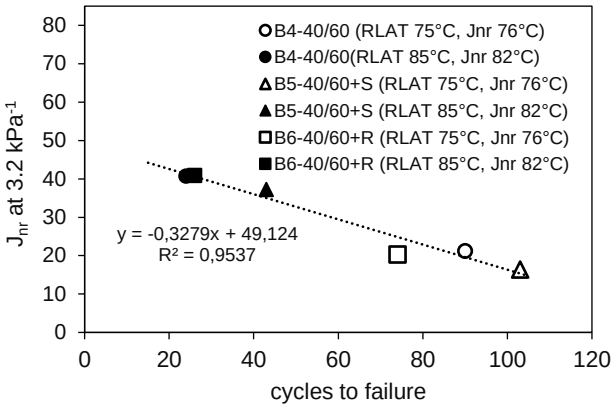

Figure 6.3. Relationship of J_{nr} at 3.2 kPa^{-1} and RLAT results for neat binders and WMA(B4, B5, B6)

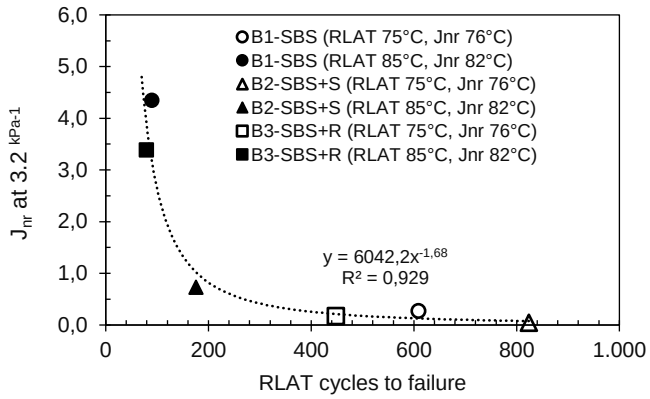

Figure 6.4. Relationship of J_{nr} at 3.2 kPa^{-1} and RLAT results for SBS modified binders and WMA (B1, B2, B3)

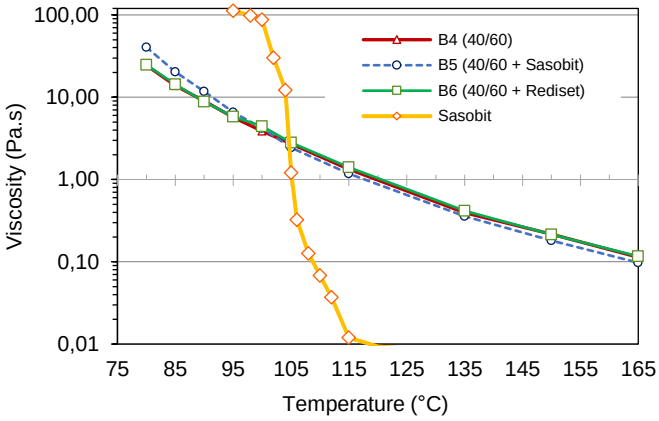

Figure 6.5. Brookfield viscometer test results

The following findings may be deduced from the MSCR and RLAT results:

- The laboratory test results showed that WMA has a rutting performance similar to, or better than HMA at the same temperature.
- Rediset LQ chemical additive has nearly no effect on the rheology of the binder and rutting performance of bituminous mixture at traffic-opening temperature. This is likely because its principal action as surfactant is only to promote coatability of aggregate and bituminous binder and thus enable the mixing at lower temperatures. Unlike Sasobit, the organic part of Rediset seems not to modify the physical properties of the bituminous binder, such as stiffness and viscosity.
- The addition of Sasobit additive improved the rutting resistance of bituminous binder and mixture significantly at traffic-opening temperature (60-85°C). This can be seen from the lower J_{nr} and higher %Recovery of MSCR test and a greater number of cycles to failure in the RLAT at high temperature.
- Reduction in viscosity at the production temperature by adding Sasobit did not increase rut depth at the temperature at opening to traffic. Rather, due to its crystallizing properties, the Sasobit additive is solid below the wax transition temperature and thus improved the stiffness and rutting resistance of the bituminous mixture.
- The permanent deformations correlate well with the non-recoverable creep compliances (J_{nr}) from the MSCR test (R2=0.91-0.95).

6.4.3. Asphalt Rutting Prediction

A simple linear-viscous method as discussed in Chapter 5 was adopted in this study for rutting prediction of WMA as compared to HMA during its early life of opening to traffic.

6.4.3.1. Viscosity-Strain Curve

The viscosity-strain curves for different test temperatures derived from the RLAT are shown in Figure 6.6 (a) to (f) for each bituminous mixture. Furthermore, the fitted trend lines and their equations are presented in Table 6.4. It was found that exponential regression provided excellent viscosity trend lines with an average R^2 of 0.968.

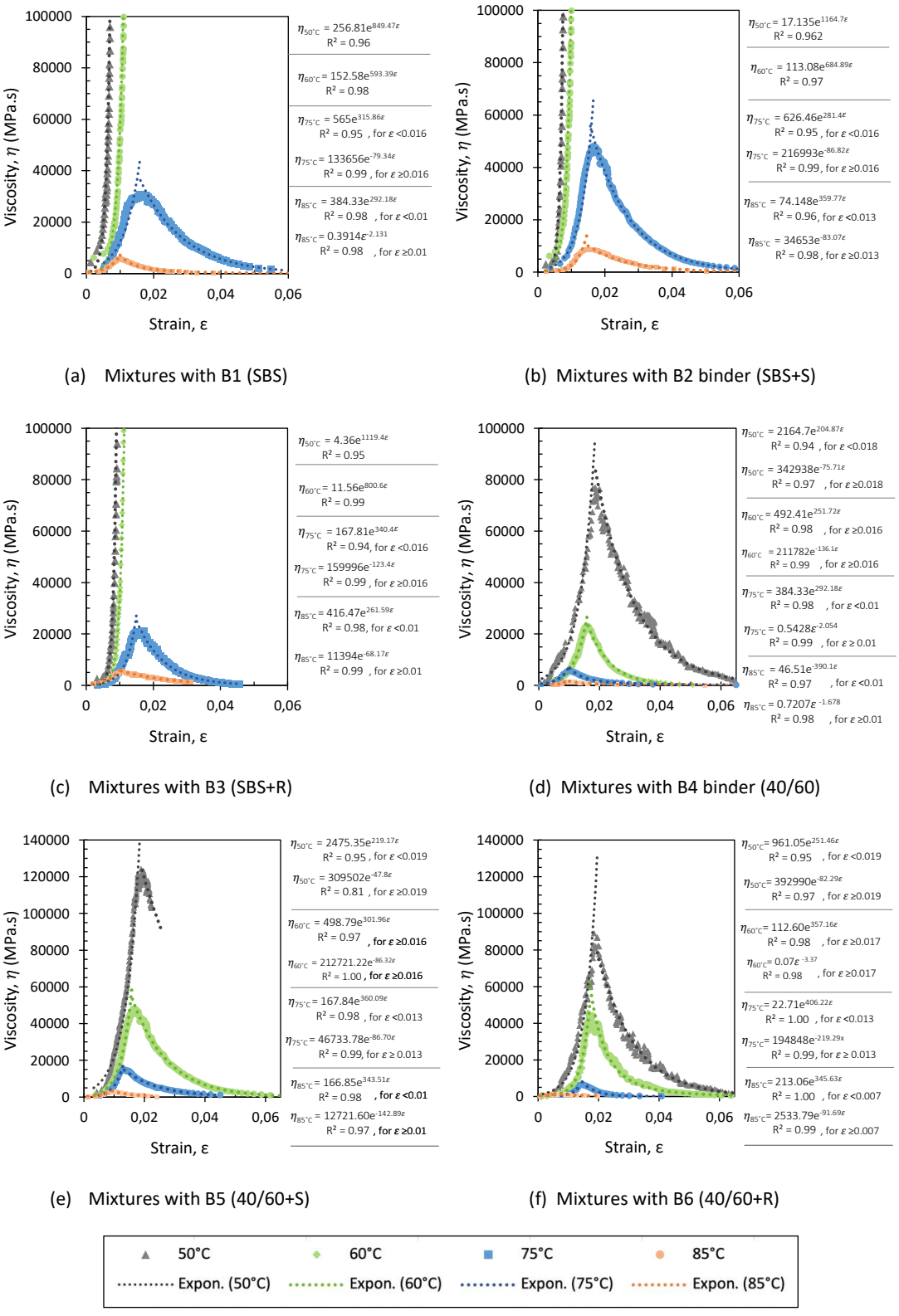

(a) Mixtures with B1 (SBS)

(b) Mixtures with B2 binder (SBS+S)

(c) Mixtures with B3 (SBS+R)

(d) Mixtures with B4 binder (40/60)

(e) Mixtures with B5 (40/60+S)

(f) Mixtures with B6 (40/60+R)

Figure 6.6 Viscosity-strain curve derived from RLAT tests for different bituminous mixtures

Table 6.4. Viscosity-strain relationship for different bituminous mixtures

Mixture with:	Temp. (°C)	Equation	Condition	R^2
B1 (SBS)	50	$\eta_{50°C} = 256.81e^{849.47\varepsilon}$		0.96
	60	$\eta_{60°C} = 152.58e^{593.39\varepsilon}$		0.98
	75	$\eta_{75°C} = 565e^{315.86\varepsilon}$	ε <0.016	0.95
		$\eta_{75°C} = 133656e^{-79.34\varepsilon}$	ε ≥0.016	0.99
	85	$\eta_{85°C} = 384.33e^{292.18\varepsilon}$	ε <0.01	0.98
		$\eta_{85°C} = 0.3914\varepsilon^{-2.131}$	ε ≥0.01	0.98
B2 (SBS+S)	50	$\eta_{50°C} = 17.135e^{1164.7\varepsilon}$		0.96
	60	$\eta_{60°C} = 113.08e^{684.89\varepsilon}$		0.97
	75	$\eta_{75°C} = 626.46e^{281.4\varepsilon}$	ε <0.016	0.95
		$\eta_{75°C} = 216993e^{-86.82\varepsilon}$	ε ≥0.016	0.99
	85	$\eta_{85°C} = 74.148e^{359.77\varepsilon}$	ε <0.013	0.96
		$\eta_{85°C} = 34653e^{-83.07\varepsilon}$	ε ≥0.013	0.98
B3 (SBS+R)	50	$\eta_{50°C} = 4.36e^{1119.4\varepsilon}$		0.95
	60	$\eta_{75°C} = 167.81e^{340.4\varepsilon}$		0.94
	75	$\eta_{75°C} = 167.81e^{340.4\varepsilon}$	ε <0.016	0.94
		$\eta_{75°C} = 159996e^{-123.4\varepsilon}$	ε ≥0.016	0.99
	85	$\eta_{85°C} = 416.47e^{261.59\varepsilon}$	ε <0.01	0.98
		$\eta_{85°C} = 11394e^{-68.17\varepsilon}$	ε ≥0.01	0.99
B4 (40/60)	50	$\eta_{50°C} = 2164.7e^{204.87\varepsilon}$	ε <0.018	0.94
		$\eta_{50°C} = 342938e^{-75.71\varepsilon}$	ε ≥0.018	0.97
	60	$\eta_{60°C} = 492.41e^{251.72\varepsilon}$	ε <0.016	0.98
		$\eta_{60°C} = 211782e^{-136.1\varepsilon}$	ε ≥0.016	0.99
	75	$\eta_{75°C} = 384.33e^{292.18\varepsilon}$	ε <0.01	0.98
		$\eta_{75°C} = 0.5428\varepsilon^{-2.054}$	ε ≥0.01	0.99
	85	$\eta_{85°C} = 46.51e^{-390.1\varepsilon}$	ε <0.01	0.97
		$\eta_{85°C} = 0.7207\varepsilon^{-1.678}$	ε ≥0.01	0.98
B5 (40/60+S)	50	$\eta_{50°C} = 2475.35e^{219.17\varepsilon}$	ε <0.019	0.95
		$\eta_{50°C} = 309502e^{-47.8\varepsilon}$	ε ≥0.019	0.81
	60	$\eta_{60°C} = 498.79e^{301.96\varepsilon}$	ε <0.016	0.97
		$\eta_{60°C} = 212721.22e^{-86.32\varepsilon}$	ε ≥0.016	1.00
	75	$\eta_{75°C} = 167.84e^{360.09\varepsilon}$	ε <0.013	0.98
		$\eta_{75°C} = 46733.78e^{-86.70\varepsilon}$	ε ≥0.013	0.99
	85	$\eta_{85°C} = 166.85e^{343.51\varepsilon}$	ε <0.01	0.98
		$\eta_{85°C} = 12721.60e^{-142.89\varepsilon}$	ε ≥0.01	0.97
B6 (40/60+R)	50	$\eta_{50°C} = 961.05e^{251.46\varepsilon}$	ε <0.019	0.95
		$\eta_{50°C} = 392990e^{-82.29\varepsilon}$	ε ≥0.019	0.97
	60	$\eta_{60°C} = 112.60e^{357.16\varepsilon}$	ε <0.017	0.98
		$\eta_{60°C} = 0.07\varepsilon^{-3.37}$	ε ≥0.017	0.98
	75	$\eta_{75°C} = 22.71e^{406.22\varepsilon}$	ε <0.013	1.00
		$\eta_{75°C} = 194848e^{-219.29x}$	ε ≥0.013	0.99
	85	$\eta_{85°C} = 213.06e^{345.63\varepsilon}$	ε <0.007	1.00
		$\eta_{85°C} = 2533.79e^{-91.69\varepsilon}$	ε ≥0.007	0.99

In general, it was observed that the viscosities of the bituminous mixtures containing PMB (B1, B2, B3) at the corresponding strains are significantly higher than those of the neat

bituminous mixtures (B4, B5, B6) at all test temperatures, indicating higher stiffness and superior rutting resistance of mixes with PMB. It was also noticed that, at the same test temperature, the peak viscosity occurred at a significantly lower strain for mixes with a neat binder. This suggests a lower number of cycles to rutting failure of mixes containing neat bituminous binder as compared to mixes with PMB. An improvement of the viscosity curve was also found with the addition of Sasobit additive to both bituminous mixtures (neat and polymer modified) at all temperatures, while the addition of Rediset additive does not significantly change the viscosity curve of the mixtures.

6.4.3.2. Rutting Prediction Results

Making use of the viscosity strain curve displayed in Figure 6.6, a linear viscous analysis was performed. The same pavement structure, load condition (B737-800 aircraft), and other assumptions used in Chapter 5 were adopted. The prediction of the number of load cycles to rutting failure for each mixture and traffic opening temperature is summarized in Figure 5.13.

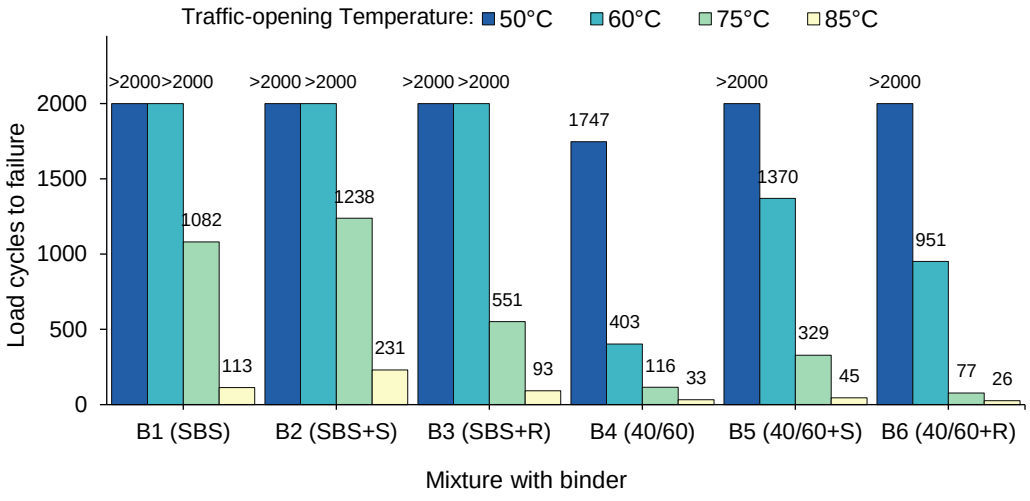

Figure 6.7. Predicted number of cycles to failure at various traffic-opening temperature for different bituminous mixtures

From the result, it was found that the addition of Sasobit additive improved the rutting performance of bituminous mixtures in the case of both neat (B5) and modified bitumens (B2). This can be seen from the greater pavement life cycles to rutting failure of mixtures containing Sasobit, compared to HMA, at all temperatures. Moreover, it was observed that the use of chemical additives (Rediset) led to slightly fewer load cycles to failure than HMA, indicating slightly lower rutting resistance. In cases where early-opening-to-traffic asphalt overlay is

essential, it is recommended to use bituminous mixture with the addition of Sasobit for asphalt overlay as it provides advantages of reduced cooling time of newly laid asphalt before opening to traffic due to a lower initial laying temperature and a higher traffic-opening temperature than HMA due to enhanced rutting resistance. However, to avoid the thermal cracking potentially caused by Sasobit, an investigation to select a Sasobit dosage rate that gives an acceptable low-temperature cracking resistance should be performed.

It should be noted that a higher traffic-opening temperature with the use of WMA-Sasobit might only be achievable in some airfield areas that are subjected to slow loading (such as taxiways and runways during initial take-off), not in the high shear areas of airport, such as in braking and turning zones, where the shear failure mode is critical. Furthermore, to see the susceptibility of WMA to shear failure in high-shear areas in airport, in the following section, the interface shear bond performance of WMA at high temperatures is assessed.

6.5. Asphalt Interface Shear Bond at Traffic Opening Temperature

6.5.1. Interface Shear Bond Test Results

The direct shear test with confinement (normal stress) for interface shear resistance assessment at high temperature performed in Chapter 5 was repeated in this chapter for warm mix asphalt (WMA). A total of 36 sandwich-block specimens were prepared in the laboratory. The SBS modified binder tack coat was applied for all specimens on the HMA surface (lower layer). Two different upper layer mixes, HMA with SBS modified binder (B1), as the control binder, and WMA with SBS and Sasobit modified binder (B2), were investigated. The test method discussed in Chapter 3 (Section 3.6.3) and Chapter 5 (Section 5.4.1.) was used for this test.

The results of ISS value of different upper layer mixtures (HMA and WMA) under different normal loads and test temperatures are presented in Figure 6.8. Each ISS value represents the average of two test specimens. For the same tack coat material, it was observed that the upper layer mixes prepared with WMA (Sasobit) exhibited a comparable measured ISS with respect to the control HMA at any temperatures and normal pressures. Although some enhanced rheological properties of bituminous binder were found with addition of Sasobit WMA additive from MSCR and DSR tests, it was observed that the use of WMA as the upper layer does not make any substantial enhancement in the adhesion or cohesion of the layer interface, as compared to HMA.

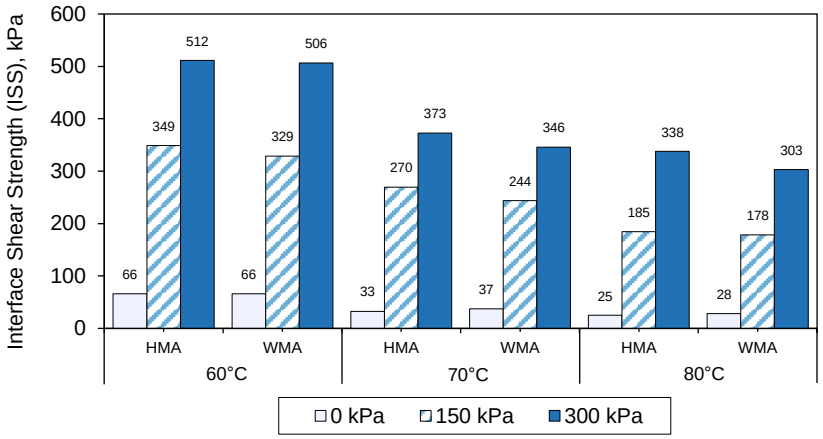

Figure 6.8 ISS of HMA and WMA at different normal stresses and test temperatures

Furthermore, a linear relationship between the ISS and the associated normal stress for both mixtures was used to obtain the failure envelope parameters, cohesion (c) and the internal friction angle (ϕ), for the analysis. The linear regression correlation coefficient R^2 as well as c and ϕ for all interface and test conditions is presented in Table 6.5 and displayed in Figure 6.9.

Table 6.5 ISS and failure envelope criteria of HMA and WMA at different normal stresses and test temperatures

Test temp.	Upper layer material	Interface Shear Strength (ISS), kPa for normal pressure:			Failure envelope criteria		
		0 kPa	150 kPa	300 kPa	c (kPa)	Internal friction angle, ϕ	R^2 (linear regression)
60°C	HMA-SBS (B1)	65.9	348.7	511.6	85.9	55.6°	0.98
	WMA (B2)	66.1	328.7	506.3	80.2	55.2°	0.99
70°C	HMA-SBS (B1)	32.7	269.6	372.8	55.0	48.0°	0.95
	WMA (B2)	37.3	243.8	345.7	54.7	45.2°	0.96
80°C	HMA-SBS (B1)	25.0	184.8	337.7	26.2	45.6°	0.99
	WMA (B2)	28.5	178.4	302.9	32.7	41.9°	0.99

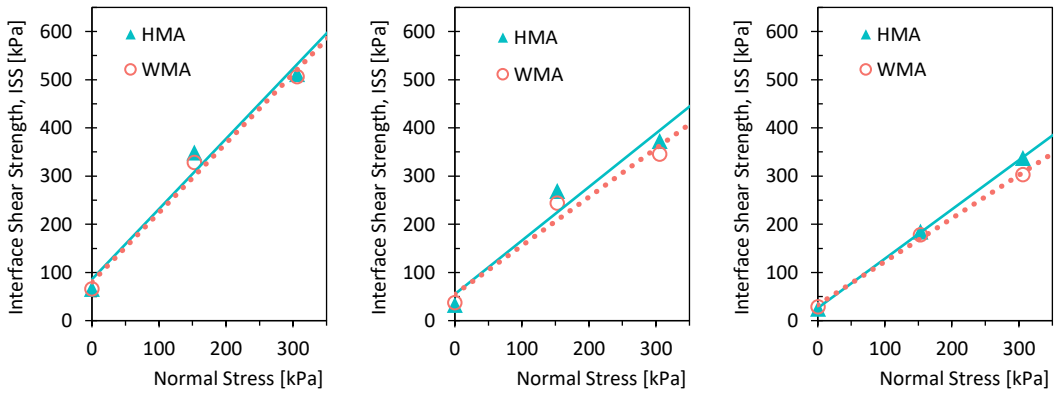

(a) 60°C (b) 70°C (c) 80°C

Figure 6.9 Failure envelopes for HMA and WMA upper materials for various test temperatures

6.5.2. Analysis of Shear Failure at Opening to Traffic

In this section, an analysis was performed to investigate the interface shear damage potential of a newly laid WMA layer as compared to HMA during the opening to air traffic. Different aircraft ground movements, including landing (L), full braking (FB), turning at a RET (RET) and taxiing (T), discussed previously in Chapter 5, were considered. The BISAR program and pavement structure used in Chapter 5 were used for this shear failure analysis. The multi-axial stress states at the asphalt layer interface (obtained from BISAR analysis) were modelled using the Mohr-Coulomb failure relationship applied to a normal-shear stress plane. The failure envelope of each asphalt mix and test temperature was acquired from the direct shear test, as presented in Table 6.5 and Figure 6.9.

The stress-to-strength ratio was used as an indicator to measure how close the layer interface was to shear failure, expressed by Eq. (5.6). The shear stress states in the WMA layer for different aircraft movements at pavement temperatures of 60°C, 70°C and 80°C along with its failure envelopes are shown in Figure 5.33(a) to (c). It was found that at 60°C, the shear stress states in the WMA layer for all aircraft load conditions were still under the failure envelope, suggesting that the interface can still resist the forces applied. As expected, the shear stress states are approaching the failure envelope at 70°C, and some are surpassing the envelope at 80°C, especially for FB-loading.

As found previously in Chapter 5, it was observed in this section that aircraft full braking (FB-loading) was the most critical loading condition and should possibly be restricted when the newly laid asphalt overlay is opened at a higher temperature (more than 70°C). Furthermore, to compare the interface shear bond performance of HMA and WMA, the maximum stress-to-strength ratio under various aircraft movements is presented in Figure 5.33 and summarized in Table 5.13. The results show that the WMA-upper layer resulted in a slightly higher stress-to-strength ratio than the HMA-upper layer at all temperatures and aircraft loading conditions, indicating slightly lower interface resistance to shear failure with WMA as the overlay layer. The small difference between the stress-to-strength ratio of WMA and HMA is likely caused by the sample variability– air voids, thickness of the samples, temperature during testing in the direct shear test which affects the failure envelope in the analysis. Further studies should be performed using a higher amount of experimental data and through statistical analysis to investigate the effect of WMA, as compared to HMA, on the interface shear strength.

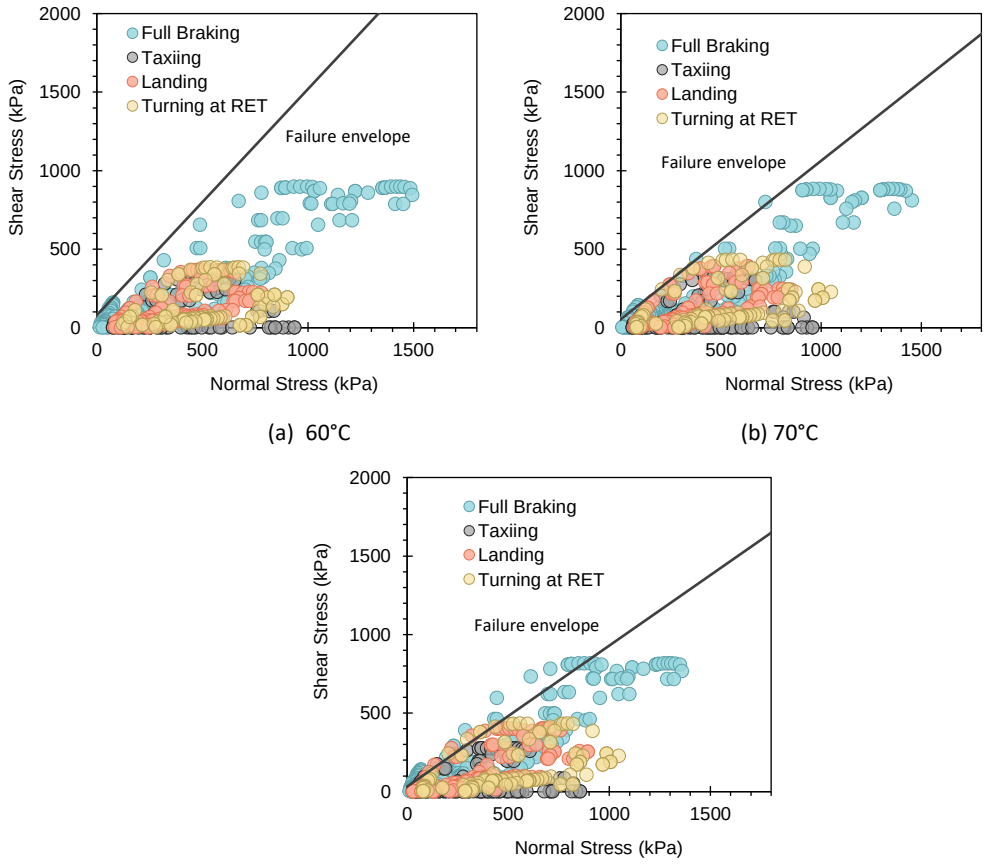

(a) 60°C (b) 70°C

(c) 80°C

Figure 6.10 Critical stress at interface under B737 aircraft at different temperature at opening to traffic for WMA

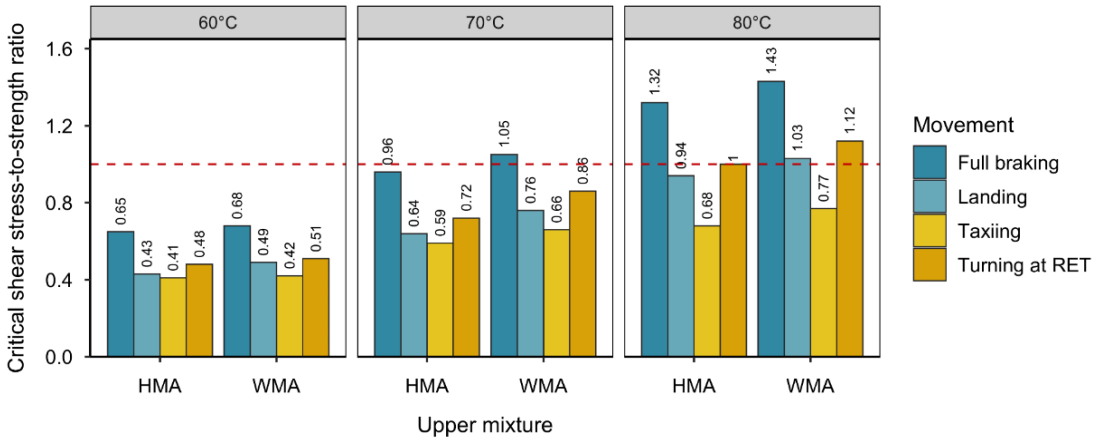

Figure 6.11 Critical stress-to-strength ratio for different B737 aircraft movement conditions at different temperatures at opening to traffic

Table 6.6. Critical stress ratio at different B737aircraft movement condition

Test temp.	Upper layer material	Critical stress ratio at layer interface for B737 aircraft movement:			
		T[a]	FB[b]	RET[c]	L[d]
60°C	HMA-SBS	0.41	0.65	0.48	0.43
	WMA	0.42	0.68	0.51	0.49
70°C	HMA-SBS	0.59	0.96	0.72	0.64
	WMA	0.66	1.05	0.86	0.76
80°C	HMA-SBS	0.68	1.32	1.00	0.94
	WMA	0.77	1.43	1.12	1.03

Notes: [a]Taxiing, [b]Full braking, [c]Turning at rapid exit taxiway, [d]Landing

In general, from the direct shear test and the analysis, it was found that at any temperature, WMA-upper layers using Sasobit additive do not obviously affect the ISS and the interface shear failure potential as compared to the corresponding HMA-upper layers. It can be concluded that, when combined with polymer modified binder, Sasobit additive could be beneficial to quickly open the new asphalt to traffic due to a lower initial laying temperature without significantly reducing the interface shear bond performance.

Overall, from the analysis of rutting and interface shear bond performance, it can be concluded that WMA mixture had similar or slightly improved performance at any particular traffic-opening temperature, as compared to HMA. In particular, WMA-Sasobit showed better rutting resistance at high temperatures, compared to HMA. However, no improvement was observed on the interface shear bond strength with addition of Sasobit additive. This suggests that, a higher traffic-opening temperature with the use of WMA-Sasobit alone (without polymer modifier) can only be achievable in the low shear areas of airport, not in others.

Finally, the WMA-Sasobit additive could be synergistically combined polymer modified binder (PMB) for superior performance during traffic opening for all areas in airport. The combination of PMB and WMA-Sasobit additives is expected to provide double advantages: (1) shortening the cooling time of the newly laid asphalt pavement due to its lower initial temperature, and (2) enabling asphalt opening to traffic at higher temperatures due to its excellent rutting resistance.

6.6. Effect of the Use of Warm Mix Asphalt on Construction Productivity

In the following section, a case study based on an airfield overlay project is presented to highlight WMA technologies for shortening the overall project nights/days of airfield runway

rehabilitation. Four different overlay thicknesses (70mm, 100mm, 70+70mm, 100+50mm) determined earlier from cooling time analyses in Chapter 4 were used to investigate the HMA and WMA construction times. The same assumptions used in Chapter 5 such as a time window of seven hours available each night, runway dimensions of 3600 x 60 m, construction stage and the work period of each stage were adopted in this analysis.

6.6.1. Cooling Time Estimation of HMA and WMA

The cooling analysis of various asphalt overlay thicknesses and mixtures in typical tropical countries during night-time construction performed in Chapter 4 was used for the analysis of construction productivity. The temperature for HMA spreading was assumed to be 150°C, in contrast, 135°C (WMA-15) and 120°C (WMA-30) were considered for WMA. The predicted cooling times from the analysis are as shown in Figure 6.12. As discussed previously in Chapter 4, it can be seen that WMA has shorter cooling times compared to HMA. The difference in cooling periods is greater for those cases with greater overlay thickness. This result suggests that using WMA with lower production temperature can be one of the strategies to reduce the cooling time of newly paved asphalt overlay and/or shorten the airfield closure. It is also noted that further cooling time savings can be made when the critical temperature at opening to traffic is raised.

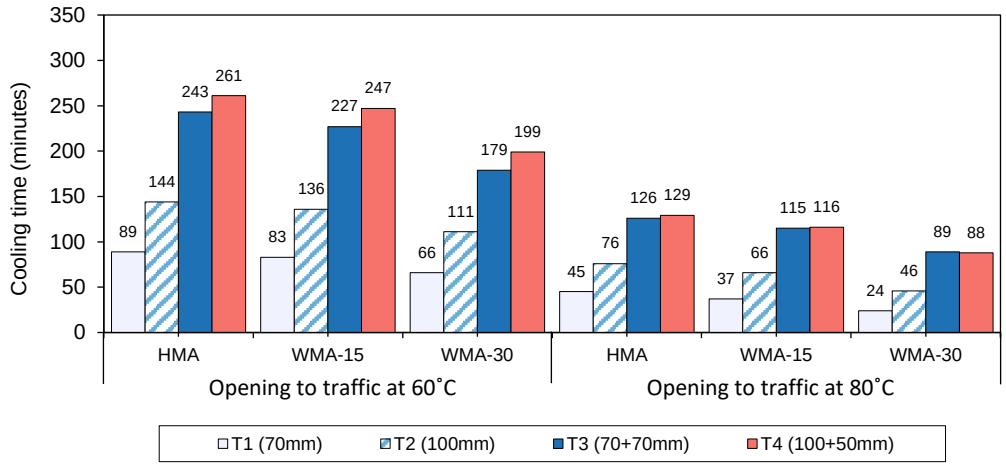

Figure 6.12 HMA and WMA cooling time needed to reach traffic opening temperature

6.6.2. Construction Time Estimation

The time available for the asphalt laying and compaction for each thickness, mixture and opening temperature strategy can be obtained by subtracting the given closure time window (7 hours, in

this case) with initial trimming and cleaning, setting up, and required cooling time presented before, as well as the site clearing, marking and lighting installation time at the end of the resurfacing work. Making use of the available time for asphalt paving work and work productivity, the volume of asphalt produced each night was computed, and thus the overall number of nights required to finish the project can be predicted. Table 6.7 lists the estimated overall number of project nights for HMA and WMA with different traffic opening strategies.

Table 6.7 Overall construction time of HMA and WMA during night-time construction

Overlay Strategy	Lift thickness (mm)	Expected overall project time on a-3600 x 60 m runway overlay (nights) for asphalt mixtures and different traffic opening temp.:					
		60°C			80°C		
		HMA	WMA-15	WMA-30	HMA	WMA-15	WMA-30
T1	70	36	35	32	31	31	31
T2	100	64	61	53	45	43	42
T3	70+70	206	169	109	79	75	66
T4	100+50	298	236	139	87	81	71

As seen in Table 6.7, for an asphalt overlay with a thickness of 100 mm in a 3600m x 60m runway, it is predicted that 64 nights are needed for asphalt overlay work to finish when the HMA is used, whereas 61 and 53 nights are needed when WMA-15 and WMA-30 are used, respectively. The nights needed to finish the overlay reduce to 43 nights when WMA-15 is opened to traffic at a higher temperature (80°C). In general, for the cases studied, as seen in Table 6.8, the use of WMA could shorten the overall project period by 1-11 nights for a single lift overlay. The reduction of asphalt overlay construction time with the use of WMA is more significant (37-159 nights) for greater lift thicknesses and multi-lift operations, as seen in Table 6.8.

Table 6.8 Construction savings nights of WMA as compared to HMA

Overlay Strategy	Lift thickness (mm)	WMA savings (nights), compared to HMA opened at 60°C, for traffic opening temp.:			
		60°C		80°C	
		WMA-15	WMA-30	WMA-15	WMA-30
T1	70	1	4	5	5
T2	100	3	11	21	22
T3	70+70	37	97	131	140
T4	100+50	62	159	217	227

The results in Table 6.8 also highlight the importance of selecting traffic opening temperature on reducing the number of pavement construction nights. As an illustration, it was

found that 18 nights could be saved (a 29% reduction), for a 100mm overlay of WMA-15, by raising traffic opening temperature, from 60°C to 80°C.

Multi lift pavement is not recommended to obtain rapid construction and rapid opening of asphalt to traffic in the case of limited time available. This is because more nights of work are needed to finish the project. In the case of large overlay thickness, it is recommended that the overlay is done in one lift and then continued for the next layer when the whole runway area is paved with the first layer. For instance, if the traffic opening temperature of 60°C is used, 36 nights are needed to finish one layer of 70 mm HMA, meaning that 72 nights are needed to finish two layers of 140mm. In contrast, it takes 206 nights to finish the project when the multi lift operation (70+70mm) is applied every night due to the slower cooling of a thick asphalt layer. However, with this strategy several drawbacks could occur, including the increased number of transverse joints and the need for interface treatment and tack coating, and there are certain to be time penalties in addressing these.

Moreover, the opening of a runway overlay to traffic does not depend only on the time of asphalt cooling but also depends on the time of restoring the lighting system and line marking at the end of each night. In the case when the time for restoring the line marking and lighting is greater than the cooling time, the use of WMA would be pointless in terms of its benefit of rapid construction. For example, it can be seen from Table 6.8, for T1 (70mm), the overall project period of WMA-30 is the same as WMA-15, when both opened to traffic at 80°C. This is because, although the cooling time of WMA-30 is 24 minutes, the assumed restoration time: 60 minutes, is used as the determining factor.

6.7. Results and Discussion

In this chapter, the use of WMA in night-time airfield rehabilitation, compared to HMA, was investigated. Two different WMA technologies (organic and chemical) were investigated through a series of laboratory tests to see the WMA rutting performance and interface shear bond behaviour at high temperatures when the newly laid asphalt overlay is opened to traffic. Furthermore, an analysis was carried out to analyze the effect of the use of WMA on improving construction productivity due to more time being available for paving each night. The following conclusions can be drawn from Chapter 6:

- The repeated load axial tests (RLAT) and rutting prediction presented in this study indicate that, in general, the WMAs have a rutting performance at high temperatures during the opening to traffic similar to, or better than HMA. It was found that, compared to HMA, WMA-Sasobit showed excellent rutting resistance at high temperature, enabling the pavement to be opened to traffic at a higher temperature in low-shear areas in airport.
- From the direct shear test on double-layered specimens, it was observed that the upper layer mixes prepared with WMA-Sasobit exhibited a comparable measured ISS compared with the control HMA, at all temperatures and normal pressures. Furthermore, based on the interface shear failure analysis, the WMA-upper layer exhibited a slightly higher stress-to-strength ratio than HMA-upper layer at all temperatures and aircraft loading conditions.
- It is recommended, for projects where rapid opening to traffic is essential or asphalt mat cooling is difficult to achieve due to the adverse hot weather conditions, to use polymer-modified binder combined with Sasobit WMA additive. It provides double advantages: (1) shortening the cooling time of the newly laid asphalt pavement due to its lower initial temperature, and (2) enabling asphalt opening to traffic at higher temperatures due to its better rutting and interface shear bond performance as compared to unmodified HMA.
- For the cases studied in this chapter, the use of WMA for asphalt overlay during off-peak period work could reduce the overall construction period by 1-11 nights for a single lift overlay– which would represent a shortening of the overlay period by 3-17%.

7. Spray Water Cooling for Early Opening of Pavement to Traffic

7.1. Overview

For the purpose of early opening to traffic, in tropical countries where the ambient air temperature is high, some contractors often practice spraying water on the newly laid asphalt to speed up the cooling process. However, there is no specific research regarding the effect of water spraying on a new asphalt surface, in term of its effectiveness and the possible detrimental impact on asphalt mechanical properties. In this chapter, the use of spray water to reduce the cooling time of newly laid asphalt pavement is examined. The heat transfer coefficients for various water cooling strategies were determined. Furthermore, the potential drawbacks of spraying water onto newly laid asphalt were investigated through laboratory testing.

7.2. Aim of Research Phase

The research question to be answered in this research phase are as follows:

- To what extent does the use of water spraying on newly laid asphalt effect reduce the asphalt cooling time so as to permit earlier trafficking? How does the spray water cooling on freshly laid asphalt affect the pavement performance, in term of durability and moisture susceptibility?

For these purposes, temperature measurements of asphalt cooling, with various strategies, were performed in the laboratory using embedded thermocouples and an infrared thermometer. A three-dimensional heat transfer analysis of the laboratory scaled model was developed in a general-purpose finite-element analyser to determine the heat transfer coefficients of the water cooling. The model was initially validated against the temperature measurement of natural asphalt cooling. Afterwards, the heat transfer coefficient of spray water

cooling was determined by trial and error matching of temperature in the validated three-dimensional (3D) model to the temperatures from thermocouple readings. The calibrated heat transfer coefficient of water cooling obtained from this analysis was then used as an input into a heat transfer model of a typical pavement structure in a tropical environment, as developed in Chapter 4, to examine the significance of forced water cooling of asphalt on reducing the cooling time of newly laid asphalt, as compared to natural cooling. The effects of water temperature, water flow-rate, cooling duration and pavement temperature on the cooling response of newly laid asphalt pavement were also reviewed.

Finally, to investigate the potential drawbacks of spraying water onto newly laid asphalt, in terms of durability and moisture damage, a series of laboratory tests were performed. Cores were taken from the asphalt slabs affected by spray water application. The Cantabro mass loss (CML) test and indirect tensile strength (IDT) test, as explained in Chapter 3 (Section 3.6.5 and 3.6.6), were then performed on the core samples to see the durability and moisture damage potential of asphalt with spray water as compared to a control asphalt mixture (with natural cooling).

7.3. Materials, Mixture Designs and Test Configuration

For the purpose of this research phase, a neat 40/60 Pen grade bituminous binder, as described in Chapter 3, was used for all asphalt mixtures. The aggregates used in this study were from existing stockpiles of granite aggregates from Bardon Hill (Leicestershire, UK). The asphalt mixtures were manufactured according to FAA Item P-401: dense graded asphalt concrete 12.5 mm (0.5 in.) maximum aggregate size (Gradation 2), as explained in Chapter 3. An asphalt bitumen content of 5.8%, obtained from the Marshall mix design test, was used for asphalt mixtures. The target air void of 4% was selected within the allowable design range of FAA specifications (FAA 2018) for airfield pavements: 2.8–4.2%. In addition, a laboratory roller compactor was used for manufacturing the slab specimens. The bulk density of the asphalt mixture was determined according to BS EN 12697-6 (BSI 2012c), while air voids percentage in the asphalt mixture was measured following BS EN 12697-8 (BSI 2018b). Based on the bulk density measurement (for sealed specimens), the air voids of prepared samples ranged between 3.4-4.4% with an average of 4.13% and a standard deviation of 0.34%. The temperature for asphalt mixture production was 155°C. This was determined based on Brookfield viscometer

tests, following BS EN 13302 (BSI 2018a), with standard viscosities between 0.15 and 0.2 Pa.s for asphalt mixing.

Five small-scale slabs with embedded thermocouples manufactured in the laboratory as detailed above in Chapter 3 (section 3.6.4) were used to measure the cooling response of newly laid asphalt with natural and forced water cooling system. Five different strategies, representing various cooling strategies, water flow intensities and cooling water temperature, as shown in Table 7.1, were used for the purpose of this study.

Table 7.1. Spray water intensity and temperature for the test.

Designation	Water intensity (V_w)	Water temp. (T_w)
Normal cooling	None	None
WC1	Rate1 (64 L/ m^2·minute)	Temp1 (10°C)
WC2	Rate1 (64 L/ m^2·minute)	Temp2 (30°C)
WC3	Rate2 (30 L/ m^2·minute)	Temp1 (10°C)
WC4	Rate2 (30 L/ m^2·minute)	Temp2 (30°C)

7.4. Test Results and Analysis

7.4.1. Laboratory Measurement of Spray Water Cooling of Newly Laid Asphalt

Temperature measurements of specimens with five different cooling strategies (as listed in Table 7.1) were carried out. The measured temperatures from thermocouple readings versus cooling time curves of the newly paved asphalt layers are presented Figure 7.1(a) to (e) for each cooling strategy. Furthermore, to compare the cooling trend of natural cooling to that of the spray water cooling, the data from the Figure 7.1(a) and (b) were plotted on Figure 7.2(a) to (d) for various depths, so that the effect of water spraying is easier to see.

For all strategies, the results reveal that, when water is sprayed, the temperature at the surface of the asphalt (Z_0) drops drastically to reach the water temperature, implying that both warming of some of the water and latent heat of evaporation of some of the water have consumed much of the asphalt surface's heat energy. The asphalt temperature then gradually rises again to air ambient temperatures, after the spraying ceases, due to heat conduction from within its thickness (warming of dry asphalt) and reduction of surface convection. So there is an immediate water warming/water latent heat of evaporation/water cooling stage followed by a warming of dry asphalt stage in sequence. Moreover, after spraying, it was noticed that there was still a visible water film on the surface of the asphalt overlay until it finally disappeared approximately 15 minutes after the spraying due to surface run-off and evaporation.

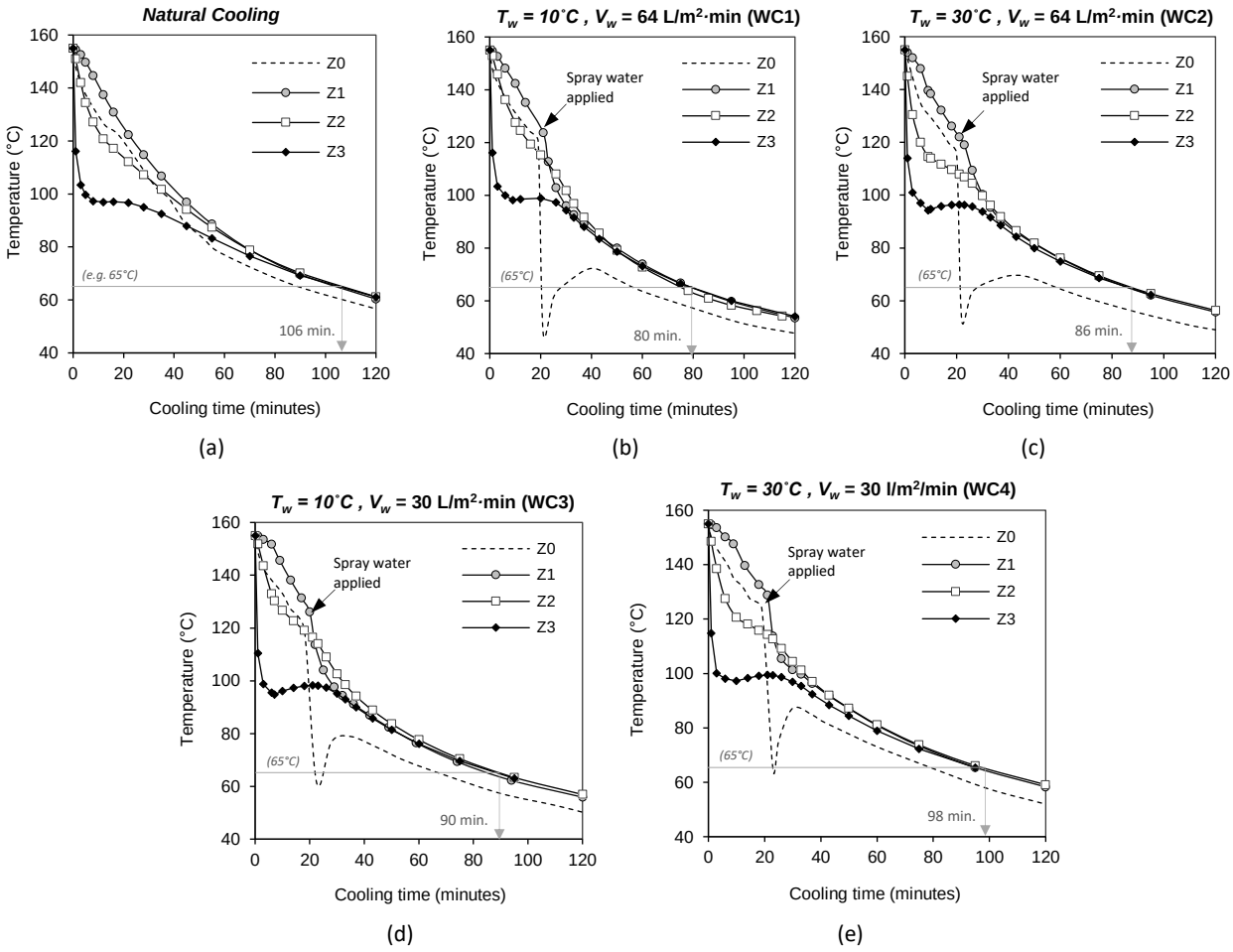

Figure 7.1. Plot of cooling temperature from thermocouple readings at various depths (Z1, Z2 and Z3) for: (a) WC1; (b) WC2; (c) WC3; and (d) WC4.

At the lower position, the Z1, Z2 and Z3 tracks show accelerated cooling due to spray application when they are at high temperatures (>100 °C) and, as seen in Figure 7.2(b) to (d), some delays were noticed in the start of cooling acceleration due to the time of travel from the asphalt surface to the depth of the location of the sensor. The delay time is dependent on asphalt depth; the higher the depth, the greater the delay time. Moreover, the delay time indicates that the asphalt has relatively low thermal conductivity, hence it does not allow the heat to be removed quickly and instantly. Overall, the experiment in this study suggests that water spraying has a great effect on reducing the temperature of newly laid asphalt at all layer depths. As seen in Figure 7.2, after 120 minutes, the differences in temperature achieved by spray-cooling range from 6.8 to 8.9°C.

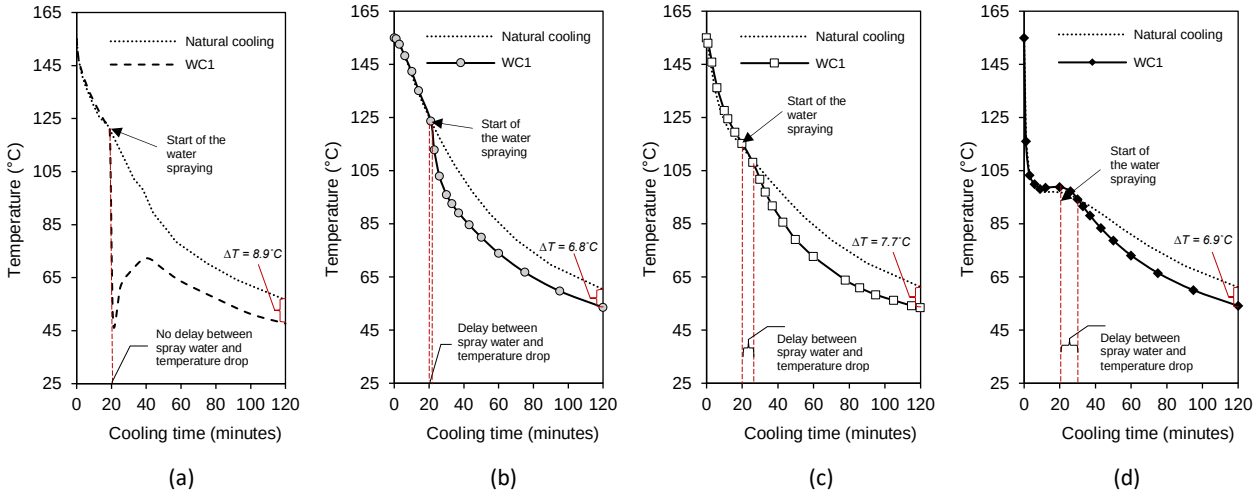

Figure 7.2. Comparison of the cooling curve of natural cooling and spray water cooling, WC1 at various depths: (a) Z0; (b) Z1; (c) Z2 and (d) Z3

The results of the experiment in this study also demonstrate that the effect of the spray water cooling on the reduction of the internal asphalt temperature is less obvious, compared to that of the asphalt surface. The effect of the water cooling becomes less apparent with depth within the specimen. For instance, as seen in Figure 7.1, when the water is applied, the temperature drops more sharply at a depth of -15mm from the surface (Z_1) compared to that of at the bottom of the newly laid asphalt (Z_3). Nevertheless, the cooling rate of the specimen with spray water cooling was still considerably higher than that of the specimen subjected to natural cooling. As an example, the time required for all lifts to cool down to 65°C for the specimen subjected to water spraying WC1 is 80 minutes, whereas, for natural cooling, it takes 106 minutes to cool down to the same temperature. These results indicate that the forced cooling with spray water could considerably affect the cooling response of newly laid asphalt at elevated temperature. However, this greatly depends on the water cooling temperature and the water flow rate.

Furthermore, reducing the temperature of the cooling water has a significant effect on the cooling response of the newly laid asphalt. The lower the water temperature (T_w), the higher the cooling rate of newly laid asphalt. It is also observed that a higher spray water flow rate (V_w) results in a faster cooling rate. For instance, as seen in Figure 7.1, to reach a temperature of 65°, 80 minutes are needed for asphalt overlay sprayed with water with a flow rate of 64L/m^2·minute (WC1), whereas it takes 90 minutes when water with a flow rate of 30L/m^2·minute (WC3) is applied. Moreover, the results from the cooling measurement of the small-scale asphalt slabs may

not reflect the real pavement structure and its boundary conditions. To investigate the effect of water cooling on a more 'representative' pavement model, in the following section, a 3D heat transfer model was developed to estimate the heat transfer coefficient of spray water cooling. Making use of the validated heat transfer coefficient, a case study with a typical pavement structure and environmental condition in a tropical country, using 1D heat transfer model as developed in Chapter 4, was then performed to evaluate the effect of spray water cooling on reducing the asphalt cooling time /lane closure before pavement traffic opening.

7.4.2. Heat Transfer Model Development

A 3D transient asphalt cooling model, as seen in Figure 7.3, using ABAQUS software was used for this research. The finite element model (FEM) was selected because of its versatility in supporting the complex three-dimensional geometric features of the asphalt specimen and the steel mould. The model also allows for a wide variety of climatic conditions and thermophysical properties of the paving material. FEM has been successfully used in many studies (Kassem et al. 2014, Wang et al. 2014b, Zhu et al. 2019) in predicting the cooling of newly laid asphalt. In this study, to model the experimental specimen, the asphalt slabs and steel mould is simulated by an 8-node linear heat transfer brick element known as DC3D8. The heat transfer model consists of asphalt overlay (70mm), existing asphalt course (40mm) and the metal mould, replicating the real specimen in the laboratory, see Figure 7.3. The thermodynamic principles: convective heat transport from wind, heat diffusion conduction into the pavement layers underneath and the surrounding steel mould, infrared radiation and heat flux from the light bulb were considered. The bottom boundary was assumed to be thermally insulated as it was placed above an insulator plate. In the first 20 minutes, before water cooling, the full model (Figure 7.3 (a)) was used. Moreover, to replicate the real condition during the water cooling experiment, a model with one side of the steel mould removed, as seen in Figure 7.3(b), was used for analysis during and after the water spraying.

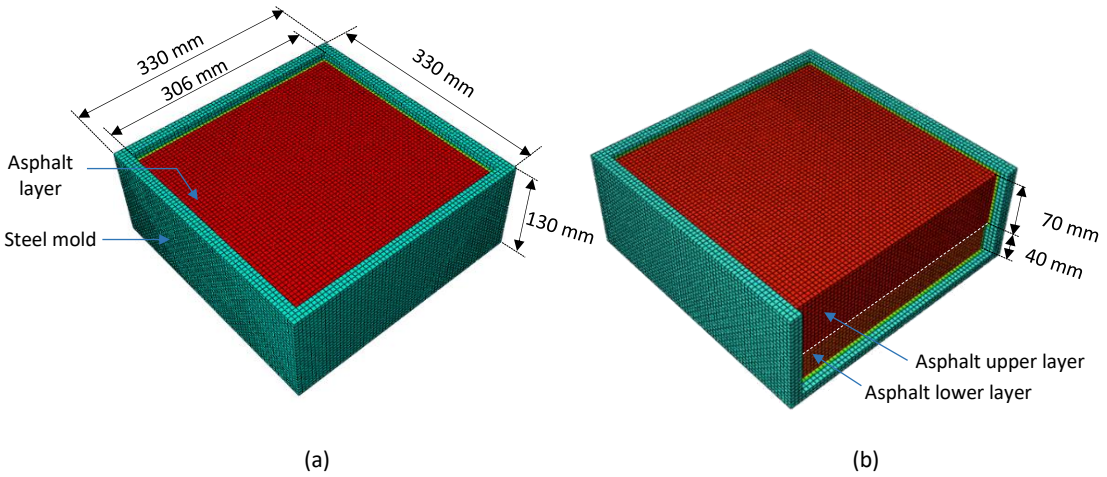

Figure 7.3. FE model of laboratory investigation of heat transfer coefficient of water cooling: (a) Full model (before water spraying) and (b) Model with one side of mould removed

7.4.3. Calibration and Validation of the Model against Laboratory Data

To calibrate and validate the developed cooling model, the temperature measurements for normal cooling of asphalt (without spray water) from the infrared-gun and thermocouples were initially used. The thermophysical properties of the material were initially assumed from a previous study by Wang et al. (2014b) and the air ambient temperature was obtained from thermocouple readings. The asphalt and steel emissivity values were obtained from a study by Zhu et al. (2019). Finally, the solar flux from the lighting bulb and the wind speeds in the laboratory were assumed using commonly used values. The adopted input parameters are listed in Table 7.2.

Table 7.2. Adopted input parameter values for the simulation model

Parameter	Values
Thermal conductivity of the bituminous mixture (W/K.m)	1.5
Thermal conductivity of steel mould (W/K.m)	200
Specific heat of bituminous mixture (W.s/kg.K)	850
Specific heat of the metal mould (W.s/kg.K)	460
Air ambient temperature (°C)	13.13
Wind speed (m/s)	0.40
Heat transfer coefficients (W/m^2 °C)	7.44
Underlying surface temp. (°C)	35
Solar flux (W/m^2)	170
Asphalt pavement emissivity	0.8
Steel mould emissivity	0.4
Albedo	0.2

A typical output of the heat transfer model, showing the pavement temperature distribution 60 mins after placing, is illustrated in Figure 7.4(a). Furthermore, the predicted temperatures from FE analysis along with the physical model's measured data, are displayed in Figure 7.4(b). It can be seen that, from the calibration and validation analysis, the estimated temperature matched the measured temperatures accurately toward the end of the cooling period. The calculation errors of the model were all less than 3°C, which are within the accepted levels for predictions of pavement temperature. Greater differences were observed between the estimated and measured temperatures at a depth of 40mm (Z2). The difference is likely to be caused by slight changes to the thermocouple bead location/depth during the compaction process. Overall, as the primary objective of the model development was to determine the heat transfer coefficient of spray water cooling, it can be concluded that the developed 3D heat transfer model was sufficiently accurate to achieve the intended objective.

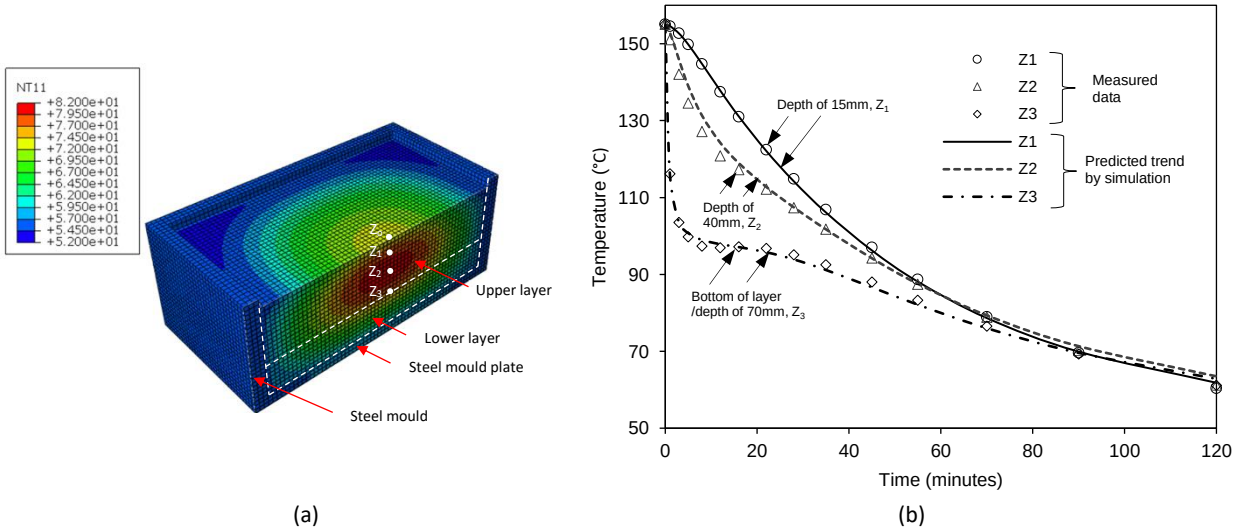

Figure 7.4. (a) Typical output of the cut section of the FE heat transfer model after 60 minutes; (b) data measurement and prediction trend of specimen temperature (natural cooling)

7.4.4. Determination of Heat Transfer Coefficient of Water Cooling

An external forced cooling using spray water is applied onto the newly laid asphalt and hence rapidly reducing the pavement temperature. During this process, the rate of the convective heat flux is a function of the temperature of cooling water (T_W), surface temperature (T_s), and the water flow rate (V_W) towards the surface to be cooled, see Figure 7.5. The overall impact of these components is accounted for in the convective heat transfer coefficient of water spraying (h_{wc}). Accurate values for h_{wc} are very complex to determine experimentally because of the difficulty

of directly measuring the convective heat flux and temperatures of the specimen (Fguiri et al. 2013) and also because the h_{wc} value depends strongly on many variables (Martin and Dulikravich 1998). One of the methods of predicting the heat transfer coefficient is by using the temperature measurements inside the material in an inverse technique (Zhang and Delichatsios 2009).

In this study, the convective heat transfer coefficient (h_{wc}) of spray water cooling at each pavement surface was estimated by trial-and-error matching of cooling profiles in the validated 3D model (developed earlier in Section 7.6.2) to those measured with thermocouple readings and infrared thermometer measurements. A similar procedure was adopted by Hulbert et al. (1997) to determine the convective heat transfer coefficient using temperature mapping measurement and heat transport modelling. Several studies (Zhou et al. 2013, Malinowski et al. 2015) have used this technique to predict the heat transfer coefficient of spray water cooling in the steel and metal industries.

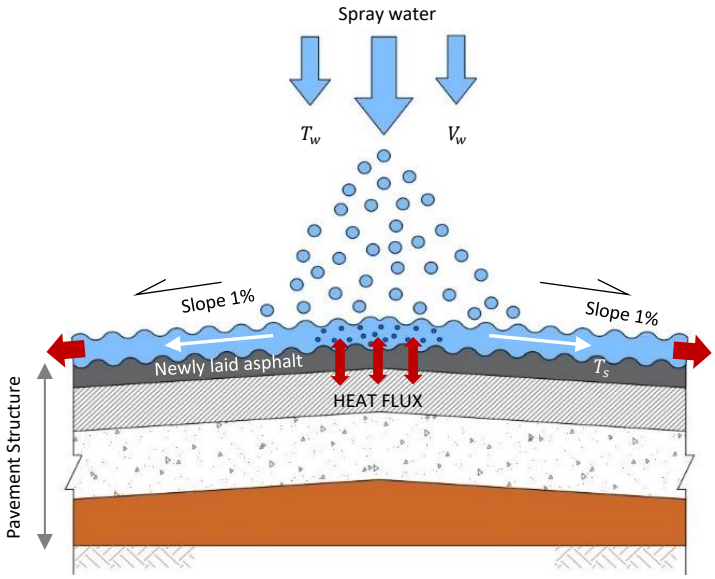

Figure 7.5. Spray cooling scheme.

For this purpose, the specific input parameters together with thermo-physical properties of all materials and boundary conditions determined earlier from the validated models, listed in Table 7.2, were used. Since the asphalt slabs' thickness and steel mould dimensions in the spray water cooling experiment were the same as the normal cooling specimen, the same finite-element mesh design used for normal cooling model analysis was also used for the spray water cooling model. The initial stage of the trial indicated that the cooling response of newly laid

asphalt with water spraying is highly dependent on the amplitude of the heat transfer coefficient distribution during the spraying, and the residual heat transfer coefficient after the spraying. In this study, the heat transfer coefficient of spray water cooling was best approximated over the asphalt surface with the block shape and exponential decay functions as shown in Figure 7.6.

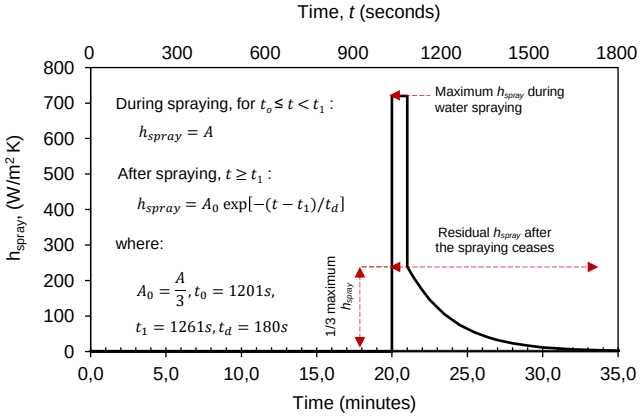

Figure 7.6. Predicted distribution of heat transfer coefficient

It is assumed that the largest value of heat transfer coefficient instantly occurs when water is sprayed. After the water spray stops, the residual heat transfer coefficient is assumed to be one-third of the ultimate value and then, it gradually decreases as the water flows to the pavement drains (due to the pavement cross-fall), and finally becomes zero after 15 minutes. These assumptions were made based on the trial and error process (to fit the temperature measurements) and also based on observation during the temperature monitoring after the water spray. Making use of this assumption, the heat transfer coefficient of spray water cooling for each strategy (WC1 to WC4) was determined using trial-and-error matching of the cooling profile. The trials were performed until the predicted temperatures from the model matched the recorded temperatures from the thermocouple readings.

In Figure 7.7, as an example, the temperatures measured by the thermocouples for different depths for WC1 are compared to the temperatures predicted by the 3D finite element heat transfer model. Overall, the temperatures predicted from the model at the thermocouple locations match the measurements with good accuracy. The average temperature difference between measured and predicted temperatures is 1.28°C. This indicates that the 3D heat transfer model is accurate for estimating the water spray heat transfer characteristics.

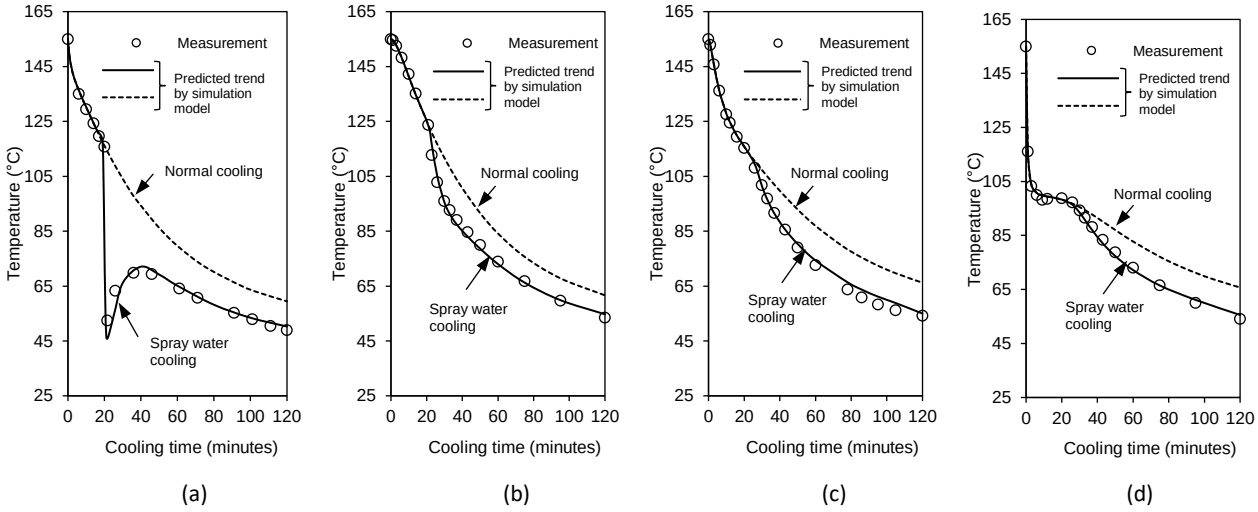

Figure 7.7. Cooling curve (data measurement and prediction) of newly laid of asphalt pavement with spray water cooling at depths: (a) Z0; (b) Z1; (c) Z2 and (d) Z3 for WC1

The maximum values of the heat transfer coefficient, h_{wc}, for each cooling strategy determined from this study are listed in Table 7.3. As expected, there is an increase in h_{wc} with the increase of spray water flow rate and with the decrease in the temperature of cooling water. Furthermore, it can be observed that the effects of the temperature of the cooling water on the h_{wc} are relatively small as compared to the water flow rate. The difference in maximum h_{wc} values between the V_w=64L/m^2·minute and V_w=30 L/m^2·minute spray-rate studies (for the same water temperature) is about 50-59%. In contrast, the difference in maximum h_{wc} values between T_w = 10°C and T_w = 30°C (for the same flow rate) is only about 18-33%.

Table 7.3. Convective heat transfer coefficients of water cooling calculated by finite element

Cooling strategy	**Water temp., T_w**	**Water Flow, V_w**	**h_{wc} (W/m^2.K)**
WC1	10°C	64 L/m^2·minute	720
WC2	30°C	64 L/m^2·minute	590
WC3	10°C	30 L/m^2·minute	360
WC4	30°C	30 L/m^2·minute	240
Literature values			131-576[a], 222-376[b], 348-553[c]

[a] spray water cooling for various metals (Bamberger and Prinz 1986), Equation (2.34) and (2.35)
[b] spray cooling system for continuous steel casting (Nozaki et al. 1978), Equation (2.36)
[c] spray cooling of steel (Ishiguro 1974) in Morales et al. (1990), Equation (2.37)

Overall, the h_{wc} values determined in this study were within the range of those reported in the literature (Bamberger and Prinz 1986, Nozaki et al. 1978) for spray water cooling experiments, with higher h_{wc} values for all cooling strategies. This is likely because the empirical

equations proposed by previous studies are intended for the cooling of steel and metals with significantly higher surface temperatures (900°C) and higher water flow rates, and thus they are not sensitive to the temperature range of asphalt production (130-150°C). Nevertheless, the estimated heat transfer coefficients from this study allow engineers to predict the cooling response of newly laid asphalt when subjected to different spray cooling strategies.

There are several sources of error in this study for determining the heat transfer coefficient of water cooling. The first source is the variability caused by errors during temperature measurements, such as the thermocouple reading errors and the depth of the thermocouple beads. The second source of error is caused by assumptions used in the 3D heat transfer model, such as surface emissivity, thermophysical properties of the materials, albedo, amplitude of the h_{wc} and heat fluxes from the light bulb. Furthermore, the heat transfer coefficient is a time- and space-dependent coefficient. In this study, the temperature measurement was only performed for one location of the asphalt slab (at various depths) in the middle of the specimen. Instead of using only one location of temperature measurement, it is recommended to employ more thermocouples or use temperature mapping/ contour on the asphalt surface. This would allow the reduction of experimental errors. Lastly, it is recognized from previous studies (Wendelstorf et al. 2009, Blagojević and Bajsić 1996) that h_{wc} greatly depends on the particle size and shape of the water droplet. In this research, these factors were not analysed. These are the limitations of this research. It is important to consider these issues for further research.

7.4.5. Example Comparisons of Natural Cooling and Spray Water Cooling

7.4.5.1. Description of Examples

Making use of the heat transfer coefficient of spray water cooling, this part outlines simulation examples to compare the cooling time lengths required by newly laid asphalt with natural cooling and spray water cooling (forced) to reach traffic-opening temperature. The one-dimensional (1D) transient cooling model of the asphalt pavement structure, developed earlier in Chapter 4, was used for this research. The same pavement structure, as used in Chapter 4, was adopted for the comparative analysis. Furthermore, the calibrated input parameters and thermal properties of each layer listed in Table 7.2 and Table 4.7 (Chapter 4) were used in this comparative analysis.

For the purpose of this study, the same cooling strategies previously used in the experiment: (1) natural cooling, (2) spray water 10L/m^2·min. at 10°C, (3) spray water 10L/ m^2·min. at 30°C, (4) spray water 60L/ m^2·min. at 10°C, and (5) spray water 60L/ m^2·min. at 30°C were considered for this comparative analysis. The heat transfer coefficient of each cooling strategy was obtained from the previous analysis. Unless otherwise noted, the spray water cooling was applied 20 minutes after the asphalt laying. All five cooling strategies were analysed for daytime (sunny) and night-time paving in a typical tropical country. A typical tropical climate was adopted for the analysis as the greater ambient temperature than other climatic regions is likely to provide a conservative cooling estimation. For this purpose, the following specific input parameter together with all other parameters determined previously in the validated model were selected:

a. Daytime paving (sunny)

- Air ambient temperature = 35°C
- Wind speed = 1 m/s
- Heat transfer coefficient of natural cooling = 9.9 W/m^2°C
- Initial temp. of asphalt overlay: 140°C
- Initial temp. of existing asphalt layer: 39°C
- Initial temp. of unbound granular base: 36°C
- Initial temp. of subgrade: 33°C
- Solar flux = 500 W/m^2

b. Night-time paving

- Air ambient temperature = 25°C
- Wind speed = 2 m/s
- Heat transfer coefficient of natural cooling = 14 W/m^2°C
- Initial temp. of asphalt overlay: 140°C
- Initial temp. of existing asphalt layer: 26°C
- Initial temp. of unbound granular base: 24°C
- Initial temp. of subgrade: 22°C
- Solar flux = 0

To examine the effect of spray water cooling on overlay thickness, two different overlay thicknesses, 70mm and 100mm were considered. In addition, to see the effect of duration of spray water cooling, three different spray water durations, 1 minute, 3 minutes and 10 minutes, were examined. Although the assumption of water spraying for 10 minutes was intended only to examine the extreme spraying condition for the purpose of this study. In reality, applying the

water spraying for 10 minutes might not be practical and require high amount of water and tankers. In addition, to see the effect of the timing of the water spraying, four different spraying times: 10, 20, 30, and 40 minutes after asphalt laying, were also simulated. In this research, the temperature at the bottom quarter (3/4 depth) of the asphalt overlay was selected as the reference location for temperature measurement as it is often the highest temperature location at traffic-opening. Moreover, a traffic-opening to temperature of 65°C, as set by many road and airport agencies, was selected for the analysis.

7.4.5.2. Comparison of Cooling Time of Water spray and Natural Cooling

The simulation results are listed in Table 7.4 for all five cooling strategies and presented in Figure 7.8 for the asphalt overlay with a water cooling strategy of WC1. The following observations may be made from the results obtained:

- For the cases studied, compared to natural cooling, spray water cooling could reduce the closure time during night-time and daytime construction by 8–31 minutes (5–34% reductions), and 13–116 minutes (3–47% reductions), respectively, depending on the asphalt lift thickness and water cooling strategy such as water cooling temperature, water flow rate, spraying duration and timing of the spray.

Table 7.4. Natural cooling and spray water cooling times needed for different cooling strategies, lift thickness and construction time

Spray water cooling strategy (duration):	The cooling time needed (minutes) for asphalt mixtures to reach traffic opening temp. of 65°C for:			
	Construction time (Lift thickness)			
	Night-time (70mm)	Night-time (100mm)	Daytime (70mm)	Daytime (100mm)
Natural cooling	91	150	248	405
WC1[a] (1 min.)	69	127	174	380
WC2[b] (1 min.)	76	134	194	386
WC3[c] (1 min.)	78	137	204	385
WC4[d] (1 min.)	83	142	221	392
WC1[a] (3 min.)	62	119	132	354
WC2[b] (3 min.)	70	128	153	364
WC3[c] (3 min.)	72	131	167	360
WC4[d] (3 min.)	79	138	182	371
WC1[a] (10 min.)*	53	106	70	298
WC1[a] (1 min.), 30 minutes after	70	128	176	380

[a] T_w = 10°C, V_w = 64 L/ m²·min.; [b] T_w = 30°C, V_w = 64 L/ m²·min.; [c] T_w = 10°C, V_w = 30 L/ m²·min.; [d] T_w = 30°C, V_w = 30 L/ m²·min.

*Might not be practical

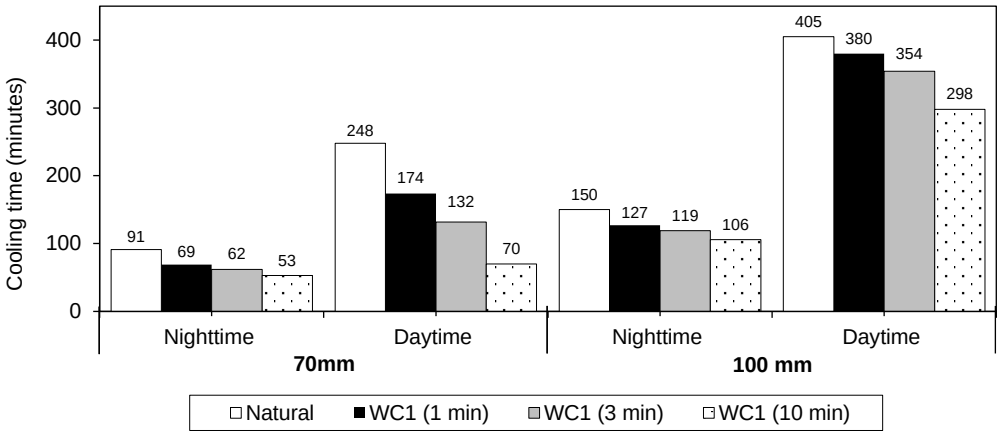

Figure 7.8. Comparison of cooling time of natural and spray water for different lift thickness, construction time and spraying duration for WC1

- The reduced cooling time with spray water cooling is dependant of the water cooling temperature and the water flow rate. The lower the water cooling temperature and the higher the water flow rate, the greater the cooling rate of the newly laid asphalt.
- The reduced cooling time due to spray water cooling is much less effective for the case with greater overlay thickness since the water only cools the crust/surface of asphalt temporarily, with the bottom of the newly laid asphalt not being much affected. For instance, the cooling time required for asphalt mixture with a thickness of 100 mm to reach 65°C during daytime construction is reduced from 405 minutes for natural cooling to 380 minutes with spray water cooling (WC1) for 1 minute – which would represent a shortening of the cooling time by only 25 minutes (6.2%). However, for asphalt with a thickness of 70mm, with the same cooling strategy, the cooling can be reduced by 74 minutes (26.1%). For thick asphalt overlays, the effect spray water on cooling time reduction can be more pronounced when the spraying duration is increased, see Table 7.4. This suggests that the statement from Asphalt Institute (2009), saying that spraying water on the new asphalt layers is ineffective, might be true for those with thick asphalt lift. However, based on the finding in this research, it might not apply to asphalt with thin layers.
- Spray water cooling duration has significant effects on the cooling rate of newly laid asphalt. It can be seen from Figure 7.9(a) and Table 7.4 that the cooling time required for new asphalt to reach the traffic opening temperature is significantly shorter when the spray water is applied for a duration of 10 minutes, compared to 1 minute and 3 minutes of spraying. For instance, for 70mm lift thickness during daytime construction, the required asphalt cooling

time with natural cooling is 248 minutes. In contrast, for the same mixture with spray water cooling strategy WC1, i.e. durations of 1, 3 and 10 minutes, the required cooling times to reach 65°C are 174, 132 and 70 minutes, respectively.

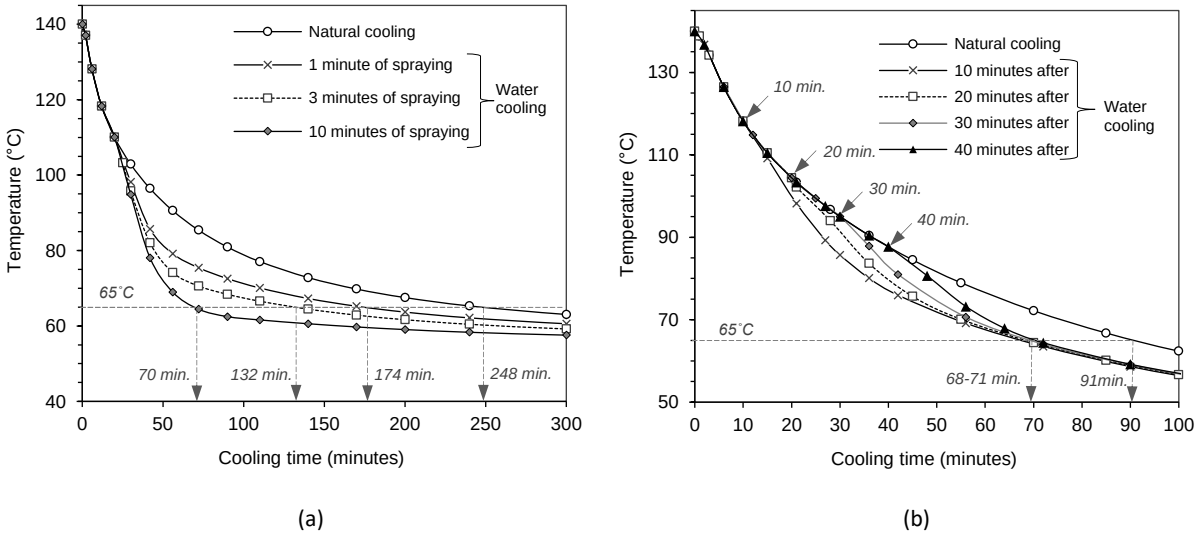

Figure 7.9. Comparison of natural and spray water cooling times for various spray water durations during (a) daytime and (b) night-time; both at a depth of 70mm and under strategy WC1

- The timing of spray water cooling after compaction, surprisingly, has no significant effect on the cooling time. As can be seen in Figure 7.9(b), the required cooling times for asphalt to reach 65°C are nearly the same for all spray start times (10, 20, 30 and 40 minutes after asphalt laying). Since the required cooling times are approximately the same, it is recommended that spray water application is applied when the surface temperature is low to avoid significant stresses and thermal shock due to temperature differences between the asphalt surface and water. In this case, water spraying 40 minutes after asphalt laying is preferred. However, in this study, the heat transfer coefficients for all spraying times (and surface temperatures) were assumed the same. In fact, a study by Bamberger and Prinz (1986) suggested that the heat transfer coefficient (h_{wc}) should be different for different surface temperatures with lower h_{wc} for lower surface temperature. With this assumption, the water cooling at high surface temperature (soon after the asphalt laying) might provide greater temperature reduction in the new asphalt.
- The effect of spray water cooling on cooling time reduction is more pronounced when applied to newly laid asphalt during daytime construction, as compared to night-time construction. This is as expected; the relatively higher ambient temperature and presence of the solar

radiation during the daytime will reduce the rate of heat loss from hot asphalt. The spray water cooling can be more beneficial when used for asphalt overlay projects during daytime. For example, the cooling time required for asphalt mixture with a thickness of 70 mm to reach 65°C during daytime construction is reduced by 74 minutes (26.1%) with the strategy WC1 for 1 minute. In contrast, for night-time construction the required cooling times would be reduced by only 22 minutes (24.2%). However, this would be highly dependent on the asphalt lift thickness, water spray duration, water cooling temperature and water flow rate.

7.4.6. Mechanical Performance of Asphalt Pavement Sprayed with Water

7.4.6.1. Cantabro Test

The core samples from specimens with natural cooling and spray water cooling were tested to investigate the effect of spray water on asphalt mixes durability. Figure 7.10 displays a visual comparison of tested asphalt specimens for the samples with natural cooling and forced spray water cooling. In addition, the results of Cantabro mass loss (CML) of the asphalt samples subjected to various cooling strategies are given in Figure 7.11. Each CML value represents the average of two core sample. The results show that the specimens with water spraying resulted in a slightly higher or equal CML (range from 2.4-3%) compared to the specimens with natural cooling (2.4%), indicating a comparable durability performance. The small difference between the CML is likely caused by the sample variability– air voids, coring process and finishing, and conditioning temperature, in the Cantabro test. Overall, the results suggest that CML of asphalt mixes was not significantly affected by the water spraying.

(a) Untested specimen (b) Sprayed water specimen (c) Natural cooling specimen

Figure 7.10. Cantabro test specimens

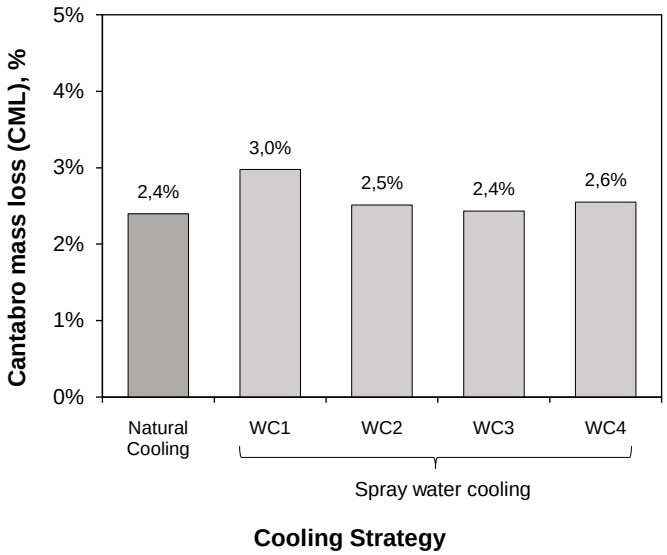

Figure 7.11. Results of Cantabro mass loss of the specimens with natural cooling and spray water cooling

In addition, among the four water cooling strategies (WC1-WC4), it was observed that no trend was found on the effect of the water temperature and flow rate on the CML. Finally, for all specimens, it can be seen that the Cantabro mass loss is relatively low (less than or equal to 3%), as compared to those reported for open-graded mixes /porous asphalt (16-25%) (Arrieta and Maquilón 2014). This might indicate that the Cantabro test is not suitable to assess the durability performance of specimens of dense graded asphalt and with low air void content (such as for airfield asphalt mixtures).

7.4.6.2. Indirect Tensile Strength Test

The indirect tensile strength, IDT (kPa) and TSR value (%) for all the asphalt samples subjected to various cooling strategies, calculated from Eq. (3.2) and (3.3), are summarized in Figure 7.12. Each value represents the average of two core sample. It can be observed from Figure 7.12 that the indirect tensile strengths of asphalt under spray water cooling strategies were slightly lower than that under a natural cooling condition. The slight decrease in the indirect tensile strength of the specimens from natural cooling condition to the spray water cooling condition might confirm that the moisture transport occurs in asphalt mixtures due to infiltration of water (during the spraying) through the pavement surface (permeability). Furthermore, to estimate how severe are the effects of spray water cooling on the moisture susceptibility of asphalt mixture, tensile strength ratio (TSR) was calculated. From the Figure 7.12, it shows that the TSR values ranged

from 92-98%, higher than the required standard TSR values, which varies from 70% to 80% (Caro et al. 2008). This finding indicates that the spray water cooling might not severely induce the moisture damage in asphalt pavement. The spray water application may have a similar impact on the pavement as the regular rainfall event. It would be worth investigating this presumption using a higher amount of experimental data and through statistical analysis to assess the effect of spray water cooling on the performance of asphalt pavement.

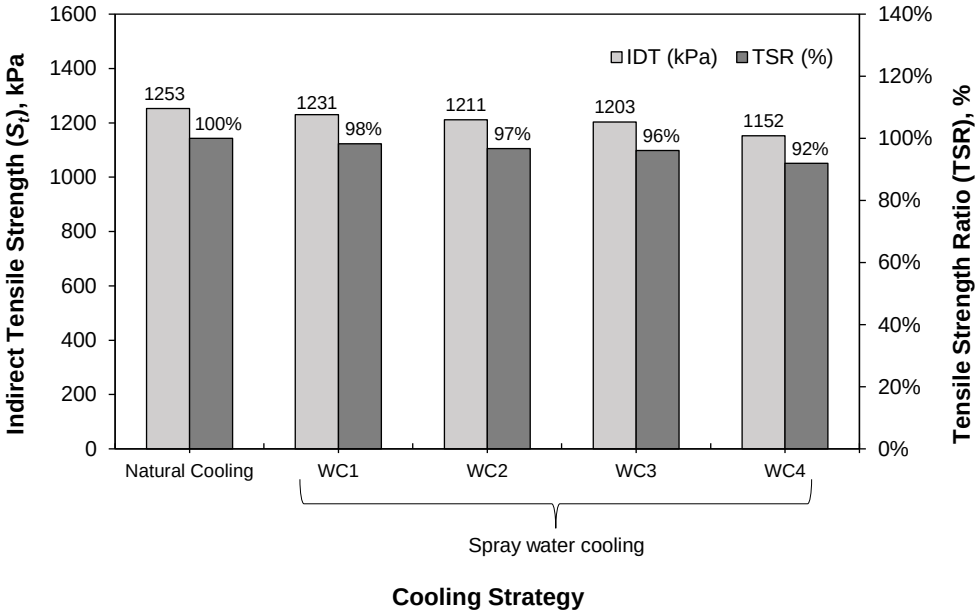

Figure 7.12. TSR results of the specimens with natural cooling and spray water cooling

Overall, the limited testing of samples presented in this research indicates that the spray water application onto the newly paved asphalt so as to permit earlier trafficking does not necessarily adversely affect the asphalt durability and or the moisture damage of asphalt pavement. Moreover, heat or thermal shock that occurs when a certain object is subjected to a rapid and sudden temperature change (too high rate of cooling) may cause shrinkage and cracking, and change in the material properties (Vilumsone-Nemes 2018, Bamberger and Prinz 1986). In addition, the water spraying onto the newly laid asphalt (at surface temperature of about 120°C) may cause reduced viscosity of the asphalt mixture (a foaming effect) and may reduce the rutting resistance of newly laid asphalt at in-service temperature. Furthermore, although it is not evidently proved in this study, the water spraying may penetrate into the layer interface and adversely reduce the bond strength between the layers, which may cause the

interface shear failure/delamination when subjected to the braking force from the traffic. Thus, a deeper research into other possible detrimental effects of spray water cooling on asphalt pavement performance through mechanical tests such as fatigue test, rutting test, and interface shear bond test is highly recommended.

7.5. Summary and Conclusion

There is no doubt that the cooling of newly laid asphalt is ideally performed under natural cooling condition. However, in the hot tropical country, the asphalt cooling time would be very lengthy to reach a targeted temperature before the newly laid asphalt can be opened to traffic. Some contractors practice spraying water on the newly laid asphalt to speed up the cooling time, despite many specifications prohibiting the practice. In this study, heat transfer experiments of spray water cooling onto newly laid asphalt were performed. The predicted heat transfer coefficients of spray water with several cooling strategies were obtained by trial-and-error matching of temperature in the validated 3D heat transfer model to those from thermocouple readings. Furthermore, to investigate the possible detrimental effect of spray water cooling onto newly laid asphalt pavement, a series of mechanical tests were carried out. From the comparative analysis the following observations are obtained:

- The 3D heat transfer model is accurate for estimating the heat transfer coefficient of water spraying. The values of the heat transfer coefficient of water cooling, h_{wc}, for various water temperatures and flow rates were determined. The values for h_{wc} (240-720 W/m^2·K) were within the range of those reported in the literature for spray water cooling experiments on metals (Bamberger and Prinz 1986, Nozaki et al. 1978). The result allows engineers to predict the cooling response of newly laid asphalt when subjected to spray water cooling.
- Simulation examples provided show that the heat loss of newly laid asphalt is greatly affected by water cooling, in particular for construction performed on sunny days. In addition, different water temperatures, flow rate, spray duration and travel time of water would result in different asphalt cooling responses.
- The reduced cooling time due to spray water cooling, however, is much less effective for asphalt with greater overlay thickness, since the water only cools the crust/surface of the asphalt temporarily, with the bottom of the newly laid asphalt not being much affected. For a thick asphalt overlay, water cooling with longer spraying duration, lower water cooling

temperature and higher water flow rate could be useful to improve the effectiveness of water spraying on cooling time reduction.

- The limited samples tested in the Cantabro test and the indirect tensile strength test in this research indicate that the spray water application onto the newly paved asphalt so as to permit earlier trafficking does not necessarily adversely affect the asphalt durability and or the moisture damage of asphalt pavement. Further studies should be performed to increase the amount of experimental data and through statistical analysis to investigate the effect of spray water cooling on the performance of asphalt pavement.
- In addition, a deeper research into other possible detrimental effects through mechanical tests such as fatigue test, rutting test and interface shear bond strength test is highly recommended.

8. Conclusions, Applications and Recommendations

8.1. Introduction

With the increase of 24-h airport operations and the number of scheduled flights at major airports, the periods available for pavement repair and overlay have become limited. In this study, to minimize delays and interruptions, early opening-to-traffic pavement rehabilitation strategies that allow work to be completed at night have been investigated. In this chapter, the conclusions from the study, their application and recommendations for the further research are presented.

8.2. Conclusions

For convenience, the detailed conclusions have been divided into five subsections relating to the different aspects of the work described in this thesis. In the first subsection, the key conclusions are presented. Afterwards, the detailed principal results and conclusions that address the research questions and existing knowledge gaps are listed.

8.2.1. Overall Conclusions

The key conclusions of this study are listed as follow:

1. There is a lack of agreement between the acceptable opening-to-traffic asphalt temperature that doesn't appear to have a strong theoretical basis
2. Current specification on opening-to-traffic asphalt temperature (60°C) as set by many agencies is reasonably acceptable for typical airfield asphalt surface material
3. Opening the newly laid asphalt overlays at a higher temperature (up to 80°C) can be achieved by using polymer modified bitumen (PMB) as the tack coat and mixture material

4. Warm mix asphalt (WMA) could shorten the airport closure and quickly open asphalt overlay to traffic, due to its lower production temperature, without notable differences in asphalt performance
5. The water spray application onto newly laid asphalt pavement does not necessarily adversely affect the asphalt durability and or the moisture damage of asphalt pavement. However, it is likely to be of limited value in accelerating cooling of overlays, except when they are relatively thin
6. Increased efficiency in night-time airport pavement overlaying can only be achieved when current cooling requirements before trafficking exceed the time needed to line and relight the pavement

Although the research in this study has been carried out in the context of airfield pavement rehabilitation and maintenance, most findings can also be applied for road and highway pavements with little or no modification.

8.2.2. Selecting the Allowable Asphalt Temperature of Opening to Traffic

Chapter 5 investigated the first strategy for reducing cooling time and addressed the first research question (the acceptable opening-to-traffic asphalt temperature) and the second research question (the effect of material selection on the decision of asphalt opening to traffic), each as listed in Section 1.2.

From the rutting and interface shear bonding test and analysis, it was concluded that newly laid asphalt with typical conventional bitumen has gained sufficient strength to resist permanent deformation and interface failure at opening-to-traffic temperature of 60°C. The results, however, suggest that different mixtures and tack coats, particularly those containing polymer-modified bitumen (PMB), could be re-opened to air traffic at considerably higher temperatures (up to 80°C) due to their superior rut resistance and interface bonding. This result should encourage airport authorities and agencies to be more flexible with the traffic-opening temperature specification, particularly for mixtures incorporating PMBs.

Selection of bituminous binder, mixtures and tack coat materials affects the decision of opening asphalt overlay to traffic, as displayed in the rutting and interface shear bond test results. Asphalt overlay rutting and bond strength could be significantly improved by use of modified bitumen and tack coat products at elevated temperatures. This suggests that the selection of

traffic-opening temperature is bituminous binder-dependent, thus it is necessary to give the pavement designer the ability to establish opening temperature based on the bituminous binder type and its performance at the selected opening-to-traffic temperature.

8.2.3. Warm Mix Asphalt (WMA) for Airfield Pavement Overlay

Chapter 6 investigated the second strategy for reducing cooling time and addressed the third research question (Comparison of rutting and interface shear strength of HMA and WMA and how the differences between HMA and WMA influence the temperature for asphalt opening to traffic).

From the repeated load axial tests (RLAT) and rutting prediction presented in this study, it was concluded that, in general, the WMAs have a rutting performance, at high temperatures, similar to, or better than HMA. Furthermore, from the direct shear test on double-layered specimens, it was observed that the upper layer mixes prepared with WMA-Sasobit exhibited a comparable measured interface shear strength (ISS) compared with the control HMA at all temperatures and normal pressures. In addition, based on the interface shear failure analysis, the WMA-upper layer exhibited a slightly higher stress-to-strength ratio than the HMA-upper layer at all temperatures and aircraft loading conditions.

Based on these results on limited WMA additive products (Sasobit and Rediset), it was concluded that the difference in production temperature of HMA and WMA has no significant difference in rutting and bond strength at in-service temperature of opening to traffic. This suggests that the use of WMA does not have a significant practical implication on the permissible temperature at opening to traffic, as compared to HMA. In addition, it was found that, compared to HMA, WMA-Sasobit showed excellent rutting resistance at high temperature, enabling the pavement to be opened to traffic at a higher temperature in the low shear areas of airport. This is likely because, at in-service temperatures, the wax additives solidify (crystallize) and thus improve stiffness and rutting resistance of the mixture.

8.2.4. Spray Water Cooling onto the Newly Laid Asphalt Pavement

Chapter 7 investigated the third strategy for reducing cooling time and addressed the fourth research question of this thesis (the cooling time of asphalt with water spraying, and the possible detrimental effect on asphalt performance).

From the temperature measurement and cooling prediction, it was concluded that the heat loss of newly laid asphalt is greatly affected by water cooling, in particular for construction performed during sunny daytime. However, it is much less effective for asphalt with greater overlay thicknesses, since the water only cools the crust/surface of the asphalt temporarily, with the bottom of the newly laid asphalt not being much affected. In this case, water cooling with longer spraying duration, lower water cooling temperature and higher water flow rate could be useful to improve the effectiveness of water spraying on cooling time reduction.

From the limited samples tested in the Cantabro test and indirect tensile strength test in this research, it was concluded that spray water application on newly paved asphalt does not necessarily adversely affect the asphalt durability or moisture damage susceptibility of asphalt pavement. Further studies should be performed using a higher amount of experimental data and, through statistical analysis, to investigate the effect of spray water cooling on the performance of asphalt pavement.

8.2.5. Reduced Cooling Time and Improved Construction Efficiency

Chapter 4 investigated the fifth research question (the effect of each strategy on reduced cooling time and improved efficiency).

From the validated cooling prediction / heat transfer model presented in this study, it was concluded that each strategy proposed in this study could significantly reduce the required cooling time before traffic opening and, thus, shorten the airport closure. From the illustrative study, raising the critical opening-to-traffic asphalt temperature and using WMA for asphalt overlays could reduce the overall construction period and improve construction efficiency, due to more volume of asphalt can be paved each night.

8.3. Applications

This section presents construction practices and applications of asphaltic concrete that will apply to repair and overlay projects which will allow rapid opening of a pavement to traffic. It is acknowledged that, the early-opening-to-traffic of asphalt may only be suitable for pavement rehabilitation in typical large and busy airports and/or projects with adverse hot weather conditions, where the runways cannot be closed for a lengthy period of time and/or the asphalt mat cooling is difficult to achieve, respectively. For less crowded airports in locations with relatively low air ambient temperature, it is unnecessary to quickly open the new asphalt to

traffic, rather it is safer to wait until the new asphalt cools to near-ambient air temperature.

The opening of a runway overlay to traffic does not depend only on the time of asphalt to cool but also depends on the time of restoring the lighting system and line marking at the end of each work period. In the case when the time for restoring is greater than the cooling time, the use of an early-opening-to-traffic asphalt strategy would be pointless in terms of its benefit for rapid construction. These are the issues that need to be considered before applying the strategies. The application of early-opening-to-traffic asphalt strategies and its performance and materials consideration is presented as a flowchart in Figure 8.1.

8.3.1. Night-time Working Hours

Time is of the essence during the off-peak time (night-time) construction. The contractor should be given as much time as possible to overlay the runway each night. The time window of 6 hours should be the least specified to reduce inefficiency.

8.3.2. Thickness and Lift Operation of Asphalt Overlay

Increasing the thickness of a mat can considerably increase the time that it will take to cool to a temperature for opening to traffic. Based on the results of this study, in the case of the limited pavement construction time available in an active airport, it is preferable to (a) select a thinner total lift depth of the asphalt overlay, and (b) avoid multi lift paving operations in a single night. In the case of large overlay thickness, it is recommended that overlay is done first in one lift and continued for the next layer only when the first layer has fully cooled (usually at least one night later). With this approach, however, several drawbacks could occur, including the increase of transverse joints, the need for interface treatment and tack coating and the need for short-duration lining and lighting.

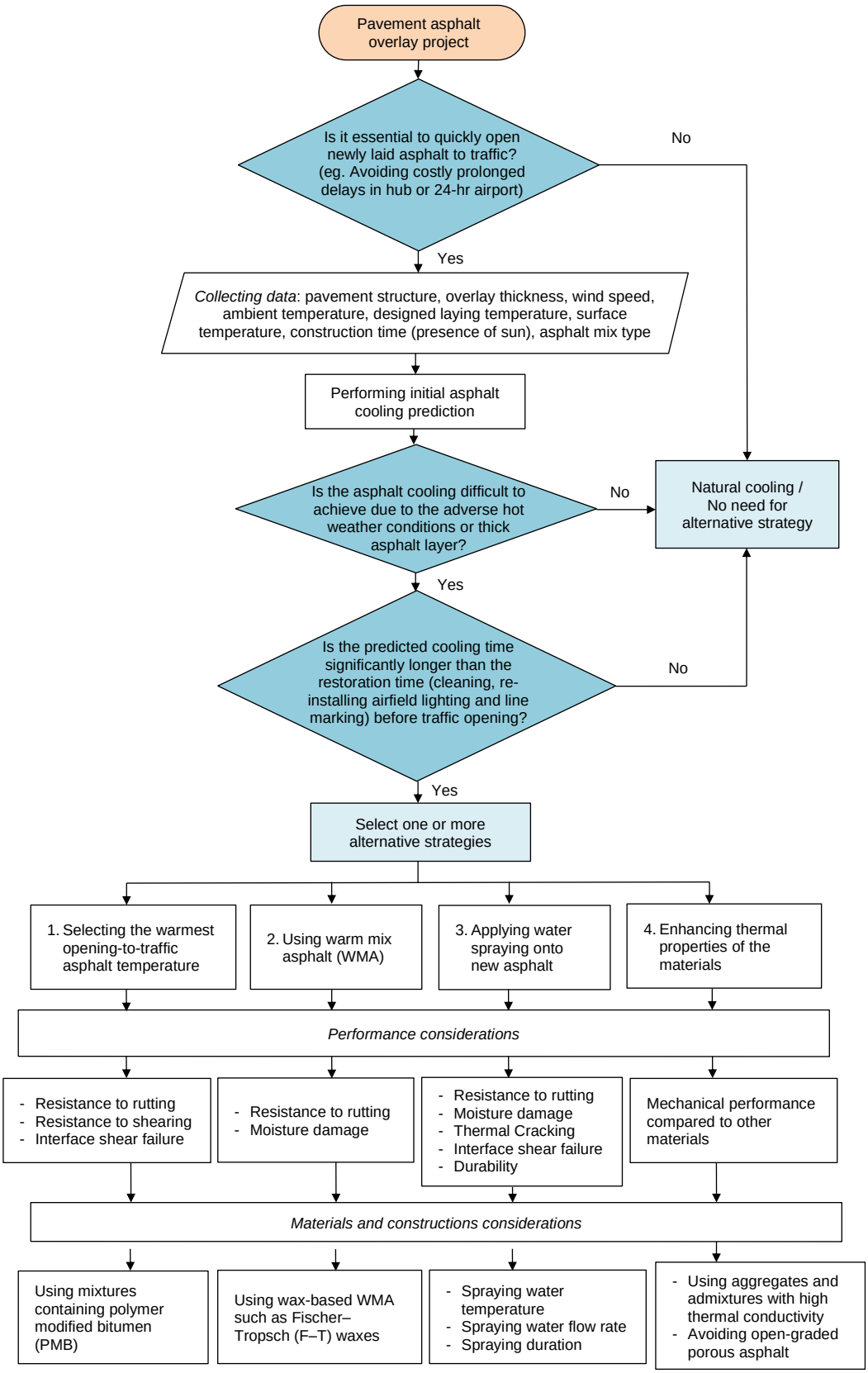

Figure 8.1 Flowchart of the application of early-opening-to-traffic asphalt strategies

8.3.3. Temperature Monitoring

For practical implementation, to avoid the mismeasurement of newly laid asphalt temperature, it is suggested that practitioners /airport authorities avoid using an infrared thermometer directed at an asphalt surface in order to gauge the amount of cooling achieved. Instead of using the temperature of the asphalt surface, it is recommended to use embedded thermocouple sensors to monitor the temperature changes at the bottom or 3/4 depth of the asphalt layer. Alternatively, if thermocouple measurement is not practical, surface temperature measurement using an infrared thermometer along with a pre-determined asphalt cooling prediction can be used instead. The internal temperature of the asphalt overlay can then be approximated using the actual surface temperature in the field and direct conversion using the estimated cooling curves (of different lift depths).

8.4. Research Limitations

The research presented in this thesis contains several unavoidable limitations. The limitations of this study are listed as follow:

- The resistance of asphalt to rutting at high temperature was mainly investigated through the RLAT test. Although the results and analysis have been validated against data from the wheel tracking test, it still may not precisely simulate the real traffic condition. A test using accelerated pavement testing or testing using a section of pavement would be useful for future research.
- For all testing temperatures (50, 60, 75 and 85°C), the cyclic compression test/RLAT was performed without confinement (unconfined). The permanent deformation and number of load cycles to failure results may therefore underestimate the rutting performance of the bituminous mixture at high temperature. As the test was performed at high temperature, confinement pressure significantly affects the development of permanent deformation. Performing the cyclic compression test with confinement or in a triaxial test is highly recommended for future study.
- The RLAT was performed over a relatively long loading time (1s loading and 1s of unloading) which represents very low vehicle speed. No adjustment was made to the time of loading (such as using time-temperature superposition principles). A future study with a

lower loading time during RLAT testing or with loading time adjustment is highly recommended.

- The load applied in the RLAT was significantly lower (1000 kPa) than actual typical commercial aircraft tires (more than 1400 kPa) due to the limitations of the laboratory equipment. In this research, however, the RLAT was primarily aimed at capturing the viscous properties of asphalt mixtures at high temperature for rutting analysis. In addition, since the RLAT specimen was uniaxial and unconfined, the test was performed at relatively low-stress levels, relative to actual aircraft tire pressures, to avoid the sample failing prematurely so that the viscous properties of the material could not be obtained.
- During the direct shear test with normal load, for interface shear bond investigation, the normal load was applied by manually pushing the compressive spring to generate load and using a simple correlation between spring stiffness and spring displacement to predict the generated normal load. It was, therefore, subject to biases and measurement errors, that may influence the interface shear bond strength analysis (in the Mohr plane). The use of more advanced apparatus to generate the normal load is highly recommended for future study.
- In this study, the temperature measurement during the water cooling experiment was only performed at one location in the middle of the asphalt slab specimen (at various depths) . Instead of using only one location of temperature measurement, it is recommended to employ more thermocouples or use temperature mapping/contours on the asphalt surface. This would allow the reduction of experimental errors.

8.5. Recommendations for Further Research

This study identified several recommendations and suggestions for further research. It also listed a number of unresolved challenges for future study. It is recommended that these issues be considered in the future. Suggestions for future research might include the following items:

- Asphalt concrete with dense grading was specifically used in this study. A future study on traffic-opening temperature of other mixtures such as stone mastic asphalt and porous asphalt is highly recommended.
- The rutting resistance and interface shear bond performance of asphalt pavement at high temperature were studied. However, the horizontal shoving or shearing of the pavement

surface or near-surface was not specifically discussed. It would be useful for future study to investigate the susceptibility of the surface to shearing during opening to traffic.

- It is acknowledged that, on the evidence of many works of literature, a higher interface shear strength value for pavement interlayers can be obtained with a milled surface. In this research, although two different pavement surfaces, asphalt and PCC, were investigated. Neither was untreated in any way so as to enhance the interface texture. It would be worth investigating enhanced interfaces (such as asphalt milled surface) and see if there is a difference in the interface shear bond of asphalt at high temperature.
- A future investigation of the performance of WMA that studies more additive types at high temperature upon opening to traffic is highly recommended. Having only two WMA additives in this study did not cover all additives that are commonly used in the field. It is recommended to study other WMA additives such as foaming or water-bearing additives, and other types of wax additive.
- In this study, the effect of spray water cooling on asphalt pavement performance was investigated only in terms of durability and moisture damage. More thorough research into other possible detrimental effects through mechanical tests, such as rutting and fatigue tests, is an issue of interest, since water spraying (onto new asphalt) may lead to thermal shock (that causes shrinkage and cracking) and lead to reduced viscosity and rutting resistance of newly laid asphalt at in-service temperature due to the foaming effect.
- Finally, it is recognized from previous studies that the heat transfer coefficient of spray water cooling greatly depends on the particle size and shape of the water droplet. In this research, these factors were not analysed. It is important to consider these factors when undertaking further research of this process.

References

AASHTO, 2008. *Mechanistic-empirical Pavement Design Guide: A Manual of Practice.* AASHTO.

Abed, A., Thom, N. and Grenfell, J. 2019. A novel approach for rational determination of warm mix asphalt production temperatures. *Construction and Building Materials,* 200, 80-93.

Aho, B., Hein, D., Dennechuk, S. and Bessom, R., 2016. 10 Years of Experience Using Warm Mix Asphalt for Airside Pavements—Boston Logan Airport. *International Conference on Transportation and Development 2016.* 1-12.

Ai, C., Rahman, A., Song, J., Gao, X. and Lu, Y. 2017. Characterization of Interface Bonding in Asphalt Pavement Layers Based on Direct Shear Tests with Vertical Loading. *Journal of Materials in Civil Engineering,* 29(9), 04017102.

Airey, G. D. 2004. Fundamental Binder and Practical Mixture Evaluation of Polymer Modified Bituminous Materials. *International Journal of Pavement Engineering,* 5(3), 137-151.

Airport Council International, 2017. Preliminary 2016 world airport traffic rankings.

Akzonobel®, 2014. *Rediset® LQ-1102CE : Warm Mix Additive and Compaction aid for hot mix* [online]. Available from: https://surfacechemistry.nouryon.com/globalassets/inriver/resources/pds_rediset_lq-1102ce.pdf [Accessed 12 November 2018 2018].

Al-Ahmadi, H. M. and Yao, S. C. 2008. Spray Cooling of High Temperature Metals Using High Mass Flux Industrial Nozzles. *Experimental Heat Transfer,* 21(1), 38-54.

Al-Mosawe, H., 2016. *Prediction of permanent deformation in asphalt mixtures.* (PhD). University of Nottingham.

Al-Mosawe, H., Thom, N., Airey, G. and Albayati, A. 2018. Linear viscous approach to predict rut depth in asphalt mixtures. *Construction and Building Materials,* 169, 775-793.

Al-Qadi, I., Wang, H., Yoo, P. and Dessouky, S. 2008. Dynamic analysis and in situ validation of perpetual pavement response to vehicular loading. *Transportation Research Record: Journal of the Transportation Research Board,* (2087), 29-39.

Al-Qadi, I. L., Yoo, P. J., Elseifi, M. A. and Nelson, S. 2009. Creep Behavior of Hot-Mix Asphalt due to Heavy Vehicular Tire Loading. *Journal of Engineering Mechanics,* 135(11), 1265-1273.

Alavi, M., Pouranian, M. and Hajj, E. 2014. Prediction of Asphalt Pavement Temperature Profile with Finite Control Volume Method. *Transportation Research Record: Journal of the Transportation Research Board,* 2456, 96-106.

Ali, A. W., Kim, H. H., Mazumder, M., Lee, M.-S. and Lee, S.-J. 2018. Multiple Stress Creep Recovery (MSCR) characterization of polymer modified asphalt binder containing wax additives. *International Journal of Pavement Research and Technology*.

Alleman, J. and Heitzman, M., 2019. *Quantifying Pavement Albedo, NCAT Report 19-09.* Ames, IA: National Concrete Pavement Technology Center.

Anderson, D., Youtcheff, J. and Zupanick, M., 2000. *Asphalt binders.* Washington DC, United States Transportation Research Board, A3B05: Committee on Safety Data, Analysis, and Evaluation.

Anderson, D. A., Christensen, D. W., Bahia, H. U., Dongre, R., Sharma, M., Antle, C. E. and Button, J. 1994. Binder characterization and evaluation, volume 3: Physical characterization. *Strategic Highway Research Program, National Research Council, Report No. SHRP-A-369*.

ARA Inc. ERES Division, 2004. *Guide for Mechanistic-empirical Design of New and Rehabilitated Pavement Structures.* Washington, D.C: Transportation Research Board of the National Academies.

Arabali, P., Sakhaeifar, M. S., Freeman, T. J., Wilson, B. T. and Borowiec, J. D. 2017. Decision-Making Guideline for Preservation of Flexible Pavements in General Aviation Airport Management. *Journal of Transportation Engineering, Part B: Pavements,* 143(2), 04017006.

Arbeider, C., Miller, S. R., Dorée, A. and Oosterveld, M., Planning the asphalt construction process: Towards more consistent paving and compaction operations. ed. *17th AAPA International Flexible Pavements Conference Exhibition 2017: Roads of the Future, Embracing Disruption*, 2017.

Archilla, A. R. and Madanat, S. 2000. Development of a Pavement Rutting Model from Experimental Data. *Journal of Transportation Engineering,* 126(4), 291-299.

Arega, Z., Bhasin, A., Motamed, A. and Turner, F. 2011. Influence of Warm-Mix Additives and Reduced Aging on the Rheology of Asphalt Binders with Different Natural Wax Contents. *Journal of Materials in Civil Engineering,* 23(10), 1453-1459.

Arepalli, U. M., Madankara Kottayi, N. and Mallick, R. B. 2019. Moisture susceptibility evaluation of Hot Mix Asphalt: combined effect of traffic and moisture. *International Journal of Pavement Research and Technology,* 12(2), 206-214.

Arrieta, V. S. and Maquilón, J. E. C. 2014. Resistance to Degradation or Cohesion Loss in Cantabro Test on Specimens of Porous Asphalt Friction Courses. *Procedia - Social and Behavioral Sciences,* 162, 290-299.

Aschenbrener, T. 1995. Evaluation of Hamburg wheel-tracking device to predict moisture damage in hot-mix asphalt. *Transportation Research Record,* 1492, 193.

ASHRAE 2010. Energy standard for buildings except low-rise residential buildings. *ASHRAE Standard 90.1-2010*.

Asifur Rahman, A., Faisal, H. M. and Tarefder, R. A., 2017. Measured versus Interconverted Viscoelastic Material Functions of Asphalt Concrete. *Airfield and Highway Pavements.* 165-175.

Asphalt Institute, 2001. *Manuel Series 5 (MS-5) Introduction to Asphalt.*

Asphalt Institute, 2009. *Asphalt Pavement Construction FAQs* [online]. Available from: http://www.asphaltinstitute.org/asphalt-pavement-construction-faqs/ [Accessed December 10 2017].

Asphalt Institute, 2015. *MS-2 Asphalt Mix Design Methods.* 7th ed.: Asphalt Institute.

ASTM, 2012. ASTM D5340-12 Standard Test Method for Airport Pavement Condition Index Surveys. West Conshohocken, PA.

ASTM, 2017. D6931-17 Standard Test Method for Indirect Tensile (IDT) Strength of Asphalt Mixtures. West Conshohocken, PA: ASTM International,.

ASTM International, 2013. SD7064/D7064M-08(2013) Standard Practice for Open-Graded Friction Course (OGFC) Mix Design. *ASTM International,.* West Conshohocken, PA.

Austin, G. 1991. Runway Resurfacing Experience. *Proceedings of the Institution of Civil Engineers,* 90(3), 575-586.

Bae, A., Mohammad, L., Elseifi, M., Button, J. and Patel, N. 2010. Effects of Temperature on Interface Shear Strength of Emulsified Tack Coats and Its Relationship to Rheological Properties. *Transportation Research Record: Journal of the Transportation Research Board,* 2180, 102-109.

Bahia, H., Hanson, D., Zeng, M., Zhai, H., Khatri, M. and Anderson, R. 2001. Characterization of modified asphalt binders in superpave mix design. NCHRP Report 459. *Transportation Research Board, Washington, DC*.

Bai, B. C., Park, D.-W., Vo, H. V., Dessouky, S. and Im, J. S. 2015. Thermal Properties of Asphalt Mixtures Modified with Conductive Fillers. *Journal of Nanomaterials,* 2015, 926809.

Bamberger, M. and Prinz, B. 1986. Determination of heat transfer coefficients during water cooling of metals. *Materials Science and Technology,* 2(4), 410-415.

Banerjee, A., de Fortier Smit, A. and Prozzi, J. A. 2012. The effect of long-term aging on the rheology of warm mix asphalt binders. 97, 603-611.

Barksdale, R. D., Laboratory evaluation of rutting in base course materials. ed. *Presented at the Third International Conference on the Structural Design of Asphalt Pavements, Grosvenor House, Park Lane, London, England, Sept. 11-15, 1972.*, 1972.

Barman, M., Ghabchi, R., Singh, D., Zaman, M. and Commuri, S. 2018. An alternative analysis of indirect tensile test results for evaluating fatigue characteristics of asphalt mixes. *Construction and Building Materials,* 166, 204-213.

Bazuhair, R. W., Pittman, C. V., Howard, I. L., Jordan, W. S., Hemsley, J. M. and Baumgardner, G. L. 2018. Conditioning and Testing Protocol Combinations to Detect Asphalt Mixture Damage. *Transportation Research Record,* 2672(28), 10-21.

Behnood, A., Shah, A., McDaniel, R. S., Beeson, M. and Olek, J. 2016. High-Temperature Properties of Asphalt Binders: Comparison of Multiple Stress Creep Recovery and Performance Grading Systems. *Transportation Research Record,* 2574(1), 131-143.

Bejan, A. and Kraus, A. D., 2003. *Heat transfer handbook.* John Wiley & Sons.

Bennert, T., Reinke, G., Mogawer, W. and Mooney, K. 2010. Assessment of Workability and Compactability of Warm-Mix Asphalt. *Transportation Research Record,* 2180(1), 36-47.

Bergman, T. L., Incropera, F. P., DeWitt, D. P. and Lavine, A. S., 2011. *Fundamentals of heat and mass transfer.* John Wiley & Sons.

Bernhard, R., Wayson, R. L., Haddock, J., Neithalath, N., El-Aassar, A., Olek, J., Pellinen, T. and Weiss, W. J. 2005. An introduction to tire/pavement noise of asphalt pavement. *Institute of Safe, Quiet and Durable Highways, Purdue University*.

Blagojević, B. and Bajsić, I. 1996. A one-dimensional numerical model of heat and mass transfer in air-water droplet flow. *Heat and Mass Transfer,* 31(6), 435-441.

Boeing, 2015. *737 Airplane Characteristics for Airport Planning.* Seattle, Washington: Boeing Commercial Airplanes.

Bognacki, C. J., Frisvold, A. and Bennert, T., Investigation of asphalt pavement slippage failures on runway 4R-22L, Newark International Airport. ed. *2007 Worldwide Airport Technology Transfer Conference Federal Aviation Administration American Association of Airport Executives*, 2007.

Bonaquist, R. F., 2011. *NCHRP Report 691: Mix design practices for warm mix asphalt.* Transportation Research Board.

Bowen, H. 1889. An apparatus for determining the relative degree of cohesion of a semi-liquid body. *School of Mines Quarterly*, 297-302.

Brisbane-Airport Australia, 25 November 2013. *BNE completes 15M runway overlay project* [online]. Available from: http://newsroom.bne.com.au/bne-completes-15m-runway-overlay-project/.

British Board Agrement 1998. Guideline document for the assessment and certification of thin surfacing systems for highways.

Brovelli, C., Crispino, M., Pais, J. and Pereira, P. 2015. Using polymers to improve the rutting resistance of asphalt concrete. 77, 117-123.

Brown, E. R. and Cross, S. A., 1991. *Comparison of laboratory and field density of asphalt mixtures.* National Center for Asphalt Technology (US).

Brown, E. R. and Foo, K. Y. 1994. Comparison of Unconfined- and Confined-Creep Tests for Hot Mix Asphalt. *Journal of Materials in Civil Engineering,* 6(2), 307-326.

Brown, E. R., Kandhal, P. S. and Zhang, J., 2001. *Performance testing for hot mix asphalt, NCAT Report 01-05.* Auburn, Alabama: National Center for Asphalt Technology Report.

Brown, S. and Snaith, M., The permanent deformation characteristics of a dense bitumen macadam subjected to repeated loading. ed. *Association of Asphalt Paving Technologists Proc*, 1974.

Bryden, J. E. and Mace, D. J., 2002. *A procedure for assessing and planning nighttime highway construction and maintenance.* Transportation Research Board.

BS Simulia, 2016. ABAQUS Analysis user's manual, Version 2016. ABAQUS.

BSI, 1996. *Method for Determining Resistance to Permanent Deformation of Bituminous Mixtures Subject to Unconfined Dynamic Loading: DD226.* London.

BSI, 2003a. *Bituminous mixtures — Test methods for hot mix asphalt — Part 22: Wheel tracking, BS EN 12697-22:2003.*

BSI, 2003b. *Concrete pavements — Part 2: Test method for the determination of the bond between two layers, BS EN 13863-2:2003.*

BSI, 2011. *Cement — Part 1: Composition, specifications and conformity criteria for common cements, BS EN 197-1:2011.* London: BSI.

BSI, 2012a. *Bitumen and bituminous binders. Determination of complex shear modulus and phase angle. Dynamic Shear Rheometer (DSR), BS EN 14770:2012.* London.

BSI, 2012b. *Bitumen and bituminous binders. Determination of the flexural creep stiffness. Bending Beam Rheometer (BBR), BS EN 14771:2012.* London.

BSI, 2012c. *Bituminous mixtures — Test methods for hot mix asphalt — Part 6: Determination of bulk density of bituminous specimens, BS EN 12697-6:2012.* London: BSI.

BSI, 2013a. *Bituminous mixtures — Test methods for hot mix asphalt — Part 22: Wheel tracking, BS EN 12697-22.*

BSI, 2013b. *Bituminous mixtures — Test methods for hot mix asphalt — Part 48. Interlayer Bonding, BS EN 12697-48.* London: BSI.

BSI, 2014a. *Bitumen and bituminous binders — Determination of the resistance to hardening under influence of heat and air, Part 1: RTFOT method, BS EN 12607-1:2014.* London: BSI.

BSI, 2014b. *Bitumen and bituminous binders — Preparation of test samples, BS EN 12594:2014.* London: BSI.

BSI, 2015a. *Bitumen and bituminous binders — Determination of needle penetration BS EN 1426:2015.* London.

BSI, 2015b. *Bitumen and bituminous binders — Determination of the softening point — Ring and Ball method, BS EN 1427:2015, BS 2000-58:2015.* BSI.

BSI, 2015c. *Bitumen and Bituminous Binders — Multiple Stress Creep and Recovery Test (MSCRT), BS EN 16659:2015.* London.

BSI, 2016. *Bituminous mixtures — Test methods for hot mix asphalt — Part 25: Cyclic compression test, BS EN 12697-25:2016.* London: BSI.

BSI, 2018a. *Bitumen and bituminous binders — Determination of dynamic viscosity of bituminous binder using a rotating spindle apparatus, BS EN 13302:2018.* London.

BSI, 2018b. *Bituminous mixtures — Test methods for hot mix asphalt — Part 8: Determination of void characteristics of bituminous specimens, BS EN 12697-8-2018.* London.

Buchanan, S. and Woods, M. E., 2004. *Field Tack Coat Evaluator (ATACKerTM), Report No. FHWA/MS-DOT-RD-04-168.* Jackson, MS: Mississippi Department of Transportation.

Buss, A., Cascione, A. and Christopher Williams, R. 2014. Evaluation of warm mix asphalt containing recycled asphalt shingles. *Construction and Building Materials,* 61, 1-9.

Butt, A. A., Harvey, J. T., Saboori, A., Ostovar, M. and Garg, N., 2019. Airfield Life Cycle Assessment: Benchmark Study of a Project at JFK International Airport. *Airfield and Highway Pavements 2019.* 456-464.

Button, J. W., Perdomo, D. and Lytton, R. L. 1990. Influence of aggregate on rutting in asphalt concrete pavements. *Transportation Research Record,* (1259).

Çanakci, H., Demirboğa, R., Burhan Karakoç, M. and Şirin, O. 2007. Thermal conductivity of limestone from Gaziantep (Turkey). *Building and Environment,* 42(4), 1777-1782.

Canestrari, F., Ferrotti, G., Lu, X., Millien, A., Partl, M. N., Petit, C., Phelipot-Mardelé, A., Piber, H. and Raab, C., 2013. Mechanical Testing of Interlayer Bonding in Asphalt Pavements. *In:* (eds), P. M. e. a. ed. *Advances in Interlaboratory Testing and Evaluation of Bituminous Materials. RILEM State-of-the-Art Reports.* Springer, Dordrecht, 303-360.

Canestrari, F., Ferrotti, G., Partl, M. and Santagata, E. 2005. Advanced testing and characterization of interlayer shear resistance. *Transportation Research Record: Journal of the Transportation Research Board,* (1929), 69-78.

Canestrari, F. and Santagata, E. 2005. Temperature effects on the shear behaviour of tack coat emulsions used in flexible pavements. *International Journal of Pavement Engineering,* 6(1), 39-46.

Capitão, S. D., Picado-Santos, L. G. and Martinho, F. 2012. Pavement engineering materials: Review on the use of warm-mix asphalt. 36, 1016-1024.

Caputo, P., Abe, A. A., Loise, V., Porto, M., Calandra, P., Angelico, R. and Oliviero Rossi, C. 2020. The Role of Additives in Warm Mix Asphalt Technology: An Insight into Their Mechanisms of Improving an Emerging Technology. *Nanomaterials,* 10(6).

Caro, S., Masad, E., Bhasin, A. and Little, D. N. 2008. Moisture susceptibility of asphalt mixtures, Part 2: characterisation and modelling. *International Journal of Pavement Engineering,* 9(2), 99-114.

Carrera, V., Garcia-Morales, M., Partal, P. and Gallegos, C. 2010. Novel bitumen/isocyanate-based reactive polymer formulations for the paving industry. *Rheologica Acta,* 49(6), 563-572.

Carvalho, R. L., 2012. *Prediction of permanent deformation in asphalt concrete.* (PhD). University of Maryland, College Park.

Cebo-Rudnicka, A., Malinowski, A., Telejko, T. and Gielzecki, J., 2012. Inverse determination of the heat transfer coefficient distribution on a steel plate cooled by a water spray nozzle. *In:* Sundé, B., Brebbia, C. A. and Poljak, D. eds. *Advanced Computational Methods and Experiments in Heat Transfer XII.* Great Britain: WIT Transactions on Engineering Sciences.

Chadbourn, B. A., Newcomb, D., Voller, V., Desombre, R. A., Luoma, J. A. and Timm, D. H., 1998. *An asphalt paving tool for adverse conditions.* St. Paul, Minnesota: Minnesota Department of Transportation.

Chaturabong, P. and Bahia, H. U. 2017. Mechanisms of asphalt mixture rutting in the dry Hamburg Wheel Tracking test and the potential to be alternative test in measuring rutting resistance. *Construction and Building Materials,* 146, 175-182.

Chen, B.-L., Rockett, L. and Mallick, R. B. 2008. A laboratory investigation of temperature profiles and thermal properties of asphalt pavements with different subsurface layers. *Journal of the Association of Asphalt Paving Technologists,* 77.

Chen, J.-S. and Huang, C.-C. 2010. Effect of Surface Characteristics on Bonding Properties of Bituminous Tack Coat. *Transportation Research Record: Journal of the Transportation Research Board,* 2180, 142-149.

Chen, S.-J. and Tseng, A. A. 1992. Spray and jet cooling in steel rolling. *International Journal of Heat and Fluid Flow,* 13(4), 358-369.

Chen, X. and Xu, Z., Effects of load and temperature on permanent deformation properties of HMA. ed. *Road Pavement Material Characterization and Rehabilitation: Selected Papers from the 2009 GeoHunan International Conference*, 2009, 49-55.

Chen, Z., Han, H., Ren, W. and Huang, G. 2015. Heat Transfer Modeling of an Annular On-Line Spray Water Cooling Process for Electric-Resistance-Welded Steel Pipe. *PLOS ONE,* 10(7), e0131574.

Cheng, J., Shen, J. and Xiao, F. 2011. Moisture Susceptibility of Warm-Mix Asphalt Mixtures Containing Nanosized Hydrated Lime. *Journal of Materials in Civil Engineering,* 23(11), 1552-1559.

Choi, Y., Sutanto, M., Collop, A. and Airey, G. 2005. Bond between asphalt layers. *Project Report to the UK Highways Agency, Scott Wilson Pavement Engineering Ltd., Nottingham, UK.*

Chowdhury, A. and Button, J. W., 2008. *A review of warm mix asphalt.* Texas Transportation Institute.

Chu, L., Zhu, B. and Fwa, T. F. 2019. Temperature Control Planning Tool for Multi-Lift Resurfacing of Airport Pavements. *Transportation Research Record,* 2673(7), 380-389.

Collop, A., Thom, N. and Sangiorgi, C., Assessment of bond condition using the Leutner shear test. ed. *Proceedings of the Institution of Civil Engineers-Transport*, 2003a, 211-217.

Collop, A. C., Cebon, D. and Hardy, M. S. A. 1995. Viscoelastic Approach to Rutting in Flexible Pavements. *Journal of Transportation Engineering,* 121(1), 82-93.

Collop, A. C., Scarpas, A., Kasbergen, C. and de Bondt, A. 2003b. Development and finite element implementation of stress-dependent elastoviscoplastic constitutive model with damage for asphalt. *Transportation Research Record,* 1832(1), 96-104.

Collop, A. C., Sutanto, M. H., Airey, G. D. and Elliott, R. C. 2009. Shear bond strength between asphalt layers for laboratory prepared samples and field cores. *Construction and Building Materials,* 23(6), 2251-2258.

Cominsky, R. J., Huber, G. A., Kennedy, T. W. and Anderson, M., 1994. *The superpave mix design manual for new construction and overlays, Report Number SHRP-A-407.* Washington, DC: Strategic Highway Research Program, 030905804X.

Cong, L., Guo, Z., Gao, Q. and Zhang, H. 2011. Permanent Deformation Characteristics and Prediction Model of Silty Subgrade Soils under Repeated Loading. *Journal of Highway and Transportation Research and Development (English Edition),* 5(2), 22-26.

Cook, D. J. and Uher, C. 1974. The thermal conductivity of fibre-reinforced concrete. *Cement and Concrete Research,* 4(4), 497-509.

Cook, K., Garg, N., Singh, A. and Flynn, M. 2016. Detection of Delamination in the HMA Layer of Runway Pavement Structure Using Asphalt Strain Gauges. *Journal of Transportation Engineering,* 142(11), 04016047.

Corlew, J. and Dickson, P., Methods for calculating temperature profiles of hot-mix asphalt concrete as related to the construction of asphalt pavements. ed. *Assoc Asphalt Paving Technol Proc*, 1968.

Côté, J. and Konrad, J.-M. 2005. Thermal conductivity of base-course materials. *Canadian Geotechnical Journal,* 42(1), 61-78.

Council, A. S. 2002. Aircraft Accident Report: Crashed on a Partially Closed Runway during Takeoff, Singapore Airlines Flight 006, Boeing 747-400, 9V-SPK, CKS Airport, Taoyuan, Taiwan, October 31, 2000. *Aviation Safety Council, Taipei, Taiwan*.

Cox, B. C., Smith, B. T., Howard, I. L. and James, R. S. 2017. State of Knowledge for Cantabro Testing of Dense Graded Asphalt. *Journal of Materials in Civil Engineering,* 29(10), 04017174.

Crispino, M., Festa, B., Giannattasio, P. and Nicolosi, V., Evaluation of the interaction between the asphalt concrete layers by a new dynamic test. ed. *Eighth International Conference on Asphalt PavementsFederal Highway Administration*, 1997.

Cross, S. A. and Shrestha, P. P., 2005. *Guidelines for Using Prime and Tack Coats.* Lakewood, CO: United States. Federal Highway Administration. Central Federal Lands Highway.

Cuciniello, G., Leandri, P., Filippi, S., Lo Presti, D., Losa, M. and Airey, G. 2018. Effect of ageing on the morphology and creep and recovery of polymer-modified bitumens. 51(5), 136.

D'Andrea, A., Russo, S. and Tozzo, C. 2013a. Interlayer Shear Testing under Combined State of Stress. *Advanced Materials Research,* 723, 381-388.

D'Andrea, A., Tozzo, C., Boschetto, A. and Bottini, L. 2013b. Interface Roughness Parameters and Shear Strength. *Modern Applied Science,* 7(10).

D'Angelo, J. 2009a. Current Status of Superpave Binder Specification. *Road Materials and Pavement Design,* 10(sup1), 13-24.

D'angelo, J., Kluttz, R. Q., Dongre, R. N., Stephens, K. E. and Zanzotto, L., Revision of the Superpave High Temperature Binder Specification: The Multiple Stress Creep Recovery Test (With Discussion). ed., 2007.

D'Angelo, J. A. 2009b. The Relationship of the MSCR Test to Rutting. *Road Materials and Pavement Design,* 10(sup1), 61-80.

D'Angelo, J. A., Harm, E. E., Bartoszek, J. C., Baumgardner, G. L., Corrigan, M. R., Cowsert, J. E., Harman, T. P., Jamshidi, M., Jones, H. W. and Newcomb, D. E., 2008. *Warm-mix asphalt: European practice.* Alexandria, VA: FHWA.

D'Andrea, A., Fustaino, C. and Tozzo, C. 2014. Recycling Dredged Sludge in Asphalt Pavement. *Journal of Materials in Civil Engineering,* 26(10), 05014005.

Dalhat, M. A. and Al-Abdul Wahhab, H. I. 2017. Performance of recycled plastic waste modified asphalt binder in Saudi Arabia. *International Journal of Pavement Engineering,* 18(4), 349-357.

Darabi, M. K., Kola, R., Little, D. N., Rahmani, E. and Garg, N. 2019. Predicting Rutting Performance of Flexible Airfield Pavements Using a Coupled Viscoelastic-Viscoplastic-Cap Constitutive Relationship. *Journal of Engineering Mechanics,* 145(2), 04018129.

Das, P. K., Tasdemir, Y. and Birgisson, B. 2012. Low temperature cracking performance of WMA with the use of the Superpave indirect tensile test. 30, 643-649.

Das, R., Mohammad, L. N., Elseifi, M., Cao, W. and Cooper, S. B. 2018. Development and Validation of a Model to Predict Interface Bonding Between Pavement Layers. *Transportation Research Record,* 2672(28), 22-30.

Dawson, A. R., Dehdezi, P. K., Hall, M. R., Wang, J. and Isola, R. 2012. Enhancing thermal properties of asphalt materials for heat storage and transfer applications. *Road Materials and Pavement Design,* 13(4), 784-803.

de Araújo, P. C., Soares, J. B., de Holanda, Á. S., Parente, E. and Evangelista, F. 2010. Dynamic Viscoelastic Analysis of Asphalt Pavements using a Finite Element Formulation. *Road Materials and Pavement Design,* 11(2), 409-433.

De Beer, M. and Maina, J., 2011. Toward Using tire road contact stresses in road pavement design and analysis. *Meeting of the Tire Society.* Pretoria, South Africa.

Dehdezi, P., Hall, M. and Dawson, A. 2011. Thermophysical Optimization of Specialized Concrete Pavement Materials for Collection of Surface Heat Energy and Applications for Shallow Heat Storage. *Transportation Research Record: Journal of the Transportation Research Board,* 2240, 96-106.

Delgadillo, R., Bahia, H. U. and Lakes, R. 2012. A nonlinear constitutive relationship for asphalt binders. *Materials and Structures volume,* 45(3), 457-473.

Delgadillo, R., Nam, K. and Bahia, H. 2006. Why do we Need to Change G*/Sinδ and How? *Road Materials and Pavement Design,* 7(1), 7-27.

Dempsey, B. J. and Thompson, M. R. 1970. A heat transfer model for evaluating frost action and temperature-related effects in multilayered pavement systems. *Highway Research Record,* (342).

Dhir, R. K., Brito, J. d., Mangabhai, R. and Lye, C. Q., 2017. 7 - Use of Copper Slag in Road Pavement Applications. *In:* Dhir, R. K.*, et al.* eds. *Sustainable Construction Materials: Copper Slag.* Woodhead Publishing, 247-277.

Diab, A., Sangiorgi, C., Ghabchi, R., Zaman, M. and Wahaballa, A. M., Warm Mix Asphalt (WMA) technologies: Benefits and drawbacks—a literature review. ed. *Functional Pavement Design: Proceedings of the 4th Chinese-European Workshop on Functional Pavement Design (4th CEW 2016)*, 29 June - 1 July 2016 2016 Delft, The Netherlands.

Diab, A., You, Z. and Wang, H. 2013. Rheological Evaluation of Foamed WMA Modified with Nano Hydrated Lime. *Procedia - Social and Behavioral Sciences,* 96, 2858-2866.

Diakhaté, M., Millien, A., Petit, C., Phelipot-Mardelé, A. and Pouteau, B. 2011. Experimental investigation of tack coat fatigue performance: Towards an improved lifetime assessment of pavement structure interfaces. *Construction and Building Materials,* 25(2), 1123-1133.

Diakhaté, M., Petit, C., Millien, A., Phelipot-Mardelé, A., Pouteau, B. and Goacolou, H., Interface fatigue cracking in multilayered pavements: Experimental analysis. ed. *6th RILEM International Conference on Cracking in Pavements; Chicago, IL; 16 June 2008 through 18 June 2008; Code 83648*, 2008-06-18 2008 CHICAGO, United States, 649-659.

Diakhate, M., Phelipot, A., Millien, A. and Petit, C. 2006. Shear Fatigue Behaviour of Tack Coats in Pavements. *Road Materials and Pavement Design,* 7(2), 201-222.

Diefenderfer, B. K., Al-Qadi, I. L. and Diefenderfer, S. D. 2006. Model to predict pavement temperature profile: development and validation. *Journal of Transportation Engineering,* 132(2), 162-167.

Do, T. C., Tran, V. P., Le, V. P., Lee, H. J. and Kim, W. J. 2019. Mechanical characteristics of tensile strength ratio method compared to other parameters used for moisture susceptibility evaluation of asphalt mixtures. *Journal of Traffic and Transportation Engineering (English Edition).*

Donovan, E. P., Al-Qadi, I. L. and Loulizi, A. 2000. Optimization of Tack Coat Application Rate for Geocomposite Membrane on Bridge Decks. *Transportation Research Record,* 1740(1), 143-150.

Dormon, G. and Metcalf, C. 1965. Design curves for flexible pavements based on layered system theory. *Highway Research Record,* 71, 69-84.

Dougan, C. E., Stephens, J., Mahoney, J. and Hansen, G., 2003. *E*-dynamic modulus: test protocol-problems and solutions, Report Number CT-SPR-0003084-F-03-3.* Connecticut Department of Transportation.

Doyle, J. D. and Howard, I. L., 2011. Evaluation of the Cantabro Durability Test for Dense Graded Asphalt. *Geo-Frontiers 2011.* 4563-4572.

Doyle, J. D. and Howard, I. L. 2016. Characterization of Dense-Graded Asphalt With the Cantabro Test. *Journal of testing and evaluation,* 44(1), 77-88.

Doyle, J. D., MejÌas-Santiago, M., Brown, E. R. and Howard, I. L. 2011. Performance of High RAP-WMA Surface Mixtures. *Journal of the Association of Asphalt Paving Technologists,* 80, 403–437.

Dublin Airport, Nov 22, 2017. *Resurfacing Dublin Airport's Runway* [online]. Available from: https://www.youtube.com/watch?v=AvnJZf586jk.

Dublin-Airport, 14 November 2016. *Runway Upgrade To Create 150 Construction Jobs* [online]. Available from: https://www.dublinairport.com/latest-news/detail/runway-upgrade-to-create-150-construction-jobs.

DuBois, E., Mehta, D. Y. and Nolan, A. 2014. Correlation between multiple stress creep recovery (MSCR) results and polymer modification of binder. *Construction and Building Materials,* 65, 184-190.

EAPA, 2004. *Environmental Impacts and Fuel Efficiency of Road Pavements.* European Asphalt Pavement Association.

EAPA, 2014. *The use of Warm Mix Asphalt, EAPA – Position Paper.* Brussels, Belgium: European Asphalt Pavement Association.

EAPA, 2017. *Asphalt in Figures 2017.* European Asphalt Pavement Association (EAPA).

Eedula, S. R. and Tandon, V., 2006. *Tack coat field acceptance criterion, Research Report TX-0-5216-1.* Austin, Texas: Texas Department of Transportation.

Eisenmann, J. and Hilmer, A., 1987. Influence of Wheel Load and Inflation Pressure on the Rutting Effect at Asphalt-Pavements-Experiments and Theoretical Investigations. *Sixth International Conference, Structural Design of Asphalt Pavements, Volume I, Proceedings, University Of Michigan.* Ann Arbor, Michigan.

Elnasri, M., Airey, G. and Thom, N. 2019. Developing the multiple stress–strain creep recovery (MS-SCR) test. *Mechanics of Time-Dependent Materials,* 23(1), 97-117.

Elseifi, M. A., Al-Qadi, I. L. and Yoo, P. J. 2006. Viscoelastic modeling and field validation of flexible pavements. *Journal of Engineering Mechanics,* 132(2), 172-178.

Emery, S. and Mihaljevic, I., Accelerated load testing of asphalt mix designs for heavy duty pavements in hot climates. ed. *ARRB Conference, 23rd, 2008, Adelaide, South Australia, Australia*, 2008.

Express, 22 Agt 2013. *Heathrow's runway was so HOT during heatwave, airport bosses had to delay resurfacing work* [online]. Available from: https://www.express.co.uk/news/uk/423967/Heathrow-s-runway-was-so-HOT-during-heatwave-airport-bosses-had-to-delay-resurfacing-work [Accessed 29th Desember 2017].

FAA, 2006. Off-peak Construction of Airport Pavements Using Hot-Mix Asphalt, AC 150/5370-13A. Washington, DC.

FAA, 2014a. *Airport Design, AC 150/5300-13A.* Washington D.C.

FAA, 2014b. *Guidelines and Procedures for Maintenenace of Airport, AC 150/5380-6C.* Washington D.C.

FAA, 2018. *Standards for specifying construction of airports, AC 150-5370-10H.* Washington D.C.

Fguiri, A., Daouas, N., Radhouani, M.-S. and Aissia, H. B. 2013. Inverse analysis for the determination of heat transfer coefficient. *Canadian Journal of Physics,* 91(12), 1034-1043.

FHWA, 2011. The Multiple Stress Creep Recovery (MSCR) Procedure. *FHWA-HIF-11-038.* Washington, DC: Office of the Pavement Technology, Federal Highway Administration.

Forough, S. A., Moghadas Nejad, F. and Khodaii, A. 2017. Predicting the tensile relaxation modulus of asphalt mixes based on the mix design and environmental factors. *International Journal of Pavement Engineering,* 18(7), 633-644.

Frank, J. E., Fuselier, G. K., Decker, C. S. and Thuma, R. G., 2013. Resurfacing the Runway to the Nation's Capital. *Airfield and Highway Pavement 2013: Sustainable and Efficient Pavements.* 742-752.

Fulton Hogan, 2011. *AIRPORTS: Our skill and experience guarantee a smooth landing.* [online]. Available from: http://www.fultonhogan.com/wp-content/uploads/2015/08/Airports-Capability-Brochure-Australia.pdf.

Fwa, T. F., 2005. *The handbook of highway engineering.* CRC Press.

Fwa, T. F., Tan, S. A. and Zhu, L. Y. 2004. Rutting Prediction of Asphalt Pavement Layer Using C-φ Model. *Journal of Transportation Engineering,* 130(5), 675-683.

Garg, N., Kazmee, H. and Ricalde, L., 2018a. Application potential of warm mix asphalt for airport pavements. *In:* Eyad Masad*, et al.* eds. *Advances in Materials and Pavement Prediction.* Doha, Qatar.

Garg, N., Kazmee, H. and Ricalde, L., Evaluation of Warm Mix Asphalt (WMA) Technologies for Use in Airport Pavements. In: Chabot, A.*, et al.*, ed., 2020 Cham: Accelerated Pavement Testing to Transport Infrastructure Innovation, 218-227.

Garg, N., Kazmee, H., Ricalde, L. and Parsons, T. 2018b. Rutting Evaluation of Hot and Warm Mix Asphalt Concrete under High Aircraft Tire Pressure and Temperature at National Airport Pavement and Materials Research Center. *Transportation Research Record,* 2672(23), 117-127.

Gayathri, V. G., Rajasekar, Y. P., Lakshmi Roja, K. and Murali Krishnan, J. 2016. Influence of Confinement Pressure on the Development of Three Stage Curve for Bituminous Mixtures. *Transportation in Developing Economies,* 2(2), 10.

Gibb, J. M., 1996. *Evaluation of Resistance to Permanent Deformation in The Design of Bituminous Paving Mixtures.* (PhD). The University of Nottingham.

Goh, S. W. and You, Z., 2011. Moisture Damage and Fatigue Cracking of Foamed Warm Mix Asphalt Using a Simple Laboratory Setup. *Transportation and Development Institute (T&DI) first Congress* 762-771.

Guercio, M. C. and McCarthy, L. M. 2015. Quantifying the Performance of Warm-Mix Asphalt and Reclaimed Asphalt Pavement in Flexible Airfield Pavements. *Transportation Research Record,* 2471(1), 33-39.

Gui, J., Phelan, P. E., Kaloush, K. E. and Golden, J. S. 2007. Impact of Pavement Thermophysical Properties on Surface Temperatures. *Journal of Materials in Civil Engineering,* 19(8), 683-690.

Hacan, 2013. *Heathrow: Runway resurfacing alters night-time flight patterns* [online]. Available from: http://www.hacan.org.uk/resources/briefings/final.ad.PDF.

Hachiya, Y., Su, K., Motono, I., Muranaga, T., Kajitani, A. and Kano, T., Implementing overnight asphalt inlay work on working runway. ed. *Proceedings of The 4th Eurasphalt and Eurobitume Congress* 2008 Copenhagen, Denmark.

Hachiya, Y., Umeno, S. and Sato, K. 1997. Effect of tack coat on bonding characteristics at interface between asphalt concrete layers. *Doboku Gakkai Ronbunshu,* 1997(571), 199-209.

Hakim, B., Widyatmoko, I., Fergusson, C. and Richardson, J. 2014. UK airfield pavement design using French asphalts. *Proceedings of the Institution of Civil Engineers - Transport,* 167(1), 27-35.

Hakimzadeh, S., Kebede, N. A., Buttlar, W. G., Ahmed, S. and Exline, M. 2012. Development of fracture-energy based interface bond test for asphalt concrete. *Road Materials and Pavement Design,* 13(sup1), 76-87.

Hall, M. and Allinson, D. 2009. Assessing the effects of soil grading on the moisture content-dependent thermal conductivity of stabilised rammed earth materials. *Applied Thermal Engineering,* 29(4), 740-747.

Hall, M. R., Dehdezi, P. K., Dawson, A. R., Grenfell, J. and Isola, R. 2012. Influence of the Thermophysical Properties of Pavement Materials on the Evolution of Temperature Depth Profiles in Different Climatic Regions. *Journal of Materials in Civil Engineering,* 24(1), 32-47.

Hamzah, M. O., Jamshidi, A. and Shahadan, Z. 2010. Evaluation of the potential of Sasobit® to reduce required heat energy and CO2 emission in the asphalt industry. *Journal of Cleaner Production,* 18(18), 1859-1865.

Han, R., Jin, X. and Glover, C. J. 2011. Modeling Pavement Temperature for Use in Binder Oxidation Models and Pavement Performance Prediction. *Journal of Materials in Civil Engineering,* 23(4), 351-359.

Hancher, D. E. and Taylor, T. 2001. Nighttime Construction Issues. *Transportation Research Record,* 1761(1), 107-115.

Harmuth, H. 1995. Stability of crack propagation associated with fracture energy determined by wedge splitting specimen. *Theoretical and Applied Fracture Mechanics,* 23(1), 103-108.

Harnsberger, P. M., Farrar, M. J., Huang, S.-C. and Robertson, R. E. 2011. Comparative Field Performance of Asphalts from Multiple Crude Oil Sources. *Transportation Research Record,* 2207(1), 62-69.

Hasheminejad, N., Vuye, C., Margaritis, A., Van den Bergh, W., Dirckx, J. and Vanlanduit, S. 2019. Characterizing the Complex Modulus of Asphalt Concrete Using a Scanning Laser Doppler Vibrometer. *Materials (Basel, Switzerland),* 12(21), 3542.

Hasiba, K., 2012. *Development of a testing approach for tack coat application rate at pavement layer interfaces.* (Master of Science). University of Illinois at Urbana-Champaign.

Hassn, A., Chiarelli, A., Dawson, A. and Garcia, A. 2016. Thermal properties of asphalt pavements under dry and wet conditions. *Materials & Design,* 91, 432-439.

Hayhoe, G. F., Dong, M. and McQueen, R. D., Airport pavement roughness with nighttime construction. ed. *Proceedings of the Third ICPT Conference*, 1998, 567-572.

He, L., Chu, L. and Fwa, T. F. 2020. Temperature-Based Criteria for Opening Newly Laid Repaired Asphalt Pavement Sections to Traffic. *Transportation Research Record,* 0(0), 0361198120908864.

Hermansson, Å. 2004. Mathematical model for paved surface summer and winter temperature: comparison of calculated and measured temperatures. *Cold Regions Science and Technology,* 40(1), 1-17.

Hesami, S., Roshani, H., Hamedi, G. H. and Azarhoosh, A. 2013. Evaluate the mechanism of the effect of hydrated lime on moisture damage of warm mix asphalt. *Construction and Building Materials,* 47, 935-941.

Hettiarachchi, C., Hou, X., Wang, J. and Xiao, F. 2019. A comprehensive review on the utilization of reclaimed asphalt material with warm mix asphalt technology. *Construction and Building Materials,* 227, 117096.

Heukelom, W. and Klomp, A., Consideration of calculated strains at various depths in connection with the stability of asphalt pavements. ed. *Second International Conference on the Structural Design of Asphalt PavementsUniversity of Michigan, Ann Arbor*, 1967.

Highter, W., 1983. Thermal properties of some asphaltic concrete mixes. *International Air Transportation Conference.* American Institute of Aeronautics and Astronautics.

Hinze, J. and Carlisle, D. L. 1990. Variables affected by nighttime construction projects. *Transportation Research Record,* 1282, 95-103.

Hobart-Airport, Feb 20, 2012. *Hobart International Airport - Runway Overlay Project* [online]. Available from: https://www.youtube.com/watch?v=jFoTDmMlEBY.

Hofko, B. and Blab, R. 2014. Enhancing triaxial cyclic compression testing of hot mix asphalt by introducing cyclic confining pressure. *Road Materials and Pavement Design,* 15(1), 16-34.

Hofstra, A. and Klopm, A., Permanent deformation of flexible pavements under simulated road traffic conditions. ed. *Presented at the Third International Conference on the Structural Design of Asphalt Pavements, Grosvenor House, Park Lane, London, England, Sept. 11-15, 1972.*, 1972.

Holguín-Veras, J., Ozbay, K., Baker, R., Sackey, D., Medina, A. and Hussain, S. 2003. Toward a Comprehensive Policy of Nighttime Construction Work. *Transportation Research Record,* 1861(1), 117-124.

Horak, E., Maina, J. W. and Emery, S., A case study: quantification and modeling of asphalt overlay delamination on an airport pavement. ed. *Bearing Capacity of Roads, Railways and Airfields. 8th International Conference (BCRRA 2009)*, 2009 Champaign, Illinois, USA.

Horonjeff, R. and McKelvey, F. X., 2010. *Planning and design of airports.* McGraw-Hill New York.

Hu, S., Zhou, F. and Scullion, T. 2011. Development, Calibration, and Validation of a New M-E Rutting Model for HMA Overlay Design and Analysis. *Journal of Materials in Civil Engineering,* 23(2), 89-99.

Hu, X. and Walubita, L. F. 2011. Effects of Layer Interfacial Bonding Conditions on the Mechanistic Responses in Asphalt Pavements. *Journal of Transportation Engineering,* 137(1), 28-36.

Huang, W., Lv, Q. and Tian, J., 2015. Effects of Tack Coat Type and Surface Characteristics on Interface Bond Strength. *New Frontiers in Road and Airport Engineering.* 25-36.

Huang, Y., Wang, X., Liu, Z. and Li, S. 2017. Dynamic modulus test and master curve analysis of asphalt mix with trapezoid beam method. *Road Materials and Pavement Design,* 18(sup3), 281-291.

Huang, Y. H., Stresses and displacements in viscoelastic layered systems under circular loaded areas. ed. *Intl Conf Struct Design Asphalt Pvmts*, 1967.

Hulbert, G. J., Litchfield, J. B. and Schmidt, S. J. 1997. Determination of convective heat transfer coefficients using 2D MRI temperature mapping and finite element modeling. *Journal of Food Engineering,* 34(2), 193-201.

Huschek, S., Evaluation of rutting due to viscous flow in asphalt pavements. ed. *Volume I of proceedings of 4th International Conference on Structural Design of Asphalt Pavements, Ann Arbor, Michigan, August 22-26, 1977.*, 1977.

Hussan, S., Kamal, M. A., Hafeez, I., Farooq, D., Ahmad, N. and Khanzada, S. 2019. Statistical evaluation of factors affecting the laboratory rutting susceptibility of asphalt mixtures. *International Journal of Pavement Engineering,* 20(4), 402-416.

IATA International Air Transport Association, 2017. *World air transport statistics, WATS 2017.* Geneva: IATA, International Air Transport Association.

ICAO, I. C. A. O., 2017. *The World of Air Transport in 2016* [online]. Available from: https://www.icao.int/annual-report-2016/Pages/the-world-of-air-transport-in-2016.aspx.

Irfan, M., Khurshid, M. B., Iqbal, S. and Khan, A. 2015. Framework for airfield pavements management—an approach based on cost-effectiveness analysis. *European Transport Research Review,* 7(2), 13.

Isailović, I., Falchetto, A. C. and Wistuba, M. 2017. Fatigue investigation on asphalt mixture layers' interface. *Road Materials and Pavement Design,* 18(sup4), 514-534.

Isailović, I. and Wistuba, M. P. 2018. Asphalt mixture layers' interface bonding properties under monotonic and cyclic loading. *Construction and Building Materials,* 168, 590-597.

Jalali, V., 2016. *Performance of warm mix asphalt compacted at reduced temperature.* (PhD). University of Nottingham.

Jalali, V., Grenfell, J. R. and Dawson, A., 2014. Temperature Effect on Warm Mix Asphalt Performance. *In:* Kim, Y. R. ed. *Asphalt Pavements.* London: CRC Press, 1966.

Jamaaoui, A., Pop, O., Ktari, R., Millien, A. and Petit, C. 2017. Analyzing of Wedge Splitting Test on Asphalt Pavement Using Optical Measurements. *Journal of testing and evaluation,* 45(6), 1959-1970.

Jamshidi, A., Hamzah, M. O. and You, Z. 2013. Performance of Warm Mix Asphalt containing Sasobit®: State-of-the-art. *Construction and Building Materials,* 38, 530-553.

Jamshidi, A. and White, G., The Challenges of Warm Mix Asphalt as a Mature Technology. In: Raab, C., ed., 2020 Cham: Proceedings of the 9th International Conference on Maintenance and Rehabilitation of Pavements—Mairepav9, 93-102.

Ji, X., Zheng, N., Niu, S., Meng, S. and Xu, Q. 2016. Development of a rutting prediction model for asphalt pavements with the use of an accelerated loading facility. *Road Materials and Pavement Design,* 17(1), 15-31.

Jia, L., Sun, L. and Huang, L., Numerical temperature prediction model and thermal properties for asphalt pavement. ed. *Advanced Characterisation of Pavement and Soil Engineering Materials* 2007 Athens, Greece.

Jones, J. P., Stamper, W. G. and Godiwalla, A., 2012. Rehabilitation of Runway 09-27 at George Bush Intercontinental Airport. *Airfield Safety and Capacity Improvements.* 37-48.

Jordan, P. and Thomas, M., 1976. *Prediction of cooling curves for hot-mix paving materials by a computer program.* Crowthorne, Berkshire: Transport and Road Research Laboratory (TRRL), 0266-7045.

Julaganti, A., Choudhary, R. and Kumar, A. 2019. Permanent Deformation Characteristics of Warm Asphalt Binders under Reduced Aging Conditions. *KSCE Journal of Civil Engineering,* 23(1), 160-172.

Kaloush, K. E., 2001. *Simple performance test for permanent deformation of asphalt mixtures.* (PhD). Arizona State University.

Kandhal, P. S. 2010. Warm mix asphalt technologies: An overview. *Journal of the Indian Roads Congress,* 71(2).

Kandhal, P. S. and Cooley, L. A., 2003. *NCHRP 508: Accelerated laboratory rutting tests: Evaluation of the asphalt pavement analyzer.* Transportation Research Board.

Kanitpong, K., Nam, K., Martono, W. and Bahia, H. 2008. Evaluation of a warm-mix asphalt additive. *Proceedings of the Institution of Civil Engineers - Construction Materials,* 161(1), 1-8.

Kar, S. S. and Nagabhushana, M., 2019. *History Of Paving Bitumen Grading System.*

Kassem, E., Garcia Cucalon, L., Masad, E. and Little, D. 2018. Effect of warm mix additives on the interfacial bonding characteristics of asphalt binders. *International Journal of Pavement Engineering,* 19(12), 1111-1124.

Kassem, H., Chehab, G. and Saad, G. 2014. An FEM-predictive tool for simulating the cooling characteristics of freshly paved asphalt concrete layers. *International Journal of Pavement Engineering,* 16(2), 157-167.

Kavianipour, A. and Beck, J. V. 1977. Thermal property estimation utilizing the Laplace transform with application to asphaltic pavement. *International Journal of Heat and Mass Transfer,* 20(3), 259-267.

Kazmee, H., Garg, N., Knieriem, R., Gerke, J. and Villafane, W., 2019. Aircraft Tire Pressure and Pavement Temperature Effects on HMA and WMA Strains. *Airfield and Highway Pavements 2019.* 322-332.

Kennedy, T. W., Huber, G. A., Harrigan, E. T., Cominsky, R. J., Hughes, C. S., Von Quintus, H. and Moulthrop, J. S., 1994. *Superior performing asphalt pavements (Superpave): The product of the SHRP asphalt research program, SHRP-A-410.* Washington, DC:

Strategic Highway Research Program, National Academy of Sciences.

Khan, A. and Mrawira, D. 2008. Influence of Selected Mix Design Factors on the Thermal Behavior of Lightweight Aggregate Asphalt Mixes. *Journal of testing and evaluation,* 36(6), 492-499.

Khanzada, S., 2000. *Permanent deformation in bituminous mixtures.* University of Nottingham.

Kheradmand, B., Muniandy, R., Hua, L. T., Yunus, R. B. and Solouki, A. 2013. An overview of the emerging warm mix asphalt technology. *International Journal of Pavement Engineering,* 15(1), 79-94.

Kheradmand, B., Muniandy, R., Hua, L. T., Yunus, R. B. and Solouki, A. 2014. An overview of the emerging warm mix asphalt technology. *International Journal of Pavement Engineering,* 15(1), 79-94.

Khweir, K. and Fordyce, D. 2003. Influence of layer bonding on the prediction of pavement life. *Proceedings of the Institution of Civil Engineers - Transport,* 156(2), 73-83.

Kim, J., Sholar, G. A. and Kim, S. 2008. Determination of accurate creep compliance and relaxation modulus at a single temperature for viscoelastic solids. *Journal of Materials in Civil Engineering,* 20(2), 147-156.

King, G., King, H., Pavlovich, R., Epps, A. L. and Kandhal, P. 1999. Additives in asphalt. *Journal of the Association of Asphalt Paving Technologists,* 68, 32-69.

Kreith, F. and Manglik, R. M., 2011. *Principles of heat transfer.* 7th ed. Boston: Cengage learning.

Kristjansdottir, O., 2006. *Warm mix asphalt for cold weather paving.* (Master of Science in Civil Engineering). University of Washington.

Kruntcheva, M. R., Collop, A. C. and Thom, N. H. 2005. Effect of bond condition on flexible pavement performance. *Journal of Transportation Engineering,* 131(11), 880-888.

Leahy, R. B., 1989. *Permanent deformation characteristics of asphalt concrete.* (PhD). University of Maryland College Park.

Lee, J., Yu, C.-H. and Park, S.-J., Effect of Water Temperature on Spray Cooling Heat Transfer on Hot Steel Plate. ed. *2010 14th International Heat Transfer Conference*, 2010, 723-729.

Lee, S.-J., Amirkhanian, S. N., Putman, B. J. and Kim, K. W. 2007. Laboratory Study of the Effects of Compaction on the Volumetric and Rutting Properties of CRM Asphalt Mixtures. *Journal of Materials in Civil Engineering,* 19(12), 1079-1089.

Leischner, S., Canon Falla, G., Gerowski, B., Rochlani, M. and Wellner, F. 2019. Mechanical Testing and Modeling of Interlayer Bonding in HMA Pavements. *Transportation Research Record,* 2673(11), 879-890.

Lekarp, F. and Dawson, A. 1998. Modelling permanent deformation behaviour of unbound granular materials. *Construction and Building Materials,* 12(1), 9-18.

Li, D. C., Fung, W. H., Widyatmoko, I., Elliott, R. C. and Larsen, B. K., 2008. Planning, Design and Implementation of Major Runway Resurfacing at Hong Kong International Airport. *Sixth International Conference on Road & Airfield Pavement Technology (6th ICPT).* Sapporo, Japan.

Li, H., Harvey, J., He, Y., Chen, Z. and Li, P. 2015. Pavement Treatment Practices and Dynamic Albedo Change in Urban Pavement Network in California. *Transportation Research Record,* 2523(1), 145-155.

Li, X., Williams, R. C., Marasteanu, M. O., Clyne, T. R. and Johnson, E. 2009. Investigation of In-Place Asphalt Film Thickness and Performance of Hot-Mix Asphalt Mixtures. *Journal of Materials in Civil Engineering,* 21(6), 262-270.

Liao, Y., 2007. *Viscoelastic FE modeling of asphalt pavements and its application to US 3.0 perpetual pavement.* (PhD). Ohio University.

Little, D. N., Button, J. W. and Youssef, H. 1993. Development of criteria to evaluate uniaxial creep data and asphalt concrete permanent deformation potential. *Transportation Research Record,* (1417).

Litzka, J. H., Pass, F. and Zirkler, E. 1994. Experiences with thin bituminous layers in Austria. *Transportation Research Record,* (1454).

Liu, J., Saboundjian, S., Li, P., Connor, B. and Brunette, B. 2011. Laboratory Evaluation of Sasobit-Modified Warm-Mix Asphalt for Alaskan Conditions. *Journal of Materials in Civil Engineering,* 23(11), 1498-1505.

Loulizi, A., Flintsch, G., Al-Qadi, I. and Mokarem, D. 2006. Comparing resilient modulus and dynamic modulus of hot-mix asphalt as material properties for flexible pavement design. *Transportation Research Record: Journal of the Transportation Research Board,* (1970), 161-170.

Luca, J. and Mrawira, D. 2005. New Measurement of Thermal Properties of Superpave Asphalt Concrete. *Journal of Materials in Civil Engineering,* 17(1), 72-79.

Lytton, R., Pufahl, D., Michalak, C., Liang, H. and Dempsey, B., 1993. *An integrated model of the climatic effects on pavements.* Washington, DC.: Transportation Research Board.

Lytton, R. L., Tsai, F.-L., Lee, S. I., Luo, R., Hu, S. and Zhou, F., 2010. *Models for predicting reflection cracking of hot-mix asphalt overlays.*

Mahmoud, A., Coleri, E., Batti, J. and Covey, D. 2017. Development of a field torque test to evaluate in-situ tack coat performance. 135, 377-385.

Mahmoud, A. F. F. and Bahia, H., 2004. *Using gyratory compactor to measure mechanical stability of asphalt mixtures.* Wisconsin Highway Research Program.

Malinowski, Z., Cebo-Rudnicka, A., Telejko, T., Hadała, B. and Szajding, A. 2015. Inverse method implementation to heat transfer coefficient determination over the plate cooled by water spray. *Inverse Problems in Science and Engineering,* 23(3), 518-556.

Mallick, R. B. and Bergendahl, J. 2009. A laboratory study on CO2 emission from asphalt binder and its reduction with the use of warm mix asphalt. *International Journal of Sustainable Engineering,* 2(4), 275-283.

Mallick, R. B., Kandhal, P. S. and Bradbury, R. L. 2008. Using Warm-Mix Asphalt Technology to Incorporate High Percentage of Reclaimed Asphalt Pavement Material in Asphalt Mixtures. *Transportation Research Record,* 2051(1), 71-79.

Mansourkhaki, A. and Sarkar, A. 2015. Plastic deformation of asphalt mixture under waveform loading. *Proceedings of the Institution of Civil Engineers - Transport,* 168(3), 200-211.

Martin, T. J. and Dulikravich, G. S. 1998. Inverse Determination of Steady Heat Convection Coefficient Distributions. *Journal of Heat Transfer,* 120(2), 328-334.

Masson, J. F., Pelletier, L. and Collins, P. 2001. Rapid FTIR method for quantification of styrene-butadiene type copolymers in bitumen. *Journal of Applied Polymer Science,* 79(6), 1034-1041.

Mazurek, G. and Nowakowski, K. 2015. The Evaluation of SMA Mixture Properties with the Surface-active Agent in WMA Technology. *Procedia Engineering,* 108, 22-29.

McArdle, J., July 2010. Overlay Project Award. *Plane Talking: Adelaide and Parafield Community and Staff Newsletter*, p. 3.

McCarthy, L., Park, S. and Mensching, D., 2012. *A Proposed Technology Evaluation Program for Warm-Mix Asphalt, NCHRP Project 20-07, Task 311.* Washington, DC: Transportation Research Board, The National Academies Press.

McLean, D. B. and Monismith, C. L. 1974. Estimation of Permanent Deformation in Asphalt Concrete Layers Due to Repeated Traffic Loading *Transportation Research Record*.

McNally, T., 2011. Introduction to polymer modified bitumen (PmB). *Polymer Modified Bitumen.* Woodhead Publishing, 1-21.

Medeiros, M. S., Chehab, G. R. and Solaimanian, M. 2012a. Investigation of Ultra-Rapid-Setting Emulsion for Tack Coat Applications. *Transportation Research Record,* 2293(1), 80-88.

Medeiros, M. S., Daniel, J. S., Bolton, H. L. and Meagher, W. C. 2012b. Evaluation of moisture and low-temperature cracking susceptibility of warm-mixture asphalt. *International Journal of Pavement Engineering,* 13(5), 395-400.

Mejías-Santiago, M., Doyle, J. D. and Rushing, J. F., 2014. Warm-Mix Asphalt for Airfield Pavements. *2014 FAA Worlwide Airport Technology Transfer Conference* Atlantic City, NJ.

Mejías-Santiago, M., Doyle, J. D. and Rushing, J. F. 2015. Performance of Grooved Warm-Mix Asphalt Pavement Surfaces Under Heavy Aircraft Load and High Tire Pressure. *Transportation Research Record: Journal of the Transportation Research Board,* 2501, 40-45.

Mejías-Santiago, M. and Rushing, J. F., 2018. *Laboratory Performance Testing of Warm-Mix Asphalt Mixtures for Airport Pavements, DOT/FAA/TC-18/26.* New Jersey: Federal Aviation Administration.

Merusi, F. and Giuliani, F. 2011. Rheological characterization of wax-modified asphalt binders at high service temperatures. *Materials and Structures,* 44(10), 1809-1820.

Mieczkowski, P. and Budziński, B. 2019. The Influence of Water on the Heat Loss of Hot Mix Asphalt. *Applied Sciences,* 9(9).

Miljković, M. and Radenberg, M. 2011. Rutting Mechanisms and Advanced Laboratory Testing of Asphalt Mixtures Resistance against Permanent Deformation. *Facta Unievrsitatis,* 9, 407.

Miller, S. R., Hartmann, T. and Dorée, A. G. 2011. Measuring and visualizing hot mix asphalt concrete paving operations. *Automation in Construction,* 20(4), 474-481.

Mo, L., Li, X., Fang, X., Huurman, M. and Wu, S. 2012. Laboratory investigation of compaction characteristics and performance of warm mix asphalt containing chemical additives. *Non Destructive Techniques for Assessment of Concrete,* 37, 239-247.

Mogawer, W. S., Austerman, A. J., Bonaquist, R. and Roussel, M. 2011a. Performance Characteristics of Thin-Lift Overlay Mixtures: High Reclaimed Asphalt Pavement Content, Recycled Asphalt Shingles, and Warm-Mix Asphalt Technology. *Transportation Research Record,* 2208(1), 17-25.

Mogawer, W. S., Austerman, A. J., Daniel, J. S., Zhou, F. and Bennert, T. 2011b. Evaluation of the effects of hot mix asphalt density on mixture fatigue performance, rutting performance and MEPDG distress predictions. *International Journal of Pavement Engineering,* 12(2), 161-175.

Mohammad, L., Bae, A., Elseifi, M., Button, J. and Patel, N. 2010. Effects of Pavement Surface Type and Sample Preparation Method on Tack Coat Interface Shear Strength. *Transportation Research Record: Journal of the Transportation Research Board,* 2180, 93-101.

Mohammad, L., Raqib, M. and Huang, B. 2002. Influence of asphalt tack coat materials on interface shear strength. *Transportation Research Record: Journal of the Transportation Research Board,* (1789), 56-65.

Mohammad, L. N., Performance Tests for Hot Mix Asphalt (HMA) Including Fundamental and Empirical Procedures. ed. *ASTM symposium STP1469*, 2006 Tampa, Florida.

Mohammad, L. N., Bae, A., Elseifi, M. A., Button, J. W. and Scherocman, J. A. 2009. Interface shear strength characteristics of emulsified tack coats. *Journal of the Association of Asphalt Paving Technologists,* 78.

Mohammad, L. N., Elseifi, M. A., Bae, A. and Patel, N., 2012. *NCHRP Report 712: Optimization of tack coat for HMA placement.* Washington, DC: Transportation Research Board, 0309213975.

Mohammad, L. N., Hassan, M. M., Vallabhu, B. and Kabir, M. S. 2015. Louisiana's Experience with WMA Technologies: Mechanistic, Environmental, and Economic Analysis. *Journal of Materials in Civil Engineering,* 27(6), 04014185.

Monismith, C. 1973. Permanent deformation studies of pavements. *FCP Research Progress Review Report, San Francisco, CA*.

Monismith, C. 1976. Rutting prediction in asphalt concrete pavements. *Transportation Research Record,* (616).

Monismith, C. L., Alexander, R. L. and Secor, K. E. 1966. Rheological Behaviour of Asphalt Concrete. *Journal of Association of Asphalt Paving Technologists,* 35, 400-450.

Monismith, C. L. and Secor, K. E., Viscoelastic behavior of asphalt concrete pavements. ed. *International Conference on the Structural Design of Asphalt PavementsUniversity of Michigan, Ann Arbor*, 1962.

Monismith, C. L., Vallerga, B. A., Harvey, J. T., Long, F. and Jew, A., 2000. Asphalt-Mix Studies: San Francisco International Airport. *The 2020 Vision of Air Transportation.* 113-124.

Morales, R. D., oacute, pez, A. G. and Olivares, I. M. 1990. Heat Transfer Analysis during Water Spray Cooling of Steel Rods. *ISIJ International,* 30(1), 48-57.

Morea, F., Marcozzi, R. and Castaño, G. 2012. Rheological properties of asphalt binders with chemical tensoactive additives used in Warm Mix Asphalts (WMAs). *Construction and Building Materials,* 29, 135-141.

Moreno-Navarro, F., Rubio-Gámez, M. C., Miró, R. and Pérez-Jiménez, F. 2015. The influence of temperature on the fatigue behaviour of bituminous materials for pavement rehabilitation. *Road Materials and Pavement Design,* 16(sup1), 300-313.

Moreno-Navarro, F., Sol-Sánchez, M., Jiménez del Barco, A. and Rubio-Gámez, M. C. 2017. Analysis of the influence of binder properties on the mechanical response of bituminous mixtures. *International Journal of Pavement Engineering,* 18(1), 73-82.

Morris, J. and Haas, R. 1972. Designing for rutting in asphalt pavements. *Canadian Technical Asphalt Association, Proceeding,* 17.

Moses, T. L., Hulsey, J. L. and Connor, B., 2009. *Airport manager's guide for the maintenance of asphalt pavements of general aviation airports.* California. Dept. of Transportation.

Motamed, A., Bhasin, A. and Liechti, K. M. 2012. Interaction nonlinearity in asphalt binders. *Mechanics of Time-Dependent Materials,* 16(2), 145-167.

Mrawira, D. and Damude, D. J., Revisiting the effectiveness of tack coats in HMA overlays: the shear strength of tack coats in young overlays. ed. *Proceedings of The Annual Conference-Canadian Technical Asphalt Association*, 1999, 115-130.

Mrawira, D. and Luca, J. 2002. Thermal properties and transient temperature response of full-depth asphalt pavements. *Transportation Research Record: Journal of the Transportation Research Board,* (1809), 160-171.

Mrawira, D. and Luca, J. 2006. Effect of aggregate type, gradation, and compaction level on thermal properties of hot-mix asphalts. *Canadian Journal of Civil Engineering,* 33(11), 1410-1417.

Muench, S. T. and Moomaw, T., 2008. *De-bonding of hot mix asphalt pavements in Washington State: an initial investigation.* Transportation Northwest (Organization).

Muslich, S., 2010. *Assessment of bond between asphalt layers.* (PhD). University of Nottingham.

Nepal, S. 2014. TIA Runway Overlay Project Failure: A Case Study from Nepal. *PM World Journal,* 3(5).

Nguyen, H. M., Pouget, S., Di Benedetto, H. and Sauzéat, C. 2009. Time-temperature superposition principle for bituminous mixtures. *European Journal of Environmental and Civil Engineering,* 13(9), 1095-1107.

Nicholls, J., 1999. *Rheological properties of polymer-modified binders for use in rolled asphalt wearing course.* Thomas Telford.

Nozaki, T., Matsuno, J.-i., Murata, K., Ooi, H. and Kodama, M. 1978. A Secondary Cooling Pattern for Preventing Surface Cracks of Continuous Casting Slab. *Transactions of the Iron and Steel Institute of Japan,* 18(6), 330-338.

Nunn, M., 1986. Prediction of permanent deformation in bituminous pavement layers. *3rd Eurobitume Conference.* The Hague.

O'Massey, R. 1978. Aircraft pavement loading: Static and dynamic. *Transportation Research Board Special Report,* (175).

Oeser, M., Pellinen, T., Scarpas, T. and Kasbergen, C. 2008. Studies on creep and recovery of rheological bodies based upon conventional and fractional formulations and their application on asphalt mixture. *International Journal of Pavement Engineering,* 9(5), 373-386.

Olard, F., Le Noan, C. and Romier, A., Innovative low energy asphalt technique for minimizing impacts from asphalt plants to road works. ed. *Choice for Sustainable Development. Pre-Proceedings of the 23rd PIARRC World Road CongressWorld Road Association-PIARC*, 2007.

Oner, J., Sengoz, B., Rija, S. F. and Topal, A. 2017. Investigation of the rheological properties of elastomeric polymer-modified bitumen using warm-mix asphalt additives. *Road Materials and Pavement Design,* 18(5), 1049-1066.

Ortiz-Ripoll, J., Miró, R. and Martínez, A. H. 2020. Semi-empirical method for the calculation of shear stress, stiffness and maximum shear strength of bituminous interfaces under in-service conditions. *Construction and Building Materials,* 258, 120374.

Ozer, H., Al-Qadi, I. L., Hasiba, K. I., Wang, H. and Salinas, A., 2013. Pavement Layer Interface Shear Strength Using a Hyperbolic Mohr-Coulomb Model and Finite Element Analysis. *Airfield and Highway Pavement 2013.* 1445-1456.

Palyvos, J. A. 2008. A survey of wind convection coefficient correlations for building envelope energy systems' modeling. *Applied Thermal Engineering,* 28(8), 801-808.

Park, S. and Schapery, R. 1999. Methods of interconversion between linear viscoelastic material functions. Part I—A numerical method based on Prony series. *International Journal of Solids and Structures,* 36(11), 1653-1675.

Pasindu, H. R., Fwa, T. F. and Ong, G. P. 2016. Analytical evaluation of aircraft operational risks from runway rutting. *International Journal of Pavement Engineering,* 17(9), 810-817.

Pasquini, E., Giacomello, G., Pasetto, M. and Canestrari, F. 2015. Laboratory evaluation of the effect of low-temperature application of warm-mix asphalts on interface shear strength. 88, 56-63.

Pei, J., Fan, Z., Liu, H., Zhang, J., Li, R. and Li, Y. 2016. Nonlinear viscoelastic model for asphalt mixture subjected to repeated loading. *Road Materials and Pavement Design,* 17(4), 892-905.

Pellinen, T. K., Witczak, M. W. and Bonaquist, R. F., 2003. Asphalt Mix Master Curve Construction Using Sigmoidal Fitting Function with Non-Linear Least Squares Optimization. *Recent Advances in Materials Characterization and Modeling of Pavement Systems.* 83-101.

Perdomo, D. and Button, J. W., 1991. *Identifying and correcting rut-susceptible asphalt mixtures.* Federal Highways Administration.

Perkins, S., 2009. *Synthesis of warm mix asphalt paving strategies for use in Montana highway construction.* Bozeman, MT, USA: Western Transportation Institute, Montana State University.

Perl, M., Uzan, J. and Sides, A. 1983. Visco-elasto-plastic constitutive law for a bituminous mixture under repeated loading. *Transportation Research Record,* 911, 20-26.

Petit, C., Millien, A., Canestrari, F., Pannunzio, V. and Virgili, A. 2012. Experimental study on shear fatigue behavior and stiffness performance of Warm Mix Asphalt by adding synthetic wax. 34, 537-544.

Pittenger, D. M. 2011. Evaluating Sustainability of Selected Airport Pavement Treatments with Life-Cycle Cost, Raw Material Consumption, and Greenroads Standards. *Transportation Research Record,* 2206(1), 61-68.

Please, A. 1961. Use of the marshall test for evaluating dense bituminous surfacings. *Journal of Applied Chemistry,* 11(2), 73-80.

Priyadharshini, Y., Maheshwari, S., Padmarekha, A. and Krishnan, J. M. 2013. Effect of Mixing and Compaction Temperature on Dynamic Modulus of Modified Binder Bituminous Mixtures. *2nd Conference of Transportation Research Group of India (2nd CTRG),* 104, 12-20.

Prowell, B. D., Hurley, G. C. and Frank, B., 2011. *Warm-mix asphalt: Best practices.* National Asphalt Pavement Association Lanham, Md, USA.

Qi, X., Sebaaly, P. E. and Epps, J. A. 1995. Evaluation of Polymer-Modified Asphalt Concrete Mixtures. *Journal of Materials in Civil Engineering,* 7(2), 117-124.

Qiao, Y., Dawson, A., Huvstig, A. and Korkiala-Tanttu, L. 2014. Calculating rutting of some thin flexible pavements from repeated load triaxial test data. *International Journal of Pavement Engineering,* 16(6), 467-476.

Raab, C., Abd El Halim, A. O. and Partl, M. N. 2012. Interlayer bond testing using a model material. *Construction and Building Materials,* 26(1), 190-199.

Raab, C. and Partl, M. N., 1999. *Methoden zur beurteilung des schichtenverbunds von asphaltbelägen.* Eidgenössisches Departement für Umwelt, Verkehr, Energie und Kommunikation, Bundesamt für Strassen.

Raab, C. and Partl, M. N., Interlayer shear performance: experience with different pavement structures. ed. *3rd Eurasphalt and Eurobitume Congress*, May 2004 Vienna, Austria

Raab, C., Partl, M. N. and El, A. E. H. O. A. 2009. Evaluation of interlayer shear bond devices for asphalt pavements. *The Baltic Journal of Road and Bridge Engineering,* 4(4), 186-186.

Rabiot, D. and Morizur, M., Polymer-Modified Bitumen Emulsions an Advantage for the Various Road Applications. ed. *Eurasphalt & Eurobitume Congress, Strasbourg, 7-10 May 1996. Volume 3. Paper E&E. 6.161*, 1996.

Raghavendra, A., Medeiros, M. S., Hassan, M. M., Mohammad, L. N. and King, W. B. 2016. Laboratory and Construction Evaluation of Warm-Mix Asphalt. *Journal of Materials in Civil Engineering,* 28(7), 04016023.

Ragni, D., Graziani, A. and Canestrari, F., Cyclic interlayer testing in bituminous pavements. ed. *Bituminous Mixtures and Pavements VII: Proceedings of the 7th International Conference'Bituminous Mixtures and Pavements'(7ICONFBMP), June 12-14, 2019, Thessaloniki, Greece*, 2019, 207.

Rahimzadeh, B., 2002. *Linear and non-linear viscoelastic behaviour of binders and asphalts.* (PhD). University of Nottingham Nottingham, UK.

Rahman, A. S. M. A., Islam, M. R. and Tarefder, R. A. 2018. Dynamic modulus and phase angle models for New Mexico's Superpave mixtures. *Road Materials and Pavement Design*, 740-753.

Rahman, T., Dawson, A. and Thom, N., The Permissible Temperature of Newly Laid Asphalt at Opening to Airfield Traffic. ed. *Bituminous Mixtures and Pavements VII*, June 12-14, 2019 2019a Thessaloniki, Greece.

Rahman, T., Dawson, A. and Thom, N. 2020a. Warm mix asphalt (WMA) for rapid construction in airfield pavement. *Construction and Building Materials,* 246, 118411.

Rahman, T., Dawson, A., Thom, N., Ahmed, I. and Carvajal-Munoz, J. S. 2020b. Determining the allowable opening-to-traffic asphalt temperature for airport pavements. *International Journal of Pavement Engineering*, 1-19.

Rahman, T., Thom, N. and Dawson, A., Strategies for Reduced Cooling Time of Asphalt for Airfield Pavement Overlay. ed. *Airfield and Highway Pavements 2019*, 2019b Chicago, Illinois, 251-265.

Read, J., Whiteoak, D., Hunter, R. N. and Self, A., 2003. *The Shell Bitumen Handbook.* Sixth ed. London: ICE Publishing.

Recasens, R. M., Martínez, A. and Jiménez, F. P. 2005. Assessing heat-adhesive emulsions for tack coats. *Proceedings of the Institution of Civil Engineers - Transport,* 158(1), 45-51.

Richard, C., Doré, G., Lemieux, C., Bilodeau, J.-P. and Haure-Touzé, J., 2015. Albedo of Pavement Surfacing Materials: In Situ Measurements. *In:* Guthrie, W. S. ed. *16th International Conference on Cold Regions Engineering.* Salt Lake City, Utah: ASCE.

Roads and Maritime Services, 2010. *QA Specification R116 Stone Mastic Asphalt.*

Roberts, F. L., Kandhal, P. S., Brown, E. R., Lee, D.-Y. and Kennedy, T. W. 1991. Hot mix asphalt materials, mixture design and construction.

Rodrigues, C. and Hanumanthgari, R., 2015. Polymer modified bitumens and other modified binders. *The Shell Bitumen Handbook.* 149-183.

Rodway, B., Asphalt deformation due to high tyre pressure. ed. *FAA airport pavement working group annual meeting*, 2009.

Rodway, B., Flexible aircraft pavement surfacing—Australian practice. ed. *8th International Conference on Maintenance and Rehabilitation of Pavements, Singapore*, 2016, 27-29.

Roffe, J.-C. and Chaignon, F., Characterisation tests on bond coats: worldwide study, impact, tests, recommendations. ed. *Proceedings of the 3rd International Conference Bituminous Mixtures and Pavements* 2002 Thessaloniki, Greece.

Rohsenow, W. M., Hartnett, J. P. and Cho, Y. I., 1998. *Handbook of Heat Transfer.* McGraw-Hill.

Romain, J., 1969. *Rut depth prediction in asphalt pavements.* Centre de Recherches Routières.

Romanoschi, S. and Metcalf, J. 2001a. Characterization of Asphalt Concrete Layer Interfaces. *Transportation Research Record: Journal of the Transportation Research Board,* 1778, 132-139.

Romanoschi, S. A. and Metcalf, J. B. 2001b. Effects of Interface Condition and Horizontal Wheel Loads on the Life of Flexible Pavement Structures. *Transportation Research Record,* 1778(1), 123-131.

Roosens, P. 2008. Congestion and Air Transport: a challenging phenomenon. *European Journal of Transport and Infrastructure Research,* 8(2).

Rowe, G. M., 1996. *Application of the dissipated energy concept to fatigue cracking in asphalt pavements.* (PhD). University of Nottingham.

Rowe, R. K., 2012. *Geotechnical and geoenvironmental engineering handbook.* Springer Science & Business Media.

Rushing, J., Mejías-Santiago, M. and Doyle, J. 2013. Assessment of Warm-Mix Asphalt for Heavy Traffic Airfields. *Transportation Research Record: Journal of the Transportation Research Board,* 2371, 41-48.

Rushing, J. F., Darabi, M. K., Rahmani, E. and Little, D. N. 2017. Comparing rutting of airfield pavements to simulations using Pavement Analysis Using Nonlinear Damage Approach (PANDA). *International Journal of Pavement Engineering,* 18(2), 138-159.

Rushing, J. F. and Little, D. N. 2014. Static Creep and Repeated Load as Rutting Performance Tests for Airport HMA Mix Design. *Journal of Materials in Civil Engineering,* 26(9), 04014055.

Rushing, J. F., Little, D. N. and Garg, N. 2014. Selecting a rutting performance test for airport asphalt mixture design. *Road Materials and Pavement Design,* 15(sup1), 172-194.

Salim, R., Gundla, A., Zalghout, A., Underwood, B. S. and Kaloush, K. E. 2019. Relationship between Asphalt Binder Parameters and Asphalt Mixture Rutting. *Transportation Research Record,* 2673(6), 431-446.

Salinas, A., Al-Qadi, I., Hasiba, K., Ozer, H., Leng, Z. and Parish, D. 2013. Interface Layer Tack Coat Optimization. *Transportation Research Record: Journal of the Transportation Research Board,* 2372, 53-60.

Sanchez-Alonso, E., Vega-Zamanillo, A., Castro-Fresno, D. and DelRio-Prat, M. 2011. Evaluation of compactability and mechanical properties of bituminous mixes with warm additives. *Construction and Building Materials,* 25(5), 2304-2311.

Sander Ty, C. and Roesler Jeffery, R. 2006. Case Study: Runway 12L-30R Keel Section Rehabilitation, Lambert ? St. Louis International Airport. *Airfield and Highway Pavement*, 872-884.

Sangiorgi, C., Collop, A. and Thom, N., Laboratory assessment of bond condition using the Leutner shear test. ed. *3rd International Conference on Bituminous Mixtures and Pavements, Thessalonkiki, Greece*, 2002a, 315-324.

Sangiorgi, C., Collop, A. and Thom, N., Non-destructive evaluation of bond between asphalt layers. ed. *XII SIIV International Congress*, 2002b.

Santagata, E., Baglieri, O., Alam, M. and Dalmazzo, D. 2015. A novel procedure for the evaluation of anti-rutting potential of asphalt binders. *International Journal of Pavement Engineering,* 16(4), 287-296.

Santagata, E., Baglieri, O., Dalmazzo, D. and Tsantilis, L. 2013. Evaluation of the anti-rutting potential of polymer-modified binders by means of creep-recovery shear tests. *Materials and Structures,* 46(10), 1673-1682.

Santagata, E., Baglieri, O., Riviera, P., Lanotte, M. and Alam, M., Influence of lateral confining pressure on flow number tests. ed. *Bearing Capacity of Roads, Railways and Airfields* 2017 Athens, Greece.

Santagata, F., Partl, M., Ferrotti, G., Canestrari, F. and Flisch, A., Layer characteristics affecting interlayer shear resistance in flexible pavements. ed. *Technical Session of the Association-of-Asphalt-Paving-Technologists. Philadelphia, PA. APR 27-30, 2008*, 2008, 221-256.

Santagata, F. A., Ferrotti, G., Partl, M. N. and Canestrari, F. 2009. Statistical investigation of two different interlayer shear test methods. *Materials and Structures,* 42(6), 705-714.

Saowapark, W., Jubsilp, C. and Rimdusit, S. 2019. Natural rubber latex-modified asphalts for pavement application: effects of phosphoric acid and sulphur addition. *Road Materials and Pavement Design,* 20(1), 211-224.

Sasol, 2008. *Sasobit –the versatile additive for asphalt mixes, Product information* [online]. Available from: https://www.sasolwax.com/fileadmin/user_upload/Asphalt_Additive_Sasobit.pdf [Accessed 13 July 2020 2020].

Sasol Wax, 2016. *A smooth landing: paving the runway* [online]. Available from: https://www.sasobit.com/files/downloads/en/slider/Interview_Airport_Focus_International_small.pdf [Accessed Spetember 9, 2020].

Shahin, M. Y., 2005. *Pavement management for airports, roads, and parking lots.* Springer New York.

Shahin, M. Y., Blackmon, E. W., Van Dam, T. and Kirchner, K., 1987. *Consequence of Layer Separation on Pavement Performance.* Champaign, Illinois: U.S. Army Construction Engineering.

Shahin, M. Y., Kirchner, K., Blackmon, E. W. and Tomita, H. 1986. Effect of layer slippage on performance of asphalt-concrete pavements. *Transportation Research Record,* 1095(1095).

Shi, X., Rew, Y., Ivers, E., Shon, C.-S., Stenger, E. M. and Park, P. 2017. Effects of thermally modified asphalt concrete on pavement temperature. *International Journal of Pavement Engineering,* 20(6), 669-681.

Sholar, G. A., Page, G. C., Musselman, J. A., Upshaw, P. B. and Moseley, H. L. 2002. Preliminary investigation of a test method to evaluate bond strength of bituminous tack coats (with discussion). *Journal of the Association of Asphalt Paving Technologists,* 73.

Shuangxi Li, Liang Tang and Kang Yao 2020. Comparison of Two Typical Professional Programs for Mechanical Analysis of Interlayer Bonding of Asphalt Pavement Structure. *Advances in Materials Science and Engineering,* 2020(5850627), 11.

Silva, H. M. R. D., Oliveira, J. R. M., Peralta, J. and Zoorob, S. E. 2010. Optimization of warm mix asphalts using different blends of binders and synthetic paraffin wax contents. *Construction and Building Materials,* 24(9), 1621-1631.

Singh, B., Saboo, N. and Kumar, P. 2017. Effect of Short-Term Aging on Creep and Recovery Response of Asphalt Binders. *Journal of Transportation Engineering, Part B: Pavements,* 143(4), 04017017.

SKYbrary, 2019. *Runway/Taxiway Construction Risks* [online]. Available from: https://www.skybrary.aero/index.php/Runway/Taxiway_Construction_Risks [Accessed August 6 2020].

Soenen, H., Blomberg, T., Pellinen, T. and Laukkanen, O.-V. 2013. The multiple stress creep-recovery test: a detailed analysis of repeatability and reproducibility. *Road Materials and Pavement Design,* 14(sup1), 2-11.

Solaimanian, M. and Bolzan, P., 1993. *Analysis of the integrated model of climatic effects on pavements.* Strategic Highway Research Program, National Research Council.

Solaimanian, M. and Kennedy, T. W. 1993. Predicting maximum pavement surface temperature using maximum air temperature and hourly solar radiation. *Transportation Research Record,* 1417, 1-1.

Soleymani, H. R., Zhai, H. and Bahia, H. 2004. Role of Modified Binders in Rheology and Damage Resistance Behavior of Asphalt Mixtures. *Transportation Research Record,* 1875(1), 70-79.

Sousa, J., Weissman, S. L., Sackman, J. L. and Monismith, C. L. 1993. Nonlinear elastic viscous with damage model to predict permanent deformation of asphalt concrete mixes. *Transportation Research Record,* (1384).

Sousa, J. B., Craus, J. and Monismith, C. L., 1991. *Summary report on permanent deformation in asphalt concrete.* Strategic Highway Research Program.

Srikanth, G., Kumar, R. and Vasudeva, R., 2018. A Review on Warm Mix Asphalt. *National Conference: Advanced Structures, Materials And Methodology in Civil Engineering (ASMMCE).*

Stewart, S., 2014. *Flying the big jets.* Crowood.

Su, K., Maekawa, R. and Hachiya, Y. 2009. Laboratory evaluation of WMA mixture for use in airport pavement rehabilitation. *Construction and Building Materials,* 23(7), 2709-2714.

Su, K., Sun, L., Hachiya, Y. and Maekawa, R. 2008. Analysis of shear stress in asphalt pavements under actual measured tire-pavement contact pressure. *Proceedings of the 6th ICPT, Sapporo, Japan*, 11-18.

Subhy, A. 2017. Advanced analytical techniques in fatigue and rutting related characterisations of modified bitumen: Literature review. *Construction and Building Materials,* 156, 28-45.

Suddeepong, A., Sari, N., Horpibulsuk, S., Chinkulkijniwat, A. and Arulrajah, A. 2020. Interface shear behaviours between recycled concrete aggregate and geogrids for pavement applications. *International Journal of Pavement Engineering,* 21(2), 228-235.

Sun, L., Jia, L. and Qin, J., Temperature distribution prediction model for asphalt pavements. ed. *10th International Conference On Asphalt Pavements-August 12 To 17, 2006, Quebec City, Canada*, 2006.

Syed, I. A., Mannan, U. A. and Tarefder, R. A. 2019. Comparison of rut performance of asphalt concrete and binder containing warm mix additives. *International Journal of Pavement Research and Technology,* 12(2), 162-169.

Syroezhko, A. M., Baranov, M. A., Ivanov, S. N. and Maidanova, N. V. 2011. Influence of natural additives and those synthesized by the Fischer-Tropsch method on the properties of petroleum bitumen and quality of floated asphalt. 54(1), 26-31.

Taamneh, M. 2016. Temperature profile prediction for flexible pavement structures. *HKIE Transactions,* 23(3), 150-156.

Taherkhani, H., 2006. *Experimental characterisation of the compressive permanent deformation behaviour in asphaltic mixtures.* (PhD). University of Nottingham.

Taherkhani, H. and Collop, A. C., Determination of the Elastic Modulus and Poisson's Ratio of Asphaltic Mixtures Using Uniaxial Creep Recovery Tests. ed. *Airfield and Highway Pavements*, October 15-18, 2008 2008 Bellevue, Washington, United States: Proceedings, 159-170.

Tan, S., Fwa, T., Chuai, C. and Low, B. 1997. Determination of Thermal Properties of Pavement Materials and Unbound Aggregates by Transient Heat Conduction. *ournal of Testing and Evaluation, JTEVA,* 25(1), 15-22.

Tarefder, R., Zaman, M. and Hobson, K. 2003. A laboratory and statistical evaluation of factors affecting rutting. *International Journal of Pavement Engineering,* 4(1), 59-68.

Tarefder, R. A. and Rahman, A., 2016. *Interconversion of Dynamic Modulus to Creep Compliance and Relaxation Modulus: Numerical Modeling and Laboratory Validation-Final Report.* Reno, NV: NDOT (Nevada department of Transportation).

Tasdemir, Y. 2009. High temperature properties of wax modified binders and asphalt mixtures. *Construction and Building Materials,* 23(10), 3220-3224.

Tashman, L., Nam, K. and Papagiannakis, A., 2006. *Evaluation of the influence of tack coat construction factors on the bond strength between pavement layers.* Washington State Department of Transportation Olympia.

Tashman, L., Nam, K., Papagiannakis, T., Willoughby, K., Pierce, L. and Baker, T. 2008. Evaluation of construction practices that influence the bond strength at the interface between pavement layers. *Journal of Performance of Constructed Facilities,* 22(3), 154-161.

Tayebali, A. A., Rahman, M., Kulkarni, M. and Xu, Q., 2004. *A mechanistic approach to evaluate contribution of prime and tack coat in composite asphalt pavements, report number FHWA/NC/2004-05.* Raleigh, North Carolina: North Carolina Department of Transportation.

Taylor, R. and Airey, G., 2015. Rheology of bitumens. *The Shell Bitumen Handbook.* 119-148.

Texas Department of Transportation, 2019. Test Procedure for Cantabro Loos, TxDOT Designation: Tex-245-F. Texas.

Thom, N., 2013. *Principles of Pavement Engineering.* Second ed. London, United Kingdom: ICE Publishing.

Thrower, E., Methods of predicting deformation in road pavements. ed. *Volume I of proceedings of 4th International Conference on Structural Design of Asphalt Pavements, Ann Arbor, Michigan, August 22-26, 1977.*, 1977.

Timm, D. H., Voller, V. R., Lee, E.-b. and Harvey, J. 2001. Calcool: A multi-layer Asphalt Pavement Cooling Tool for Temperature Prediction During Construction. *International Journal of Pavement Engineering,* 2(3), 169-185.

Tozzo, C., D'Andrea, A., Cozzani, D. and Meo, A. 2014a. Fatigue investigation of the interface shear performance in asphalt pavement. *Modern Applied Science,* 8(2), 1.

Tozzo, C., D'Andrea, A. and Al-Qadi, I. L. 2016a. Dilatancy in the Analysis of Interlayer Cyclic Shear Test Results. *Journal of Materials in Civil Engineering,* 28(12), 04016171.

Tozzo, C., Fiore, N. and D'Andrea, A. 2014b. Dynamic shear tests for the evaluation of the effect of the normal load on the interface fatigue resistance. *Construction and Building Materials,* 61, 200-205.

Tozzo, C., Fiore, N. and D'Andrea, A., Investigation of Dilatancy Effects on Asphalt Interface Shear Strength. In: Canestrari, F. and Partl, M. N., ed., 2016b Dordrecht: 8th RILEM International Symposium on Testing and Characterization of Sustainable and Innovative Bituminous Materials, 335-346.

Tran, N., Willis, R. and Julian, G., 2012. *Refinement of the bond strength procedure and investigation of a specification.* Auburn, AL: National Center for Asphalt Technology,.

Transportation Safety Board of Canada, 2000. *Aviation Investigation Report A00Q0094, Runway Excursion.*

Tsai, B. W., Monismith, C. L., Dunning, M., Gibson, N., D'Angelo, J., Leahy, R., King, G., Christensen, D., Anderson, D., Davis, R. and Jones, D. 2005. Influence of Asphalt Binder Properties on the Fatigue Performance of Asphalt Concrete Pavements. *2005 Journal of the Association of Asphalt Paving Technologists: From the Proceedings of the Technical Sessions,* 74, 733-789.

Tsai, J. and Lai, J. 2010. Evaluating constructability and properties of warm mix asphalt. *Georgia Institute of Technology (Atlanta), Final report*.

Tschegg, E. K., Kroyer, G., Tan, D.-M., Stanzl-Tschegg, S. E. and Litzka, J. 1995. Investigation of Bonding between Asphalt Layers on Road Construction. *Journal of Transportation Engineering,* 121(4), 309-316.

Tsubokawa, Y., Mizukami, J., Esaki, T. and Hayano, K., Study on infrared thermographic inspection of de-bonded layer of airport flexible pavement. ed. *FAA Worldwide Airport Technology Transfer Conference. Atlantic City, New Jersey*, 2007.

Tw Kennedy, F. L. R. R. B. M., 1984. *Effects of Compaction Temperature and Effort on the Engineering Properties of Asphalt Concrete Mixtures Placement and Compaction of Asphalt Mixtures.* West Conshohocken, PA: ASTM International.

Uddin, W. 2003. Viscoelastic characterization of polymer-modified asphalt binders of pavement applications. *Applied Rheology,* 13(4), 191-199.

Uzan, J. 2004. Permanent Deformation in Flexible Pavements. *Journal of Transportation Engineering,* 130(1), 6-13.

Uzan, J., Livneh, M. and Eshed, Y., Investigation of adhesion properties between asphaltic-concrete layers. ed. *Association of Asphalt Paving Technologists Proc*, 1978.

Vallerga, B. A., Jew, A. and Nokes, W. A., 2000. Case Study of an Innovative High Stability Asphalt Mix for Heavy Aircraft Wheel Loads. *The 2020 Vision of Air Transportation.* 334-345.

Vangla, P. and Latha, G. M. 2015. Influence of Particle Size on the Friction and Interfacial Shear Strength of Sands of Similar Morphology. *International Journal of Geosynthetics and Ground Engineering,* 1(1), 6.

Vargas-Nordcbeck, A., 2012. *Physical and structural characterization of sustainable asphalt pavement sections at the NCAT test track.*

Vargas-Nordcbeck, A. and Timm, D. 2011. Validation of Cooling Curves Prediction Model for Nonconventional Asphalt Concrete Mixtures. *Transportation Research Record: Journal of the Transportation Research Board,* (2228), 111-119.

Vasenev, A., Bijleveld, F., Hartmann, T. and Dorée, A., A real-time system for prediction cooling within the asphalt layer to support rolling operations. ed. *5th Eurasphalt and Eurobitume Congress*, 13-15 June 2012 Istanbul, Turkey.

Vilumsone-Nemes, I., 2018. 12 - Fusing of cut textile components. *In:* Vilumsone-Nemes, I. ed. *Industrial Cutting of Textile Materials (Second Edition).* Woodhead Publishing, 189-205.

Walubita, L. F., Hoeffner, J. and Scullion, T., 2012. *New Generation Mix-Designs: Laboratory-Field Testing and Modifications to Texas HMA Mix-Design Procedures.* Texas. Dept. of Transportation. Research and Technology Implementation Office.

Wang, H. and Al-Qadi, I. L., Impact of non-uniform aircraft tire pressure on airfield pavement responses. ed. *Transportation and Development Institute Congress 2011: Integrated Transportation and Development for a Better Tomorrow*, 2011, 844-853.

Wang, H., Li, M. and Garg, N., Simulation of NAPTF High Tire Pressure Tests with Advanced Finite Element Modeling. ed. *2014 FAA Worldwide Airport Technology Transfer Conference*, 2014a Galloway, New Jersey.

Wang, H., Li, M. and Garg, N. 2016. Investigation of shear failure in airport asphalt pavements under aircraft ground manoeuvring. *Road Materials and Pavement Design,* 18(6), 1288-1303.

Wang, H., Liu, X., Apostolidis, P. and Scarpas, T. 2018a. Review of warm mix rubberized asphalt concrete: Towards a sustainable paving technology. *Journal of Cleaner Production,* 177, 302-314.

Wang, J., Yuan, J., Xiao, F., Li, Z., Wang, J. and Xu, Z. 2018b. Performance investigation and sustainability evaluation of multiple-polymer asphalt mixtures in airfield pavement. *Journal of Cleaner Production,* 189, 67-77.

Wang, W., Tan, G., Liang, C., Wang, Y. and Cheng, Y. 2020. Study on Viscoelastic Properties of Asphalt Mixtures Incorporating SBS Polymer and Basalt Fiber under Freeze–Thaw Cycles. *Polymers,* 12(8), 1804.

Wang, X., Su, Z., Xu, A., Zhou, A. and Zhang, H. 2017. Shear fatigue between asphalt pavement layers and its application in design. *Construction and Building Materials,* 135, 297-305.

Wang, Y., Zhu, S. and Wong, A. S. T. 2014b. Cooling Time Estimation of Newly Placed Hot-Mix Asphalt Pavement in Different Weather Conditions. *Journal of Construction Engineering and Management,* 140(5), 04014009.

Wasage, T. L. J., Stastna, J. and Zanzotto, L. 2011. Rheological analysis of multi-stress creep recovery (MSCR) test. *International Journal of Pavement Engineering,* 12(6), 561-568.

Wasiuddin, N. M., Selvamohan, S., Zaman, M. M. and Guegan, M. L. T. A. 2007. Comparative Laboratory Study of Sasobit and Aspha-Min Additives in Warm-Mix Asphalt. *Transportation Research Record,* 1998(1), 82-88.

Wellner, F. and Hristov, B. 2015. Numerically Supported Experimental Determination of the Behavior of the Interlayer Bond in Asphalt Pavement. *Transportation Research Record,* 2506(1), 116-125.

Wen, H., Kutay, M. and Shen, S. 2011. Evaluation of the Effects of Asphalt Binder on the Properties of Hot Mix Asphalt at Intermediate Temperatures. *Journal of testing and evaluation,* 39(3), 321-326.

Wendelstorf, J., Spitzer, K. H. and Wendelstorf, R. 2008. Spray water cooling heat transfer at high temperatures and liquid mass fluxes. *International Journal of Heat and Mass Transfer,* 51(19), 4902-4910.

Wendelstorf, J., Wendelstorf, R. and Spitzer, K.-H. 2009. Spray Cooling Heat Transfer and Calculation of Water Impact Density for Cooling of Steel Sheet Materials by Inverse Process Modelling. *steel research international,* 80(9), 639-644.

Wendt, P., Voltes-Dorta, A. and Suau-Sanchez, P. 2020. Estimating the costs for the airport operator and airlines of a drone-related shutdown: an application to Frankfurt international airport. *Journal of Transportation Security,* 13(1), 93-116.

Wensel, M., Shalaby, A., Thiessen, M. and Mah, V., Investigation of asphalt pavement rutting at two Canadian airfields. ed. *4th Transportation Specialty Conference of the Canadian Society for Civil Engineering, Montreal, Canada*, 2002.

West, R., Rodezno, C., Julian, G., Prowell, B., Frank, B., Osborn, L. and Kriech, T. 2014a. NCHRP Report 779: Field Performance of Warm Mix Asphalt Technologies. *Transportation Research Board of the National Academies, Washington, DC*.

West, R., Rodezno, C., Julian, G. and Prowell, D. 2014b. Engineering properties and field performance of warm mix asphalt technologies. *National Cooperative Highway Research Program, Washington, DC, USA, NCHRP Final Report Project,* (09-47A).

West, R. C., Watson, D. E., Turner, P. A. and Casola, J. R., 2010. *Mixing and Compaction Temperatures of Asphalt Binders in Hot-Mix Asphalt, NCHRP Report 648.* Washington, DC: Transportation Research Board, The National Academies Press.

West, R. C., Zhang, J. and Moore, J. 2005. Evaluation of bond strength between pavement layers. *NCAT report*, 05-08.

White, G., Developing Warm Mix Asphalt for Airports. ed. *Proceedings of the 15th International Flexible Pavement Conference*, 2013.

White, G., Cyclic shear deformation of asphalt at Melbourne Airport. ed. *FAA Worldwide Airport Technology Transfer Conference (ATTC)*, 5–7 August 2014 2014a Galloway: Innovations in Airport Safety and Pavement Technologies, 1–19.

White, G., New airport pavement technologies from the USA. ed. *Proceedings 2014 Australian Airport Association National Conference, Gold Coast, Australia*, 2014b, 23-27.

White, G., 2015a. *Systematic diagnosis of factors leading to cyclic shear creep of airport asphalt surfaces.* (PhD). University of the Sunshine Coast.

White, G. 2015b. Warm Mix Asphalt For Australian Airports. *International Journal on Pavement Engineering & Asphalt Technology (PEAT),* 16(1).

White, G. 2016a. The Impact of Rainfall During Asphalt Paving Operations- Technical Note. *The International Journal of Pavement Engineering and Asphalt Technology (PEAT),* 17(2), 7.

White, G. 2016b. Shear stresses in an asphalt surface under various aircraft braking conditions. *International Journal of Pavement Research and Technology,* 9(2), 89-101.

White, G. 2016c. State of the art: interface shear resistance of asphalt surface layers. *International Journal of Pavement Engineering,* 18(10), 887-901.

White, G., 2017a. Expedient runway upgrade technologies. *In:* Loizos, A., AlQadi, I. and Scarpas, T. eds. *10th International Conference on the Bearing Capacity of Roads, Railways and Airfields.* Athens, Greece: Taylor & Francis Group, 1735-1741.

White, G. 2017b. State of the art: Asphalt for airport pavement surfacing. *International Journal of Pavement Research and Technology,* 11(1), 77-98.

Widyatmoko, I., 1998. *The performance of polymer modified bituminous mixtures.* (PhD). Sheffield Hallam University.

Williams, B. A., Willis, J. R. and Ross, T. C., 2019. *Asphalt Pavement Industry Survey on Recycled Materials and Warm-Mix Asphalt Usage: 2018.*

Williams, R. and Prowell, B. 1999. Comparison of laboratory wheel-tracking test results with Wes Track performance. *Transportation Research Record: Journal of the Transportation Research Board,* (1681), 121-128.

Wills, W., 1982. *Current Practices on Nighttime Pavement Construction Asphaltic Concrete.* US Department of Transportation, Federal Aviation Administration.

Witczak, M. W., 2005. *Simple performance tests: Summary of recommended methods and database, NCHRP Report 547.* Transportation Research Board.

Witczak, M. W., Kaloush, K., Pellinen, T. and El-Basyouny, M., 2002. *Simple performance test for superpave mix design, NCHRP Report 465.* Washington DC: Transportation Research Board, 0309067154.

Wu, S., Chen, H., Zhang, J. and Zhang, Z. 2017. Effects of interlayer bonding conditions between semi-rigid base layer and asphalt layer on mechanical responses of asphalt pavement structure. *International Journal of Pavement Research and Technology,* 10(3), 274-281.

Xiao, F., Amirkhanian Serji, N. and Zhang, R., Rheological Investigation of Non-Foaming WMA Additives at Mid-Temperature. ed. *Emerging Technologies for Material, Design, Rehabilitation, and Inspection of Roadway Pavements*, 2020/07/11 2011: Proceedings, 1-8.

Xiao, F., Amirkhanian Serji, N. and Zhang, R. 2012. Influence of Short-Term Aging on Rheological Characteristics of Non-Foaming WMA Binders. *Journal of Performance of Constructed Facilities,* 26(2), 145-152.

Xiao, F. and Amirkhanian, S. N. 2009. Laboratory investigation of moisture damage in rubberised asphalt mixtures containing reclaimed asphalt pavement. *International Journal of Pavement Engineering,* 10(5), 319-328.

Xiao, F., Wang, J., Yuan, J., Liu, Z. and Ma, D. 2020. Fatigue and Rutting Performance of Airfield SBS-Modified Binders Containing High Modulus and Antirutting Additives. *Journal of Materials in Civil Engineering,* 32(3), 04019366.

Yang, K., Li, R., Yu, Y., Pei, J. and Liu, T. 2020. Evaluation of interlayer stability in asphalt pavements based on shear fatigue property. *Construction and Building Materials,* 258, 119628.

Yin, F., Epps Martin, A. and Arámbula-Mercado, E. 2016. Warm-Mix Asphalt Moisture Susceptibility Evaluation for Mix Design and Quality Assurance. *Transportation Research Record: Journal of the Transportation Research Board,* 2575, 39-47.

Yinfei, D., Shengyue, W. and Jian, Z. 2015. Cooling asphalt pavement by a highly oriented heat conduction structure. *Energy and Buildings,* 102(Supplement C), 187-196.

Yu, J. Y., Feng, Z. G., Zhang, H. L. and McNally, T., 2011. 9 - Ageing of polymer modified bitumen (PMB). *Woodhead Publishing Series in Civil and Structural Engineering.* Woodhead Publishing, 264-297.

Yunus, A. C. 2003. Heat transfer: a practical approach. *MacGraw Hill, New York*.

Zaniewski, J. P. and Pumphrey, M. E. 2004. Evaluation of performance graded asphalt binder equipment and testing protocol. *Asphalt technology program,* 107, 376-384.

Zapata, C. E. and Houston, W. N., 2008. *Calibration and validation of the enhanced integrated climatic model for pavement design, NCHRP Report 602.* Transportation Research Board, 0309099293.

Zaumanis, M., 2014. Warm Mix Asphalt. *In:* Gopalakrishnan, K., Steyn, W. J. and Harvey, J. eds. *Climate Change, Energy, Sustainability and Pavements.* Berlin, Heidelberg: Springer Berlin Heidelberg, 309-334.

Zhang, J. and Delichatsios, M. A. 2009. Determination of the convective heat transfer coefficient in three-dimensional inverse heat conduction problems. *Fire Safety Journal,* 44(5), 681-690.

Zhang, J., Ray Brown, E., Kandhal, P. and West, R. 2005. An Overview of Fundamental and Simulative Performance Tests for Hot Mix Asphalt. *Journal of ASTM International,* 2(5).

Zhang, J., Walubita, L. F., Faruk, A. N. M., Karki, P. and Simate, G. S. 2015. Use of the MSCR test to characterize the asphalt binder properties relative to HMA rutting performance – A laboratory study. *Construction and Building Materials,* 94, 218-227.

Zhang, J., Wu, S., Ven, M. and Chen, F. 2012. Dynamic Viscosity Analysis of Base Bitumen with the Addition of Rediset. 476-478, 1621-1625.

Zhang, J.-p., Wu, S.-h., Pel, J.-z. and Li, Y.-w. 2014. Analysis of Mechanical Responses of Asphalt Pavement Interlayers Based on Shear Spring Compliance. *Journal of Highway and Transportation Research and Development (English Edition),* 8(1), 1-6.

Zhang, W. 2017. Effect of tack coat application on interlayer shear strength of asphalt pavement: A state-of-the-art review based on application in the United States. *International Journal of Pavement Research and Technology,* 10(5), 434-445.

Zhang, W., Cui, B., Gu, X. and Dong, Q. 2018. Comparison of Relaxation Modulus Converted from Frequency- and Time-Dependent Viscoelastic Functions through Numerical Methods. *Applied Sciences,* 8(12), 2447.

Zhang, Y., Birgisson, B. and Lytton, R. L. 2016. Weak Form Equation–Based Finite-Element Modeling of Viscoelastic Asphalt Mixtures. *Journal of Materials in Civil Engineering,* 28(2), 04015115.

Zhao, Y., Tang, J. and Liu, H. 2012. Construction of triaxial dynamic modulus master curve for asphalt mixtures. *Construction and Building Materials,* 37, 21-26.

Zhou, F. and Scullion, T., 2004. *Input parameters of enhanced VESYS5, Report number FHWA/TX-05/9-1502-0 1-4.* Austin, Texas: Texas Department ofTransportation.

Zhou, F., Scullion, T. and Chen, D.-H. 2002. Laboratory Characterization of Asphalt Mixes of SPS-1 Sections on US281. *Road Materials and Pavement Design,* 3(4), 439-453.

Zhou, X., Thomas, B. G., Hernández B, C. A., Castillejos E, A. H. and Acosta G, F. A. 2013. Measuring heat transfer during spray cooling using controlled induction-heating experiments and computational models. *Applied Mathematical Modelling,* 37(5), 3181-3192.

Zhu, B., Chu, L. and Fwa, T. F. 2019. Cooling characteristics of warm mix asphalt for multi-lift pavement repair and resurfacing. *International Journal of Pavement Engineering*, 1-12.

Zhu, H., Sun, L., Yang, J., Chen, Z. and Gu, W. 2011. Developing Master Curves and Predicting Dynamic Modulus of Polymer-Modified Asphalt Mixtures. *Journal of Materials in Civil Engineering,* 23(2), 131-137.

Zhu, H., Xie, Z., Fan, W., Wang, L. and Shen, J. 2013. Effects of Warm Mix Asphalt (WMA) Additives on the Properties of WMA Mixtures. *Applied Mechanics and Materials* 275-277, 2097-2102.

Ziari, H. and Babagoli, R. 2015. Evaluation of Fatigue and Rutting Behavior of Asphalt Binder Containing Warm Additive. *Petroleum Science and Technology,* 33(17-18), 1627-1632.